The Measurement and Characterisation of Aerosol in the Urban Atmosphere (PM$_{10}$) and an Evaluation of the Sources of these Particles by Number

by

Andrew Lindsay Dye

A thesis submitted to the University of Plymouth
in partial fulfilment for the degree of

DOCTOR OF PHILOSOPHY

Department of Environmental Sciences
Faculty of Science

LIBRARY STORE

The Measurement and Characterisation of Aerosol in the Urban Atmosphere (PM$_{10}$) and an Evaluation of the Sources of these Particles by Number

Andrew Lindsay Dye

Abstract

The link between human health and the mass of fine particulate matter below 10 μm (PM$_{10}$) in air is well documented. Current research suggests that the number, size and shape of particles may be of most concern and that in the urban atmosphere combustion sources of PM$_{10}$, especially diesel engine sources, dominate the fine (< 1 μm) and ultra-fine (<0.1 μm) particles. Despite this, the number, size and shape of particles in urban air has not been reported to any great extent or detail, and the percentage contribution to the numbers of particles from different sources is largely unknown. The objectives of this research were to characterise fine particles with respect to their morphology and thus apportion the sources of particles by number.

Urban aerosol above 1 μm was initially examined to study the fluctuations in PM$_{10}$ number and make retrospective analysis of periods of elevated PM$_{10}$ for source identification in Plymouth, UK. Aerosol was collected *via* a Burkard spore trap and examined using light microscopy with image analysis between 16 March 1995 and 31 August 1996, at a background site in Plymouth, UK. Two periods, 19 January-4 February and 10-25 March 1996, identified as UK wide PM$_{10}$ episodes, were retrospectively studied and compared with PM$_{10}$ mass measurements. The mean number count for the whole period was 10.5 x 10^4 ± 7.9 x 10^4 particles m^{-3}. The two PM$_{10}$ episodes had elevated average number concentrations of 13.5 x 10^4 ± 7.6 x 10^4 particles m^{-3} for 19 January - 4 February 1996, and 13.0 x 10^4 ± 9.7 x 10^4 particles m^{-3} for 10-25 March 1996. During the periods of elevated PM$_{10}$ the tapered element oscillating microbalance (TEOM) mass of particles had a low correlation with the particles less than 5 μm and an increased correlation to the particles greater than 5 μm in size. Outside of these peak periods the PM$_{10}$ TEOM mass was most closely correlated with the number of particles less than 5 μm in size. This work shows the difference in urban aerosol during periods of air quality guideline exceedence. These findings agree with literature that an aged continental aerosol source has a key role in the generation of UK wide PM$_{10}$ mass exceedances.

Further analysis of the fine urban aerosol (< 1 μm) was made using direct sampling of urban aerosol on to porous carbon films (PCF) developed in this research. The efficiency of collection was low (*ca.* 5%) but the samples were representative and enabled transmission electron microscopy (TEM) for sub-micron particle analysis. Measurement was made of the fractal dimensions and diameter of particles. This was used to identify any ageing and ultimately the sources of aerosol.

PCF were used in the simultaneous collection of urban roadside and background aerosol, on seven dates between December 1996 and August 1997 in Plymouth, UK. The average perimeter fractal dimension (PFD) of aerosol was consistently significantly greater at the roadside than the background (+ 0.02), indicative of a smoother, aged aerosol at the background site.

The sampling of a variety of combustion engines was made for source identification purposes. The particle morphology produced from the diesel engines showed great uniformity of particle morphology with varying speed and load; no consistent significant differences were found. The morphology results were comparable to other density fractal dimensions and perimeter fractal dimension values found in other studies for diesel. A natural log relationship between the median particle size and the median PFD was found for the diesel engine sources but not in petrol samples. This natural log trend was considered as a tentative 'fingerprint' of diesel engine combustion and was in harmony with literature values of PFD for diesel engine particles.

Using the fractal measures, size and particle classification the bulk of aerosol was identified as from hydrocarbon combustion sources; *ca.* 88-92% of the roadside and *ca.* 77-86% of background. A component of carbon ceno-spheres were identified contributing *ca.* 6-12% of both the roadside and background aerosol. Non-combustion particles increased from *ca.* 1-4% of the roadside to *ca.* 7-9% of the background, as did the proportion of aged combustion particles, from 0-1% of roadside to 2-3% of the background aerosol. A strong correlation for the median size *vs.* PFD morphology curve between, the roadside and diesel sources (0.93 - 0.95) and the background and petrol sources was found (0.95). The roadside aerosol was significantly different to the petrol source in the 120-220nm size range (p=0.007) and there was a low correlation of the petrol and the roadside size *vs.* morphology curve (0.66). This suggests the domination of roadside aerosol by diesel engine particles. The background aerosol was similar to both diesel and petrol engine sources, especially from a dilution tunnel, thus indicative of a mixture of sources and an aged combustion aerosol. Roadside sources thus dominate the fine and ultra fine urban aerosol by number as compared to most other studies which have only apportioned the sources of particles in the air by mass.

Contents

Section   **Page**

Chapter One : Introduction

Chapter Two : Urban Aerosol measured using a Burkard Spore Trap

Chapter Three : Experimental Methods for Urban Aerosol Analysis

Chapter Six : Source Apportionment of Urban Aerosol

Chapter Seven : Conclusions and Future Work

References

Appendix One

Appendix Two

List of Figures

Chapter One : Introduction

Chapter Two : Urban Aerosol measured using a Burkard Spore Trap

Chapter Three : Experimental Methods for Urban Aerosol Analysis

Chapter Four : The Morphology and Sources of Urban Aerosol Analysis

Chapter Six : Source Apportionment of Urban Aerosol

List of Tables

Chapter One : Introduction

Chapter Three : Experimental Methods for Urban Aerosol Analysis

Chapter Four : The Morphology and Sources of Urban Aerosol Analysis

Chapter Five : The Morphology of Aerosols from Diesel and Spark Ignition Engines

Chapter Six : Source Apportionment of Urban Aerosol

Appendix Two
A2.1 Data for Average Aerosol Morphology for each study day

Abbreviations

2D	Two Dimensional
3D	Three Dimensional
AZ	Arizona
CCSEM	Computer Controlled Scanning Electron Microscopy
COMEAP	Committee on the Medical Effects of Air Pollutants
CO_x	Oxides of Carbon
DEP	Diesel Engine Particulate matter
DETR	Department of the Environment and Transport
DFD	Density Fractal Dimension
DI	Direct Injection
DLA	Diffusion Limited Aggregation
EDXS	Energy Dispersive X-ray Spectroscopy
ESEM	Environmental Scanning Electron Microscopy
g	gram
hr	hour
IDI	Indirect Injection
kV	kilo-volt
l	litre
$l\ min^{-1}$	litre per minute
m	metre
mg	milligram
ml	millilitres
nm	nano-meter
Nm	Newton metre
NO_x	Oxides of Nitrogen
NPF	Nuclepore Filter
PAH	Polycylic Aromatic Hydrocarbon
PCF	Porous Carbon Film
PFD	Perimeter Fractal Dimension
PM_{10}	Particulate matter with an aerodynamic diameter less than 10 microns, usually used with reference to the mass of particulate matter
ppb	parts per billion
ppm	parts per million
PTFE	Teflon
QUARG	Quality of Urban Air Review Group
SEM	Scanning Electron Microscope
SI	Spark Ignition
SO_x	Oxides of Sulphur
STEM	Scanning Transmission Electron Microscope
TEM	Transmission Electron Microscopy
TEOM	Tapered Element Oscillating Microbalance
UK	United Kingdom
US	United States of America
UTHSCSA	University of Texas Health Science Centre at San Antonio
μg	microgram
μm	micrometer or micron

Glossary

Agglomerate

Used to describe the structure of a particle made up of a number of primary units, usually formed in combustion.

Ceno-sphere

A spherical soot particle formed in combustion which form agglomerate particles of soot.

Density Fractal Dimension

A measure of the space filling capability of the area or volume of the structure.

Euclidean geometry

The geometry of perfect, ideal shapes i.e. circles, squares, triangles and smooth surfaces.

Fractal

A descriptive term coined by B.B. Mandelbrot for complex patterns which can be described using the concepts of fractal geometry. A fractal object self similar i.e. its morphology is in a statistical sense, unvaried regardless of whether the entire object or only a small part of it is considered.

Fractal Dimension

A measure of the ruggedness and space filling ability of a structure.

Fractal Geometry

Tackles the problems of describing the rugged surfaces and structures found in nature.

Koch islands

A mathematical curve bounding a finite area but with an infinite perimeter and are formed from repeated operations to the perimeter of a triangle (triadic island) or a square (quadratic).

Occlusion

The hiding of details of something by pacing something in front of it. This commonly occurs with two dimensional projections of three dimensional objects where the upper most part of the object obscures the detail below.

Perimeter Fractal Dimension

A measure of the ruggedness of the boundary or perimeter of a structure and the effectiveness with which the perimeter fills space.

Self similarity

An object may be described as self similar if it can broken up into smaller copies of itself, i.e. a straight line, a square. This is a key concept in fractal geometry.

Sierpinski gasket

A classic theoretical fractal formed by a repeated pattern of triangles, named after Waclaw Sierpinski (1882-1969).

Thresholding

A term used in image analysis to describe the process of choosing the point in the grey scale at which you want pixels to be selected to make a binary image.

Acknowledgements

CHAPTER ONE
Introduction

1.1 Urban Air Quality

During the 1950's the major contributor to urban air pollution in the UK was domestic coal use (QUARG, 1996). One smog episode in London had sulphur dioxide and smoke levels of 4000 μg m^{-3}, it lasted four days, and caused an estimated 4,000 deaths from respiratory or cardiovascular disease (O'Neill, 1985). In 1956 the Clean Air Act was introduced in the UK and these smog's were prevented from occurring again (BéruBé et al., 1997).

In the UK today there is a growing contribution to air pollution from vehicle emissions as well as other anthropogenic sources (Brown, 1994). Oxides of nitrogen (NOx), oxides of carbon (COx), oxides of sulphur (SOx) and ozone are all of concern in relation to vehicle emissions but most concern has been raised over particles smaller than 10 microns in aerodynamic diameter (PM_{10}). The pivotal role of the motor vehicle in our society and economy is beginning to be questioned seriously (Shrimsley, 1997). Issues of road congestion, road rage, road deaths, and road building have all intensified along with total emissions, as car use has increased (Clover, 1995; Langley, 1996 a).

1.1.1 Gaseous and Particulate Pollutants

There are a number of different pollutants which are cause for concern in terms of air quality. Sulphur dioxide (SO_2) is historically linked with air pollution and was the major contributor to the urban smogs of the 1950's (QUARG 1993a). With the introduction of the Clean Air Act in 1956 levels of SOx in urban areas have been following a decreasing trend since 1960 (QUARG, 1993a). With the introduction of low sulphur diesel fuels, levels of sulphur dioxides will most likely show no further increase (QUARG, 1993 b). However some caution is still necessary in areas with a large smoke contribution from domestic fires. Belfast is the most notable case in the UK, as here there is no option of natural gas heating (QUARG, 1996; cf. Section 1.1.5). Sulphur dioxide is also known to

play a role in acid aerosol formation, which perceived wisdom is indicating to be more and more significant (COMEAP, 1995; Seaton *et al.*, 1995).

1.1.2 Urban aerosol

Urban airborne particulate matter, especially the respirable fraction below 10 μm (PM_{10}), in size, is important in terms of public health, having been linked to increases in respiratory and cardiovascular death rates (Dockery *et al.*, 1993; Pope *et al.*, 1995 a). As the health impacts of PM_{10} have become more widely acknowledged it is apparent that more detailed studies of the respirable particles are required (QUARG, 1993 a, b; Read, 1994; COMEAP, 1995; QUARG, 1996). Air quality standards for PM_{10} levels are based on mass measurements per cubic metre of air and most studies have linked health effects to PM_{10} mass measurements (Dockery and Pope, 1994; Schwartz, 1994). Recent work has indicated that it is the number, size and shape of PM_{10} particles which are of most significance (Seaton *et al.*, 1995). It has been suggested that the urban particulate cloud may contain up to 100000 nano-meter sized particles per ml in what may be a gravimetric concentration of only 100-200μg m^{-3} (Seaton *et al.*, 1995). An epidemiological study has concluded that the 24 hour PM_{10} standard of 150μg m^{-3} in the United States does not represent a threshold pollution level below which adverse respiratory health effects are negligible, and that respiratory effects can be observed at PM_{10} levels well below the national US standard (Dockery and Pope, 1994). These results suggest that the present standards for ambient PM_{10} concentrations may be inadequate, and that the characteristics of the fine (< 1 μm) and ultra-fine (< 0.1 μm) particles need to be more fully understood in order to interpret the impact of airborne particulate pollution upon health. Consequently the quantification of particle concentration by number and investigation of the size, shape and composition of the particles is now an area growing in importance and interest (Xie *et al.*, 1994 a, b; Katrinak *et al.*, 1995).

Emissions of diesel engine particulate matter (DEP) have been identified as a major contributor to urban PM_{10} (QUARG, 1993 b). Such emissions are of major importance in the route of organic and inorganic toxic substances deep into the lungs (QUARG, 1993 a, b). Kao and Friedlander, (1995), in California in the US used a chemical mass balance receptor model to identify aerosol sources. They found that that DEP may contribute as much as a quarter of PM_{10} by mass of the aerosol in the urbanised South Coast Air basin of California. In a study of particle numbers and elemental composition measured by energy dispersive x-ray spectroscopy, by Katrinak *et al.*, (1995), over 30%, by number, of particles less than 2 microns were inferred to be from anthropogenic combustion sources in Phoenix, AZ. USA.

1.1.3 Diesel engine, perceived benefit, popularity & future trends

The efficiency of diesel in a direct injection vehicle has always made it the preferred option for commerce and industry (QUARG, 1993, b ; *cf.* Section 1.2.2). With growth in the last seven years in the environmental movement, and moves toward greater fuel efficiency in general there has been a move towards diesel engine vehicles amongst private car owners (QUARG, 1993, b). The promoted and perceived benefits are, a greater energy efficiency and thus a reduced carbon dioxide contribution to 'greenhouse' gases, lower maintenance, and lower lead emissions than gasoline engines (QUARG, 1993, b). A favourable lower tax on diesel as compared to petrol in the UK has encouraged this shift in public opinion. From 1987-1997 diesel has consistently been priced 4-8 pence per litre cheaper than 4 star leaded petrol and during 1989, 1992 and 1993 cost the same or less than unleaded petrol (DETR *Recent Statistics*, Spring 1997). With increased acknowledgement of the problems associated with diesel engine exhaust emissions (QUARG, 1993 a, b; QUARG, 1996, COMEAP, 1995), diesel fuel has been priced accordingly between leaded and unleaded petrol, and there has again been a shift in media perception of diesels and public opinion

(Langley, 1996 b). A recent report even suggests that future UK taxation policy may again shift in favour of petrol and against diesel fuel (Leake and Macaskill, 1997). Thus, after the rapid growth of diesels from 6% of the vehicle fleet in 1991 to 25% at the end of 1993 (QUARG, 1996), the sale of diesel cars actually reversed during 1995 (Langley, 1996 b). Consequently the early, worst case, predictions of road transport particle emissions by the Quality of Urban Air Review Group (QUARG 1993 a ,b), using 49% vehicle penetration of diesels in to the car fleet, have not occurred and are less likely to happen in the present climate of public opinion and fuel cost.

1.1.4   Health effects of gaseous and particulate pollutants

There are two main concerns about air pollution, the long term chronic and the short term acute health effects (COMEAP, 1995).   The long term chronic effects are possible carcinogenic effects and increases in the numbers of asthmatics (QUARG 1993a; Green, 1995; *cf.* Section 1.1.4.1 and 1.1.4.2). The short term acute effects are perhaps easier to pin point; hour on hour increases in air pollution have been linked to respiratory problems, exacerbation of existing respiratory problems, and links to increases in cardiovascular problems (Schenker, 1993; Green, 1995; *cf.* Section 1.1.4.3). The following four sections deal with the health effects of gaseous and particulate pollutants, much of the information quoted here and detailed accounts of the respiratory system and medical studies of particulate may also be found in COMEAP (1995).

1.1.4.1 The Chronic effects of PM_{10} on asthma

Asthma is a chronic disease caused by aggravated and swollen airways that are predisposed to abrupt contraction; without medication attacks can be violent and life threatening (Cookson and Moffatt, 1997). In the last twenty years the number of people diagnosed with asthma has doubled to 1 in 7 in the UK, and 1 in 3 of all emergency paediatric visits in

the US are asthma related (Cookson and Moffatt, 1997). Whilst susceptibility to asthma is determined by our genetic make up, it is not likely that this has changed significantly within the last century. The current asthma epidemic must be therefore be due to environmental factors (Seaton *et al.*, 1994; Cookson and Moffat, 1997).

There is a tendency amongst laymen, scientist and medical professional alike to immediately look to increases and changes in air pollution as the likely cause of the asthma epidemic. Certainly it is clear that air pollution exacerbates asthma in people already diagnosed and its may even trigger some otherwise non-diagnosed asthma suffers to be found to be asthmatic (*cf.* Section 1.1.4.3). However air pollution does not seem to be the causal factor in the underlying massive asthma increase (Seaton *et al.*, 1994). Studies comparing the prevalence of asthma and allergies in Germany between the west and the east found that both were lower in the more polluted east than in the west (von Mutius *et al.*, 1992). In addition the same authors reported there was a lower chance of younger children suffering from asthma (von Mutius *et al.*, 1994). Respiratory infections are more common in the east than in the west and also the youngest children are most likely to catch numerous infections from their siblings (Cookson and Moffatt, 1997). Cookson and Moffatt, (1997) have used this evidence to hypothesise that childhood infection may actually protect against asthma. In support of this hypothesis investigators in Japan have shown a correlation between decrease in childhood tuberculosis and the increase in asthma. (Shirakawa *et al.*, 1997). It has also been postulated that a change in diet during the last twenty years has contributed to the asthma increase (Seaton *et al.*, 1994). This work noted that a decline in consumption of fresh fruit (26%), green vegetables (51%) and of potatoes (37%) has reduced the UK general population intake of anti-oxidants and vitamins, and postulates that this is a possible cause of the asthma epidemic. A multifactorial cause of increased asthma seems most likely

(Green, 1995), however house ventilation, dust mites and an increase in domestic pets have been suggested as insignificant causal factors (Shirakawa *et al.*, 1997).

1.1.4.2 PM_{10} and Chronic Effects

The problems associated with the study of the chronic effects of long term exposure to suspended particulate matter are numerous. Studies of this type have to account for the changes in socio-economic conditions, medical services, occupations, smoking habits, diet, and house moves of study subjects over their whole lifetimes (COMEAP, 1995). Thus although early studies have linked air pollution to long term health effects, they have often been discounted because of inadequately documented confounding factors (Pope *et al.*, 1995 a). The best evidence for long term health effects has been provided in two well designed recent studies. The Harvard six city study (Dockery *et al.*, 1993) looked at the effects of air pollution on mortality, whilst controlling for individual risk factors. Survival analysis was conducted on the data from a 14-16 year mortality follow up of 8111 adults in six US cities. After removal of smoking and other confounding factors, Dockery *et al.*, (1993) found that air pollution was positively associated with lung cancer and cardiopulmonary disease and mortality from these diseases was most strongly associated with fine particulate matter. A larger study was made by Pope *et al.* (1995 b), as cited in Pope *et al.* (1995 a), using data from over 500,000 adults and ambient air pollution levels in 151 US cities, during an eight year period. As with the six city study, fine particles were associated with mortality after the removal of confounding factors. Sulphate particles were found by Pope *et al.*, (1995 b) to be significantly associated with all cause, cardiopulmonary and lung cancer mortality. For a more complete review of these and other studies refer to COMEAP (1995) and Pope *et al.*, (1995 a)

The organic extract from urban aerosol has been shown to be mutagenic by numerous *in vitro* studies using Salmonella typhimurium assays (Siak *et al.*, 1985; van Houdt, J.J., 1990; Viras *et al.*, 1990; Bayona *et al.*, 1994; Hannigan *et al.*, 1994; Kado *et al.*, 1994). The mutagenic activity of urban aerosol organic extract in total and particle size fractionated samples was measured in Bologna, Italy (Pagano *et al.*, 1996). This study found that the mutagenic activity of urban aerosol organic extract is not associated to coarse particles (>2.5 μm), but to fine particles, and the mutagenicity increases as the size of particle decreases. The increased mutagenic activity with decreasing size is believed to be due to the increased absorbing surface of fine particles produced in combustion processes (Pagano *et al.*, 1996). In support of the work by Pagano *et al.* (1996), diesel engine combustion particles (DEP), which make up a large proportion of fine urban aerosol (QUARG 1993 b), have been shown to be potentially carcinogenic (Scheepers and Bos, 1992). DEP consist of a carbon core with polycyclic aromatic hydrocarbons (PAH) attached, which are known to be genotoxic (Scheepers and Bos, 1992). However studies comparing carbon black having no adsorbed PAH against DEP, found a similar rat lung tumour response for each (Nikula *et al.*, (1995) as cited in Driscoll *et al.*, (1996), which questions the role of polycyclic aromatic hydrocarbons in tumour formation. It has been proposed that low solubility carbon particles cause tumour formation as a generic response to their persistent inflammation of the lung (Driscoll *et al.*, 1996).

1.1.4.3 The Acute Health Effects of PM_{10}

The study of the acute health effects of PM_{10} examines the relationship between daily changes in mortality or morbidity and air pollution (COMEAP, 1995). It is generally accepted that acute effects arise through an exacerbation of existing ill-health on a short term basis, as opposed to the studies of chronic effects which look at the relationship between long term exposure to PM_{10} and the development of chronic disease (COMEAP,

1995). Numerous epidemiological studies have shown that periods of elevated PM$_{10}$ concentrations correspond to significant increases in adverse acute health effects (Dockery and Pope, 1994; Pope *et al.*, 1994; Schwartz, 1994; Thurston *et al.*, 1994; Pope *et al.*,1995 a; Katsouyanni, 1997). Increases occur in mortality, especially cardiovascular mortality, respiratory disease hospitalisation, exacerbation of asthma, incidence and duration of respiratory symptoms, decline in lung function and restricted activity as summarised in Table 1.1.

Health Endpoint	Percentage change in health indicator per each 10 μgm^{-3} increase in PM$_{10}$
Increases in daily mortality	
Total deaths	*1.0*
respiratory deaths	*3.4*
cardiovascular	*1.4*
Increase in hospital usage	
Admissions	*0.8*
Emergency department visits	*1.0*
Exacerbation of asthma	
Asthmatic attacks	*3.0*
Bronchodilator	*2.9*
Emergency department visits	*3.4*
Hospital admissions	*1.9*
Increase in respiratory systems reports	
Lower respiratory	*3.0*
Upper respiratory	*0.7*
Cough in children	*1.2*
Decrease in lung function	
forced expired volume	*0.15*
peak expiratory flow	*0.08*

Table 1.1 Combined effect estimates of daily mean particulate pollution based on the correlation of PM$_{10}$ with various health endpoints from a number of studies, after Dockery and Pope (1994)

It has been observed that there is no threshold level of PM$_{10}$ below which the association of mortality and morbidity, as given in Table 1.1, do not hold (Brown, 1994; Pope *et al.*, 1995 a). This means that an increase in PM$_{10}$ from 10 to 20 $\mu g\ m^{-3}$ causes the same percentage increase in health effects as the increase from 100 to 110 $\mu g\ m^{-3}$ of PM$_{10}$. This relationship

between PM_{10} and health effects has been generally attributed to the fact that the general population includes a 'sensitive' proportion made up of the old, young and infirm who are susceptible to environmental change (COMEAP, 1995; Seaton *et al.*, 1995).

The weight and consistency of epidemiological evidence has made it impossible or at least imprudent not to regard the association between PM_{10} and health effects as causal (COMEAP, 1995). This cautious approach to causality will be taken by many until a clear toxicological mechanism is elucidated (Schenker, 1993; COMEAP, 1995; Green, 1995). Because the mass increases of PM_{10} linked to health effects is very small *i.e.* $10\mu g\ m^{-3}$ for a 1% mortality increase, then traditional toxicological methods and explanations based on mass are not useful (Seaton *et al.*, 1995; BéruBé *et al.*, 1997). Whilst the mass of a $1\mu m$ particle is the same as one thousand $0.1\mu m$ particles, the increase in surface area is ten times as great. Therefore a small mass increase can account for a very large increase in the number and surface area of particles impacting in the lungs (COMEAP, 1995). The fine nature of particles means they can penetrate and irritate the alveolar regions of the lungs (COMEAP, 1995; Driscoll *et al.*, 1996). Desorption or deposition of any material on to the wall of the lungs may then occur, possibly PAH in the case of combustion particles (Scheepers and Bos, 1992; Pagano *et al.*, 1996). The large surface area of these fine particles also increases the likely hood of synergistic effect with other pollutants and gases entering the lungs (Schlesinger, 1995). Ozone has been especially implicated as having a much greater toxic effect when mixed with $PM_{2.5}$ than either ozone or $PM_{2.5}$ alone (Kleinman, 1995). These interactions complicate any attempt to study the toxicology of particles in order to make a human risk assessment (Schlesinger, 1995).

Seaton *et al.*, (1995) have hypothesised that acidic ultra fine particles ($0.02\mu m$), either themselves or the attached surface chemicals, provoke alveolar inflammation which causes

changes in blood coagulability and the release of mediators which exacerbate lung disease. This hypothesis indicates the number, size and shape of particles as the most important factors. It also accounts for the observed increase in cardiovascular mortality during PM_{10} peak periods (Table 1.1). In support of this theory a recent study has shown evidence of increased plasma viscosity during periods of high concentrations of sulphur dioxide (mean $200\mu g$ m^{-3}) and total suspended particles (mean $98\mu g$ m^{-3}), as measured in 3256 adults during a 13 day period in Ausberg, Germany (Peters *et al.*, 1997)

Evidence from particle toxicology on rats demonstrates the acute action of very fine particles (Warheit *et al.*, 1990; Ferin *et al.*, 1992; Driscoll *et al.*, 1996). Driscoll *et al.* (1996) exposed rats to chronic and sub chronic levels of carbon black for 6 hr/day, 5 days/week for up to 13 weeks. This work ascertained that at a sub chronic inhalation of $1.1mg$ m^{-3} of carbon black with a mass median aerodynamic diameter of 0.88 μm by rats had no adverse health effects, whereas similar earlier research using Teflon fume particles of $0.03\mu m$ in diameter at a much lower concentration of 200 μg m^{-3} showed acute pulmonary toxicity in rats (Warheit *et al.*, 1990). Ultrafine particles (~20nm) have been shown to access the pulmonary interstitium to a larger extent than fine particles (~250nm) where they are then retained for a longer period of time, and may enter the lymphatic system or rarely enter the bloodstream (Ferin *et al.*, 1992). The study by Ferin *et al.* (1992), also suggested that inflammation was affected by processes occurring during the exposure period and less by the lung burden or particle redistribution after exposure.

1.1.4.4 Urban Gaseous Pollutants: Physiological effects

Carbon monoxide is a major component of both petrol and diesel engine emissions (*cf.* Table 1.4). It is produced as a result of incomplete oxidation of the fuel, and is much more abundant in petrol exhaust than diesel (QUARG, 1993 a). When inhaled carbon monoxide

is favoured over oxygen in combination with the blood haemoglobin, thus leading to a deoxygenation of the blood (O'Neill, 1985) . The effect is lethal at high doses but at low doses brain function is impaired, those with coronary heart disease may suffer heart pain and there may be a risk to unborn children (Read, 1994). The reaction is reversible and after exposure to high carbon monoxide levels the body can return to normal levels in a matter of hours (O'Neill, 1985).

Most hydrocarbons and organic compounds are particulate bound, but in any case either particulate or gaseous, hydrocarbons represent a major group of toxins emitted to the air (QUARG, 1993 a). The mutagenic properties particulate bound organic compounds have been investigated by numerous studies (Siak *et al.*, 1985; van Houdt, J.J., 1990; Viras *et al.*, 1990; Hannigan *et al.*, 1994; Kado *et al.*, 1994; Bayona *et al.*, 1994; Pagano *et al.*, 1996), which are discussed in Section 1.1.4.2. Volatile organic compounds released in combustion range in toxicity, but effects range from irritation to nervous system damage (QUARG 1993a). Benzene has been identified as the volatile organic compound of most concern and in sufficient doses can cause leukaemia (Read *et al.*, 1994).

Oxides of Nitrogen (NOx) are also a significant anthropogenic pollutant (QUARG, 1993a; Read, 1994). Most of the NOx produced in combustion is in the form of NO, which is quickly oxidised in air to NO_2 (QUARG, 1993 a; O'Neill, 1985). The exposure to NO_2 causes constriction of the airways and an increase in airway resistance (QUARG, 1993 a). Cilia which coat the airway and beat in a regular pattern acting as a cleansing mechanism for the lungs are also disrupted by roadside concentrations of NO_2, so increasing the vulnerability to infection (Read, 1994). Elevated levels of NO_2 may trigger asthmatic attacks, and has also been associated with increased respiratory infection in children (Read,. 1994). High concentrations of NO_2 are associated with any combustion process and a

special area of concern is the high concentrations produced by domestic gas cooking appliances (QUARG, 1993 a; Read, 1994).

None of the pollutants present in air, act in isolation in the respiratory tract. Exposure to gas/particle mixtures can result in an additive synergistic toxic effect (Schlesinger, 1995). The interaction between gas and particles can be in terms of physical adsorption, chemical reactions on particle surfaces, or an alteration of the pulmonary environment which allows other components to have an effect. Thus the sum of the urban pollutant cocktail can be greater than its individual parts, of which the particle component is the most important in terms of mass transfer and toxicity (Cole, 1996).

1.1.5   Standards and Air Quality Criteria

The UK air quality strategy was published in March 1997, setting out the details of standards and objectives for air quality in the UK. Each of the standards and objectives is health based, set in the context of current research by either the UK Expert Panel on Air Quality Standards or by the World Health Organisation. The present air quality standards are summarised in Table 1.2.

Pollutant	Standard	Objective - to be achieved by 2005
Benzene	5 ppb (running annual mean)	5 ppb
1,3-Butadiene	1ppb (running annual mean)	1 ppb
Carbon monoxide	10 ppm (running 8 hour mean)	10 ppm
Lead	0.5 $\mu g \, m^{-3}$ (annual mean)	0.5 $\mu g \, m^{-3}$
Nitrogen Dioxide	150 ppb (1 hour mean) 21 ppb (annual mean)	150 ppb (hourly mean) 21 ppb (annual mean)
Ozone	50 ppb (running 8 - hour mean)	50 ppb (97th percentile)
PM$_{10}$	50 $\mu g \, m^{-3}$ (running 24 - hour mean)	50 $\mu g \, m^{-3}$ (99th percentile)
Sulphur Dioxide	100 ppb (15 minute mean)	100 ppb (99.9[th] percentile)

ppm = parts per million; ppb = parts per billion

Table 1.2 The Standards and Objectives of the UK National Air Quality Strategy (NetCen, 1998)

The greatest exceedance of these standards in the UK occurs with respect to the PM_{10} measurements. The number of exceedences of PM_{10} standards for just 6 of the 43 UK sites are illustrated in Table 1.3. In 1996 the number of exceedances of the PM_{10} standard ranges from maximum of 134 exceedance days at Belfast to a minimum of 11 exceedances days measured in Edinburgh centre. To meet the set objective for 2005, the number of exceedances has to be 4 days or less (99th percentile). Clearly not even the cleanest sites monitored in the UK meet these objectives at present and most sites have about 5-10 times the number of exceedances required.

Site	1996 (no. of days)	1995 (no. of days)	1994 (no. of days)
Belfast Centre	134	40	32
Birmingham Centre	36	24	23
Bristol Centre	37	27	31
Swansea Centre	24	41	---
Leicester Centre	21	8	18
Edinburgh Centre	11	18	3

Table 1.3 Selected sites and the number of exceedances of PM_{10} recommendations

(Table 1.2)

Other UK standards and objectives are generally, easily met. No exceedances of the standards for benzene or 1,3-butadiene were recorded at any site from 1994-1996 (NetCen, 1998). For nitrogen dioxide the most exceedances are recorded in London, Cromwell Road, at only 9 hourly exceedances of 150ppb in 1995 (NetCen, 1998). Significant carbon monoxide exceedances were not measured at any sites during 1996, and a maximum of 13 hourly exceedances were recorded in Belfast during 1995 (NetCen, 1998). The exceedances of sulphur dioxide represent the only large scale exceedances of the air quality standards along with the PM_{10} exceedances. Belfast exhibits by far the worst record with 666 exceedances in Belfast east (NetCen, 1998). It is the case that the number of

exceedances due to sulphur dioxide occur mostly during the winter months when domestic fires are in use. In Belfast coal fires are still widely used in the absence of natural gas (QUARG, 1996).

It is apparent therefore that PM_{10} represents the pollutant of most immediate concern in terms of its impact on air quality. Whilst the exceedances concentrate on PM_{10}, the research focus is shifting to fine particles below 2.5 microns (QUARG, 1996). Current research has indicated that it may be the number, size and shape of fine and ultra fine airborne particles which is of most concern as discussed previously (Seaton *et al.*, 1995; QUARG, 1996; *cf.* Sections 1.1.2 and 1.1.4).

1.2   Particle Fundamentals

1.2.1   Natural formation of Primary particles

The action of the wind blowing over dry and loose soils leads to the suspension of particles in the air. This commonly happens over sandy and sparsely vegetated areas such as deserts. In the northern hemisphere the Sahara may contribute to as much as half of the total dust burden of this source in the air. The atmospheric burden of dust from this source in the northern hemisphere, excluding the Sahara, is 3 million tonnes. The size range of these mechanically generated aerosols is large, typically 1-10 microns (Murphy, 1984). The large size of these particles relative to the majority of airborne particles, means that deposition occurs quickly and their residence time in the atmosphere is low. Dust may then be resuspended again under dry, windy conditions (QUARG, 1996; Twomey, 1977; Murphy, 1984).

As the UK is surrounded by sea the contribution of sea salt to the atmospheric aerosol load in the UK is significant (QUARG, 1996). This is especially true in coastal cities such as

Plymouth. Wind and wave action causes spray which, as the water evaporates, leaves sea salt suspended in the atmosphere. The crystalline nature of salt and the mechanical nature of the spray formation means that the aerosol tends toward the coarse size of particles from 0.5-10 μm (Murphy, 1984). The salt burden in the atmosphere is increased in the winter when salt is commonly added to the roads to prevent ice formation (Twomey, 1977; Murphy, 1984; QUARG, 1996).

Biological particles such as spores, pollens, viruses and fibres, have a range of sizes between 0.01-10 microns in the air (Murphy, 1984). Although governed by the same physical properties as other non biological particles, these are generally of most concern in terms of their allergenic properties and biological activity (COMEAP, 1996; QUARG, 1996).

1.2.2 Anthropogenic Sources of Primary Airborne Aerosol

High temperature (>100°C) combustion and smelting are the largest primary anthropogenic contributors of aerosol material to the air, reported at 73% in 1993 (COMEAP, 1995). Combustion processes vary greatly from source to source. Diesel combustion has been identified as the single most significant contributor of fine particulate material to the urban air, at 20% in 1993 (COMEAP, 1995; BéruBé et al., 1997). During diesel combustion a fine fuel spray is introduced to the combustion chamber. The fuel spray is then incompletely burnt to leave a fine aerosol of pyrolysed and unburnt fuel, which is emitted from the exhaust (Barnard and Bradley, 1985). During petrol combustion, carbon atoms join together to form carbon particles within the combustion zone. Coal combustion leaves a residue of fly ash formed from carbon and non combustible minerals contained within the coal (QUARG, 1996). Particles produced in combustion processes are very fine in size (Murphy, 1984). They may have a mass mode of a few hundred nanometers and a number mode of a few tens of nanometer (Carpenter and Johnson, 1979; Medalia and Rivin, 1982).

This ultra-fine size means that the aerosol produced has a large surface area, and a very deep penetration in to the lungs (Twomey, 1977; Murphy, 1984). This makes combustion sources of particles of most concern in terms of public health (Seaton *et al.*, 1995).

Metallurgical processes and refuse burning produce fine metallic rich vapour which may be emitted to the air (QUARG, 1996). The high metallic content of these particles makes them of special concern in terms of their toxicity and despite best efforts fumes may still be emitted to the air (QUARG, 1996).

In the South West UK, the china clay industry is a significant contributor of aerosol to the air through its mining operations (ECC International, 1986). Dust is generated from both the exposed mine and the china clay wastes (Department of the Environment, 1996). China clay is also a major ingredient of cement which is manufactured in Plymouth, UK. Dusts can be blown from the site or generated during the cement manufacturing process (ECC International, 1986). These sources are of significant concern for workers health and dust levels are carefully monitored under government Health and Safety at Work regulations (Health and Safety Executive, 1998). Generally, the dusts produced from mining processes are in the order of a few microns to a few millimetres in size and are therefore large enough to be of minor concern in terms of their respiratory penetration (Murphy, 1984). However cement manufacture includes a high temperature process to chemically form the cement. It is during this process where there is perhaps most concern, as smaller particles (*ca.* 1 μm) may be produced, and these may be expelled in the exhaust from the cement ovens.

Other anthropogenic sources of wind blown dusts in urban areas include dust from tyre wear, brake shoes, road markings, and in fact any part of the exposed urban environment which tends to degrade (QUARG, 1993 a). Although these sources may contribute

significantly to the total mass of aerosol, especially under strong wind conditions, the low temperature mechanical process under which they form leads to a large aerodynamic size and less significant respiratory penetration (Twomey, 1977).

1.2.2.1 Combustion Engines

Incomplete combustion of oil-based fuels results in the emission of pollutants such as nitrogen oxides, hydrocarbons, carbon monoxide, particulate matter, sulphur dioxide, carbon dioxide and organic compounds, e.g. aldehydes, benzene and polycyclic aromatic hydrocarbons (Barnard and Bradley, 1985; QUARG, 1993a). Complete combustion does not occur in the internal combustion engine as the reaction is kinetically limited, in other words the time in the combustion chamber is less than the time it takes for combustion reaction to be complete (Barnard and Bradley, 1985).

Petrol and diesel engines differ in both their ignition and combustion processes. In a petrol engine the air and fuel is premixed. Ignition occurs through an electric spark hence the term spark ignition to denote this type of engine. Combustion then proceeds in a flame front across the chamber. Fuel will only burn when the air to fuel ratio (mass/mass) lies between 10 and 20 to 1 (Barnard and Bradley, 1985). In a petrol engine the carburettor provides this air to fuel ratio, and in this sense petrol engines are quantity governed i.e. an approximately constant air/fuel is maintained by the carburettor. The torque of the engine (the fundamental output of the internal combustion engine) is limited by the amount of air/fuel mix entering the combustion chamber. (Rogers and Mayhew, 1992)

In a diesel engine cylinder the compression stroke raises the air temperature. When the piston reaches the minimum volume position the air temperature is sufficiently high that when liquid fuel is sprayed into the combustion chamber in droplets the fuel self ignites.

The term compression engine (CI) is therefore commonly used to describe diesel combustion engines. The ignition is only achieved if air compression is between 20 and 22 to 1. In a spark ignition engine if compression exceeds 9 then the air fuel mix explodes prematurely. The thermal efficiency of an engine is governed by the compression ratio (Barnard and Bradley, 1985) and thus the high compression ratio in a diesel engine leads to a better fuel economy. Diesel engines are in this sense quality governed, *i.e.* the air/fuel ratio varies for different speeds and load conditions, which determines the torque.

There are two forms of diesel engine combustion, indirect injection (I.D.I.), direct injection (D.I.). In relatively small vehicles such as cars and light vans indirect injection (I.D.I.) is used (Barnard and Bradley, 1985). In I.D.I. combustion starts in a pre-chamber which contains a proportion of the total air charge. The fuel is injected into this chamber at a compression ratio above 20:1. The mixing of the fuel and air is aided by the turbulence produced in the combustion process in this fuel rich mix (Haddad and Watson, 1984). The high pressure developed by the combustion process in the pre chamber projects the unburnt fuel together with the early combustion products into the main chamber at high velocity causing rapid air mixing in the space over the piston. Larger vehicles such as buses and trucks tend to use direct injection. Mixing is dependent on the spray characteristic which introduces the fuel to the chamber (Murayama *et al.*, 1986). The spray characteristic of the injector must be arranged to produce a rapid air and fuel mixing. The air motion in the chamber helps to do this (Rao *et al.*, 1993). Further details of the internal combustion processes may be found in Barnard and Bradley (1985), Haddad and Watson (1984) and Pemberton (1996).

Table 1.4 compares the emissions from different engine types. It is apparent that emissions from diesel engines are low in carbon monoxide and carbon dioxide but high in nitrogen

oxides and particulate matter when compared to petrol engines that have a three-way catalyst. The higher emissions of sulphur dioxide from diesel engines can be attributed to the presence of sulphur in diesel fuel, whereas petrol does not contain sulphur. However greater fuel efficiency and lower maintenance make diesel vehicles more economical than petrol and therefore an attractive option for the private owner and for industry (Brown, 1994). It is predicted that an increased market penetration of diesel cars at the expense of three-way catalyst petrol cars will on balance have a negative effect on urban air quality (QUARG, 1993 b; cf. Section 1.1.3)

Pollutant	Petrol without catalyst	Petrol with three way catalyst	Diesel without catalyst	Diesel with oxidation catalyst
Nitrogen oxides	****	*	**	***
Hydrocarbons	****	**	***	*
Carbon monoxide	****	***	**	*
Particulate matter	**	*	****	***
Aldehydes	****	**	***	*
Benzene	****	***	**	*
1, 3-Butadiene	****	**	***	*
PAH	***	*	****	**
Sulphur dioxide	*	*	****	****
Carbon dioxide	***	****	*	**

Key: * ~ lowest emissions **/*** ~ intermediate **** ~ highest emissions

Table 1.4 A Relative Comparison of Emissions From Petrol Cars with Three Way Catalysts and Diesel cars. (QUARG, 1993 b)

Diesel engine particles (DEP) are of major importance in the route of organic (PAH, N-PAH) and inorganic toxins (*i.e.* metals) deep into the lungs (QUARG 1993 a, b). The organic fraction of DEP are of special concern because of the possible long term carcinogenic effects of polycyclic aromatic compounds (QUARG 1993 b; cf. Section 1.1.4.2). As previously discussed (cf. Section 1.1.2) studies in the USA have indicated that DEP may contribute to much as a quarter of PM_{10} by mass (Kao and Friedlander, 1995) or over 30% of particles less than 2 microns by number (Katrinak *et al.*, 1995).

1.2.2.2 The Mechanism of Diesel Engine Soot Formation

A three phase formation of soot has been proposed (Scheepers and Bosh, 1992; Barnard and Bradley, 1985). The first stage consists of a simultaneous cracking, pyrolysis, dehydrogenation and pyrosynthesis of compounds at a temperature of 2000 - 2300°C, to form naphthalene radicals which combine together. Figure 1.1 illustrates the formation and growth of a naphthyl radical from C_2 species as proposed by Frenklach *et al.*, (1987, 1990). The growth continues until a critical size of carbonaceous nuclei is reached at a size of 0.001 - 0.01 μm. Agglomeration of theses nuclei occurs to form spherical primary soot particles, also know as carbon ceno-spheres (Medelia and Rivin, 1988). In the third phase chains of primary soot form through aggregation (*cf.* Section 1.5.2).

1.2.2.3 The Mechanisms of Spark Ignition Engine Soot Formation

The relative masses of particulate matter produced from different road vehicles are compared in Table 1.5. It is evident that the mass of particulate matter from spark ignition (gasoline) engines is much lower than from diesel engines. In 1995 the source contribution of PM_{10} to the UK atmosphere was put at 46.3×10^3 tonnes from diesels and 10.9×10^3 tonnes for petrol sources (QUARG, 1996). This was while the UK vehicle fleet comprised only between 10-20% of diesel vehicles in the same year (DETR, 1998). Furthermore the contribution of petrol engine particles to PM_{10} is predicted to fall, as unleaded fuel becomes more and more widely used.

The formation of particulate matter in spark ignition combustion is less well studied than for diesel soot formation. A similar process is postulated for gasoline as for diesel engines (Barnard and Bradley, 1985; QUARG, 1996). However gasoline fuel is much lighter than

diesel fuel. Therefore in combustion there is much less tendency to form the intermediates proposed for soot formation (Figure 1.1) and thus the soot output is much lower.

Vehicle Type	Amount of Particles Produced (g l^{-1})
Light Duty Diesel Vehicles	4-7
Heavy Duty Diesel Vehicles	7-14
Petrol Vehicles	0.65

Table 1.5 Relative mass of particulate produced per litre of fuel for different vehicle types.(QUARG, 1993 b)

In leaded fuels, the formation of lead oxides and other lead compounds is a major contributor to the particulate output. Lead compounds may either be produced as discrete particles or as an integral part of carbonaceous agglomerate (Barnard and Bradley, 1985). There is some evidence for the action of lead compounds in the seed for carbonaceous nuclei agglomeration on the surface (Steiner *et al.*, 1992).

After the formation of primary soot particles, either including lead compounds or not, aggregation of soot to form chain like structures, again occurs, which may follow a number of models (*cf.* Section 1.5.2).
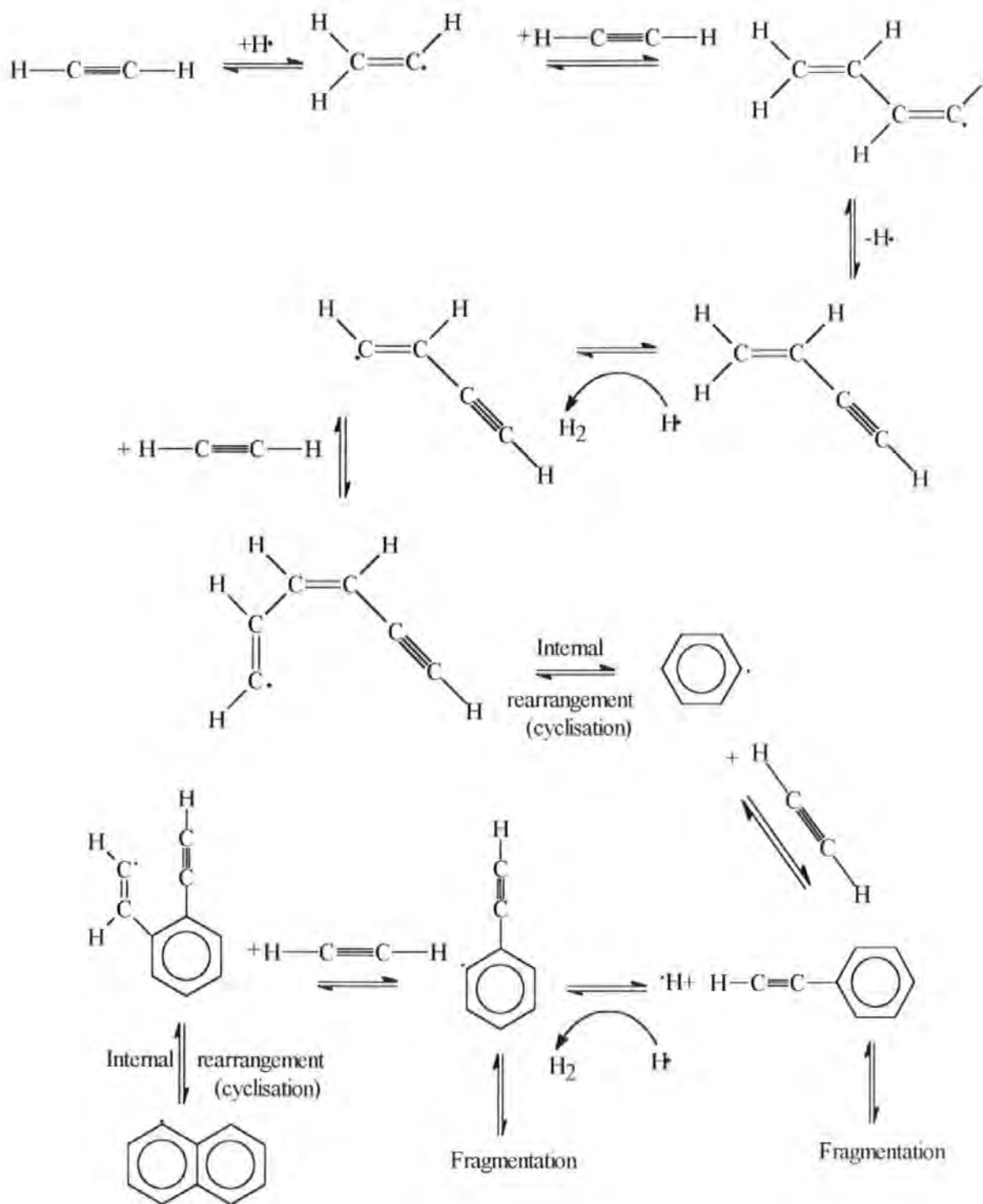
Figure 1.1 The formation and growth of a naphthyl radical from C_2 species as proposed by Frenklach et al. (1987, 1990). The formation of PAH from the naphthyl radical follows the same route as that from phenyl radical to naphthyl radical

1.2.3 Anthropogenic Sources of Secondary particles

Particles that are produced from within the atmosphere are termed secondary particles. Secondary particles are not produced directly from an anthropogenic process, but anthropogenic processes contribute indirectly to the formation of particles within the atmosphere (Twomey, 1977).

Sulphates make up a large proportion of secondary particles and up to 20% of the UK particulate matter by mass (QUARG, 1996). Sulphates are formed when sulphur dioxide produced during combustion, oxidises, in the atmosphere. In the (UK) atmosphere a fine sulphuric acid mix may then form and this is readily neutralised by ammonium, emitted widely from sewage decomposition (QUARG, 1993), to produce ammonium bisulphate and then ammonium sulphate (QUARG, 1996).

NO_2 is formed in combustion and by the rapid oxidation of NO, also from combustion sources (O'Neill, 1985). Further oxidation produces nitric acid in the air and this may react with ammonia to produce ammonium nitrate, in the particulate phase (QUARG, 1993). HCl gas emitted from combustion processes, especially coal, may also react with ammonia to produce ammonium chloride particles (COMEAP, 1995; QUARG, 1996).

Hydrocarbons in the atmosphere can react with each other and undergo reactions to form involatile and semi-volatile particles (QUARG, 1996). Asphalt, from road construction, is an example of a source of hydrocarbons to the atmosphere and vapour from asphalt rapidly cools and condenses on any pre-existing particles (QUARG, 1996). Such process are important in terms of the high mass and toxicity of such hydrocarbons (QUARG, 1993 a)

Further details of the formation and contribution of secondary particles to urban aerosol may be found in QUARG, 1993 a and QUARG, 1996.

1.2.4   The Physico-chemical properties of particles

1.2.4.1 Fundamental Physical Properties

The fundamental physical and chemical properties of particles govern their agglomeration, their residence time in the atmosphere, their capture by filters, and their penetration and deposition in the respiratory system. Understanding of these properties is therefore vital for any study of fine particles (QUARG, 1996).

Brownian motion is the result of the impaction and transfer of kinetic energy from molecules of air to particles (Twomey, 1977). The motion induced in the particle is random, and in fine particles (<0.1μm) this random walk plays a significant role in the movement and impaction of particles to form agglomerates (Murphy, 1984). During the agglomeration process particles tend to adhere and not break up. This is a result of weak Van der Waals forces between particles (Twomey, 1977; Destephen and Choi, 1996). These inter-molecular forces dominate in holding the particle together, until the particle becomes big enough such that other stress and strain forces, induced by the movement of the particle through the air become of greater significance. Brownian motion is the most significant factor in the deposition of fine particles in the alveolar regions of the lungs (COMEAP, 1995)

Sedimentation of particles is the settling of particles due to gravity. The amount and size of particles which are removed from the atmosphere by sedimentation is dependent upon atmospheric stability (Twomey, 1977). The effect of Brownian motion on small particles (<

2 μm) is more significant than sedimentation processes and so particles of this size tend to stay suspended in the air for long periods of time (QUARG, 1996).

Impaction occurs when the air flow carrying particles must deviate around an object, such as a tree or at a bronchial junction in the lungs (COMEAP, 1995). Particles with sufficient momentum will then be unable to follow the air flow and will impact upon the surface in question (COMEAP, 1995). At the point of impaction the particle will either bounce or adhere to the surface (QUARG, 1996). The chance of adherence is governed by the surface itself and the particle (QUARG 1996). The forces involved in adhesion of particles to surfaces or other particles are not well understood, but the concepts of Van der Waals are widely used; these concepts are further discussed in Destephen and Choi (1996), Twomey (1977) and Elzo et al. (1996). Sticky surfaces increase the efficiency of particle adherence after impaction. For instance in the lungs a mucus carpet is used to capture particles (COMEAP, 1995). For this reason, sticky surfaces are sometimes used to increase the efficiency of impaction samplers, notably the Burkard spore trap uses a gelatine gel to trap particles (Burkard Ltd., Bucks.). Interception of a particle occurs when the air flow takes the particle very close to a surface and is then intercepted by the surface. The process of interception becomes significant over rough or sticky surfaces (QUARG, 1996).

Fine particles can have a major role in the scattering of solar radiation in the atmosphere (QUARG, 1996). In fact there are theories proposing a world wide 'nuclear winter' if such a war was to occur, based solely on the amount of debris that would be ejected into the atmosphere and by the effect it would have on the amount of solar radiation reaching the biosphere (Kaye, 1993). Fine agglomerate particles produced from combustion engines can have a significant effect on the scattering of light in the urban atmosphere because of their very convoluted structure (Kaye, 1993).

The interaction of a particle with water vapour is governed by the hydrophilic or hydrophobic nature of the substance in question. Hydroscopic substances such as sea salt and ammonium nitrate will take up water at moderate and high relative humidities (QUARG, 1996). Such an interaction may greatly affect the particle morphology and also changes the light scattering and deposition properties of the particle (QUARG, 1996). Repeated chamber cloud processing, consisting of water condensation and evaporation, upon particles from butane combustion was performed by Colbeck *et al.* (1990). This work showed that there was a significant compaction of particle structures consisting of greater than 10^3 primary spherules. In a similar study by Huang *et al.* (1994), cloud processing was performed on diesel engine particles, whilst in an environmental scanning electron microscope. This process caused the collapse of structural morphology after a number of hours and was most significant in the case of diesel engine particles generated from low sulphur fuel. Such ageing of particles affects both the aerodynamic diameter and the surface area of a particle.

1.2.4.2 Particle size

The size of particle is the overriding influence on its physical activity (QUARG, 1996). In turn the size of a particle is governed by the formation process (*cf.* Sections 1.2.1, 1.2.2 and 1.2.3). Atmospheric particles may be usefully classified in to three major groups (QUARG, 1993 a; QUARG, 1996):

(i)   Nucleation mode

Commonly particles less than 0.2 μm have been attributed to this mode (QUARG, 1993 a ; COMEAPS, 1995). However particles within this mode are small, less than 100 nm in diameter and typically 1-10nm (Twomey, 1977; Murphy, 1984; QUARG, 1996). They are

short lived in the atmosphere with a large Brownian motion driving diffusion limited aggregation of the particle towards the accumulation mode (Twomey, 1977; Katrinak *et al.*, 1993). There may be many atmospheric particles in the nucleation mode, in terms of number (*ca.* $10^6 - 10^9$), yet due to their size they may not have a significant mass (QUARG, 1996). The smallest particles consist of only a few molecules, formed during combustion and evaporative processes, by condensation and nucleation of molecules of a substance. Gas to particle conversions of condensation and nucleation occur when the kinetic energy against the condensation of molecules is overcome by the bonding energy between molecules (Murphy, 1984). Nucleation and condensation theory are further discussed in detail in Twomey (1977).

(ii)   Accumulation mode

Particles in the accumulation mode are between about 0.05 µm and 2 µm in diameter (QUARG, 1996). Particles accumulate in this range *via* the agglomeration of particles from the nucleation mode (Murphy, 1984). Within this mode particles are little affected by Brownian motion and gravitational settling (Twomey, 1977; *cf.* Section 1.2.4.1) and thus have a high atmospheric residence time due to inefficient atmospheric removal (QUARG, 1996). The size distribution and morphology of accumulation mode particles may be greatly affected by cloud processing (Colbeck *et al.*, 1990; Huang *et al.*, 1994; QUARG, 1996). Chemical reaction and evaporation results in a particles size increase and compositional changes in aerosol (*cf.* Section 1.2.4.1). Agglomeration opportunities increase within clouds because of the high aerosol density and thus cloud processes generally increase particle size (QUARG, 1996).

(iii)   Coarse mode

Particles in this range are between *ca.* 2 μm and 100 μm in diameter and generally consist of mechanically generated wind blown dusts (Murphy, 1984). Their large size means they have a high settling velocity and consequently a low residence time in the atmosphere (QUARG, 1996). The large particle size means that they may contribute a significant mass of aerosol whilst being low in number (QUARG, 1996). Comminution of materials rarely generates particles smaller than 5 μm, but anthropogenic processes contribute to this process through, for example, mining processes and road dusts (Twomey, 1977; Murphy, 1984). Fly ash is a special comminution aerosol formed where coal is crushed to form a powder which is burnt, or where oil spray is used in combustion (QUARG, 1996).

1.3   Measurement of Coarse, Fine and Ultrafine particles

1.3.1   Mass Measurements of Airborne Particles

Hourly mass measurements of PM_{10} at 43 sites around the country are routinely made as part of the Enhanced Urban Network of air quality monitoring (NetCen, 1998). Measurements are made using Tapered Element Oscillating Microbalances (TEOM), which have proved reliable for this purpose although there is some doubt concerning the loss of volatile material (QUARG, 1996). The mass *vs.* size distribution shows that the urban aerosol has a bi-modal distribution, with modes at about 10 μm and 0.5 μm (QUARG, 1996). The mass of one 1μm particle is equal to that of one thousand 0.1μm particles (COMEAP, 1995). As health evidence indicates that it is the numbers of particles impacting in the lungs that may be of most importance then mass measurements alone may be misleading as to the true potential health impact of an aerosol (Seaton *et al.*, 1995).

1.3.2. Counting Airborne Particles

Interest in the numbers of particles in the urban atmosphere has led to the development of methods of particle counting, *e.g* laser particle counting, condensation particle counters, and light and electron microscopy techniques (Murphy, 1984). Measurements of ambient urban air typically show that the number *vs.* size distribution is dominated by the fine and ultrafine particles (QUARG, 1996). Particle counting studies have shown that there may be upto 100000 particles per ml of air, having a mass concentration of only 150 μg m^{-3} air (Seaton *et al.*, 1995; QUARG, 1996)

1.3.3 Size Distribution Measurements of Airborne Particles

The size of an airborne particle is fundamental to its toxicity, consequently size distribution measurements of aerosol are of paramount importance (Twomey, 1977). Measurement of the size distributions of aerosols may be achieved by a number of methods. Traditionally, impactors have separated the aerosol by aerodynamic diameters. Separated portions of the aerosol could then be weighed (Murphy, 1984). More recently scanning mobility particle sizers attached to condensation particle counters have allowed the size distribution of particles by number to be determined (COMEAPS, 1995).

1.3.4 Measuring Particle Morphology

Measurements of asbestos morphology are made using scanning or transmission electron microscopy (Basu *et al.*, 1986; Spurny, 1994). However there has been little work relating to the morphology of urban aerosol (*cf.* Section 1.5.3). Studies using electron microscopy have described 'chain-like' aggregates but such descriptions are subjective and open to misinterpretation (BéruBé *et al.*, 1997; QUARG, 1996). In contrast a study by Katrinak *et al.*, (1993), in Phoenix, AZ., USA, used to concepts of fractal geometry to quantitatively and objectively describe the morphology of urban aerosol (*cf.* Section 1.5.3). Related

disciplines have also made use of aerosol measurement techniques (*cf.* Section 1.5) and there has been work to identify aerosol particles according to their morphology albeit for only relatively large particles (>1µm) (Xie *et al.*, 1994 a, b; Kim and Hopke, 1988; Kindratenko *et al.*, 1994; Hopke and Song, 1997; *cf.* Section 1.5). There has also been no work to relate quantitative measurements of morphology to particle toxicity, although there is evidence to support assumptions about different morphologies and their toxic nature (COMEAP, 1995).

1.4 Particle analysis using microscopy

1.4.1 Light microscopy

Light microscopy has been used extensively in both the analysis of biological aerosols such as pollens (Hirst, 1952) and the measurement of asbestos fibres in air (Basu *et al.*, 1986; Spurny *et al.*, 1994). In general the optical microscope may be used for the identification of particles above 0.8 µm in size (Murphy, 1984). The minimum size is imposed because of the size of the wavelength (0.55 µm for green light) which is a limitation on the resolution of a microscope.

A novel study has recently been conducted by Battarbee *et al.*, (1997) using optical microscopy for the analysis of urban aerosol. These authors used a Burkard volumetric spore trap (Burkard Ltd., Bucks.) to collect a continuous trace of particles. From this trace an optical count of airborne particles was made, and compared with other measurement techniques. The advantage of this collection method is the continuous and permanent nature of the particle trace, allowing retrospective analysis of areas of interest (Battarbee *et al.*, 1997; *cf.* Chapter 2). Optical microscopy has been used, labour intensively both for the counting and identification of particle types (Murphy, 1984; Glikson *et al.*, 1995; Battarbee *et al.*, 1997). In these studies the microscope operator classifies the particle type, usually as

either biological or non-biological. This is useful for identifying the contribution of allergen inducing particles, such as spores and pollens. However the non biological urban aerosol is not adequately described by the use of generic terms such as 'soot'(Glikson *et al.*, 1995), and objective measurements are of greater use in the description of this fraction (Katrinak *et al.*, 1993; Kindratenko *et al.*, 1994; *cf.* Section 1.3.4).

1.4.2   Electron microscopy

1.4.2.1 Urban Aerosol Characterisation using Scanning Electron Microscopy (SEM)

Computer controlled scanning electron microscopy (CCSEM) has become a method almost synonymous with individual particle analysis (Van Borm and Adams, 1988; Saucy *et al.*, 1991; Katrinak *et al.*, 1995; Xie *et al.*, 1994a,b; Kim *et al.*, 1988; Kim and Hopke, 1988; Hamilton *et al.*, 1994; Hopke and Song, 1997). It allows the continuous automated analysis of individual particles as found and detected by the computer. Typically studies usually have a lower limit of 0.4 - 0.5 µm (Van Borm and Adams, 1988; Saucy *et al.*, 1991), dependent on the aerosol of most interest to the study. The most detailed study using CCSEM with an electron microprobe and energy dispersive X-ray spectrometer, by Katrinak *et al.*, (1995), reported particle counts of 1-10 x 10^6 m^{-3} in Phoenix, Az., USA. These authors used a relatively high resolution to 0.1 µm diameter sized particles. Of the 11209 fine particles analysed in Phoenix, 32% were reported as zero - count particles, most likely to be vehicle generated carbonaceous particles, 32% mineral rich particles, 12.1% metal rich particles, 7.4% sulphur rich particles, 0.2 % salt particles. However this work accepts that most vehicle generated carbonaceous particles will be found below the size resolution limit of study.

1.4.2.2 Urban Aerosol Characterisation using Transmission Electron Microscopy

The obvious limitations of CCSEM are those of resolution. In most studies the smallest particles measured were 0.4 μm in diameter, which is a major limitation when looking at urban aerosol. Since more than half of the number of urban PM_{10} are found below 0.1 μm (QUARG, 1996). Using transmission electron microscopy (TEM) the ultra fine particles below 0.1 μm may be resolved (Waller, 1967; Carpenter and Johnson, 1979; Medalia and Rivin, 1982; Katrinak *et al.*, 1993; BéruBé *et al.*, 1997). However few studies have used TEM, despite the importance of this fraction to atmospheric integrity and public health, probably as a result of the cost or time for analysis. Carpenter and Johnson, (1979) used TEM to analyse the physical characteristics of diesel particulate matter, and found that individual carbon spheres had a mean size of 47.9 nm and 43.6 nm in diluted and undiluted exhaust respectively. Measurements made of London aerosol by Waller, (1967) using TEM showed concentrations of particles of less than 5 μm in the order of 10^4 cm^{-1} with an median number particle size between 90 and 130 nm.

1.4.2.3 TEM sampling and Preparation

Past studies have used the Jaffe washing method of sample collection to accurately assess the numbers of particles in urban air (Spurney, 1994; *cf.* Figure 3.2, Chapter 3). In this method aerosol is collected on a 0.1 μm nuclepore filter (NPF), coated with a carbon film, and the NPF is then dissolved leaving the carbon film and particles intact (Robards and Wilson, 1993). This preparatory stage subjects the collected aerosol to a vacuum coating process and to chloroform, which may both cause particle collapse, and the open structure of urban aerosol may be obscured (Robards and Wilson 1993). To reduce the likelihood of this problem, PM_{10} may be directly collected onto TEM grids for immediate analysis. Direct particle TEM collection has been previously used for the sampling of welding fumes of mostly greater than 1 μm in aerodynamic diameter (Farrants *et al.*, 1988; Karlsen *et al.*,

1992). In those studies the momentum of the large, heavy metallic particles caused them to impact on a non-porous carbon film suspended over a copper 300 mesh TEM grid (Farrants *et al.*, 1988). Other direct sampling has used a thermophoretic precipitator to deposit <100nm particles on to carbon films (Maynard, 1995).

The bulk of the number distribution of urban aerosol resides below 100 nm and is largley carbonaceous (QUARG, 1996). This presents a difficult aerosol mix to sample directly because of the widely varying physical behaviour of particles of different sizes (Twomey, 1977; *cf.* Section 1.2.4). The thermophoretic method fulfils the sampling of ultra fine aerosol (< 100nm) directly but lacks portability because of its power needs (Maynard, 1995). There is also some question about the structural changes which may occur in particles in high temperature environments (Maynard, 1995). However those particles below 1 μm are far less likely to impact due to their momentum as in the direct sampling methods (Farrants *et al.*, 1988; Karlsen *et al.*, 1992). The development of a fine aerosol sampling technique for TEM has thus formed part of this research (*cf.* Section 1.6)

1.4.3 Image analysis

Morphological analysis of any object has the inherent difficulty in describing an object in ways which can then be used and repeated in a uniform way (Kaye, 1993). Past studies have used qualitative expressions to describe the morphology of vehicle generated particles (Medalia and Rivin, 1982; BéruBé *et al.* 1997; Waller, 1967). Medalia and Rivin, (1982) described particulate carbon as falling into four groups; aciniform carbon, carboniferous microgel, carbon ceno-spheres, and coke and char fragments. A study of the atmosphere of London by Waller (1967) described smoke aggregates, crystals and irregular particles. These measures are useful in conveying the quality of the aerosol but are difficult to use in a repeatable manner and confusion of terms can easily arise between different workers. It is

possible to measure various parameters of an aerosol from electron micrographs by hand, but with the advent of powerful image analysis instruments more quantitative measurements of particle morphology have become possible (Kaye, 1993). Concurrent to the increase in computing power has been the development in the use fractal geometry in fine-particle characterisation (Schwarz and Exner, 1980).

1.5 Particles and Fractal Geometry

1.5.1 Fractal Analysis

The concepts of fractal analysis have been applied from coastlines to the fluctuations of the stock markets (Kaye, 1993). The first successful use of applied fractal geometry was by Medaila, (1975) who described the profiles of carbon black by plotting the perimeter estimate *vs.* the resolution of inspection. At an increased resolution of inspection greater detail in the object is measured and thus the perimeter estimate increases. The gradient of the perimeter *vs.* resolution of inspection, on a logarithmic chart, allows for the calculation of the fractal dimension of the object (*cf.* Section 3.6). General concepts of fractals and applied fractal geometry are thoroughly dealt with by Kaye (1993).

The measurement of fractal dimensions are easily applied using an image analyser (Schwarz and Exner, 1980; Kaye *et al.*, 1993), and much work has been done to develop various techniques of measuring fractal dimension (Kaye, 1991). Multiple fractal dimensions have been used to quantify airborne particle shapes by Xie *et al.* (1994 a). This study suggested that more than one fractal dimension was needed to characterise particle shape, and it was successful in characterising three typical aerosol shapes, spherical, blade and aggregate. Characterisation of agglomerated aerosols using image analysis of TEM pictures has also been done (Kruis, 1994); in this work aspects of analysing whole agglomerates and the individual primary spheres were discussed which are important for powder and particle

engineering in manufacturing processes. Combinations of chemical composition and shape factors, other than fractal dimensions, have also been used to classify particles using, multivariate clustering techniques (Kim *et al.*, 1988; Kim and Hopke, 1988), and artificial neural networks (Xie *et al.*, 1994b; Wienke *et al.*, 1994).

The fractal dimension is closely associated to our normal understanding of dimensions of either one, two or three dimensions in the x, y and z planes (Barnsley *et al.*, 1988). For Euclidean objects such as a cube, square or line the fractal dimension is equal to their Euclidean dimension (Kaye, 1993).

The general rule is that the one dimensional line can be divided into N segments each scaled down by the ratio $r = 1/N$. For two dimensional objects such as a square in a plane it may be divided in to N similar parts each of which is scale down by $r = 1/\sqrt{N}$. Likewise a three dimensional object may be divided up in to N parts each of which is scaled by the ratio $r = 1/\sqrt[3]{N}$. (Barnsley *et al.*, 1988). It follows then that in general a D dimensional object may be divided in to N smaller self similar parts each scale by a ratio of :

- $r = 1/\sqrt[D]{N}$ or $N = 1/r^D$

So the self similarity dimension or fractal dimension of the object is given by:

- $D = \log(N)/\log(1/r)$ (Barnsley *et al.*, 1988)

In the work described herein two different types of fractal dimension have been used. A boundary or perimeter fractal dimension has been used which describes the texture of the perimeter of the image, this is a linear fractal dimension (Kaye, 1993; *cf.* chapter 3). A

density fractal dimension has been used which describes the space filling quality of the image, this is a two dimensional fractal dimension (Barnsley *et al.*, 1988).

1.5.2 Fractal Combustion Particles and Formation Dynamics

The concepts of fractal dimension have proved particularly successful in the application to combustion aerosols. Studies have characterised particles from the combustion of diesel at different loads (Skillas *et al.*, 1997), combustion of diesel with different sulphur content (Huang *et al.*, 1994), acetylene combustion (Samson *et al.*, 1987) and the combustion of petrol, fuel oil, paraffin oil, butane and wood (Colbeck *et al.*, 1997). Aggregates from high temperature sources of iron, zinc and silicon dioxide have also been measured using fractal geometry (Forrest and Witten, 1979). The aim of such investigations is to provide information concerning the specific nature of the particles produced in the combustion processes (Kaye and Clark, 1991; Kaye, 1993). Fractal measurements are useful as a quantitative measure of the structural morphologies of particles, and can be directly related to the physical properties of the particle (Nyeki and Colbeck, 1994). The fuel and combustion process are directly related to the fractal dimension of the particle and thus are indicative of the source of the particle (Katrinak *et al.*, 1993; Colbeck *et al.*, 1997; Skillas *et al.*, 1998).

A number of models have been used to describe the formation of agglomerate aerosols, such as diesel engine particles as shown in Table 1.6. Each model yields a characteristic fractal dimension, which is usually independent of chemical composition (Katrinak *et al.*, 1993). The model values may therefore be used in comparison with measured values to postulate the mechanisms of agglomerate formation.

In the monomer-cluster model, primary particle spheres (monomers) attach to a cluster of particles one by one. Such attachment yields a high fractal dimension of 2.5 or 3 in three dimensions and 2 when measured in two dimensional projections (Skillas *et al.*, 1998; Katrinak *et al.*, 1993). This highlights the limitations of measurement of two dimensions. The projection of a three dimensional object onto a two dimensional surface, such as in transmission electron microscopy and image analysis, results in the loss of information (Kaye, 1993). This loss of information is known as occlusion and may be experimentally assessed (*cf.* Section 3.4.4). Thus using two dimensional projections no differences between monomer-cluster formation using diffusion limited aggregation or ballistic trajectories can be distinguished (Katrinak *et al.*, 1993). This is not too much of a problem since most aerosol measurements yield density fractal dimensions below 2 (Katrinak *et al.*, 1993). The cluster-cluster model describes the growth of aggregates through the collision of groups of monomers (Jullien *et al.*, 1987). The characteristic fractal dimension produced from these models are lower than 2 and are thus suggested to be more applicable to the formation of aerosol (Katrinak *et al.*, 1993; *cf.* Table 1.6).

Aggregation model	*Trajectory of particle or cluster*	*Fractal Dimension*
monomer - cluster (primary soot particles added to each cluster one by one)	ballistic (linear) diffusion limited aggregation (DLA)	3.00^a, 2^c 2.50^a, 2^c
cluster - cluster (growth of agglomerates by collisions between clusters)	ballistic (linear) diffusion limited aggregation (DLA)	1.95^a 1.91^b 1.80^a 1.78^b
tip-to-tip variation of cluster-cluster (clusters have opposite charges on their tips)	electrostatic effects dominate (chemical model)	1.42^b
tip-to-tip variation of monomer-cluster model (cluster tips and monomers have opposite charges)	electrostatic effects dominate (chemical model)	1.0^b

a. Skillas *et al.*, 1998
b. Jullien *et al.*, 1987
c. Katrinak *et al.*, 1993, 2 dimensional measurement of particles formed in three dimensions
Table 1.6 Aggregation models and Characteristic fractal dimensions (density fractal dimensions; cf. Chapter 3)

The trajectories, size and electrostatic properties of particles all also influence the resultant agglomerate fractal dimensions (Jullien *et al.*, 1987). In the early stages of a combustion process the spherules formed are small (< 50nm) and the mean free path between particle collisions is lengthened because of the high temperature (Mountain *et al.*, 1986; Katrinak *et al.*, 1993). Within this environment free molecular flow predominates and particles follow ballistic, *i.e.* linear, trajectories (Jullien *et al.*, 1987; Katrinak *et al.*, 1993). As monomers or clusters of particles move away from the combustion event, in time and space, the temperature falls, the mean free path of particles is reduced, and larger clusters of particles form (Katrinak *et al.*, 1993). Within this environment diffusion limited aggregation (DLA) predominates and particles follow random-walk, *i.e.* Brownian motion, trajectories (Skillas *et al.*, 1998; Katrinak *et al.*, 1993). In other cases if electrostatic effects occur between particles the trajectory becomes immaterial and the fractal dimension of resultant structures is reduced (Jullien *et al.*, 1987). An aerosol particle may endure a series of different conditions during its lifetime, and thus combinations of the aggregation models shown in Table 1.6, are probably necessary to explain the fractal dimensions of aerosols found in the urban environment (Katrinak *et al.*, 1993).

1.5.3   Fractal Measurements of Urban Aerosol Particles

Little work has been carried out on the fractal properties of atmospheric aerosol particles. Measurements of the fractal dimension of carbonaceous aggregates has been made for particles collected in Phoenix, Arizona (Katrinak *et al.*, 1993), confirming the fractal nature of particles, and suggesting ageing and formation processes. Classification of aerosol particles has been made using fractal dimensions (Xie *et al.*, 1994, Kindratenko *et al.*, 1994). In both of these studies of particle identification, multiple fractal dimensions were suggested to be most useful in the quantitative description of particle shape. In such a way

chemically similar fly ash and soil dust can be distinguished according to morphology (Kindratenko *et al.*, 1994), and classification of spherical, bladelike and fused particles can be made (Xie *et al.*, 1994). It is clear then that the fractal measurement of images can be used in the investigation of ageing, formation and sources of an aerosol (Katrinak *et al.*, 1993).

1.6 Objectives of Study

There are three stages to the research presented here:

- PM_{10} is currently measured using mass based TEOM measurements as part of the automatic urban network. Such measurements give no insight to the size distribution or number count of the aerosol and peak episodes can not be analysed in more detail retrospectively. In the first stage this work a method collection and measurement of 1- 10 μm aerosol by optical microscopy and image analysis has been developed. Using this method an 18 month monitoring programme of airborne particulate was made at the University of Plymouth. The aim of this work was to study the trends and periodical variation of particulate matter number concentration in Plymouth Retrospective analysis of periods of interest was made, with the aim of identifying the size and sources of peak episodes of PM_{10} with comparison to TEOM measurements of the same episodes (*cf.* Chapter 2).

- In the second stage of this work methods of collection and analysis were developed for the analysis of fine (1 μm) and ultra fine airborne (0.1 μm) particles by transmission electron microscopy and image analysis.(*cf.* Chapter 3). It was aimed to collect enough aerosol for analysis, with the minimum opportunity for structural changes. The method used has needed to be portable, cheap, and easy to use.

- The method developed for direct sampling of aerosol for TEM was used the characterisation of aerosol at the background and the roadside. This has been made using two fractal dimensions, which quantitatively describe the morphology of the particle. A simple comparison of morphologies does not account for the large size range of aerosol examined. Thus a detailed breakdown and comparison of morphologies within their size ranges has shown the true differences between particles and the most important size of particles (*cf.* Chapter 4). The data was used aimed to examine the differences in ageing and composition in the roadside and background aerosol. In the same way a Perkins Prima 2 litre diesel engine source was extensively sampled using the developed techniques and other engine particles were sampled from a dilution tunnel as a comparison. The effects of speed, load and engine type on the morphologies of particles produced has been investigated. In this work a source 'fingerprint' morphology of engine particles was sought (*cf.* Chapter 5).

- The source characterisation and other literature available characterising sources was used in comparison with the urban aerosol samples. A tentative identification of the percentage contribution of particulate sources by number to the roadside and background aerosol in Plymouth has been made. Groups of fresh and aged particles from hydrocarbon combustion were identified, as well as individual carbon ceno-spheres and non-combustion particles. The differences in roadside and background aerosol composition were thus found. A correlation between urban aerosol and source aerosol morphologies was also used as an aid to 'fingerprint' the major contributor of particles to the roadside and background (*cf.* Chapter 6)

CHAPTER TWO
Urban Aerosol measured using a Burkard Spore Trap

2.1 Introduction

Urban airborne particulate matter, especially the respirable fraction below ten microns (PM_{10}), in size has been linked to increases in respiratory and cardiovascular death rates (Dockery *et al.*, 1993; Pope *et al.*, 1995). Air quality standards for PM_{10} levels are based on mass measurements per cubic metre of air and most studies have linked health effects to PM_{10} mass measurements (Dockery and Pope, 1994; Schwartz, 1994). However there is some debate about the significance of mass *vs.* number of particles (*cf.* Section 1.1.2) (Seaton *et al.*, 1995; COMEAP, 1995). Despite this interest there is little information on the size distribution and morphology of PM_{10} in the urban air, especially over a period of time. The number and morphology of airborne particles is thus of research interest. In this chapter the use of a Burkard spore trap is reported for the daily monitoring of ambient air particulate number concentration and morphology. This application of an existing particle trapping method for the collection of urban aerosol has been previously described by Battarbee *et al.*, (1997). In this research, which was developed coincidentally, a Burkard spore trap has also been used but further developments in image analysis have been made for automated particle measurement. The aims of this work were to use the developed method to make an 18 month study of the particle number and size in Plymouth, UK, to examine any periods of interest retrospectively, and to consider the effects of local traffic sources and meteorology on particle number.

2.2 Experimental Details

2.2.1 Site Review and Sampling Apparatus

Daily samples of airborne pollen and particulate matter were collected during 16 March 1995 to 31 August 1996 using a *Burkard Volumetric Spore Trap* (Burkard Ltd. Bucks.). Sampling took place at the Issac Foot building, University of Plymouth at approximately 30m above ground level and over 150m from the nearest main road (*cf.* Figure 4.1; Section

4.2). The spore trap consists of a gel strip attached to a metal drum which rotates at 2mm per hour. The glycerine jelly used is composed of a mixture of gelatine (10 g), glycerol (54 ml), distilled water (60 ml) and phenol (1.4 g), and is painted on to the melinex tape. The gel is designed to minimise particle bounce, to swell shrunken spores and to preserve specimens (Burkard Spore Trap Manual, Burkard Ltd). Air is sampled at a rate of 10 l min^{-1}, particulate matter enters through an orifice of dimensions 14 x 2 mm and impacts onto the gel strip. The Burkard recording drum and orifice are illustrated in Figure 2.1. Slides corresponding to periods of 24 hours, are made up from the gel strip using saffranine stain (1:250) and used in microscopic analysis. Saffranine stain is used to stain any biological material for easy identification, but does not affect other particulate material. The efficiency of the spore trap is quoted as 70% ± 20%, based on wind tunnel tests for Lycopodium spores approximately 40 microns in diameter (Hirst, 1952). No collection efficiency curves exist for the Burkard spore trap but further calculations have shown that the theoretical efficiency drops to < 50% for particles <2 µm in size (Long, X. in: Battarbee et al., 1997).
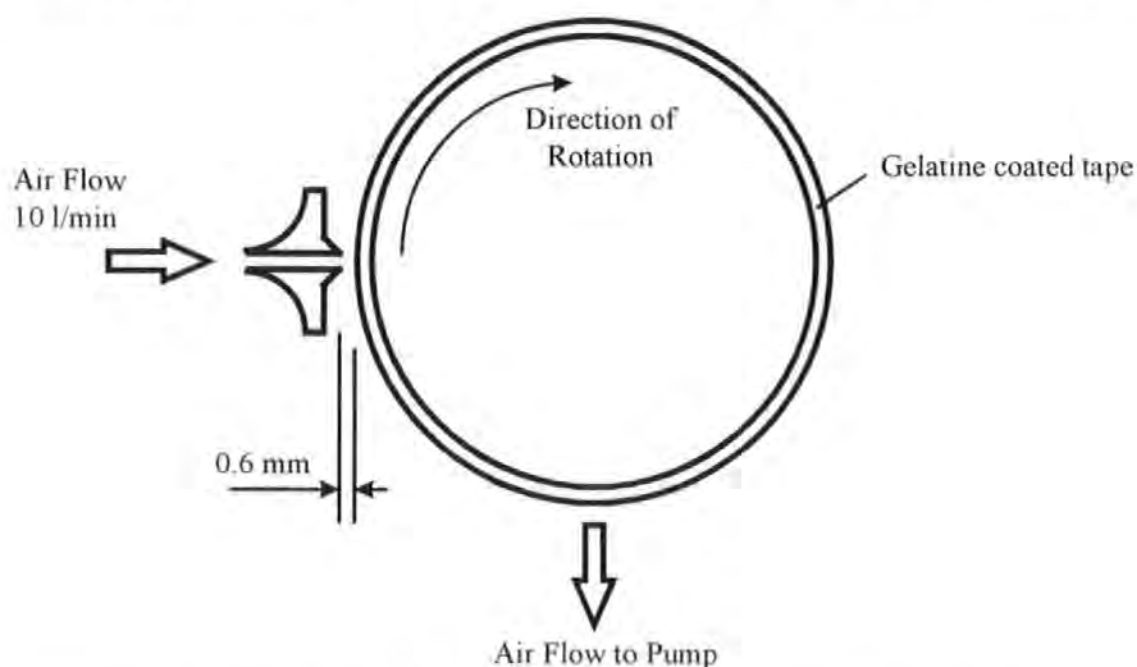
Figure 2.1 Diagram of the Burkard recording drum and orifice (After Operating

Instructions, Burkard Manufacturing Co. Ltd.).

2.2.2 Slide Preparation

Slides are prepared from the gel strip simply and provide a permanent record of airborne aerosol. The gel strip was removed from the sampling drum and cut in to pieces corresponding to 24 hour periods. Each piece, corresponding to 24 hours, was attached to a slide using a drop of distilled water. This procedure was carried out with care to avoid the formation of air bubbles under the gel strip. The cover slip was then lowered over the slide to cover the gel strip and was attached using a permanent mounting solution with saffranine stain, made up from saffranine powder and water (1:250).

In initial use of spore slides with image analysis, Gelvatol permanent mountant was used (35 g Gelvatol, 100 ml distilled water, 50 ml glycerol, 2 g phenol). It was noted that areas containing air bubbles had to be disregarded, so to avoid the erroneous counting of bubbles as particles. Consequently to this slide preparation was revised and air bubbles were eliminated through greater care in slide preparation. The gel used for staining the slides was also changed to a medium known as Farrants solution. This eliminated all small air pockets and was suitable for staining of pollen material Unfortunately Farrants solution did not set quickly enough for the purpose of daily spore counting. In addition the solution seeped, reducing slide quality and making slide handling difficult. For this reason the staining gel was switched to glycerine jelly, also used as the spore impaction surface on the melinex tape, with saffranine stain added. This stain/gel mix was heated and then applied to the slide using a pipette. There was no tendency for small bubbles to form on the slides, the staining of pollen material was clear, the slides dried quickly and were robust enough for use soon after completion.

Early work was performed using dark field microscopy, but improvements to the slide quality allowed the use of bright field microscopy. This increased the quality of image

detection and of particle data, and allowed the collection of data on particle greyness and the variance of greyness over a particle.

2.2.3 Slide Analysis

Slides were analysed using an optical microscope attached to a *Quantimet 570 Image Analyser* (*Cambridge Instruments Ltd., UK*). Image analysis enables the properties and parameters of 2D images to be recognised and measured.

Image collection was made using a *Fujitsu* low light level camera attached to a mono-focal light microscope. A macro programme was written to automatically measure particle size, shape and shading (*cf.* Appendix 1). Image processing and thresholding for detection were governed by operator judgement, with the aim of optimum image quality and detection. Measurements of particle roundness diameter, area and greyness were taken at a magnification of 400 times, and are defined below:

- Diameter is defined as the diameter of a circle with the same area as the 2D projected image of the particle measured

- Roundness = $(perimeter)^2 \div (4 \times \pi \times Area)$

1 = round, <2 = square, ~2 = triangle, 5-10 = fibre, >20 = strand

- Greyness a linear scale from 0 (black) to 255 (white), the grey value for a particle is the average calculated from the greyness of each pixel within the particle boundary

For each slide during the 18 month period a single transverse across the slide was selected and six view fields along that transverse were analysed *via* optical microscopy and image

44

analysis, as described above. The size of view field, area of slide and volume of air sampled are all known variables, thus allowing the number of particles between 1 - 10 μm in a cubic meter of air to be calculated.

The slide for one single 24 hour period was measured in detail, to coincide with meteorological measurements. For this day six areas were measured at 2 mm intervals along the transverse of the slide, corresponding to each hour of the day. In this way a detailed picture of short term variation over one day (24 h) is considered.

2.3   Results and Discussion

2.3.1   Urban Particle Monitoring

The daily Plymouth ambient particle concentrations for 16 March 1995 to 31 August 1996 are shown in Figure 2.2, with the PM_{10} mass from a tapered element oscillating micro-balance (TEOM) in Bristol, UK shown for comparison. The mean concentration over the total sample period was 10.5×10^4 particles m^{-3}, and have a range of 0.5×10^4 - 55.8×10^4 particles m^{-3}. The number of particles exhibits large periodical and daily variations similar to the PM_{10} TEOM mass.

Over the 18 month sampling period the particle number concentration appears to decrease (Figure 2.2). There is a significant difference (t-test $p<0.001$) between the mean particle count before 22 September 1995 and after 10 October 1995. For the period 16 March to 22 September 1995 the mean particle number concentration was 14.7×10^4 particles m^{-3} with a range of 2.03×10^4 - 55.8×10^4 particles m^{-3}. For the period 10 October 1995 - 31 August 1996 the mean was 7.9×10^4 with a range of 0.5 - 47.1×10^4. Method developments which have been discussed (*cf*. Section 2.2) were made before the study period began and methodology used during the 18 month period was consistent. The

45
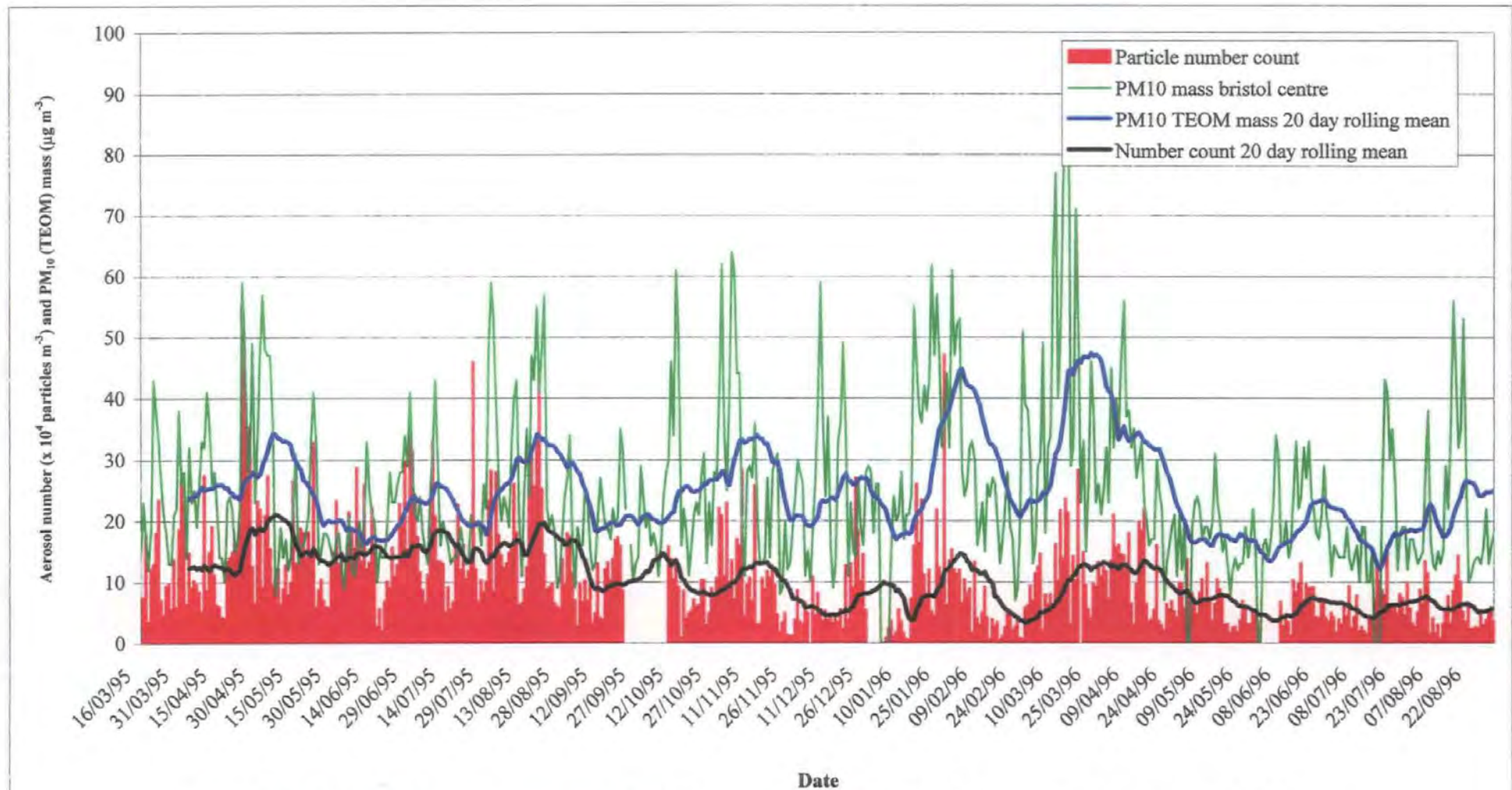
Figure 2.2 Daily burkard number concentration (Plymouth) and PM $_{10}$ TEOM mass, (Bristol central), 16.3.95 - 31.8.96

observed trend is most probably as a result of spore trap maintenance between 22 September 1995 and 10 October 1995.

Interpretation of the implications of the ambient particle concentrations is complicated by the fact that much of the previously reported work on particle concentrations that induce a respiratory response take account of only the mass of ambient PM_{10}, not the number. It is mass that is currently used in air quality standards. Work at the University of Birmingham UK reported by Seaton *et al.*, (1995), using a condensation particle counter, has shown that total numbers of particles range between 1×10^9 - 50×10^9 m^{-3}, sometimes rising to 100×10^9 m^{-3}. Concentrations in Phoenix, Arizona USA, have ranged between 0.5×10^6- 50×10^6 m^{-3} for particles less than 2 μm (Katrinak *et al.*, 1995). The particle counts determined in the present study are in the range of 0.5×10^4 - 55.8×10^4 particles m^{-3} which is lower than the concentration reported either in the Birmingham or Phoenix studies. However in the Birmingham study, counts were made of all particles smaller than *ca.* 4 μm in aerodynamic diameter, and in Phoenix for particles between 2-0.2 μm. Thus both studies include the counts of fine particles smaller than 1 μm and the Birmingham study includes ultra-fine particles below 0.1 μm (100nm). The work reported here must be considered as complementary and not in direct comparison with these other studies. The greatest number of airborne particles are below 1μm in diameter which were not efficiently collected by the Burkard spore trap (*cf.* Section 2.2.1) and observation of particles with a diameter less than 0.5 μm is impossible using light microscopy. Therefore our values which are 10^5 times lower than determined in Birmingham and 10^2 times lower than that measured in Phoenix, are not indicative of cleaner air but simply of the larger and limited size range of particles measured.

A further contrast between the study described herein and the previous studies in Birmingham and Phoenix is the definition of diameter. In the present study particle sizes have been measured as the diameters of circles with areas equal to the 2D image of the particle. In contrast aerodynamic diameter was used in the Birmingham and the Phoenix studies. This influences the particle number count as follows; the drag on a particle between 1 and 10 microns falling through air is described by Stokes Law:

- ***Drag force (F) = $6\pi\eta aus$*** *(Murphy, 1984)*

Where η = fluid viscosity (air = 1.82×10^{-4} g s^{-1} cm^{-1}), a= equivalent sphere radius of particle, u=velocity at an instant, s=shape factor (sphere =1), a dimensionless constant.

The forces acting upon 3 particles at terminal velocity are shown in Figure 2.3. Particle *A* describes a spherical particle, with shape factor (*s*) of one.

- ***A)*** $m_a g = 6\pi\eta au_a s$ at the velocity u_a.

And Particle *B* describes a particle with shape factor (*s*) >1 thus :

- ***B)*** $m_b g = 6\pi\eta au_b s$ at the velocity u_b,

- where $u_b < u_a$ and $m_a g = m_b g$

Particle *C* has a smaller radius (*a*) and mass (*m*) and shape factor (*s*) of one, but for a unit reduction in radius the mass decreases by $4\pi/3$.

So :

- $6\pi\eta a_a u_a s >> 6\pi\eta a_c u_c s$

Where $a_a > a_c$ but because of the decrease in mass (*m*) by $4\pi a^3/3$ it follows that $u_a > u_c$.

Therefore in certain cases

- $u_a > u_b = u_c$

Aerodynamic diameter is defined as, the diameter of a sphere of unit density with the same settling velocity as the particle in question. Consequently in terms of equivalent circle diameter particle A is equal to particle B, however when considering the aerodynamic diameter particle B is equal to particle C.
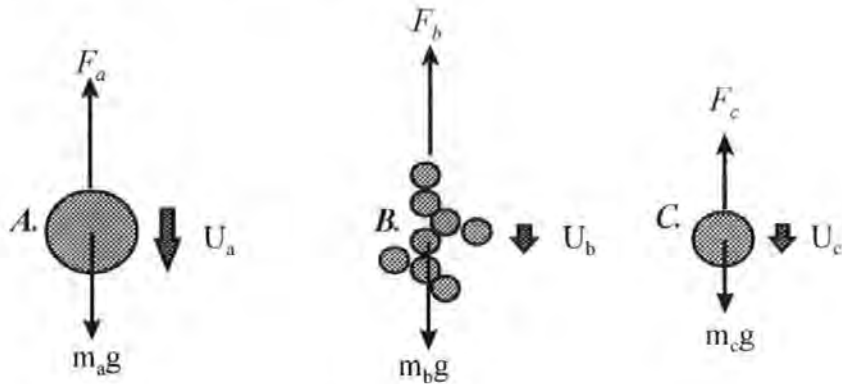
Figure 2.3 The Forces acting upon a particle at terminal velocity ($mg=6\pi\eta aus$)

In practise, the shape factors (s) of particles has a maximum of approximately two. So for a particle of equivalent circle diameter of 10 μm with a shape factor equal to two, the drag acting upon the particle according to Stokes law, multiplied by the shape factor is equal to twice the drag upon a 10 μm spherical particle. However the mass of both particles is the same, thus the down force expression (mg) is the same for both particles. Hence all other factors being equal the downward velocity (u) is halved. If this velocity was expressed in terms of a spherical particle, the down force term (mg) would be halved to balance. So the mass of the particle would be half and for a particle of the same density, the radius would be reduced by $1/(\sqrt[3]{(4\pi/3)})$, *i.e.* for a 5 μm equivalent circle radius particle the aerodynamic radius would be 3.5 μm. Thus the aerodynamic diameter of a particle with a shape factor of 2 and an equivalent circle diameter of 10 μm, would be *ca.* 7 μm. At smaller particle sizes this effect is less significant as diffusion becomes more dominant than sedimentation in governing the motion of particles (*cf.* Section 1.2.4). Therefore particles of 10-20μm in diameter, and of irregular shape, may in some cases be within 10 μm in aerodynamic

diameter but greater than 10 μm by equivalent circle diameter. As a consequence, those particles measured in this study include some above 10 μm in diameter, however this does not greatly affect the overall particle number count owing to the scarcity of these particles. Conversely a small number change in such large particles may significantly affect the TEOM PM_{10} mass. For example one 20 μm particle may have the same mass as eight thousand 1 μm particles, of the same density and eight million 0.1 μm particles of the same density. Therefore in contrast to studies in Birmingham and Phoenix the use of equivalent circle diameter allows the influence of large irregular shaped particles to be assessed. In short, aerodynamic size is important as this plays a part in atmospheric integrity, true exposure levels to humans and levels of impaction within the respiratory tract. Conversely equivalent circle diameter gives a better indication of the mass of each particle which may enter the lung. The study of both is complimentary for the full understanding of fine particles. This effect is probably small and further study of the data on the roundness and area of the particle may reveal an indication of aerodynamic behaviour.

2.3.2   Retrospective particle number analysis

The movement of the drum of the Burkard spore trap with time produces a trace from which changes of atmospheric particle number concentrations with time may be calculated. Slides produced from this trace are permanent and thus are suitable for retrospective analysis. In the present study a detailed analysis of particle number and distribution during the periods 6 Jan -16 Feb 1996 and March 1996 has been made. In addition a detailed retrospective analysis has been made of a single 36 hour period, to examine the influence of local meteorology and local sources upon the numbers and size distribution of aerosol. The 36 hour period chosen was selected as it was considered 'typical' of unsettled conditions in Plymouth, inclusive of both rain and wind periods.

During the first three months of 1996 there were two periods of UK wide elevated concentrations of PM_{10}, as measured by tapered element oscillating micro-balance (TEOM) in the automatic urban network (AUN). From 19 Jan to 4 February the overall urban PM_{10} (TEOM) concentration was 43 $\mu g\ m^{-3}$, with >50 $\mu g\ m^{-3}$ on 6 of 17 days. From 10-25 March the country wide mean PM_{10} (TEOM) concentration was 57 $\mu g\ m^{-3}$, with >50 $\mu g\ m^{-3}$ exceedences on 11 of 16 days (King and Dorling, 1997). Back trajectory calculations for these periods has shown that the air masses associated with these elevated concentrations came from the east, from mainland Europe. As a result, it has been suggested the elevated concentrations of PM_{10} mass (TEOM) are not due to local vehicle generated sources as previously suggested (QUARG 1993 b; QUARG 1996; Brown, 1994), but from the long range transport of continental aerosol. (King and Dorling 1997; Stedman 1997). In this research we have aimed to examine these elevated periods of PM_{10} mass in terms of particle number and distribution. It is aimed to identify any significant changes in aerosol size composition during these times as an indicator of the introduction of a different aerosol mass. It is also aimed to show any correlation between PM_{10} mass (TEOM) and particle number and further conclude the implications of the size distribution of aerosol during PM_{10} mass exceedences on the perceived toxicity of elevated PM_{10} mass concentrations.

The particle number count for Plymouth, UK., as measured using the Burkard spore trap is shown for the period 6 Jan - 16 Feb 1996 (*cf.* Figure 2.4) and March 1996 (*cf.* Figure 2.5). Also shown is the PM_{10} (TEOM) mass for Bristol centre (data from The National Air Quality Information Archive : http://www.aeat.co.uk/netcen/aqarchive/archome.html) for the same periods. Both charts seem to show a corresponding increase in PM_{10} number and PM_{10} mass for the same periods as the UK wide episodes reported by King and Dorling, (1997) (*cf.* Figures 2.4 and 2.5).
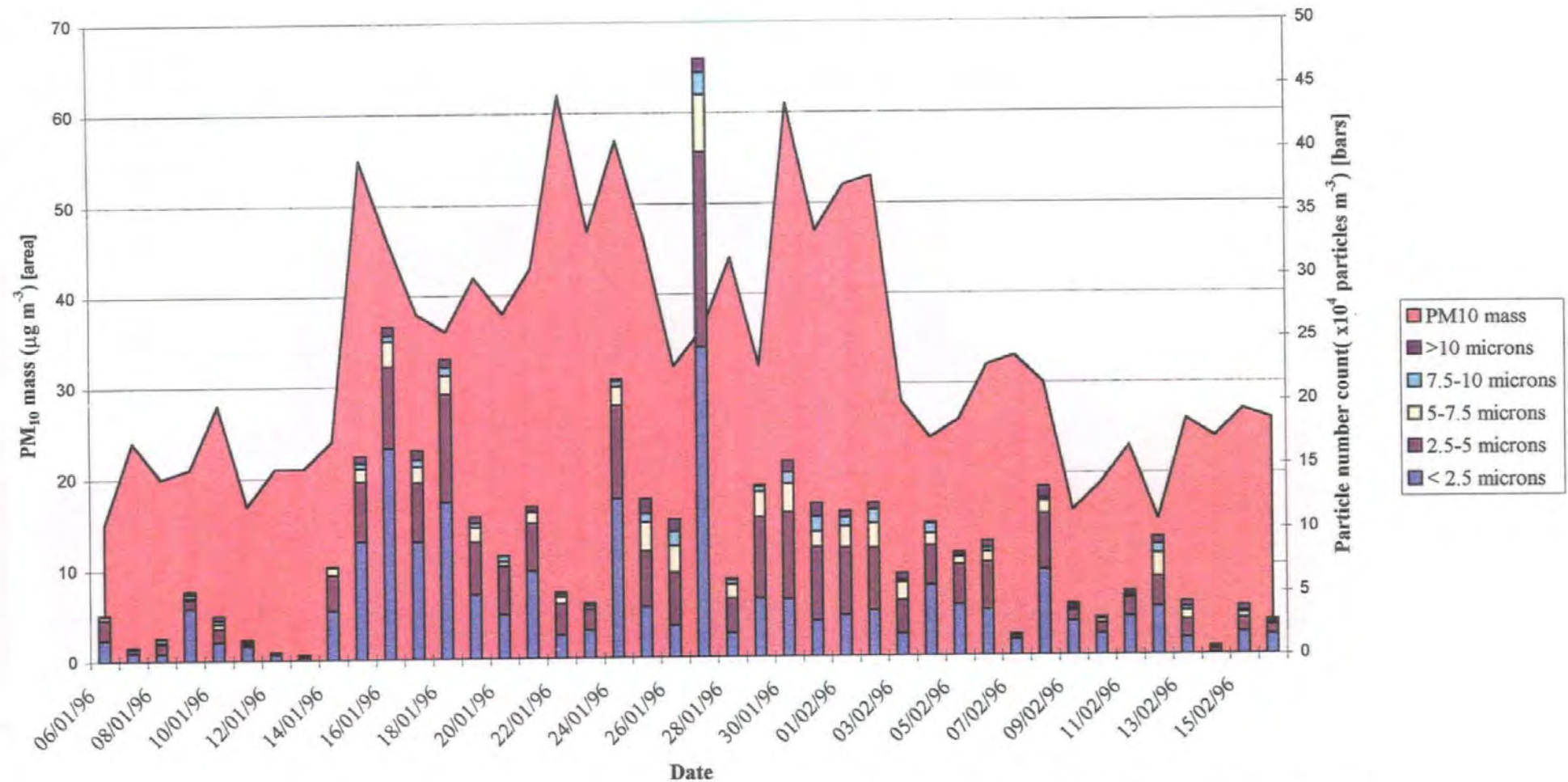
Figure 2.4 PM $_{10}$ mass (TEOM, Bristol Center) and Particle number count (University of Plymouth) for the period 6 Jan - 16 Feb 1996
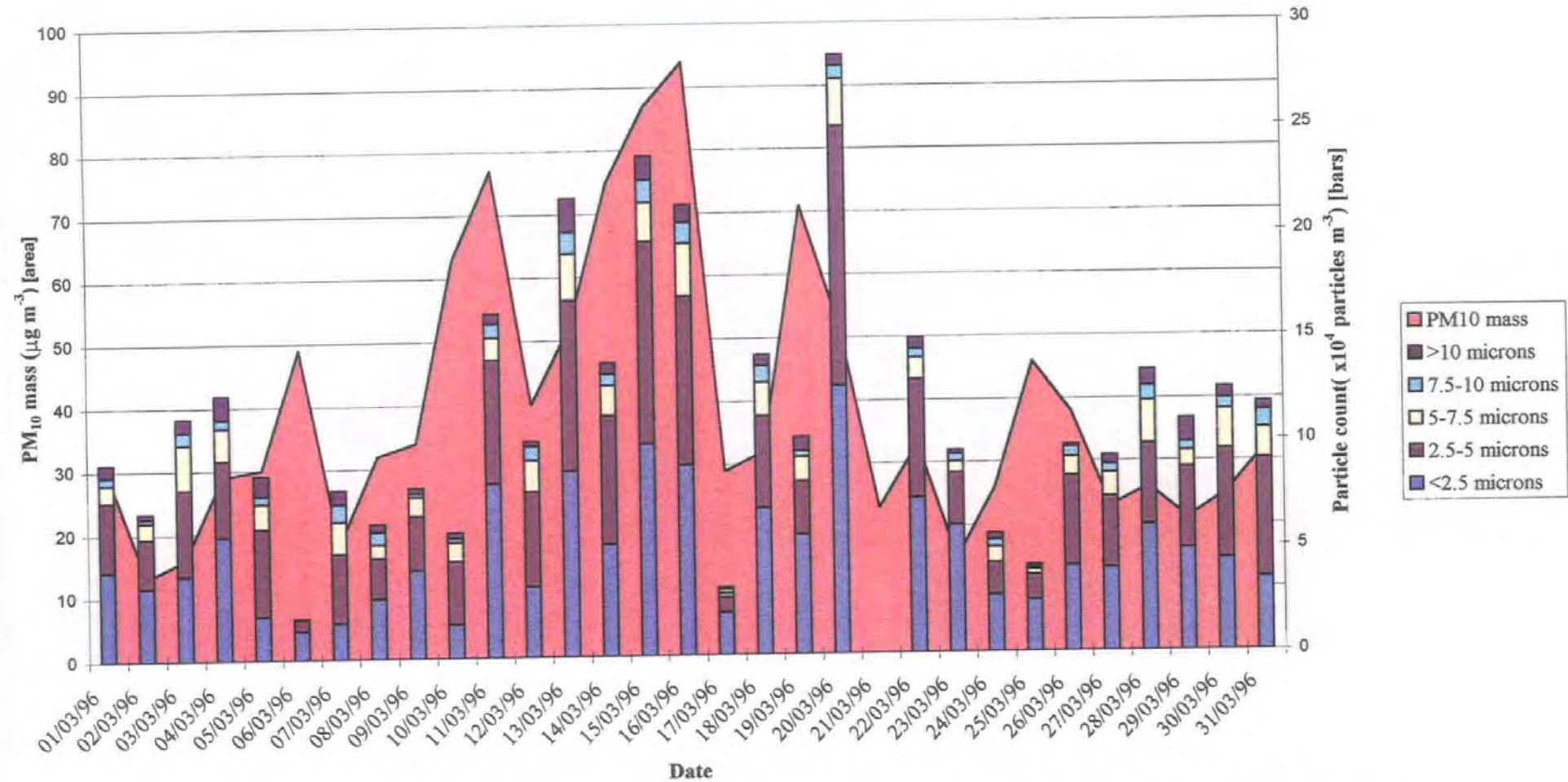
Figure 2.5 PM $_{10}$ mass (TEOM, Bristol Center) and Particle number count (University of Plymouth) for March 1996

From 19 Jan to 4 Feb the average particle number was $13.5 \times 10^4 \pm 7.6 \times 10^4$ particles m^{-3}, and the average PM_{10} (TEOM) mass was 51 ± 24 μg m^{-3}. From the 10 - 25 March the mean particle count was $13.0 \times 10^4 \pm 9.7 \times 10^4$ particles m^{-3}, and the mean PM_{10} (TEOM) mass was 43 ± 11 μg m^{-3}. However as with other work (Battarbee *et al.*, 1997) the correlation between PM_{10} mass and total number is low, with a slightly negative correlation (correlation co-efficient $r = -0.05$) for 19 Jan- 4 Feb and a low correlation ($r = 0.49$) for 10-25 March.

The particle size groupings are also given in Figures 2.4 and 2.5 with the percentage contributions of each size range to the total number illustrated in Figures 2.6 and 2.7. Figure 2.6 illustrates the period for January to February 1996 and has some notable features. Prior to 19 January the 2.5-5 μm fraction ranges between 10-40% of the collected aerosol number, almost always lower than the <2.5 μm which makes up 25-65% of the collected aerosol. During the peak episode this trend reverses and the <2.5 μm fraction falls to between 20-50% and the 2.5-5 μm fraction increases to between 25 -45% of the collected total particle count. Between 25 Jan-3 Feb the reversal in trends of collected fine (<2.5 μm) and coarse (>2.5 μm) aerosol is most apparent as the 5-7.5 μm fraction increases from *ca.* 5% to between 10-20% of the collected total particle count. After the peak episode ends (Feb 4) the collected particle fractions return to their pre-episode ranges.

For the whole of the peak period, correlation of particle number with the PM_{10} (TEOM) mass is low (<0.02) for all size fractions. However for the period from 29 Jan - 4 Feb the size range < 2.5 μm is poorly correlated (-0.07), but >2.5 μm sizes show good correlation (> 0.62) with the PM_{10} (TEOM) mass. Out side of the peak period the correlation for <2.5 mm particles with the PM_{10} (TEOM) mass is especially good (0.72).
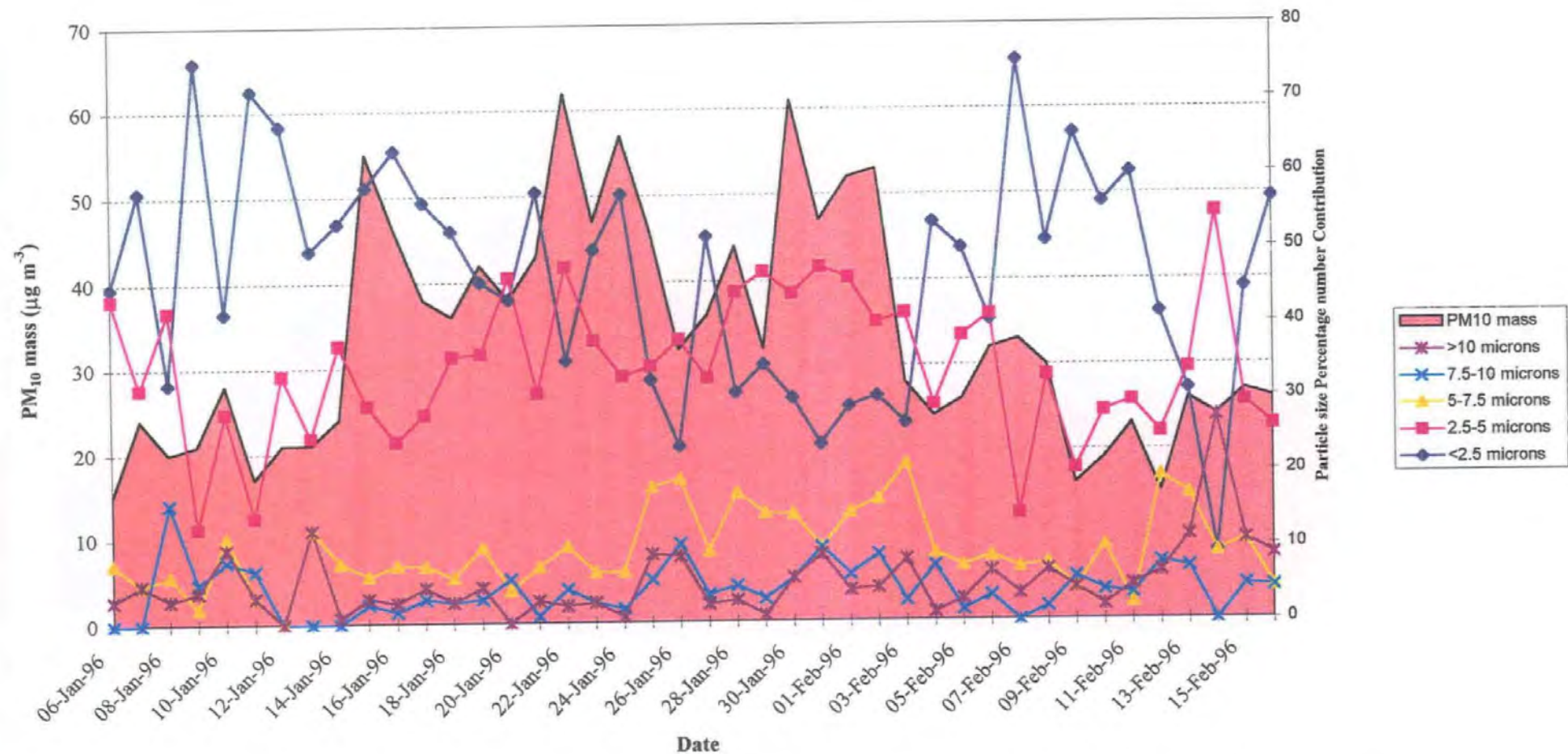
Figure 2.6 Percentage Contributions to the particle number by size (University of Plymouth) and the PM$_{10}$ mass
(TEOM, Bristol centre) for the period 6 Jan - 16 Feb 1996
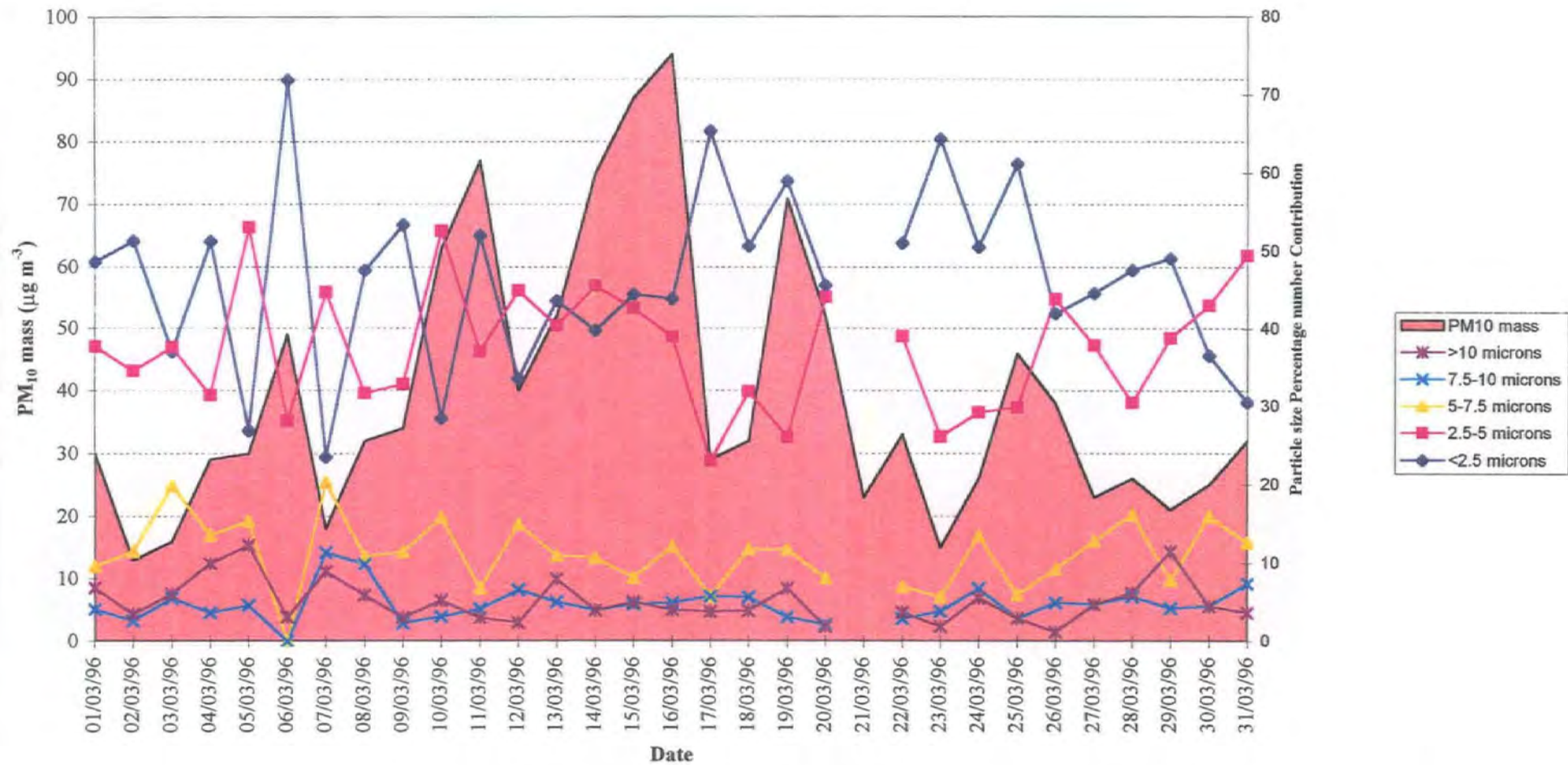
Figure 2.7 Percentage Contributions to the particle number by size (University of Plymouth) and the PM $_{10}$ mass (TEOM, Bristol centre), March 1996

These results suggest that fine sources of aerosol (vehicle generated) were most dominant prior to the peak period, but fluctuated according to the general meteorology of the south west of England. The introduction of a continental air mass from the east caused an increase in the particle count, which it seems is greatly due to the >2.5 μm size fraction of aerosol, despite some air mass mixing or local effects. After the peak period, fine sources of aerosol resume their dominance.

A similar increase in particle number and PM_{10} mass (TEOM) is observed in March 1996 (Figure 2.5, and Figure 2.7), although is not quite as obvious. The correlation of PM_{10} mass (TEOM) and total particle number for the whole period is low (0.47), but increases to 0.5 for <5 μm particles and decreases (0.26) for < 5 μm particles. This supports the association of fine (vehicle generated) particles with day to day fluctuations of particle mass. For the peak period 6-21 March the correlation of <5 μm particles with PM_{10} (TEOM)mass drops (<0.45) and the correlation of >5 μm particles with PM_{10} (TEOM) mass is increased (>0.42). This is indicative of the greater association of >5μm particles with the PM_{10} (TEOM) mass peak period. This is further evidence that the mainland European air mass brings with it a > 2.5 μm aerosol, which then greatly affects the PM_{10} mass measurements.

The analysis of the size distribution of particles clearly supports the hypothesis of other studies (King and Dorling, 1997; Stedman, 1997), which suggest that aerosols, distinctly different in source, are introduced to the UK atmosphere during periods of PM_{10} (TEOM) mass exceedence. The work herein has shown that during these periods the PM_{10} (TEOM) mass is most closely associated with coarse particles (>2.5 μm).

The hourly particle count and rainfall for a 24 hour period is shown in Figure 2.8. During this period the average hourly particle count was 8.8×10^4 particles m^{-3}, rising to 19.4×10^4 particles m^{-3} during the rush hour peak at 16:00 hours and falling to 2.7×10^4 particles m^{-3} at 01.00 hours. The dominance of the smaller aerosol is shown, with those particles <5 μm making up on average 73% of the aerosol. The diurnal fluctuation of particle concentrations is shown here at morning (6-9am) and evening (3-6pm), consistent with other studies of particle number (Battarbee *et al.*, 1997; QUARG 1996) and particle mass (QUARG 1996).

Combustion particles are known to be predominantly generated in the fine (<2.5 μm) size range (Katrinak *et al.*, 1995; Carpenter and Johnson, 1979). It may be expected then that during rush hour periods the percentage contribution of fine particles would increase. The contribution of each size range is shown in Figure 2.8, and the percentage contribution from each size range in Figure 2.9. Both diagrams show that during the rush hour periods there is no obvious change in the contribution to the aerosol of each size range, suggesting that under consistent meteorological conditions, prior to the rain event, the aerosol size distribution is reasonably stable. Thus, an input of fine vehicle generated aerosol increases the overall number of particles, but agglomeration of aerosol ensures a self preserving size distribution. This is in agreement with theoretical concepts of agglomerate aerosol behaviour (Twomey, 1977; Jain and Kodas, 1998). The size distribution of the aerosol returns to the pre-rainfall consistency less than one hour after precipitation ends (*cf.* Figure 2.9), thus showing that meteorological effects, although influential, are only short term.
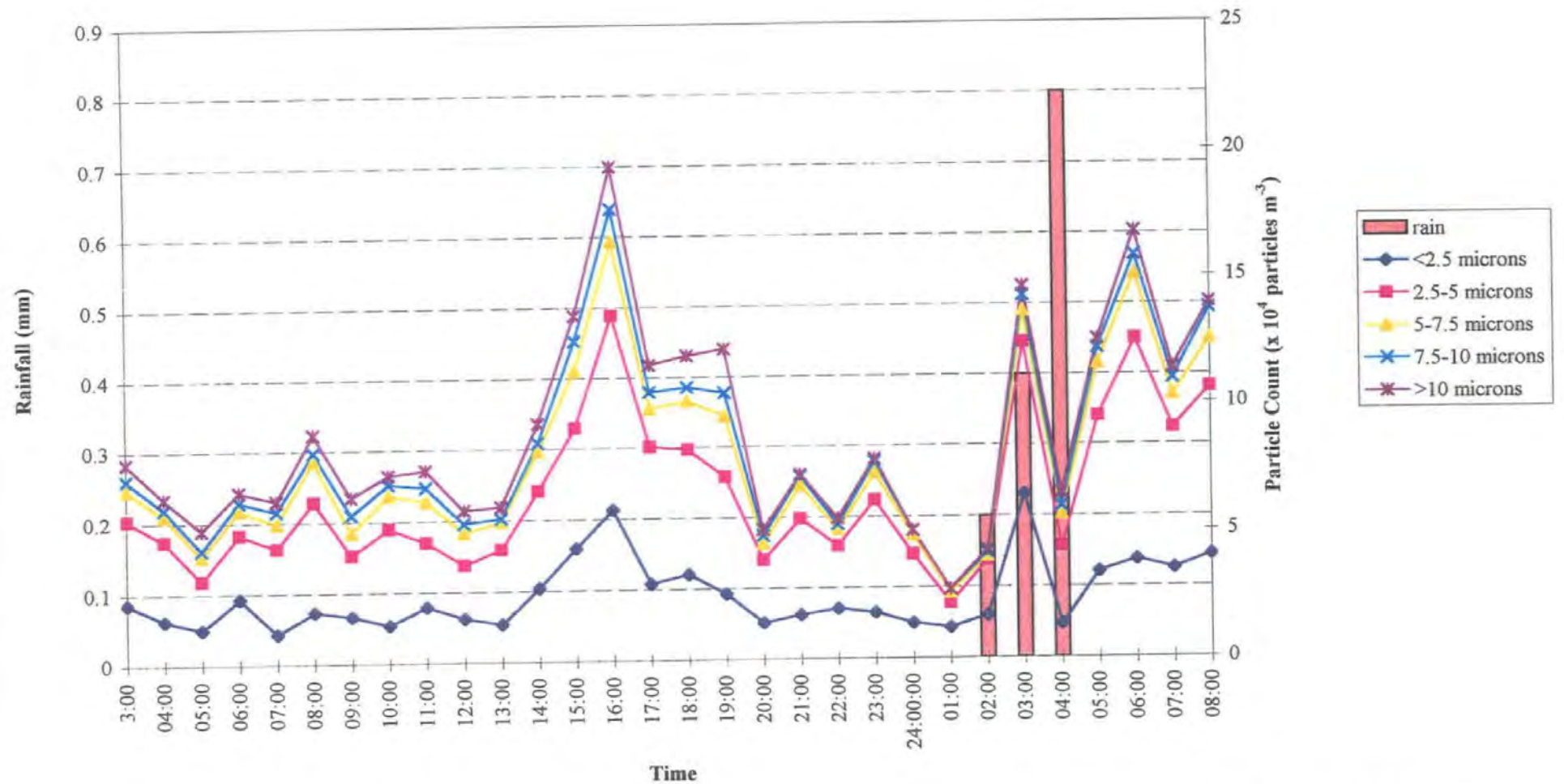
Figure 2.8 Size fractionated Particle count (University of Plymouth) and rainfall (University of Plymouth) for the period 03.00 ,19.9.96 - 08.00, 20.9.96
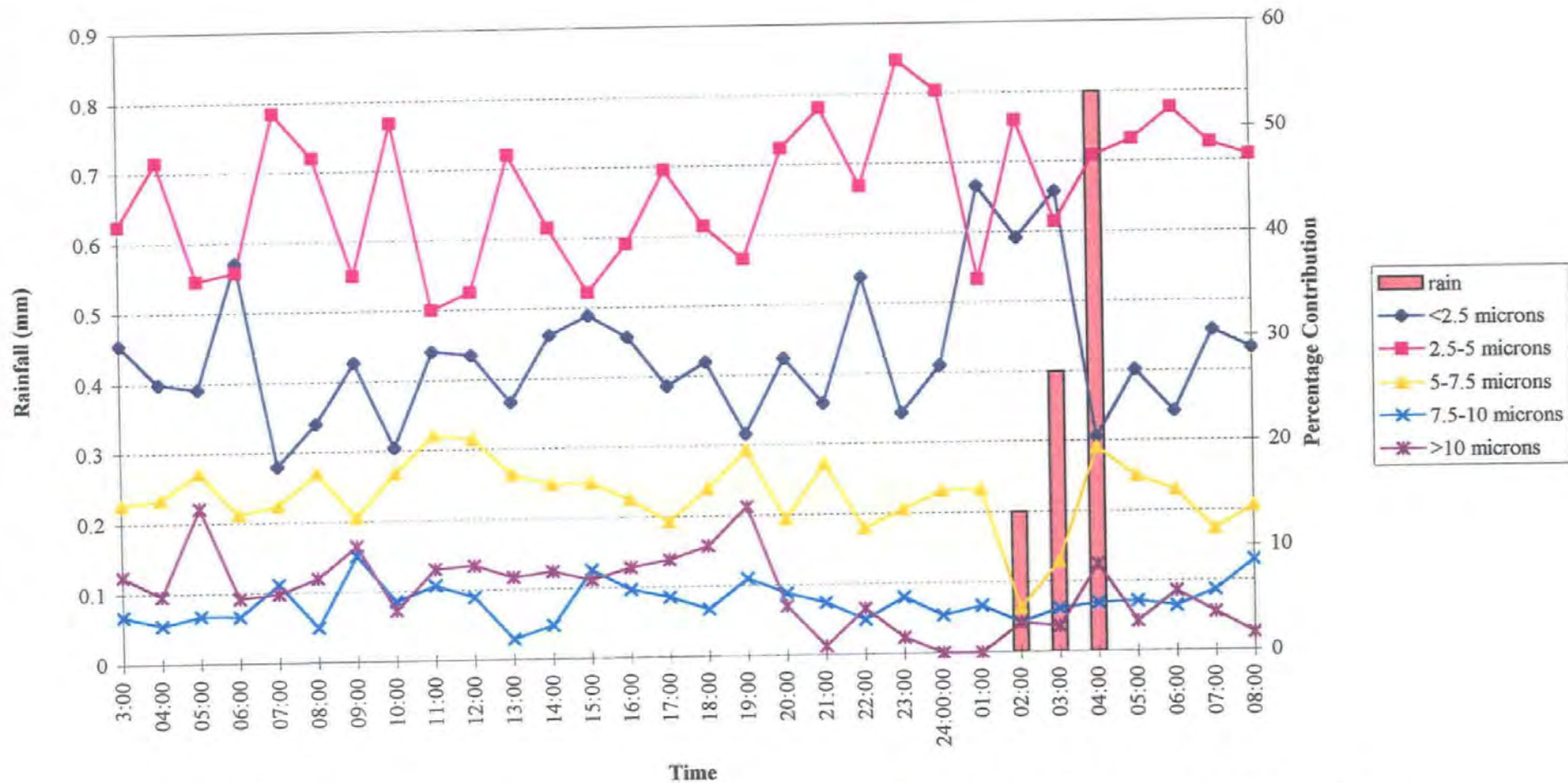
Figure 2.9 Size range percentage contribution to particle count and rainfall at the Univerisity of Plymouth, from 03.00, 19.9.96 to 08.00 am 20.9.96

The rainfall during the 36 hour period was only slight, (1.4 mm total), and only lasted for 3-4 hours, in the early morning (*cf.* Figure 2.8 and 2.9). Despite this the particle concentration and distribution during the same period shows a large fluctuation (Figures 2.8 and 2.9). Contrary to expectation, the particle number concentration actually peaks during this period. When the percentage contribution of sizes is examined during this period, it is evident that there is a fall in all the >5 μm size range particles to less than 10% of the total aerosol, and the <2.5 μm aerosol increases to > 50% contribution to the aerosol. The removal of larger size particle by precipitation has also been demonstrated by Battarbee *et al.*, (1997). However Battarbee *et al.*, (1997) did not report either an increase or decrease in the fine particle concentration. The reason for the increase in <2.5 micron particles in the present study is unclear. It is possible that the increased count may be from fine rain nuclei or perhaps particle resuspension on impaction with the ground.

2.4   Conclusions

In the work described herein a Burkard spore trap has been used and developments have been made using image analysis particle number counting and size measurement. The methods developed have been used to make an 18 month study of the particle number and size in Plymouth, UK. Two periods of UK wide elevated PM_{10} mass (TEOM) were retrospectively studied, and a 36 hour period was studied in detail to consider the effects of local traffic sources and meteorology on particle number. The results can be summarised thus:

- The mean concentration over the total sample period was 10.5×10^4 particles m^{-3}, and has a max/min range from 0.5×10^4 - 55.8×10^4 particles m^{-3}. The number of particles exhibits large periodical and daily variations similar to the PM_{10} (TEOM) mass.

- The particle number found was 10^5 times lower than determined in Birmingham and 10^2 times lower than that measured in Phoenix, but are most probably not indicative of cleaner air but simply of the larger and limited size range of particles measured.

- The use of equivalent circle diameter as opposed to aerodynamic diameter allows the influence of large irregular shaped particles to be assessed in comparison with PM_{10} mass.

- The analysis of the size distribution of particles clearly supports the hypothesis of other studies (King and Dorling, 1997; Stedman, 1997), which suggest that the introduction of a distinctly different aerosol occurs during periods of PM_{10} (TEOM) mass exceedence. The work herein has shown that during these periods the PM_{10} (TEOM) mass is most closely associated with coarse particles (>2.5 µm).

- The diurnal fluctuation of particle concentrations is shown here at morning (6-9am) and evening (3-6pm), consistent with other studies of particle number (Battarbee *et al.*, 1997; QUARG 1996) and particle mass (QUARG 1996).

- The slight rainfall during the 24 hour period causes a large fluctuation in the particle concentration and distribution. Contrary to expectation, the particle number concentration actually peaks during this period due to an increase in fine (<2.5 µm) aerosol from an unknown source.

The interaction of a number of sources and effects in the urban atmosphere is observed in this study. Local sources of fine aerosol, generally vehicle generated, contribute greatly to diurnal fluctuations. Local meteorology affects the PM_{10} and particle distribution hour by hour. Large scale air masses affect the regional meteorology and accumulation of particles in stable conditions, and the input of micron sized aerosol from continental Europe can push PM_{10} mass concentrations over excedence levels. Consequently although micron size continental aerosol input may cause urban PM_{10} mass excedences, the overall particle

number may not be greatly affected, as most urban aerosol is found below 1μm in diameter. In terms of possible health effects, fine particles (<1μm) have been singled out as of most concern because of their deep respiratory penetration and large surface area (COMEAP, 1995). Therefore PM_{10} (TEOM) mass measurements give a good indication of the input of micron size material from the continent, causing excedences of the EPAQS limit of 50 μg m^{-3}, however they may be of less use in determining the possible health impact of an aerosol. The present study has demonstrated that the study of particle size distribution and morphology is essential for understanding the potential toxicological impacts of an aerosol (*cf.* Chapters 3 - 6).

As mentioned previously the vast majority of ambient air particles are found below 0.5 μm which is below the limit of detection using optical analysis. Further work then is presented in Chapters 3 and 4, showing the detailed morphological analysis of sub-micron particles. The results of sub-micron analysis are useful for assessing the true number of particles and contribution by different sources to urban aerosol.

Despite reservations, the analysis of particle number on spore trap slides has a number of advantages. Burkard spore samplers are widespread therefore it would be quite simple to extend particle number measurements using this method to many other areas. The slides give a permanent record of the airborne particulate matter hour by hour which can be stored or transported for image analysis in another area. Research is continuing in the counting and characterisation of urban aerosol by number of which this study has made an initial attempt and the method is open to development.

CHAPTER THREE
Experimental Methods for Urban Aerosol Analysis

3.1   Introduction

The size, shape and number of urban aerosol are important parameters which determine its health impact (Seaton *et al.*, 1995; QUARG, 1996; *cf.* Section 1.1.2).   Microscopy and electron microscopy can be used in the analysis of these factors (Waller, 1967; BéruBé *et al.*, 1997; Battarbee *et al.*, 1997).   There are specific problems associated with the representative sampling and analysis of urban aerosol for electron microscopy (*cf.* Section 1.4.2).   Membrane filters may be used for the efficient sampling of aerosol for SEM, but the lower limit of resolution is usually above the modal size of urban aerosol (Murphy, 1984; Katrinak *et al.*, 1995; *cf.* Section 1.4.2).   Post sampling processing of filters may be used to make analysis using TEM possible, thus allowing resolution of nano-meter size particles (Spurney, 1994).   However this process can cause sample artefacts and is thus not best for detailed morphological analysis of aerosol (Robards and Wilson, 1993).   Direct sampling methods of aerosol for TEM have been developed but are either inefficient for fine particles (Farrants *et al.*, 1988) or use high temperatures which may affect particle morphology (Maynard, 1995).   Thus as part of this research a method has been developed to directly sample fine and ultra fine urban aerosol for TEM whilst fulfilling aims of: collecting a representative of sample, portability, low cost and ease of use.

The application of fractal geometry to the measurement of engine particles has received some attention (Kaye, 1993; Colbeck *et al.*, 1997; Skillas *et al.*, 1998), whilst application to urban aerosol has had little interest (Katrinak *et al.*, 1993; *cf.* Section 1.5).   The fractal geometry of a particle is directly related to its physical properties (Nyeki and Colbeck, 1994), it can give insights in to the formation dynamics (Kaye and Clark, 1991; Katrinak *et al.*, 1993) and thus can be used to indicate particle sources (Katrinak *et al.*, 1993; *cf.* Section 1.5).   The measurement of fractal morphology is therefore very useful, but has a number of complexities.   Information is lost in analysis of the morphology of three

dimensional particles from two dimensional images, which has to be accounted for (Kaye, 1993). This work has applied two fractal measures to the analysis of urban aerosol and a quantification of occlusion effects has also been made.

This chapter details the experimental techniques used throughout in the analysis of aerosol in this research and is in six sections. Sampling and Treatment are discussed in Section 3.2. The Electron microscope facilities and the application of TEM to aerosol analysis are described in Sections 3.3 and 3.4, respectively. Image analysis techniques are outlined in Section 3.5, and the application of fractal measures using image analysis in Section 3.6. The final section gives details of the statistical techniques used (*cf.* Section 3.7)

3.2   Experimental Methods: Sampling and Treatment

3.2.1   Aerosol Sampling Apparatus

Two portable sampling pumps were used to collect aerosol samples, an AS808 (Aztec Instruments Ltd), and a MCS 10 Portable Sampler (SKC Ltd Cat no.901-10, Dorset, UK). Both were used at sampling rates between 2 and 10 l min^{-1} over periods ranging from 30 seconds to 2 hours. The pump flow was checked using a flow meter before and after sampling. The short time periods involved meant that the decrease in flow was not measurable. The accuracy of flow was controlled to $\pm$ 0.25 l min^{-1} set using the flow meter.

Cyclone sampling heads were used for all sampling. The cyclone used was the European Cyclone sampling head (SKC Cat No. 225-69, Dorset, UK). It is made in conductive plastic to minimise static build up and varying the flow rate enables different fractions of the aerosol to be collected. When used at a flow rate of 1.9 l min^{-1} the particle sampling efficiency follows the British Medical Research Council (BMRC) curve, with a 50% efficiency at 5 microns (Vincent, 1989). This curve assumes an efficiency of close to 100%

for < 1μm particles, thus the number and distribution of particles reaching the filter is representative of a < 5 μm aerosol.

3.2.2 SEM sampling and Coating

Aerosol samples for SEM were made using the cyclone sampling head (*cf.* Section 3.2.1) loaded with filter or loaded with the direct sampling set up (*cf.* Section 3.2.3.2).

3.2.2.1 Filtration

Whatman PTFE membrane filters and Whatman Cellulose filters were initially used but the filter structure was found not to be suitable for scanning electron microscopy (SEM). Cellulose and PTFE membrane filters have a highly three dimensional structure, as in Figure 3.1 a, making any particle analysis difficult. Whatman Cyclopore membrane filters (Whatman Cat no. 7060-2501) were established to be most suitable for SEM and are commonly known as nuclepore filters. These filters are thin (7-20μm) and microporous with round cylindrical pores and a flat surface, shown in Figure 3.1b. These allow the collection of particles with a high degree of certainty and a close to theoretical particle to membrane interaction (Spurny and Lodge, 1968; Fukami, 1992). The smooth surface allows all particles collected to be viewed in the same plane of focus and there are no hidden particles within the structure of the filter as in fibrous filters.
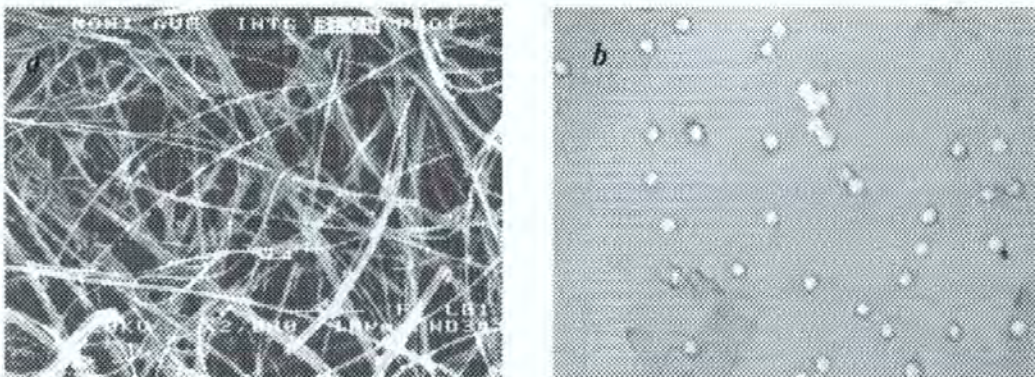
Figure 3.1 Scanning micrograph of (a)Glassfibre filter and (b) Cyclopore filter (pores 100nm)

The filtration of particles is governed by the fundamental physical properties of aerosol which allow particles to be removed from the air stream (*cf.* Section 1.2.4). The efficiency of a 0.1 μm nuclepore (cyclopore) filter has been calculated at approximately 100%. Aerosols larger than the pore size are collected on the filter. Aerosols smaller than the pore size are collected by diffusion deposition. (Fukami, 1992).

3.2.2.2 Coating

For SEM a filter piece must be cut to a size approximately 8 x 8 mm, the filter piece was attached to the stub using a carbon adhesive disc (G3347 AGAR) and Acheson 915 silver DAG (G3648 AGAR). The sample was coated with a conductive surface which allows any charge build up to dissipate. Charging is characterised by a very bright area in the image caused by the deflection of any electrons which were scanning the area in question.

Sample stubs were coated in gold initially in a POLARON SEM coating unit E5100 with Film thickness monitor E5500 (Polaron Equipment Ltd., Hertfordshire, UK) with Edwards High Vacuum pump EDM2 (Edwards High Vacuum, BOC Ltd., Sussex, UK). Latterly gold coating was made in an EMITECH K550 (EMITECH Ltd., Kent, UK) with Edwards RV5 pump (Edwards High Vacuum, BOC Ltd., Sussex, UK). Typical coatings were 5 - 10nm in thickness. Gold is very good for preventing charging but obscures elemental information, if EDXS is to performed.

Carbon coating was carried out on a variety of instruments. An Edwards TB 500 sputter coating unit was used for a rough deposition of carbon for SEM at 0.05 torr vacuum. Higher quality carbon coating required the use of an Edwards 306 or an Auto Edwards 306 carbon coating unit operating at between 10^{-4} and 10^{-5} torr vacuum. Both of these units use

high temperature evaporation of carbon, which then coats every available surface within the vacuum. The vacuum chamber in the Edwards 306 was achieved using a diffusion pump, and in the Auto Edwards 306 using a turbo pump. Carbon coating is less good at preventing charging but does not obscure the elemental nature of the sample as greatly as the gold coat.

3.2.3 Sampling for Transmission Electron Microscopy (TEM)

Aerosol was collected on a 0.1 μm nuclepore filter (NPF) and coated with a carbon film. The NPF was dissolved leaving the carbon film and particles intact. Dissolution of the filter was performed in a Jaffe Washer using a stainless steel mesh bridge (Catalogue no. G252, AGAR) and chloroform (AnalaR, BDH, Poole, UK) atmosphere as in Figure 3.2. This preparatory stage subjects the collected aerosol to a low pressure coating process and also to chloroform. The low pressure and the solvent may both cause particle collapse, thus the open structure of urban aerosol may be obscured (Robards and Wilson, 1993). To reduce the likelihood of this problem, PM_{10} may be directly collected onto TEM grids for immediate analysis.
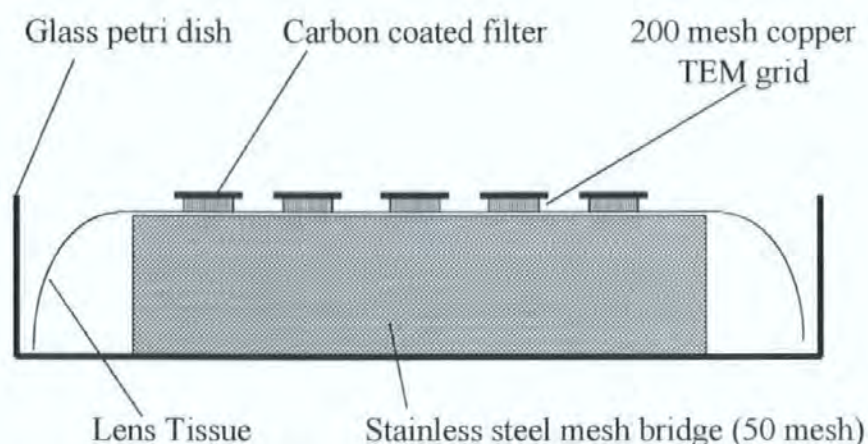
Figure 3.2 Design of the Jaffe washer used in the preparation of clean Porous Carbon Film (PCF) and Nulcepore Filter (NPF) collected samples for TEM

3.2.3.1 Porous Carbon Film collection of Aerosol

The direct sampling developed here was designed to fulfil the collection of a representative aerosol sample, in reasonable quantities for analysis, with the minimum of particle structure interference, to be simple in construction, low cost and portable.

Development was made of a porous carbon film with known filtration characteristics, and transparent to a TEM beam (cf. Section 3.3.2). The Jaffe wash method and the direct method of sampling both require the use of carbon films extensively. Initially a carbon film using an Edward TB 500 sputter-coating unit was used, however this produced films of very low quality and not transparent to the TEM electron beam. Higher quality carbon films were produced using an Auto 306 Edwards coating unit. It was found by a number of trials that the optimum positioning of carbon source and filter substrate was upward coating on to a filter (10-15cm separation), held in place using a specially designed holder. Upward coating was used to reduce contamination of the thin carbon films by large carbon particles settling out on to the filter. Early trials found that a very thin film (ca. 10 nm) of carbon was the best, surviving filter dissolution and giving good transparency on the TEM. On replacement of the original carbon rods, it was found that this thickness of film could then not survive the nuclepore filter dissolution. Again after further trials a film thickness of 15-18nm was used. The Auto 306 Edwards was not available for most of the study period and an Edwards 306 Carbon coating unit was used. This unit is not automated but did not take significantly more time to use and the quality of films produced were comparable in stability and condition.

3.2.3.2 Procedure of Porous Carbon Film preparation and Sampling

A 0.1 μm nuclepore filter (NPF) was coated with carbon to 15-20 nm in an Edwards 306 coating unit. The filter was cut in pieces and placed on top of 200 mesh TEM grids in the

Jaffe washing apparatus (*cf.* Figure 3.2). Adequate washing took at least 24 hours to remove the polycarbonate film and leave a porous carbon film (PCF) over the copper grid. The film was checked for quality and a blank count of particles on the grid was made using a Jeol 2000 ex II TEM at 200kV. Counting was performed at 40K including all particles between 0.02-10 microns in 10 areas (1.5 μm^2) on 15 different grid squares. Using an analysis of variance (ANOVA), the variation in count between different grid squares was examined to check that particle distribution across the film was uniform. In the case of a non uniform count a Dixons Q test removed the outlying group of data or the film was discarded and another used. By this procedure a clean PCF was produced which had a regular pore size of 0.1 μm for the filtration of particles (*cf.* Figure 3.1b). The PCF will have the same pore-size and therefore the same filtration character as the NPF that is used to make it (*cf.* Section 3.2.2.1).

A clean PCF was attached to another clean NPF using carbon cement around the edges of the grid. Care was paramount in this procedure to prevent the large proportion of the PCF becoming contaminated with the cement. Filter and attached grid were used in a 5 μm cyclone sampling head at 1.9 l min^{-1}. A cyclone sampling head causes the air flow to follow a spiral path before reaching the filter. The centrifugal force acting on the particles causes the larger particles with a greater momentum to be removed from the air stream and in to a grit pot, so preventing the filter from overloading.

The efficiency of collection was determined by comparison of aerosol collected using the Jaffe washing method and the porous carbon film collection method as described above. The sampling site was Charles Cross, Plymouth, which has high traffic flow at most times of the day. A nearby junction on Cobourg street, Plymouth receives traffic from Charles Cross and has in excess of 1000 vehicles per hour passing through during the working day (Devon

County Council, 1996; cf. Figure 4.1, Section 4.2). Therefore Charles Cross is a suitable location to sample vehicle generated aerosol. During the collection of samples, weather conditions and other factors were noted for use in interpretation of the results.
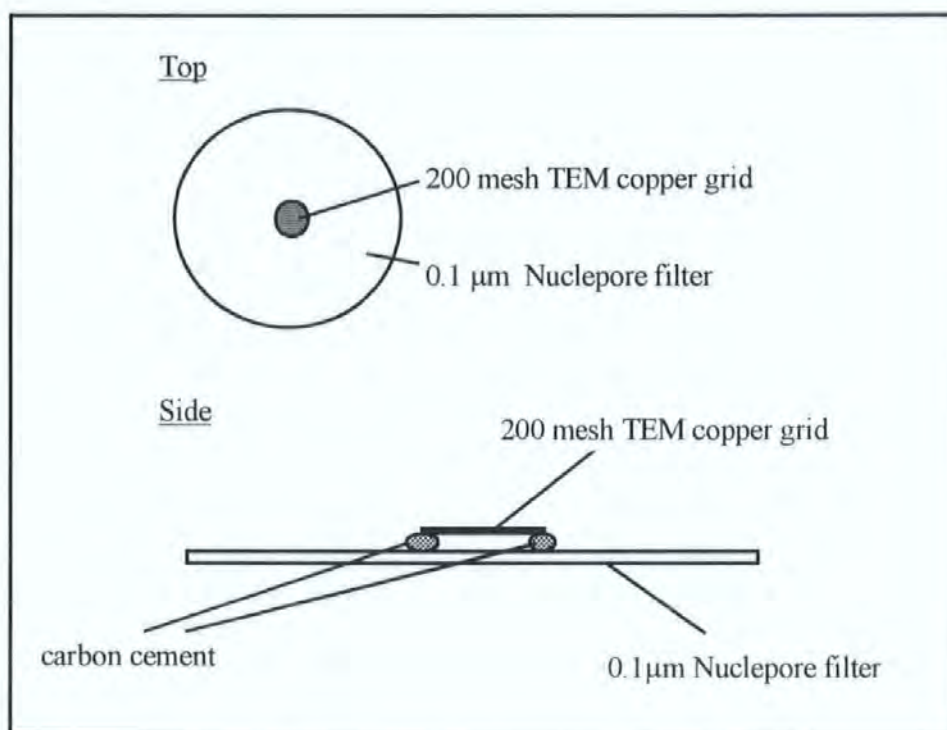
Figure 3.3 Diagram of the TEM grid attachment to the nuclepore filter for direct sampling

Immediately after sampling the PCF grid (*cf.* Figure 3.3) was removed and re-counted as described and a PM_{10} count calculated by subtracting the blank count. The NPF used in the sampling was coated in the auto Edwards 306 with 15-20 nm carbon. It was cut and placed on top of 200 mesh copper grid in the Jaffe Wash apparatus and again washed for at least 24 hours. A 0.1 μm NPF has a collection efficiency of approximately 100% because of diffusion deposition of particles smaller than the pore size (Fukami *et al.*, 1992). The PM_{10} count on the NPF washed samples was therefore considered to be the true count. The efficiency of the direct sampling of PM_{10} could then be calculated by dividing the direct

sample PM_{10} count by the true sample PM_{10} count. The efficiency of other film, calculated as a comparison, are shown in Table 3.1.

The bias of collection was determined by the comparison of >150nm particles to <150nm particles. This was calculated as the change in the proportion of fine (<150 nm) particles in the directly collected sample as compared to the proportion of fine particles in the NPF sample.

Film Type	Description	Efficiency of collection ± 95% confidence interval	Fine particles (<150 nm) bias. i.e. (directly sampled % of fine PM / NPF sampled % of fine PM)
Formvar (Robards & Wilson, 1993)	non-porous plastic film	$3.8 \pm 0.6\%$	0.7
Holy Carbon Film (AGAR)	Irregular pore size (0.1-5 µm) but not very clean	$9.9 \pm 2.9\%$	
Porous Carbon Film (PCF) (This research)	Regular pore size (0.1 µm)	$5.5 \pm 0.7\%$ $4.7 \pm 1.0\%$ $4.7 \pm 1.8\%$ $7.9 \pm 2.9\%$	1.06

Table 3.1 Efficiency and representative nature of direct sampling media

3.3   Electron Microscope Analysis Facilities

3.3.1   Scanning Electron Microscopy (SEM)

Three SEM instruments were used extensively during the period of study, a JEOL 5200, JEOL 5300 and a JEOL 6100 with EDXS and Link eXL analytical system. The JEOL 6100 was used most extensively having the greatest resolution of the SEM instruments. Typically the beam kV for the 6100 was set to 35kV allowing a useable resolution of 20-50nm. The theoretical resolution of such an instrument is much higher towards one or two nano-meters spatial resolution. In practice however, this quality of resolution is difficult and time

consuming to achieve. In consequence TEM was the preferred choice for nano-meter resolution of particles.

Scanning electron micrographs were obtained from the camera attachment to the JEOL 6100, both polaroid (SM 45150) and roll film (MP 35031) attachments were used. Photographic materials used were Polaroid 53, 4 x 5" coaterless film, 800/30 ISO, (Catalogue no. P9335, AGAR) and Kodak TMAX 100 Pro, TMX120, 100 ISO (AGAR). Development of roll film was made using ILFORD D19 developer and Kodak Uni Fix. Micrographs were enlarged using a Devere 504 enlarger (AGAR) and ILFORD 165 x 216 mm glossy 100 0-5 paper. Development was made using ILFORD paper developer (P9153 AGAR), Kodak Uni fix (AGAR P9140) and Agfa Stop Bath G182b (P9166). Development criteria were to produce high contrast pictures without obscuring any features.

Micrographs were also collected electronically through the Link eXL analytical system and directly from a monitor producing a TV signal of the SEM image. These images could be stored to disk, and transferred directly to image analysis software. Images captured in this way have the advantage of little degradation over time, no materials are used to capture the image and in most cases produce an end result more rapidly. The resolution of images is dependent on the lines scanned on the image. From a TV signal the image is collected quickly because the resolution (570 lines) is not great. Images with more lines taken from the Link eXL had a higher resolution but were more time consuming to collect.

Stereo pair images were collected using the JEOL 6100 to analyse the three dimensional nature of the particles captured. Images were collected either using negatives or electronic methods. An area of interest was found and centred and a micrograph of the area was taken. The sample was then tilted by 5-10 degrees, keeping the image centred on the same

area of interest. The image should stay central if eucentric alignment has been completed (Robards and Wilson, 1993). The stereo-pair may then be viewed in a number of ways. A stereopair may be viewed with the naked eye focusing each eye separately on each image this is not required however if stereo pair glasses or a viewer is available. A stereoviewer allows each eye to see only one of the images. The parallax difference in the images produced by the differences in angle convince the viewer that the image is three dimensional (Robards and Wilson, 1993). With knowledge of the parallax and the angle of difference between the pictures, measurements may be taken from a stereo pair of the depth of the object.

3.3.2 Transmission Electron Microscopy

Two Transmission Electron Microscopes were used, a JEOL 1200 ex II and a JEOL 2000 fx II.

3.3.2.1 JEOL 1200 ex II and Electronic Image Capture

The JEOL 1200 ex II was used, with beam voltage between 80 and 120 kV. Magnification used varied from 400 to 300,000 times on the microscope its self. Magnifications of 1,500,000 could be achieved using the TV mode, whilst reducing the spot size to increase the resolution, this was made possible by the video image enhancer.

Micrographs were captured using the camera attachment within the microscope. Kodak Electron Microscopy Film Estar Thick base 4489 65 x 90mm (P972 AGAR) was used for this purpose. Development and printing was the same as with SEM micrographs (cf. Section 3.3.1).

A system was developed to capture images from the microscope to a 486 PC using an video capture card (miroVIDEO DI video card, Miro Computer Products AG, Braunschweig, Germany). The video camera within the body of the microscope was situated below the TEM, in the same area as the photographic camera. Images were collected by switching to TV mode, which activated the video camera. Individual frames were collected from the TV signal using the image capture software on the computer and saved to disk for future use in image analysis. Contrast was optimised to give the maximum edge clarity as an aid to image analysis.

3.3.2.2 JEOL 2000 fx II

The JEOL 2000 fx II was used, with beam voltage between 120 and 200 kV. Magnification used varied from 400 to 600,000 times on the microscope its self. This microscope was equipped with a scanning transmission electron microscope (STEM) unit EM-ASID20, enabling high resolution SEM and STEM images simultaneously of the same area. Also two EDXS detectors were used, a high angle beryllium window detector, and a windowless detector at right angles to the TEM column.

Micrographs were obtained from the JEOL 2000 microscope in two ways. A normal TEM internal column camera was use to collect TEM micrographs. The STEM unit was equipped with camera attachment allowing roll film (Jeol MP 35031) or Polaroid (SM 45150) camera body attachment, this unit recorded scanning and scanning transmission micrographs. Using the STEM facility with the EDXS system an area of image could be selected in spot mode for elemental analysis. Morphological and elemental analysis of the same particle could be made using the micrographs and EDXS in tandem.

Three guidelines were followed during the analysis. For EDXS qualitative analysis a significant peak should be 3 times the standard deviation of the background, the total count rate was kept below 3000 s^{-1} for best energy resolution and the EDXS was be calibrated within 10 eV of the tabulated literature values (Newbury *et al.*, 1981).

3.4 Application of Transmission Electron Microscopy to Aerosol Analysis

3.4.1 When is a Particle a Particle?

The identification of discrete particles for analysis is obvious at scales of a few microns (*cf.* Figure 3.4), but as shown in Figure 3.5, at scales of a few nano-meters identification can be more difficult. The edges of particles are so thin that there is no distinct visual break between the background matrix and the particle in question. A useful definition of a particle is a grouping of molecules that exceed a certain minimum size or which maintains its integrity for a certain minimum time (Twomey, 1977). Twomey (1977) suggests that a minimum size of 1 nm or 10^{-9} m is useful although particles of this size are short lived, adhering strongly to surfaces within seconds and coagulating quickly.
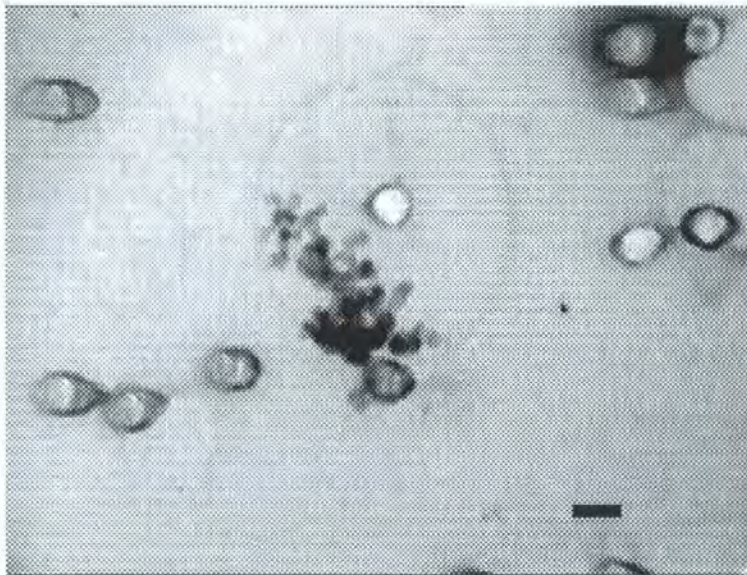
Figure 3.4 Easily identifiable micron sized agglomerate particle, scale bar =100nm
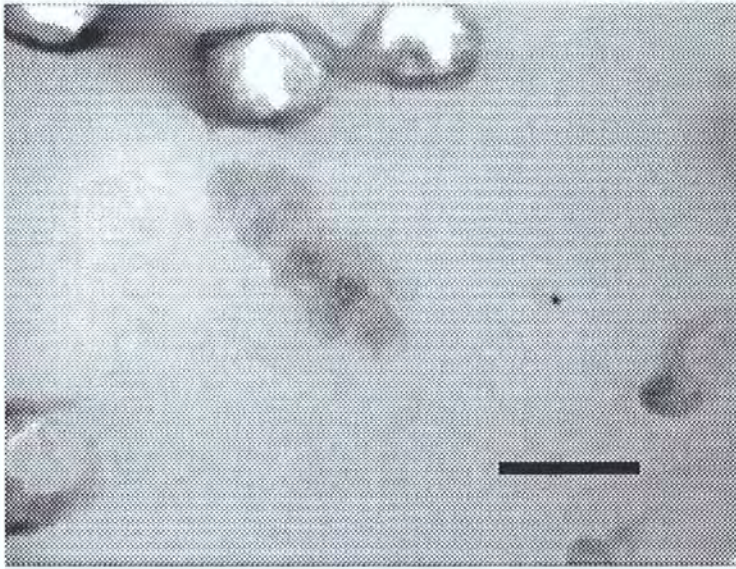
Figure 3.5 Sub-micron particle with undefined edges, scale bar = 100nm

For this study certain irreducible conditions for particle identification were imposed. Particles had to be stable in the vacuum and in the electron beam of the microscope for at least long enough to collect a micrograph. This was not the case for some particles which were vaporised in the beam, which accounted for much less than *ca.* 1% of particles examined. There is also a proportion of volatile particles which can never be seen under high vacuum TEM conditions. In general particle size had to be greater than two or three nano-meters in its longest aspect to be distinguished as a particle. Operator experience was relied upon to distinguish any dubious particles although in the majority of cases identification of particles was obvious.

3.4.2 Morphological and EDXS analysis on the 2000

Early work involved morphological and elemental analysis using the JEOL 2000 ex II (*cf.* Section 3.3.2.2). Direct particle collection was used in confidence that the particle structure was changed as little as possible. After counting particles on the grid, random particles or groups of particles, were selected at x100,000 magnification using the TEM and physical movement of the sample. When an object was found one or more pictures were taken in

TEM mode, the TEM was then switched to Scanning TEM (STEM) mode with electron microprobe. Using the electron microprobe the area of the particle was selected for Energy Dispersive X-ray spectroscopy (EDXS). An EDXS spectra was collected for 100 seconds and stored. Negatives were developed and then subjected to image analysis, to measure the morphological nature of particles collected (*cf.* Section 3.5.1.2).

3.4.3 JEOL 1200 Image Capture Developed

The method described in Section 3.4.2 was very time consuming and the quantity of analysis obtained was small, whilst being highly detailed. A further method was developed to concentrate on the morphological analysis of particles.

After counting particles on the grid, random particles or groups of particles, were selected at x100,000 magnification using the TEM and physical movement of the sample. The physical movement of the sample has a certain random nature built in, but in reality the random particle selection is as the particles are encountered. The random nature is therefore reliant on a random and uniform distribution of particles on the porous carbon film.

3.4.3.1 Fixed Magnification Analysis

Initially micrographs of particles were all taken at 100,000 magnification, thereby ensuring that all image analysis measurement was the same. This method of fixed magnification pictures is useful for making a series of linear or area measurements for micrographs, but the particles are not normalised for the fractal measurement so only fractal measurements of particles of the same size may be compared. True fractals are not size dependent (Kaye, 1993), but there are limitations of box measurement. The finite box sizes used for measurement mean that large boxes are not very useful for measuring very small images and

large particle images induce edge effects in analysis. Feret diameter normalisation of particles of different sizes is needed for comparable fractal measurements.

3.4.3.2 Normalised Analysis

Normalisation of particles according to their maximum feret diameter was performed to allow comparable measures of fractal dimensions. Normalisation of feret diameters was made as closely as possible within the limitations of fixed integer magnifications of the TEM. In practical terms normalisation was made using a guide ring attached to the monitor within which particle were centred and normalised. The normal size was designed to be 30-40% of the total width of the image. Normalised particles of this size could be measured on the image analyser without being too small for accurate measurement using the series of finite square sizes or too large for edge effect interference from the image analyser frame of measurement.

3.4.3.3 Comparison of Normalised *vs.* Fixed Magnification

The choice between normalised and fixed magnification was difficult because both have useful advantages and conversely both have disadvantages. Normalisation allows fractal comparison between groups of particles, it is a standard for fractal work (Kaye, 1993, Katrinak *et al.*, 1993) and measurement of fine particle detail is made. There is some error in normalisation, caused by the limited choice of magnifications on the TEM (*cf.* Section 3.4.3.2), and linear measurements using image analysis have to be calibrated for each individual picture. Without normalisation fractal comparison can only be made between particles of the same size, but data on the textural nature of particles is more comparable. A series of textural qualities caused by the carbon cenospheres are more easily identified with a fixed magnification analysis, occurring at the same resolution of measure. Also linear measurements are more easily made without normalisation. Normalisation was preferred

because of the advantages in group analysis which was required to group particles as to their sources from their morphological character. Table 3.2 compares the average density fractal dimension and perimeter fractal dimension measured using either fixed focus or normalised particle images.

Sampling site and fractal dimension measured	Fixed	Variable
Road PFD	1.18 ± 0.10	1.20 ± 0.10
Road DFD	1.77 ± 0.07	1.54 ± 0.10
Background PFD	1.14 ± 0.17	1.13 ± 0.10
Background DFD	1.76 ± 0.09	1.55 ± 0.08

Table 3.2 Comparison of means from fixed and variable analysis of the same particles

The greatest effect in use of normalised analysis is on the measurement of the density fractal dimension (*cf.* Table 3.2). The average DFD in the normalised analysis is 0.2 lower than the fixed magnification method. The reduction being probably due to the elimination of both edge effects and the use of oversized boxes on small particles. Particles in the fixed analysis method may fill the analysis area and the edge of this area may limit the number of boxes used as a measure. This limitation causes an over estimate of the density fractal dimension. Figures 3.6 and 3.7 show the comparison of fixed and normalised analysis for the same particles. The chart of PFD (*cf.* Figure 3.6) suggests there is some correlation, however weak, between values gained in fixed and normalised methods. Figure 3.7 of DFD shows no clear correlation of methods at all. It is clear that all fractal measurement methods should be reported in detail, thus facilitating the comparison of research which may produce very different results.
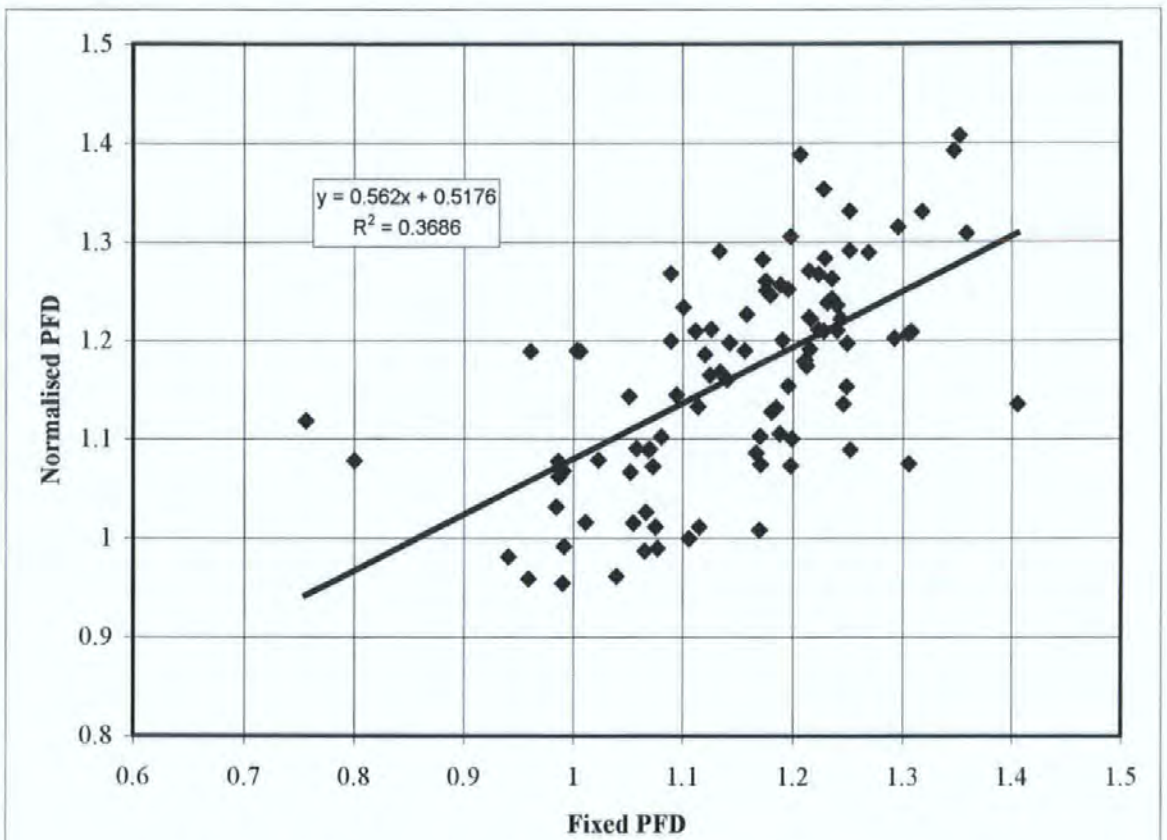
Figure 3.6 Comparison of Perimeter Fractal Dimension as measured by Fixed magnification and normalised image methods.
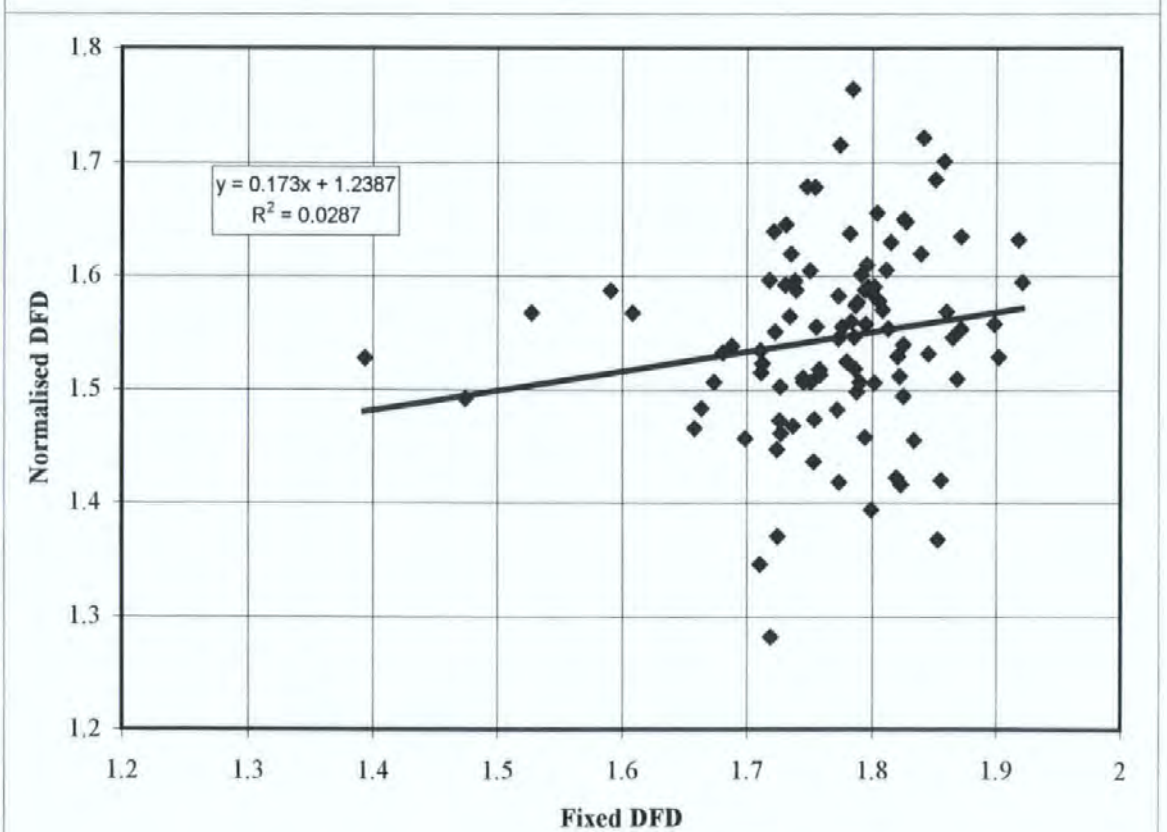
Figure 3.7 Comparison of Density Fractal Dimension as measured by Fixed magnification and normalised image methods

3.4.3.4 Image Calibration

For normalised images particle size was measured using Image Tool (*cf.* Section 3.5.2). The calibration of images was made at magnifications ranging from 2.5K times to 15K with 2160 lines/mm cross grating (S106 AGAR). Magnifications from 15K to 200K were calibrated with ferritin quad structure with 1.25 nm spacing (S126 AGAR).

3.4.4 Occlusion Study

Occlusion effects can lower the apparent roughness of an agglomerate when projected into two dimensions (Samson *et al.*, 1987; Kaye *et al.*, 1994; Wu *et al.*, 1994). The three dimensional nature of particles is not taken into account when analysed on a two dimensional TEM picture. One particle (AD1113), is shown in Figure 3.8, part a) displays the large variation in particle morphology and size when viewed from different angles and part b) is a stereo-pair which reveals the highly three dimensional nature of the particle not accounted for in two dimensional measurements. The change in two dimensional density and perimeter fractal dimensions (*cf.* Section 3.6) can be measured. This was performed in order to quantify the region of error of using a single two dimensional image to account for the fractal dimension of a particle. Measurements were made of perimeter fractal dimension, density fractal dimension and equivalent circle diameter for seven selected agglomerates at various angles of observation. The variation in these measurements with changing angle is shown in Figures 3.9 ,3.10 and 3.11. Although all measurements were still made on two dimensional projections, the statistical variation in fractal dimensions and diameter for the same agglomerate at different angles of observation is shown in Table 3.3. It is also possible to study the occlusion effect at $0°$ as opposed to the average fractal dimensions as seen from a number of angles (cf. Table 3.4).
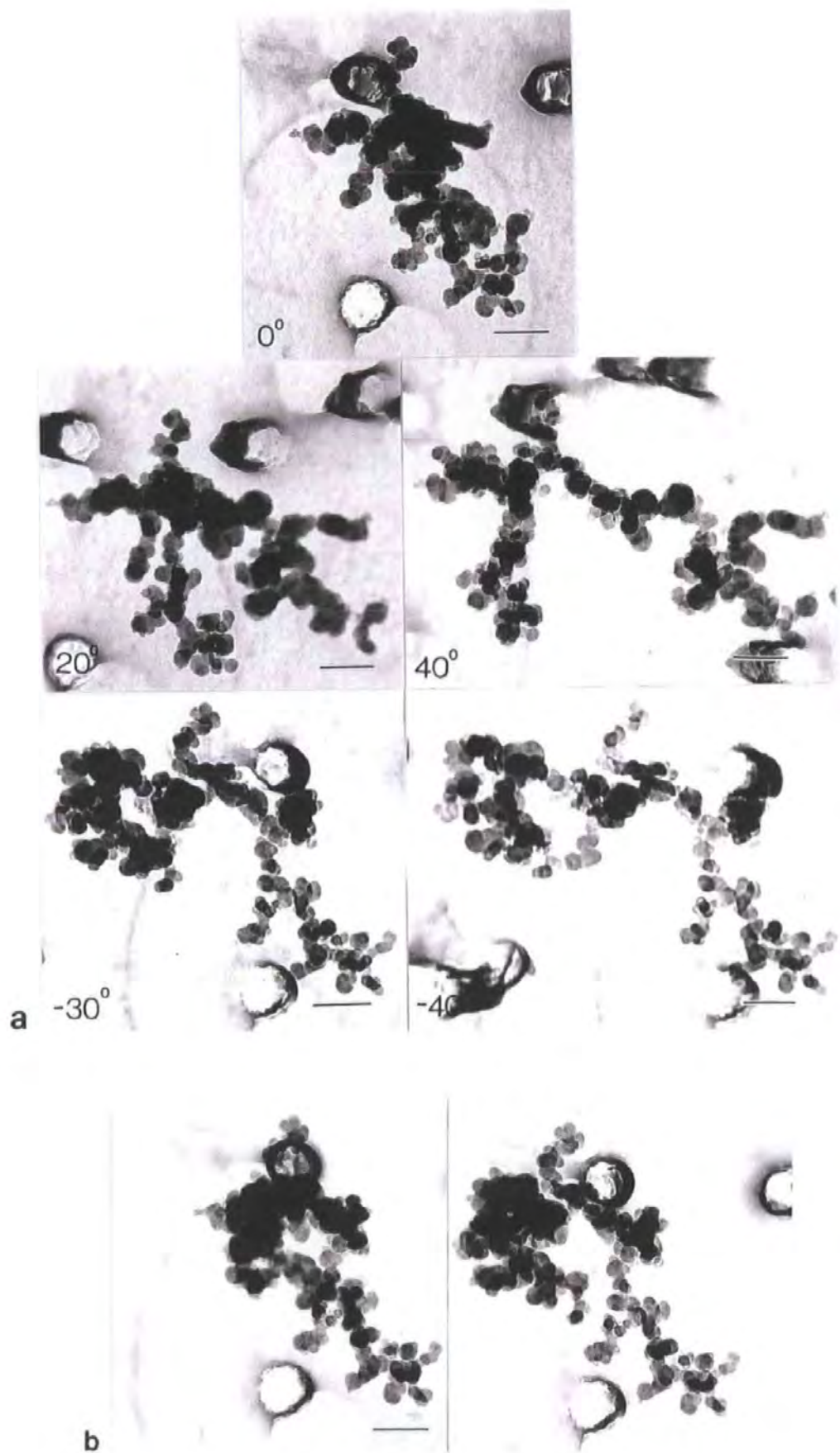
Figure 3.8 Illustration of the three dimensional nature of agglomerate particles. (a) a series of TEM micrographs of particle AD1113 showing the high variability of particle shape and size when viewed from changing angles, scale bar = 100nm. (b) A stereo picture of AD1113 which may be viewed to give a true three dimensional impression of the particle.
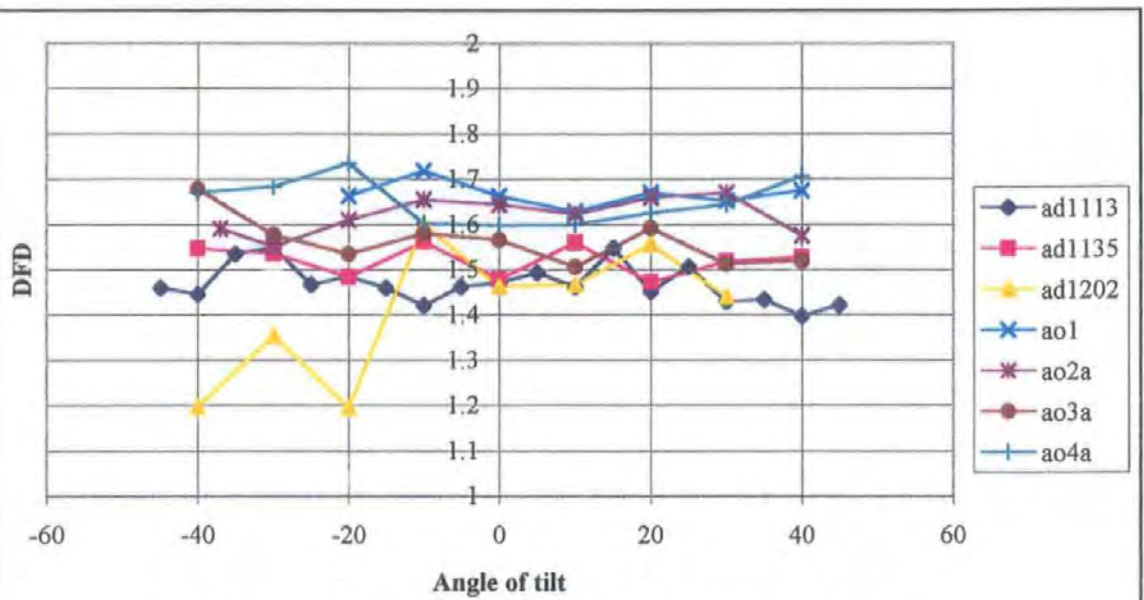
Figure 3.9 Density fractal dimension vs Tilt angle
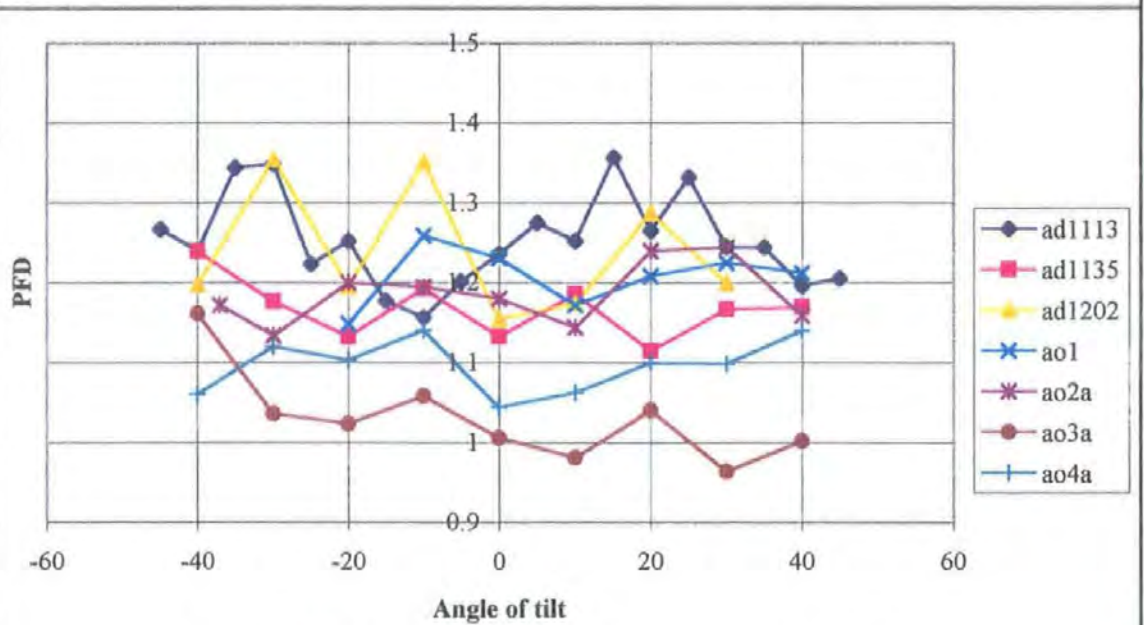
Figure 3.10 Perimeter fractal dimension vs Tilt angle
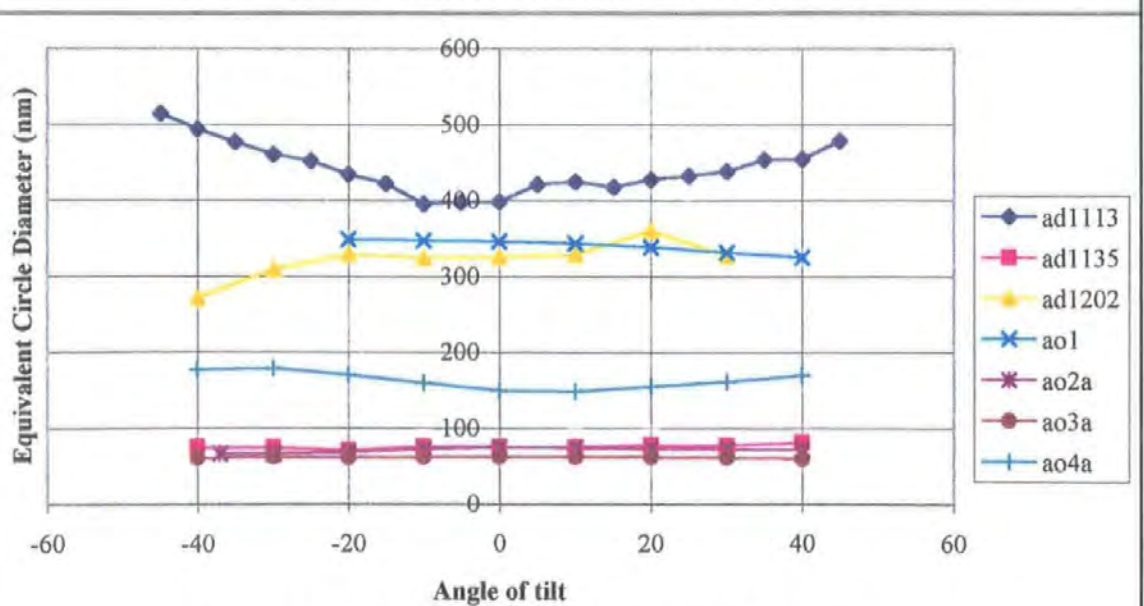
Figure 3.11 Equivalent Circle Diameter vs Tilt angle

Occlusion Particle	DFD	± DFD S.D. (RSD)	PFD	± PFD S.D (RSD)	Diameter	± Diameter S.D. (RSD)
ad1113 (19)	1.47	0.043 (2.7%)	1.25	0.058 (4.6%)	441	32.7 (7.4%)
ad1135 (9)	1.52	0.035 (2.3%)	1.17	0.038 (3.6%)	75.6	2.96 (3.9%)
ad1202 (8)	1.50	0.061 (4.1%)	1.24	0.080 (6.5%)	322	24.9 (7.7%)
Ao1 (7)	1.66	0.027 (1.6%)	1.21	0.037 (3.1%)	340	9.03 (2.7%)
Ao2 (9)	1.62	0.041 (2.5%)	1.19	0.039 (3.3%)	71.3	3.31 (4.6%)
Ao3 (9)	1.56	0.054 (3.5%)	1.03	0.057 (5.5%)	61.7	0.795 (1.3%)
Ao4 (9)	1.65	0.050 (3.0%)	1.10	0.035 (3.2%)	163	11.2 (6.8%)
Average	1.57	0.046 (2.9%)	1.17	0.052 (4.4%)	210	16.5 (7.9%)
Ave of errors	n/a	0.044 (3.2%)	n/a	0.049 (4.9%)	n/a	14.5 (4.9%)

Table 3.3 of Average Fractal dimensions and diameter for selected particles measured at a variety of sample orientations to the microscope beam with standard deviations (SD) and relative standard deviations in brackets (RSD).

The mean relative standard deviation of the fractal dimensions and diameter is less than ± 5% and consistent in magnitude at different agglomerate sizes (*cf.* Table 3.3).

Particle No.	DFD at 0°	DFD (ave)	DFD diff	PFD at 0°	PFD (ave)	PFD diff.	diam. at 0°	diam. (ave)	diam. diff.
ad1113	1.473	1.47	0.003	1.237	1.25	-0.014	434	441	-7
ad1135	1.480	1.52	-0.04	1.133	1.17	-0.037	70.5	75.6	-5.1
ad1202	1.463	1.50	-0.037	1.155	1.24	-0.085	329	322	7
Ao1	1.663	1.67	-0.007	1.231	1.21	0.021	349	340	9
Ao2	1.644	1.62	0.024	1.180	1.19	0.010	68.3	71.3	-3
Ao3	1.566	1.56	0.006	1.006	1.03	-0.024	61.8	61.7	0.1
Ao4	1.598	1.65	-0.052	1.044	1.096	-0.052	170	163	7
Ave.			-0.002 ± 0.03 (-0.03%)			-0.029 ± 0.03 (-2.2%)			1.1 ± 6.5 (-0.5%)

Table 3.4 The difference between average measurements from a range of sample angles and the measurement made at 0° tilt.

Matched pair t-tests were performed comparing the average fractal dimension with the measurement at zero degrees to examine if the occlusion effect decreases the measured values of DFD, PFD or diameter (cf. Table 3.4). Using a one tailed test looking for a significantly lower values than the average, the difference was not significant in the case of

DFD (p = -1.37) or the diameter (p = 0.46). For the PFD the test statistic (p) was -2.234 with 6 degrees of freedom, so greater than the t value at 95% confidence (p $_{0.05,6}$ = -1.94). Therefore the PFD values at 0° are significantly lower than the average PFD values. The average PFD under calculation is -0.029 ± 0.034 (cf. Table 3.4). Although statistically significant this is only 2-3% of the typical PFD values as calculated by a single observation at 0° and is lower than the average standard deviation of PFD values at different angles (cf. Table 3.3).

3.5 Image Analysis

Image analysis is simply the measurement of certain parameters i.e. length of an image. This is a time consuming process if performed manually, but using image analysis software allows complex processing and measurement to be conducted quickly. Dedicated systems such as the Cambridge Quantimet 540 image analyser which was used extensively in this work (cf. Section 3.5.1), or image analysis software for use on an IBM compatible PC such as UTHSCSA Image Tool (cf. Section 3.5.2), may be used for this purpose.

3.5.1 Quantimet 540

Fractal measurements were made using a Quantimet 540 image analyser. Images were either acquired from TEM negatives using a CCD camera or from Zip disk (iomega Ltd., Utah, US). Grey image enhancement, detection, binary image modification and measurement were all performed on this instrument as illustrated in Figure 3.12.
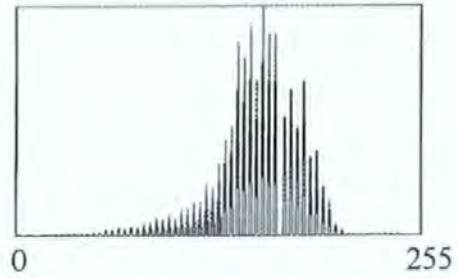
Collected Image
8 bit grey scale tiff
594x444 pixels

Thresholding

Binary
image
modification
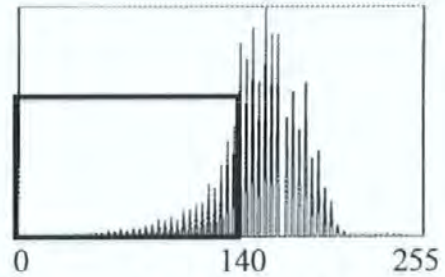
Image after selection of a maximum
threshold greyscale value.
Here all pixels below 140 grey scale
value are selected and shown in black

Binary image after the selection of
the area for analysis and removal of
interference

*Figure 3.12 Image processing, showing thresholding and modification
of the grey scale image*

3.5.1.1 Macro Programs for Automated Image Analysis

Automation of image analysis is the great advantage of computer use. The Quantimet 540 uses a special Quantimet 540 QUIC BASIC (QBASIC) language to automate image analysis processes. Programs were designed to allow user input to decide on grey image enhancement and choices in binary image modification and detection, with measurement functions completely automated for speed (*cf.* Figure 3.12).

3.5.1.2 Procedure using Images on Negatives

The image analyser was set up and programmed to measure TEM negatives at x100,000 magnification. Initially QBASIC macro named FRACBOX was used, this included the basic procedures of setting the image and measurement frames, acquisition and image detection with the facility to manually select areas of interest (*cf.* Figure 3.12). Measurement was made automatically, overlaying 5 different grid sizes for fractal measurement (*cf.* Figure 3.13), and counting the boxes. FRACBOX2 developed the facility for the user to change the image set up for best contrast and brightness in acquisition and a change in detection to clean the image. FRACBOX3 included a function to fill holes in particle areas for detection. FRACBOX4 allowed a multi-detection of the negative for a better acquisition, this version was design to make a box count of the image outline as well as the whole area. FRACBOX5 allowed measurements to be saved directly to disk, this was the final version of image analysis programme using negatives.

The images were collected and stored on the computer through a macro camera directed at the negative on a light box. Fractal analysis was made using a box counting technique (*cf.* Figure 3.13) for the density fractal dimension and the changing measure in perimeter at different box sizes was noted for the calculation of the boundary fractal dimension.

• Binary image is overlaid with 5 grids of different square size
• DFD = count any squares touching the image.
• PFD = count squares touching image edge (not holes)

DFD   PFD
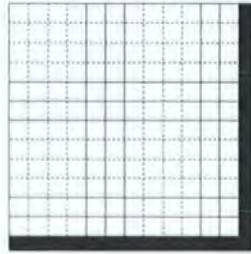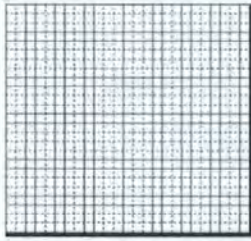
Density Fractal Dimension
• $Db = 2-s$
• s = slope of ln (box size) vs ln (n x box area)

Perimeter Fractal Dimension
• $Dp = 1-s$
• s = slope of ln (box size) vs ln (n x box size)

Density Fractal Dimension Chart

$y = 0.5516x + 8.0941$
$R^2 = 0.9213$

ln (n x box area)
ln box size

Perimeter Fractal Dimension Chart

$y = -0.1841x + 7.2451$
$R^2 = 0.7055$

ln (n x box size)
ln box size
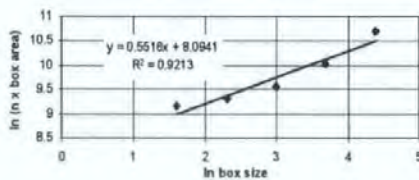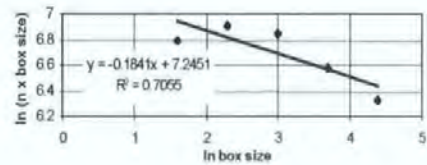
$Db = 2-0.5516 = \textbf{1.4484}$ $Dp = 1- -0.1841 = \textbf{1.1841}$

Figure 3.13 Image fractal analysis, using box counting

3.5.1.3 Procedure using Images on Disk

The measurement of images from disk was similar as from negative, the differences being in acquisition. FRACTIF5 allowed 8bit grey scale TIFF images to be imported for analysis similar to FRACBOX4. Image acquisition from Zip drive, measurement of boundary fractal dimension and saving to disk were included in FRACTIF6. FRACTIF7 had slightly changed detect levels so as no to automatically over-detect. FRACTIF8 was the final version of macro programme allowing images to be imported from hard disk. All programmes a presented in Appendix 1.

3.5.2 Image tool

Some image analysis was performed using UTHSCA Image Tool version 1.27 (developed at the University of Texas Health Science Centre at San Antonio, Texas. V1.27 and 2.00 alpha available from the Internet by anonymous FTP from http://ddsdx.uthscsa.edu/dig/itdesc.html). Measurement of equivalent circle diameters were made, with each magnification separately calibrated (cf. Section 3.4.3.4). Image Tool was also used for number counting of particles.

3.6   Fractal Measurement using Image Analysis

Measurement of the fractal dimensions of images have been made by other studies in a wide range of fields from coastlines to combustion products (Mandelbrot, 1977; Peitgen et al., 1992). They provide a useful measure of the morphology of an image (Schwarz and Exner, 1980). Fractal dimensions of agglomerate aerosol are directly related to their formation (Kaye and Clark, 1991) and fundamental physical properties (Colbeck and Wu, 1994). Fractal dimensions have been measured from images in two ways in this study: an area measurement, quantifying how the image fills space, known as a density fractal dimension (DFD) and a fractal measure quantifying the roughness or ruggedness of the image

boundary, known variously as the structural, boundary or perimeter fractal dimension (PFD). Both methods are shown in Figure 3.13.

For a statistically fractal (exactly self similar) object which is composed of N copies of itself each of which is scaled down by the ratio r, the fractal dimension D of an object may be described by the equation (Barnsley *et al.*, 1988):

- $1 = Nr^D$ (1)

Estimates of the fractal dimension (D) using a box counting method, shown in Figure 3.13, may be made for the Density (Db) and Perimeter (Dp) Fractal Dimensions thus:

Density Fractal Dimension (DFD) (Barnsley *et al.*, 1988)

- $N \propto r^{-Db}$ (2)

- $N = Cr^{-Db}$ (3)

N = Number of boxes covering any part of the image

Db = Density Fractal Dimension

C = constant

r = square size in pixels

Total area (A) covered as in Figure 3.13:

- $A = Nr^2 = Cr^{-Db}.r^2 = Cr^{2-Db}$ (4)

∴ applying the natural logarithm

- $ln\ A = 2-Db.ln\ r$ ∴ $2-Db = (\Delta ln\ A)/(\Delta ln\ r) = s$ (5)

s = slope in the ln A vs ln r chart (Figure 3.13)

- $Db = 2-s$ (6)

Perimeter Fractal Dimension (PFD)(Kaye, 1993; Barnsley *et al.*, 1988)

As in (1) and (2) where:

- $N = Cr^{-Dp}$ (7)

N = number of boxes covering any part of the image perimeter

Dp = Perimeter Fractal Dimension

C = constant

r = square size in pixels

Total perimeter (P) covered as in Figure 3.13:

- $P = Nr = Cr^{-Dp}.r = Cr^{1-Dp}$ (8)

- $ln\ P = 1-Dp.ln\ r$ $\therefore$ $1-Dp = (\Delta ln\ P)/(\Delta ln\ r) = s$ (9)

s = slope in ln P vs ln r chart

- $Dp = 1-s$ (10)

In practise Db (6) and Dp (10) are easily obtained from the ln A/ln r and ln P/ln r graph, examples are shown in Figure 3.13. In many cases in this research the ln/ln graph for a single particle exhibited different gradients, especially for the PFD as in Figure 3.13. Detailed research of this multiple fractal phenomenon has been made by other researchers for DFD (Katrinak *et al.*, 1993) and PFD (Kaye 1993; Kaye *et al.*, 1994). In general the low resolution part of the curve (larger ln r value) relates to the structural nature of the particle. The high resolution part of the curve (smaller ln r value) relates to the fine textural nature of the particles. For agglomerate particles the textural dimension can be non fractal because the self similarity breaks down at the resolution of the primary units. In other

research the multiple PFD has been used for particle characterisation (Kindratenko *et al.*, 1994; Xie *et al.*, 1994) but in this research a single average PFD is used. Normalisation means that the same box sizes may resolve different textural or structural qualities dependent of the size of the primary units and the overall agglomerate size. Thus for clarity one PFD is used which combines textural and structural effects and comparison of particles has been made within these ranges.

3.6.1 Measurement of Theoretical Fractals

Theoretical fractals are mathematical images produced by a set equation, which defines their fractal dimension. Measurement was made of three theoretical fractals with known dimensions. The Sierpinski gasket, shown in Figure 3.14 c, was used to determine the accuracy of density fractal measurement. A triadic and a quadratic island as shown in Figure 3.14 a and b, were measured to determine the accuracy of measurement of perimeter fractal dimensions.

From (1) $N \propto r^{-D}$ or $D = \log N/\log (1/r)$

Sierpinski gasket (Figure 3.14c)

- Area ~ Length^{DFD}

The Sierpinski gasket is made up of 3 parts scaled by a length ratio of 1/2 from the original

- Sierpinski gasket = log 3/log 2 = 1.58

Koch Islands (Figure 3.14a and b)

A triadic Koch curve or island it is comprised of N=4 sub-segments each scaled by ratio r=1/3 from the original. For the quadratic Koch island, it consists of N = 8 subsegments each scaled by a ratio r= 1/4

- Triadic Island PFD= log 4/log 3 = 1.26

- Quadratic Island PFD= log 8/ log 4 = 1.50

So knowing the Sierpinski Density fractal dimension = 1.58 and the Koch island fractal dimensions of triadic = 1.26 and quadratic = 1.50, the accuracy fractal dimension measurement using the box counting technique in this work may be discerned.
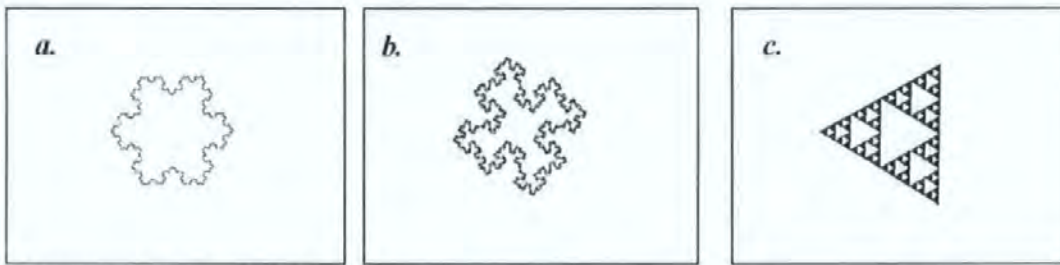
(Barnsley *et al.*, 1988)

Figure 3.14 A triadic Koch island (a), a quadratic Koch island (b)and a Siepenski gasket (c)

Each of the theoretical fractals were scanned on to disk from a pictorial image, this was done to simulate the process of saving a digital image from a non digital real image. Each image feret diameter was normalised to 1/3 of the image width in the same way as the images of particles collected (*cf.* Section 3.4.3.2). Analysis was performed using FRACTIF8, and the data compared with theoretical values (*cf.* Table 3.5).

Fractal	Measured fractal dimension	Theoretical	Difference	Underestimate
Sierpinski carpet	1.44	1.58	-0.14	9.1%
Quadratic	1.29	1.50	-0.21	13.9%
Triadic	1.19	1.26	-0.07	5.4%

Table 3.5 Theoretical fractal measurement using image analysis

There is a significant underestimate of the true theoretical dimension (*cf.* Table 3.5). This is due to the finite box sizes used in determination of the fractal dimension, edge effects and choice of centre (Katrinak *et al.*, 1994). Weber (1992) has also shown that density fractal dimensions may be underestimated by as much as 20% dependent upon the complexity of the structure (*cf.* Sections 3.4.4 and 3.6.2). More complex structures will be under estimated by a greater amount because of the limitations of using finite boxes to cover an image. Most of the perimeter fractal dimensions calculated in our study are close to that of the triadic island so we may infer an underestimate of 5-6 % in the measurement of the fractal, not including the occlusion effects (*cf.* Section 3.4.4).

3.6.2 Comparison of 2D and 3D density fractal dimensions

The density fractal dimensions calculated using image analysis are by definition limited to two dimensions so information is lost (*cf.* Section 3.4.4). The three dimensional density fractal dimension of agglomerates has been determined using a number of techniques, the aerodynamic diameter and the absolute mass (Nyeki and Colbeck, 1994), kinetic coagulation (Wu *et al.*, 1994), volume equivalent diameter and aerodynamic diameter (Colbeck and Wu, 1994; Wu and Colbeck, 1996) and from light scattering experiments (Gangopadhyay *et al.*, 1991; Sorensen *et al.*, 1992; Weber, 1992).

An electron micrograph of an agglomerate was provided by Ian Colbeck (University of Essex) with a known density fractal dimension as determined by the technique described in Colbeck *et al.*, (1997). The density fractal dimension was then measured using the method described in this work (*cf.* Section 3.5 and 3.6). A comparison of the DFD measured by three dimensional and two dimensional techniques is shown in Table 3.6.

Method	Density Fractal Dimension
Colbeck *et al.*, (1997)	2.3 ± 0.2
I.A. of 2D projection	1.54± 0.05
	1.7 ± 0.05 (adjusted according to underestimate[1])

1. Underestimate from section 3.6.1

Table 3.6 Comparison of fractal measurement techniques

With no adjustment according to the underestimate in this study (*cf.* Section 3.6.1), the difference between the methods is 0.66 (*ca.* 29% increase from 2D to 3D) or after adjustment this difference is 0.5 (*ca.* 22% increase). There is a loss of information of *ca.* 25% when the density fractal dimension is measured from a projected image. This will affect the sensitivity of this parameter and in this work will decrease the selective nature of the density fractal dimension in distinguishing different particle sources. The amount of information lost will be dependent on the density fractal dimension of the individual particle. The method used by Colbeck *et al.*, (1997) examined micron sized agglomerates with large three dimensional structures, so the loss of information owing to occlusion effects will be great. Smaller agglomerates or more planar agglomerates submicron in size, will have less convoluted three dimensional structures and so less information will be lost in projection. The particles examined in this work are all submicron, so it is reasonable that the loss in information will be unlikely to be as great as 25%. This is not quantifiable without a study of the loss of information from submicron particle projection.

3.7 Statistical Techniques

Statistics and analysis were performed using Microsoft EXCEL 95 v7.0 also using xlSTAT Pro. v.2-v.3 (Fahmy, 1996). XLSTAT is a low cost, add in module for Microsoft EXCEL which allows advanced statistical functions to be performed within the worksheet.

Various statistical techniques were used such as t-tests, matched pair t-tests and ANOVA. (Dowdy and Wearden, 1991; Miller and Miller, 1993), all in order to enhance the interpretation of the results.

CHAPTER FOUR
The Morphology and Sources of Urban Aerosol

4.1   Introduction

The size, shape and number of urban aerosol are of current concern in terms of air quality and public health (QUARG, 1996). However there have been few studies, previous to this work, of urban aerosol morphology (Waller *et al.*, 1967), and the fractal nature of urban aerosol (Katrinak *et al.*, 1993). No other studies have been made using fractal analysis to quantify the difference between aerosol morphology simultaneously at the roadside and in the background aerosol. Despite the number median urban aerosol size of *ca.* 100nm (COMEAP, 1995) and the public health concern over fine and ultra fine aerosol (Seaton *et al.*, 1995), other studies have only examined fractal particles of a mean size of one micron (Kindradeko *et al.*, 1994; Xie *et al.*, 1994).

In this work a simultaneous collection of roadside and background aerosol has been made (*cf.* Section 4.2). The novel technique for sampling of aerosol developed at the University of Plymouth (Dye *et al.*, 1997; *cf.* Chapter 3) has enabled the analysis of a representative aerosol (number median *ca.* 80nm). A measurement of the density fractal dimension, perimeter fractal dimension and the size of this aerosol was subsequently made using computer aided image analysis (*cf.* Section 3.6). The aim of this work has been to identify any ageing processes acting upon the aerosol and ultimately identify sources of aerosol (*cf.* Chapter 6).

4.2   Site Review

Samples of the urban ambient background aerosol were taken from the top of the Fitzroy building at the University of Plymouth, UK. (Figure 4.1) between December 1996 and July 1997.
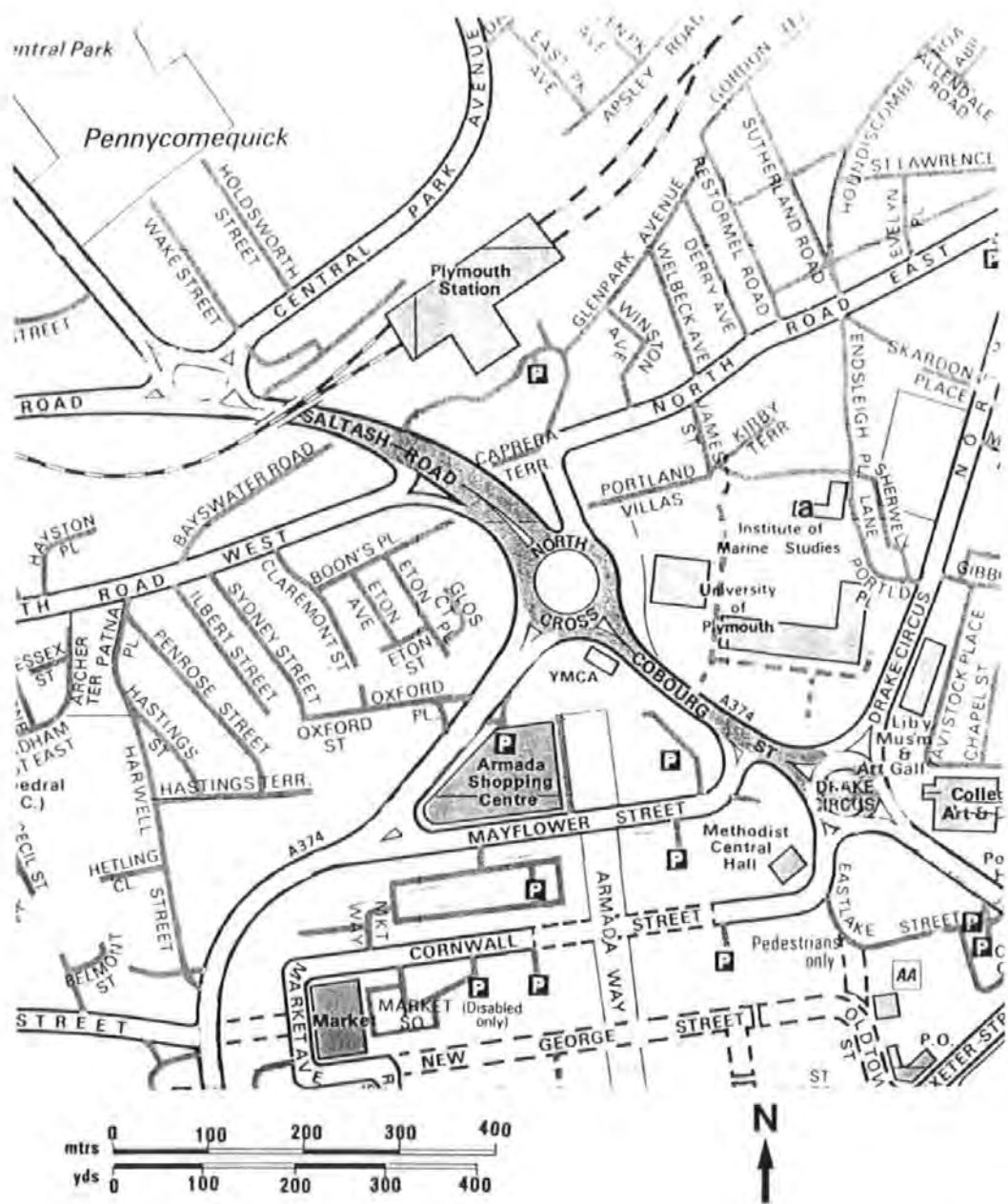
Figure 4.1 Map showing the background sampling site, (a) the Fitzroy building at the University of Plymouth, and the roadside sampling site (shaded area) along Saltash road and Cobourg street. (Automobile Association, 1995)

Urban background sites are supposed to represent typical air pollution exposure conditions for members of the public. The site should not be within:

30m of a very busy road (>30,000 vehicles/day)

20m of a busy road (10,000-30,000 vehicle/day)

10m of any other road (< 10,000 vehicles/day)

(QUARG, 1993 a)

The map in figure 4.1 shows that the closest road to the Fitzroy building is over 150m away, and has a load of between 10,000 and 20,000 vehicles per day, therefore this site fits the criteria of an urban background site. It was also the site of meteorological readings made using an automatic weather station (Meteorological Data Archive, University of Plymouth) and the Burkard Spore trap (*cf.* Chapter 2). The site is in an elevated position of *ca.* 30m and is used on the assumption that the boundary layer is always well mixed (Oke, 1978). For particles above *ca.* 1µm, in still air conditions over a period of days this assumption may not always be true (Twomey, 1977). Most of the particles analysed in this work were below 0.5µm and so any effect of elevation on number distribution is negligible.

Samples of the roadside aerosol were taken by Saltash Road and Coburg Street, Plymouth, UK (*cf.* Figure 4.1). These roads have a load of 10000-20000 vehicles/day, peaking at around 3-4pm with 1300 vehicles/hour (Department of Environmental Services, Plymouth). Pollutant concentrations fall rapidly moving away from the roadside (QUARG, 1993 a), so roadside proximity is very important. Measurements were made on the roadside pavement, 1-2m from the kerb, using the portable sample pump and sampling head (*cf.* Section 3.2). Sampling was made at 1-1.5m above ground level so as to most closely represent public exposure.

4.3   Experimental

4.3.1   Sampling

Aerosol sampling was conducted on seven dates between December 1996 and July 1997. Sampling was performed simultaneously at the roadside and background sites (*cf.* Section 4.2). Porous carbon films were used for aerosol sampling, allowing immediate TEM analysis (Dye *et al.*, 1997; *cf.* Section 3.2.3.2). European cyclone sampling heads were used with pump sampling rates set to 1.9 l/min (*cf.* Section 3.2.1 and Section 3.2.2). Sampling was conducted for periods of approximately one hour at the road side and two hours for background samples, between 1200 and 1400 hours on the selected dates. The longer collection time for background samples was to allow the collection of sufficient aerosol for analysis (*cf.* Table 4.1).

4.3.2   Analysis

Immediately after sampling, the grids with porous carbon film (PCF) were removed. The nuclepore filter (NPF) used in sampling was coated in carbon and processed in a Jaffe wash apparatus (*cf.* Section 3.2.3).

The PCF, with sample, was analysed in the JEOL 1200 fx II TEM (*cf.* Section 3.3.2.1). Approximately 50 particle images each were taken from the roadside and the background samples using either normal TEM micrographs or capture onto disk (*cf.* Section 3.3.2.1). Particles were either captured at a fixed magnification (*cf.* Section 3.4.3.1) or were normalised (*cf.* Section 3.4.3.2). Image analysis was performed on a Quantimet 540, using a macro programme written by Paul Russell at the University of Plymouth (*cf.* Section 3.5). Box counting techniques were used to calculate the perimeter fractal dimension (PFD) and the density fractal dimensions (DFD) (Barnsley *et al.*, 1988; Kaye, 1994; *cf.* Section 3.6).

Statistical analysis of the data was performed using Microsoft EXCEL v.7.0 with xlSTAT pro. EXCEL add-in (Fahmey, 1996; *cf.* Section 3.7).

4.4   Results and Discussion

4.4.1   Morphology Description of Urban Aerosol

The majority of particles were observed to be agglomerate in structure, comprising of a number of individual spheres. These spheres are variously referred to as primary paracrystaline units (Abrahamson, 1977), ceno-spheres (Medalia and Rivin, 1982) and spherules (Katrinak *et al.*, 1993), this text will consistently refer to the term ceno-spheres. The carbonaceous nature of these agglomerates was confirmed using energy dispersive x-ray spectroscopy (EDXS) (*cf.* Section 3.4.2) on a Jeol 2000fx II. The EDXS trace shown in figure 4.2 shows the typical result from the analysis of carbon ceno-spheres. The carbon peak (C) accounts for the particles and porous carbon film and the copper peak (Cu) results from the TEM grid. A simple qualitative classification of particles was made visually, as micrograph collection took place (*cf.* Table 4.1). Identification was made between agglomerates of ceno-spheres and non agglomerates. The non-agglomerate particles were further described according to their morphology.

The Table 4.1 shows that agglomerate particles of carbon ceno-spheres dominated the aerosol samples in every case, on different days and at the different locations. The contribution of agglomerates to urban aerosol has been noted in previous studies (Waller, 1967; Katrinak *et al.*, 1992; Katrinak *et al.*, 1993; QUARG, 1996; BéruBé *et al.*, 1997). The source of such agglomerates from hydrocarbon combustion sources such as diesel and spark ignition engines is well documented (Medalia and Rivin, 1982; Köylü *et al.*, 1995; Colbeck *et al.*, 1997).
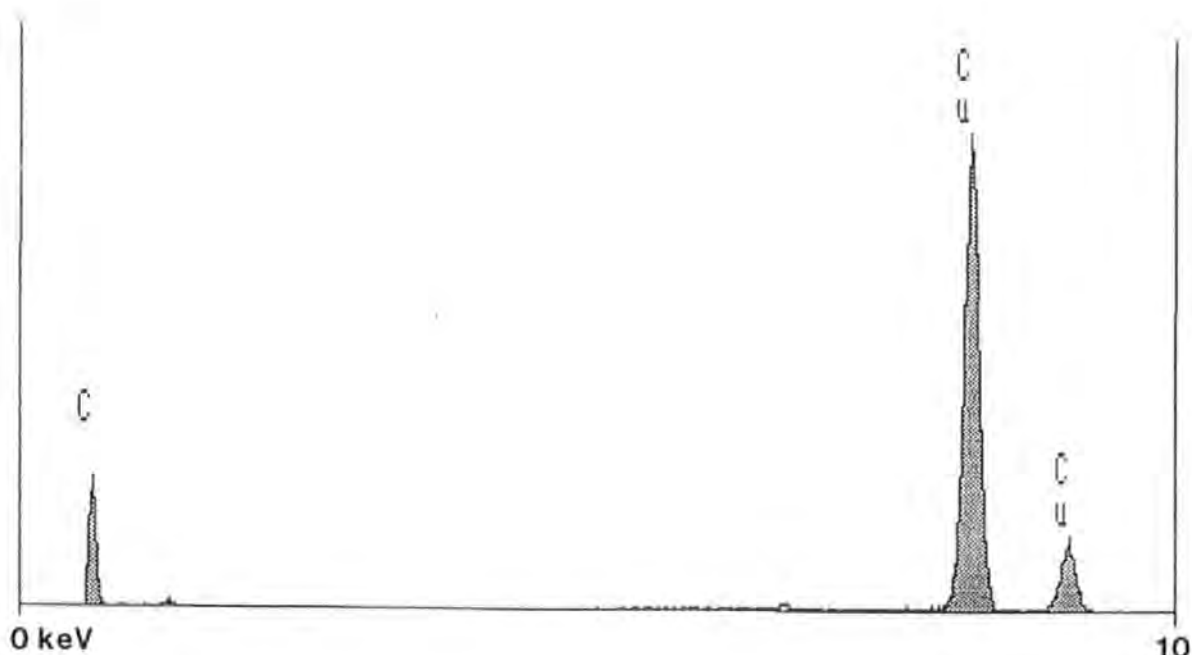
Figure 4.2 A typical EDXS trace from the analysis of carbon ceno-spheres captured by direct sampling on to a 200 mesh copper grid (analysis on a Jeol 2000 fx II)

[1.] *The carbon peak (C) is a Kα peak at 0.16 keV and is a result of the carbon ceno-sphere and the porous carbon film. The two copper (Cu) peaks are Kα and Kβ from left to right, occurring at 7.82 and 8.68 keV respectively and are as a result of the copper grid supporting the porous carbon film. (Newbury et al., 1981)*

Collection Date	Roadside		Background	
	Agglomerate Number	Non-Agglomerate Number + Description	Agglomerate Number	Non-Agglomerate Number + Description
4.12.96	44	4 Irregular	41	3 Irregular 1 Large Sphere
3.2.97	54	2 Irregular	43	6 Irregular
10.3.97	50		45	3 Irregular 4 Ceno-spheres, 2 Large Spheres,
3.4.97	49		46	4 Irregular
12.5.97	46	4 Irregular 1 Ceno-sphere	48	3 Irregular 2 Ceno-spheres
2.6.97	46	3 Ceno-spheres 1 Large sphere	45	1 Irregular 3 Ceno-spheres 1 Old agglomerate
21.7.97	46	1 Irregular, 2 Ceno-spheres 1 Large sphere	42	2 Irregular 2 Ceno-spheres 4 Old agglomerates
All (%)	94%	6%	88%	12%

Table 4.1 The numbers of differing particles types, classed by observation, at the roadside or background site.

The agglomerate domination of aerosol was slightly reduced in the background aerosol where other, non-roadside, sources had a contributory effect (*cf.* Table 4.1). Typically the agglomerates examined had a filigree open structure with a large surface area (*cf.* Figure 4.3 and 4.4). Each agglomerate was made up of upwards of two individual ceno-spheres and the mean individual ceno-sphere size was 36 nm ± 21 nm, this was in agreement with the mean size found in Phoenix, Arizona, USA, of 26nm (Katrinak *et al.*, 1993), and in London of *ca.* 50nm (Lawther *et al.*, 1968).

Initially particles were examined using qualitative EDXS as an aid to the determination of the source. Plymouth has a marine contribution of aerosol salt (*cf.* Figure 4.5), indicated by the presence of sodium (Na) and chlorine (Cl) in analysis (*cf.* Figure 4.6).
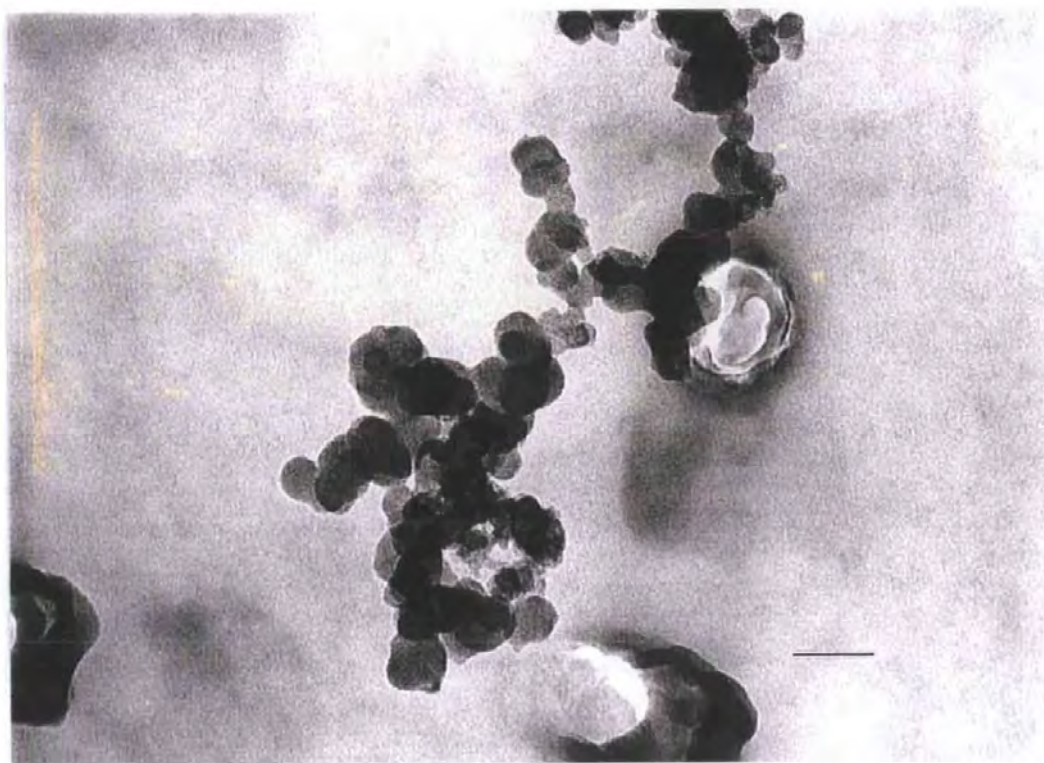
Figure 4.3 TEM micrograph of an agglomerate particle from the Plymouth background site, showing its construction of carbon ceno-spheres in clusters and chains, scale bar = 50nm
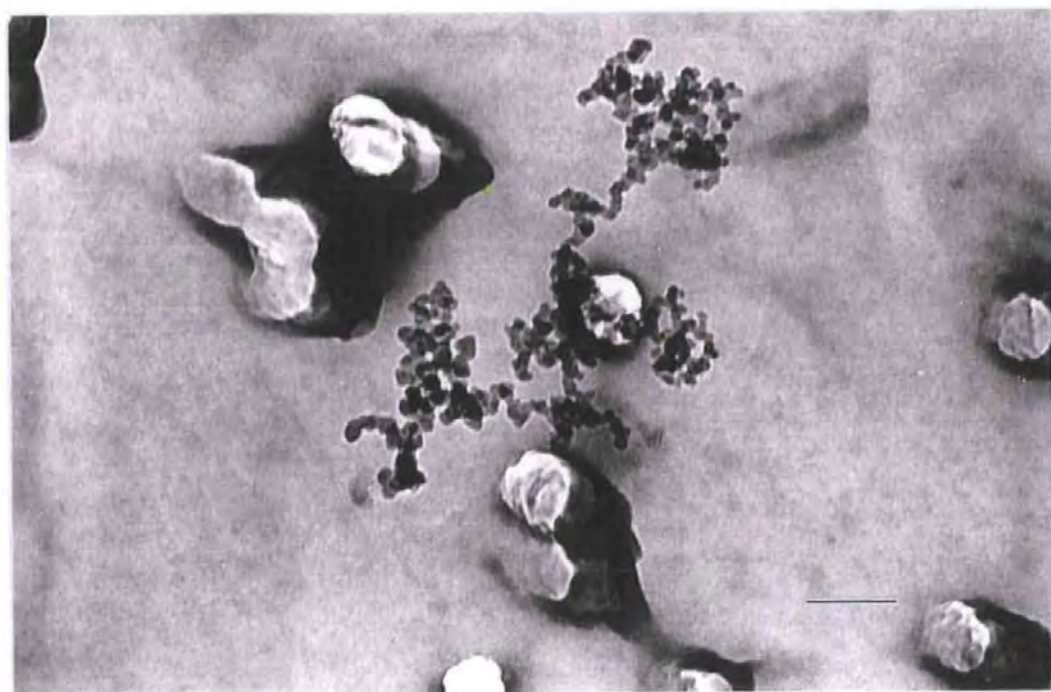
Figure 4.4 TEM micrograph of an agglomerate particle from the Plymouth background site, with a typical filigree structure and large surface area, scale = 100nm

Figure 4.5 TEM micrograph of a salt particle from the Plymouth background site, a very small salt crystal but still showing a partially cubic crystalline structure and exhibiting the EDXS trace in figure 4.6, scale bar = 50nm
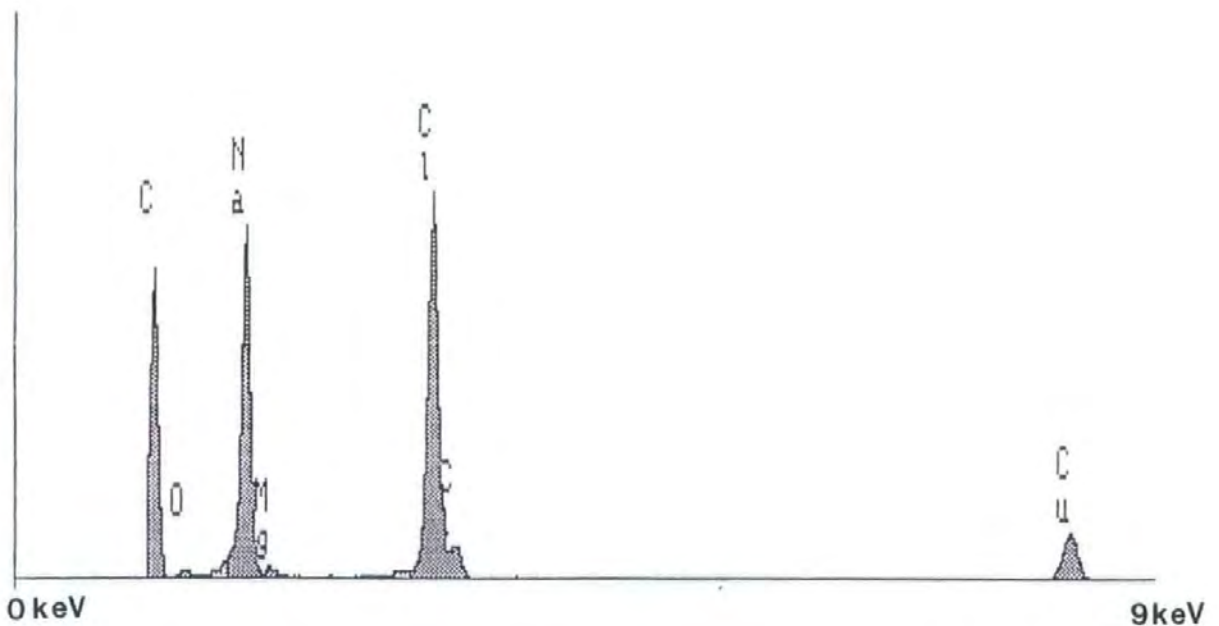
Figure 4.6 EDXS trace of the particle shown in figure 4.6, the carbon (C) peaks are from the PCF film and Copper (Cu) from the TEM grid. Sodium (Na) and Chloride (Cl) form the main bulk of the particle with some other elements of magnesium and oxygen, the marine source of this salt crystal is likely

In other coastal areas sea salts contribute a significant proportion of the mass of aerosol, 18% in Brisbane, Australia (Chan *et al.*, 1997) and 1-2% in Rubidoux, California, USA (Chow *et al.*, 1992). Other non-agglomerate particles analysed by EDXS, contained various proportions of ions of calcium, silicon, iron, chromium and copper. The mass contribution to the aerosol of such elements is significant in material from the geosphere and marine aerosols. In California, aerosol contributions of 30-50% of crustal material, 1-8% of marine aerosol and 20-35% of motor vehicles by mass have been calculated (Kao and Friedlander, 1995). When aerosol is examined by number the vehicle sources of aerosol have an increased influence. In a study of aerosol of 1.1 μm mean diameter in Phoenix, Arizona, USA, contributions of 35% of crustal material, 0.2 % of marine aerosol and 32 % of motor vehicle aerosol by number were calculated (Katrinak *et al.*, 1995). In the research reported here an aerosol of representative size (*ca.* 0.1μm mean; *cf.* Section 4.4.2.1) has been studied and accurately reflects the number domination of aerosol by fine carbonaceous agglomerates (*cf.* Table 4.1). Crustal and marine aerosols are relatively low in number and large in mass and size compared to motor vehicle sources of urban aerosol and are therefore much less significant by number. Fine carbonaceous particles are especially difficult to analyse by EDXS because of their small size, and can often be better distinguished by morphology, owing to the similarity of their elemental profile (Kindratenko *et al.*, 1994). Carbon films were used to collect particles and so a carbon peak was always present in the EDXS trace. With this in mind, the elemental nature of particles becomes a less significant factor compared to the structural information contained within the carbonaceous agglomerate particles, making up 85-95% of the aerosol by number (*cf.* Table 4.1).

Non-agglomerate particles varied considerably in structure and included individual ceno-spheres (*cf.* Figure 4.7), flakes (*cf.* Figure 4.8), large round spheres (*cf.* Figure 4.9) and old or coated agglomerate particles (*cf.* Figure 4.10).
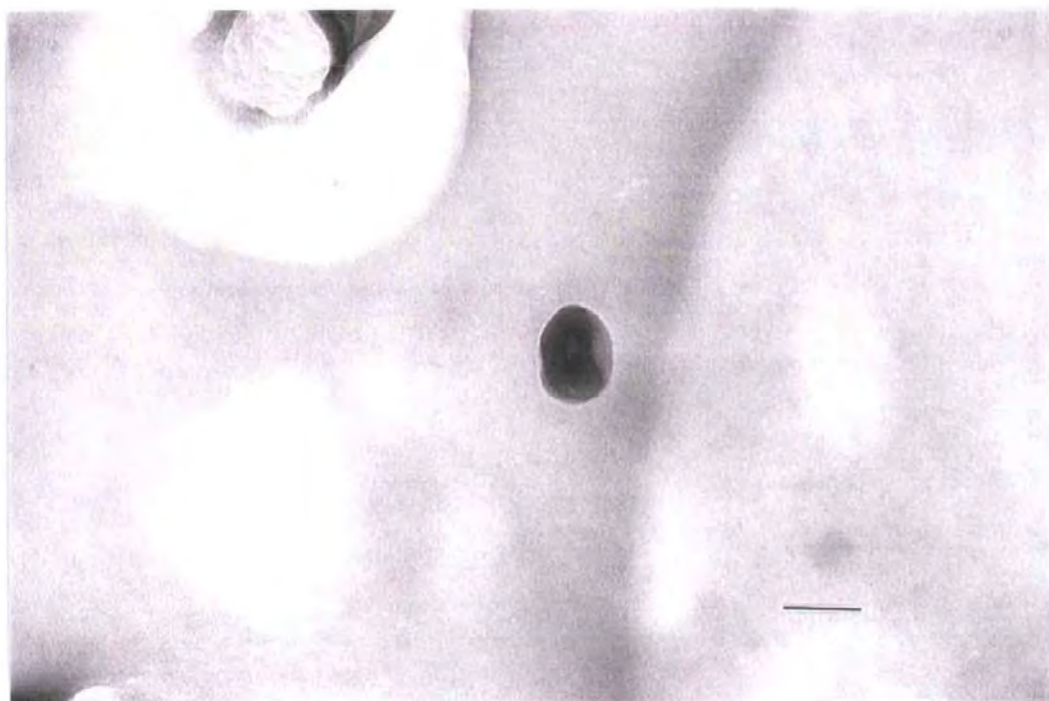
Figure 4.7 TEM micrograph of a single carbon ceno-sphere from the Plymouth background site of typical size ca. 40 nm in diameter, scale bar = 50nm

Figure 4.8 TEM micrograph of a mixed particle from the Plymouth roadside site, inclusive of 'flake' type particles with regular morphology and other amorphous material, scale bar = 50nm
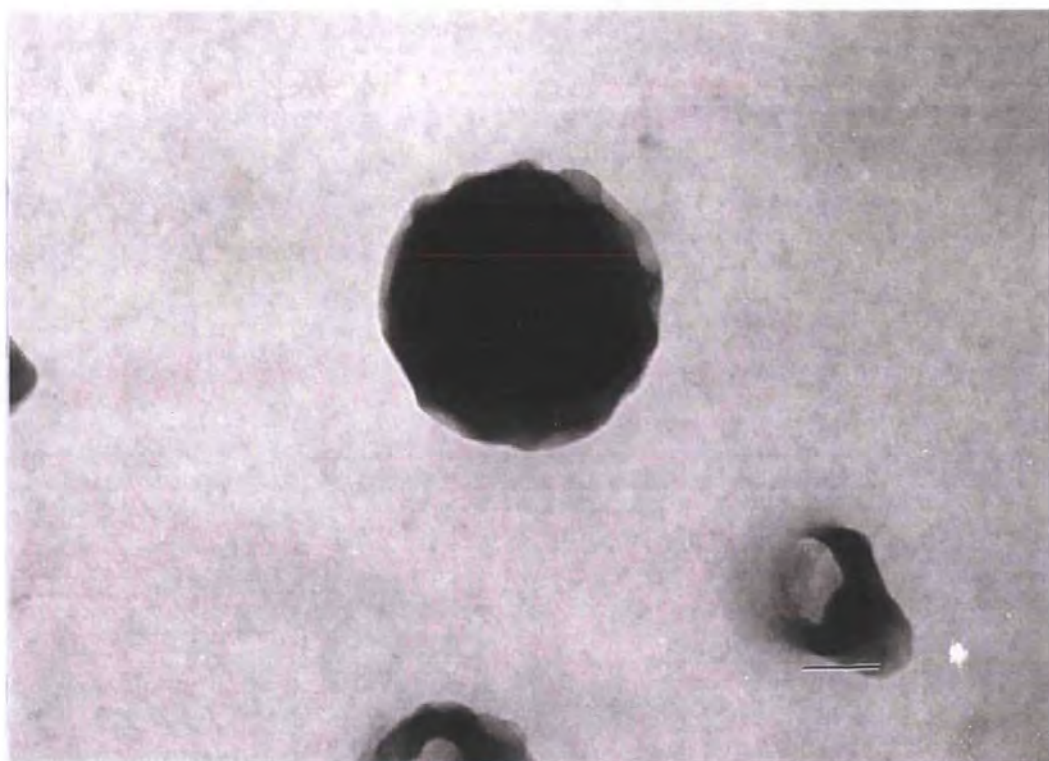
Figure 4.9 TEM micrograph of a spherical particle from the Plymouth background site, possibly a ceno-sphere from a vehicle combustion source of the maximum size of any ceno-spheres measured with a diameter of ca. 120nm, scale bar = 50nm
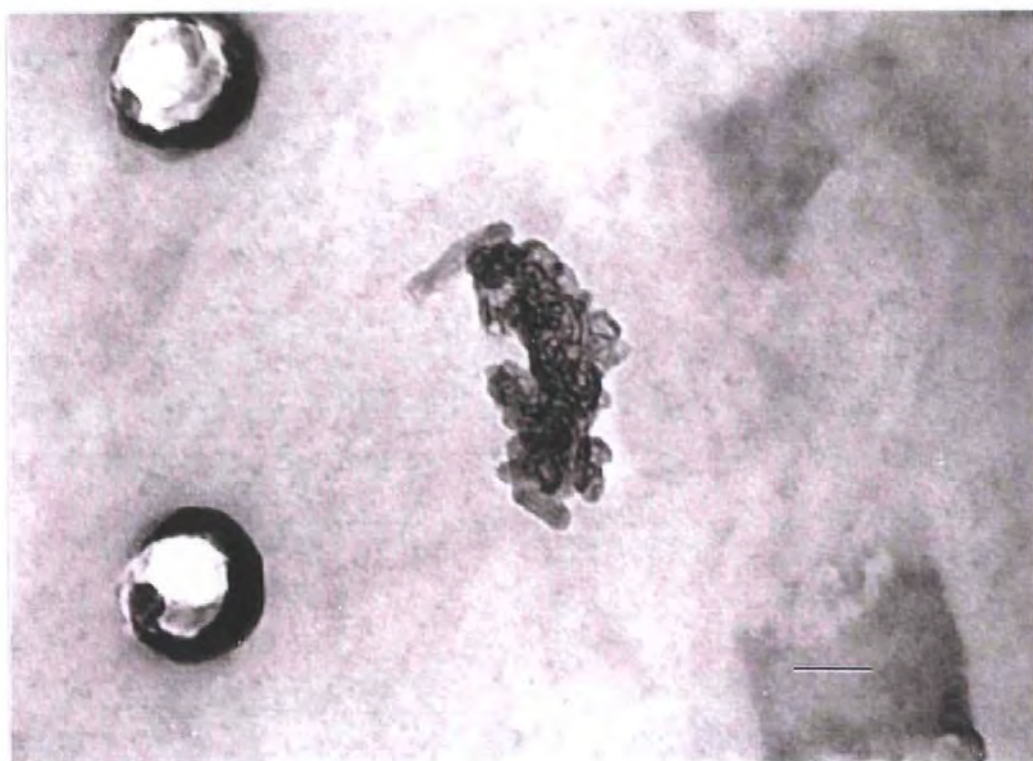
Figure 4.10 TEM micrograph of an agglomerate particle from the Plymouth roadside site, exhibiting a compacted agglomerate structure with individual ceno-spheres obscured this is indicative of a aged agglomerate (Katrinak et al., 1993), scale bar = 50nm

Coated or compacted agglomerate particles (*cf.* Figure 4.11 and Figure 4.12) have been previously noted by Katrinak *et al.* (1993). Such particles are very dense but because the coating is transparent to the electron beam the hidden agglomerate can be discerned. Agglomerates have been shown to collapse whilst acting as cloud condensation nuclei (Colbeck *et al.,* 1990), with organic material added in the form of a coating. (Katrinak *et al.,* 1992; Katrinak *et al.,* 1993). Such particles are formed as a result of post-emission processes and thus indicative of aged aerosol (Katrinak *et al.,* 1993). The appearance of aged particles only at the background aerosol site in Plymouth, suggests a similar process (*cf.* Table 4.1). In general 'fresh' agglomerates thus make up the majority of fine urban aerosol in Plymouth (*ca.* Table 4.1). The processes of agglomeration begin to remove agglomerates from the fine size fraction as soon as they are emitted to the air (QUARG, 1996; Twomey, 1977), therefore the observation of fine material will generally signify fresh particles *i.e.* a few hours to a few days old. This does not mean that the aerosol is necessarily locally generated as aerosol may travel many miles in a day (Twomey, 1977). However locally generated aerosols would seem to be the most likely source.

The agglomeration of mineral and combustion material in air causes the formation of mixed structure agglomerates (*cf.* Figure 4.11). These few cases have been classed as agglomerate. Mixed agglomerates are indicative of an aged aerosol where combustion aerosol has become attached to other particles in the atmosphere.

The internal structure of carbon ceno-spheres has previously been studied using Electron Energy Loss Spectroscopy (Katrinak *et al.,* 1992). This work suggests that combustion derived particles have internal structures of graphite with associated amorphous areas of hydrocarbons, and the presence of surface coatings during the summer.
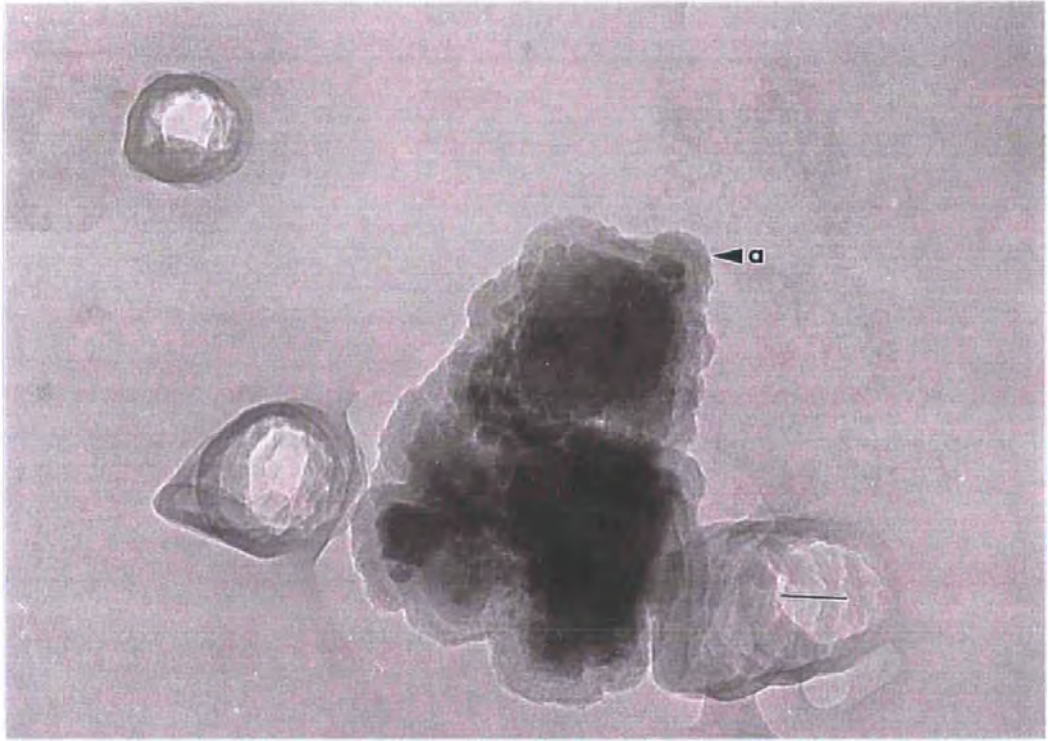
Figure 4.11 TEM micrograph of a compacted agglomerate particle with (a) surface coating, from the Plymouth background site, scale bar = 50nm

Figure 4.12 TEM micrograph of an agglomerate particle from the Plymouth roadside site, compacted and coated but the agglomerate of ceno-spheres is still visible, scale bar = 50nm

Some of the individual carbon ceno-spheres examined in this study exhibited an internal structure of a dark nucleus structure surrounded by carbon, although the nucleus is rarely central (*cf.* Figure 4.13, 4.14 and 4.15). This supports the postulation of soot formation *via* a stable soot nucleus and the addition of radical and non radical platelets (Abrahamson, 1977). Other carbon structures as postulated by Abrahamson (1977) were also routinely found in this work, primary paracrystaline units (*cf.* Figure 4.13, 4.14 and 4.15), agglomerated paracrystaline units (*cf.* Figure 4.16 and 4.17), soot chains with structure (*cf.* Figure 4.18 and 4.19), and soot chains of primary units (*cf.* Figure 4.20 and 4.21). Although these structures may be distinguished, in reality there are many varieties of agglomerate structure between each postulated extreme.

4.4.2 Quantitative Fractal Analysis of Urban Aerosol

Particle morphologies were quantified using two fractal measurements, perimeter fractal dimension (PFD) and density fractal dimension (DFD), and measurement of the equivalent circle diameters for all particles (*cf.* Chapter 3). The fractal dimension is a dimensionless quantity used to characterise morphologies outside of the scope of description using conventional Euclidean measurements, *i.e.* length/breadth ratios. Fractal measures are therefore less intuitively understandable on the part of the observer. A scale of fractal dimensions of both PFD and DFD has been constructed using real particle shapes found in this study (*cf.* Figure 4.22). This scale allows a better understanding of the differences between small increments in fractal dimension. In general as a PFD tends toward two, this indicates a more rugged boundary (PFD of 1 = round boundary), and as a DFD tends toward two this indicates an increasing density of structure (DFD of 2 =filled circle).
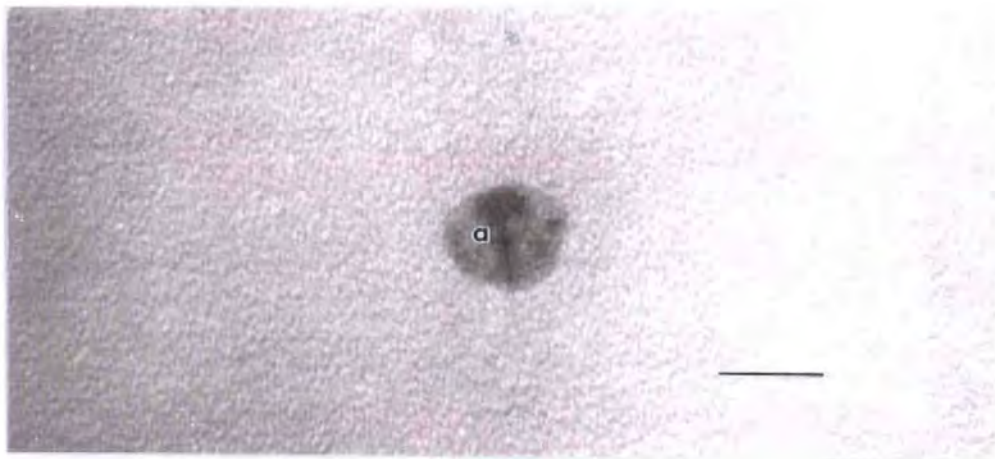
Figure 4.13 TEM micrograph of a ceno-sphere (primary para-crystalline unit) from the Plymouth roadside site, ca. 8nm in diameter and with (a) an internal 'nucleus' structure, scale bar = 10nm
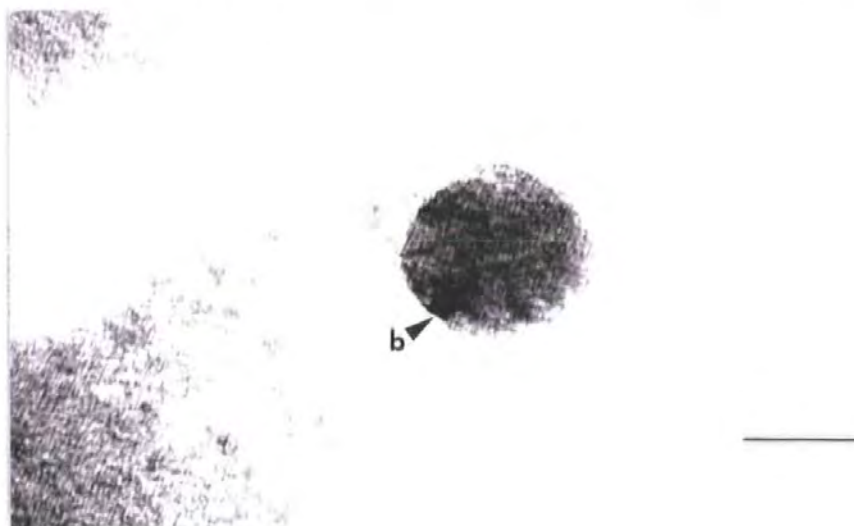
Figure 4.14 TEM micrograph of a ceno-sphere (primary para-crystalline unit) from the Plymouth roadside site, ca. 20nm in diameter with (b) a dark 'nucleus' structure, scale bar = 20nm
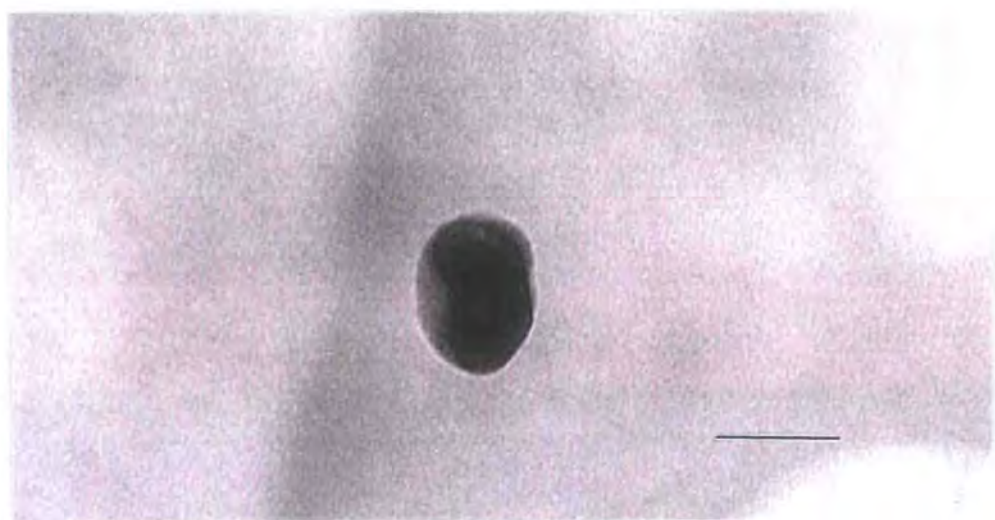
Figure 4.15 TEM micrograph of a ceno-sphere (primary para-crystalline unit) from the Plymouth background site ca. 40nm in diameter with some faint internal structure, scale bar = 50nm
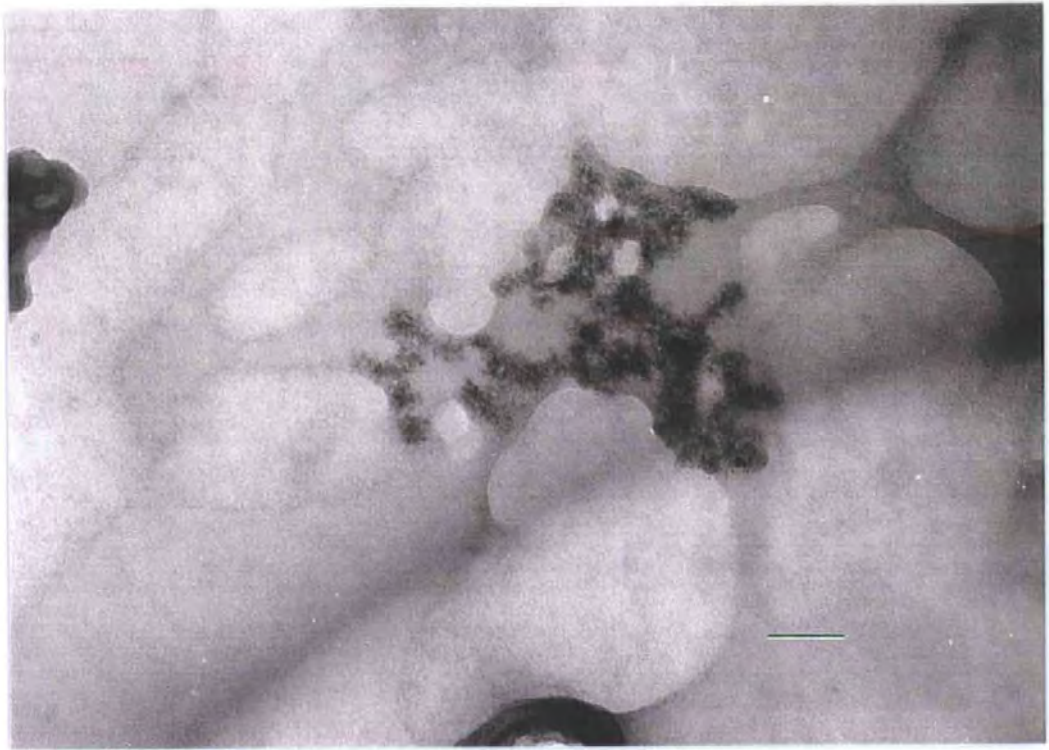
Figure 4.16 TEM micrograph of an agglomerate of para-crystalline units (Abrahamson, 1977), exhibiting a coating, from the Plymouth background site, scale bar = 50nm
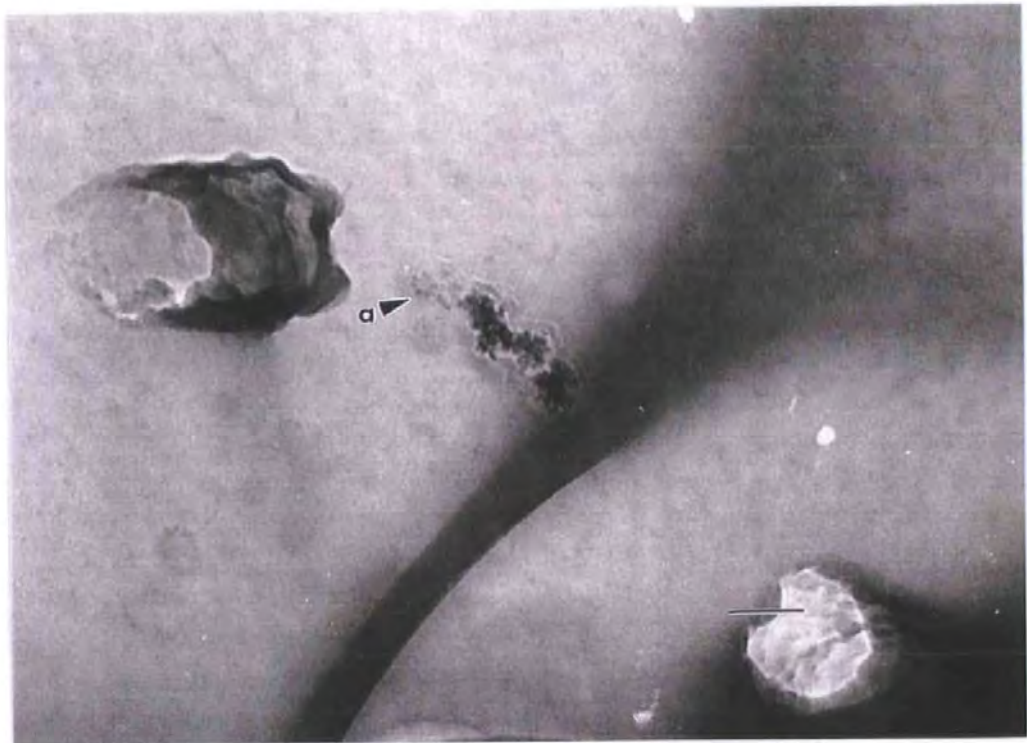
Figure 4.17 TEM micrograph of an agglomerate of para-crystalline units (Abrahamson, 1977), showing (a) some break up in to para-crystaline units on impaction with the PCF, from the Plymouth background site, scale bar = 50nm
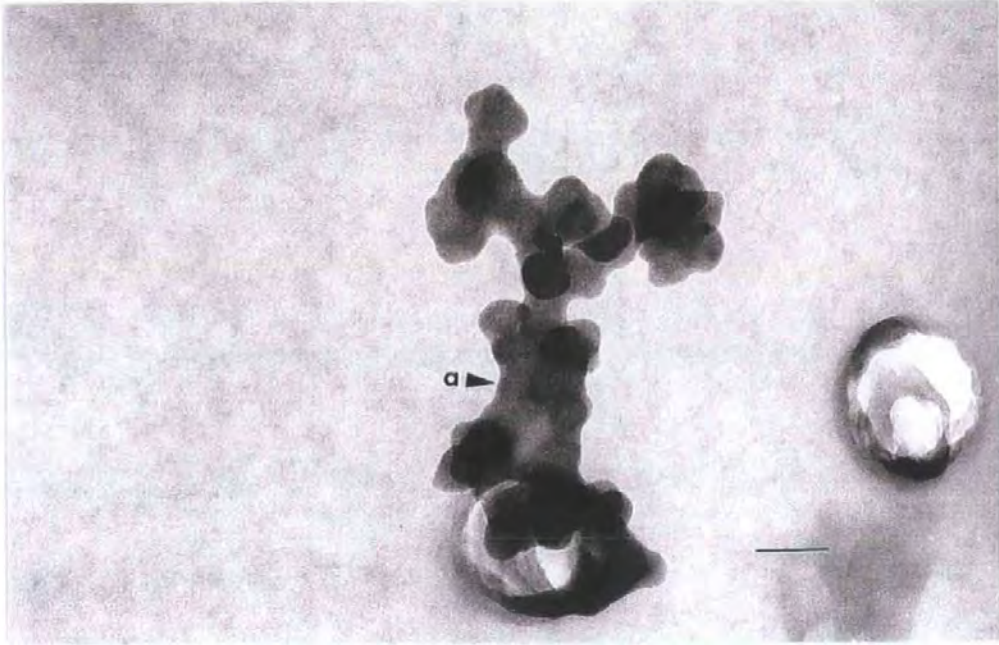
Figure 4.18 TEM micrograph of a fused agglomerate particle from the Plymouth background site, exhibiting (a) fused bridges over the whole structure, also described as soot chain with structure (Abrahamson, 1977), scale bar = 50nm
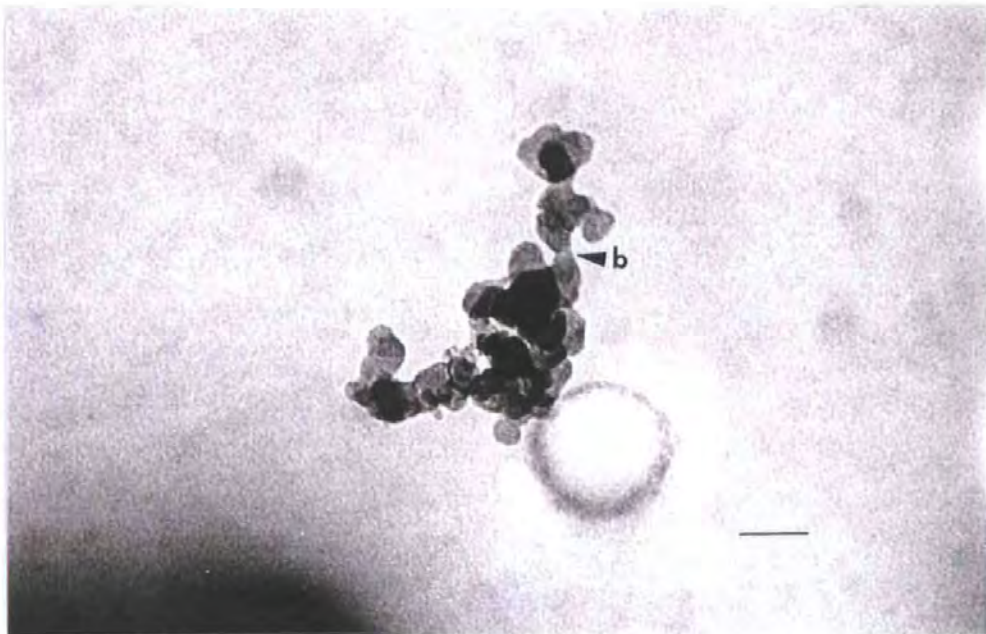
Figure 4.19 TEM micrograph of agglomerate particle from the Plymouth roadside site, with some (b) fused bridges between ceno-spheres, also coming under the description as soot chain with structure (Abrahamsom, 1977), scale bar = 50nm
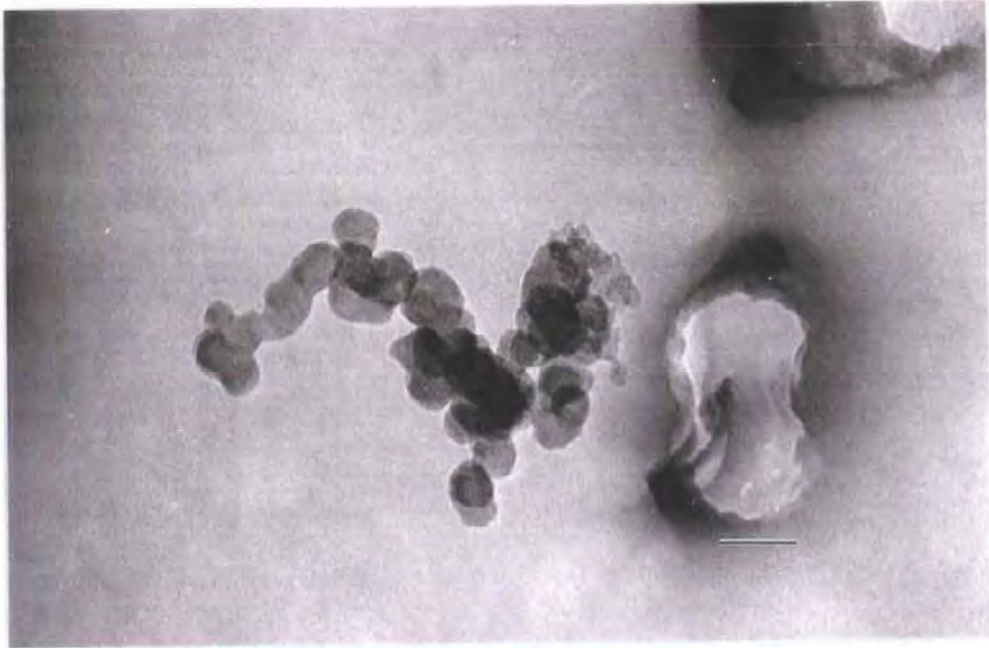
Figure 4.20 TEM micrograph of an agglomerate particle from the Plymouth background site, constructed from distinct recognisable carbon ceno-spheres, this structure is also known as a soot chain of primary units (Abrahamson, 1977), scale bar = 50nm
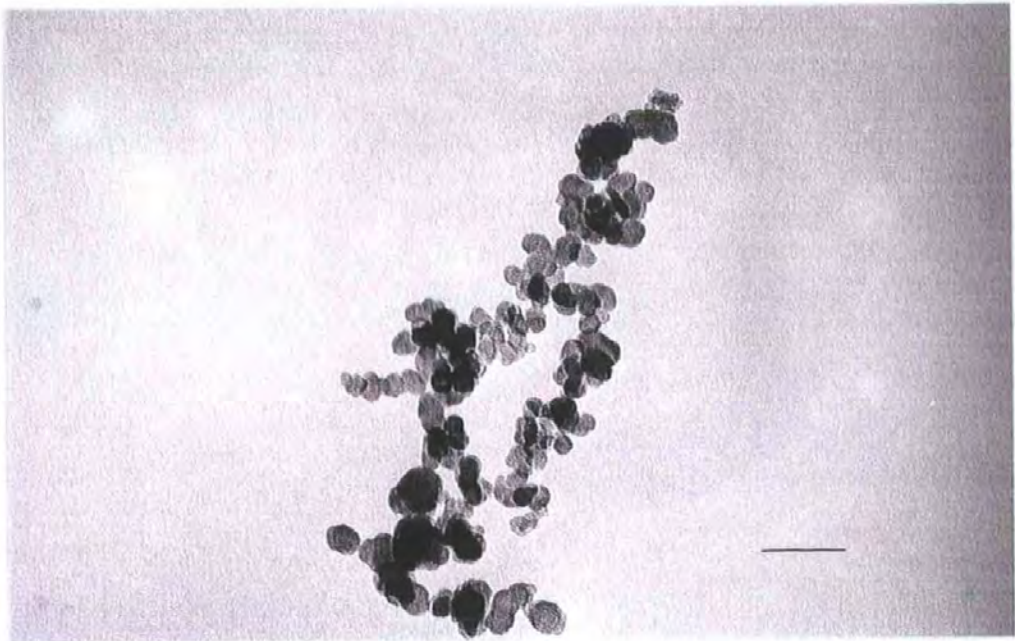
Figure 4.21 TEM micrograph of an agglomerate particle from the Plymouth roadside site, with a clear ceno-sphere construction also known as a soot chain of primary units (Abrahamson, 1977) and is illustrative of the large surface area and complex morphologies possible, scale bar = 100nm
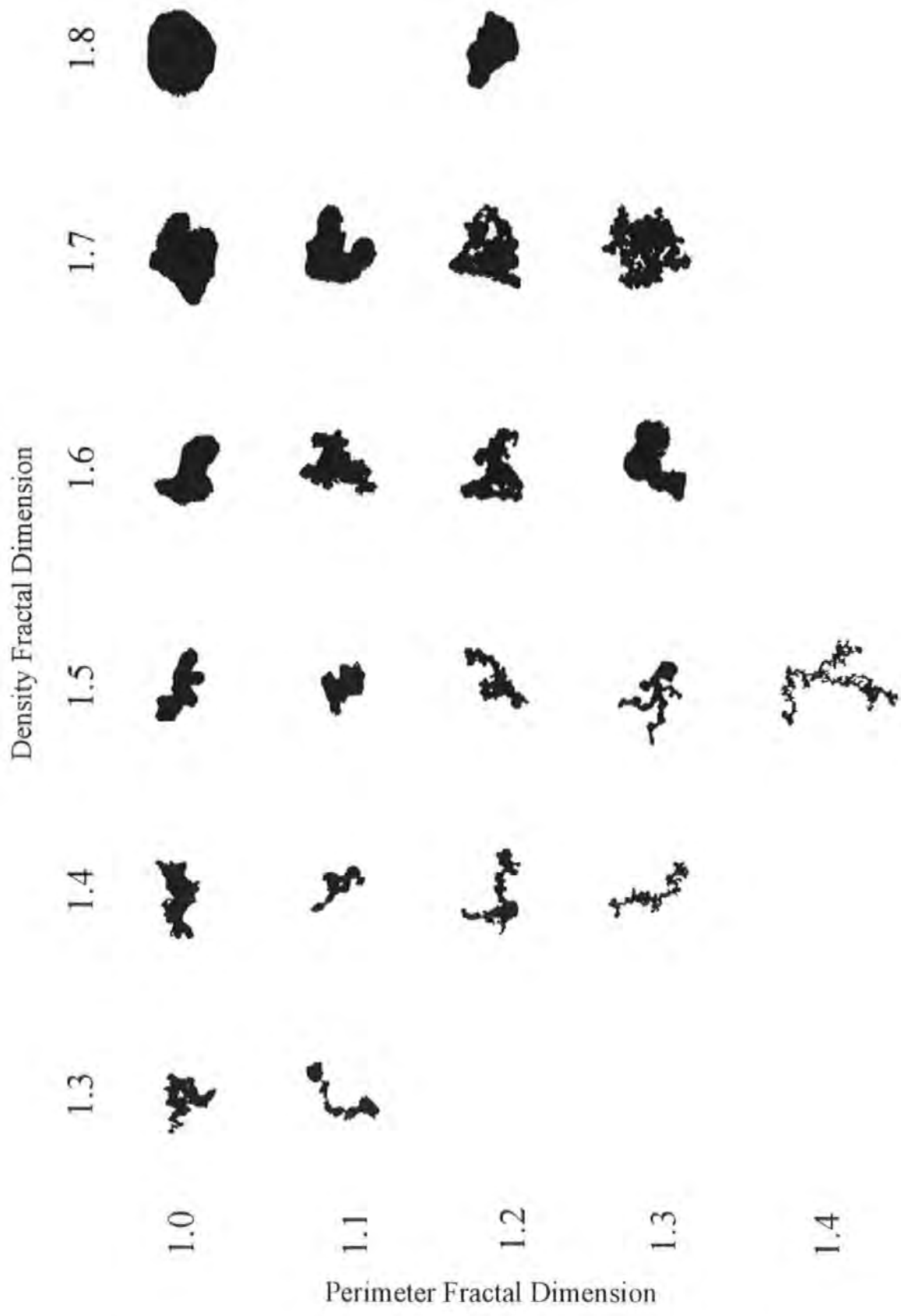
Figure 4.22 Scale of Perimeter and Density Fractal Dimension
using real particle shapes

4.4.2.1 All Data Summary Analysis

The mean DFD, PFD and size results from the analysis of particles using the fixed magnification method (*cf.* Section 3.4.3.1), and the normalised method (*cf.* Section 3.4.3.2) are shown in Tables 4.2 and 4.3. The PFD, DFD and size distribution of fixed analysis data is shown in Figures 4.23, 4.24 and 4.25. The Normalised study PFD, DFD and size distributions are shown in Figures 4.26, 4.27 and 4.28.

Sampling Site (no. of particles)	DFD ± S.D.	PFD ± S.D.	Equivalent Circle Diameter ± S.D. (nm)	Number Median Diameter (nm)
Roadside (167)	1.62 ± 0.20	1.16 ± 0.10	96 ± 70	71
Background (189)	1.63 ± 0.19	1.10 ± 0.12	103 ± 70	83
t-test pvalue	p=0.47	p< 0.0001	p=0.32	

Table 4.2 The mean DFD, PFD and equivalent circle diameter from the fixed magnification analysis of roadside and background aerosol (for the dates 4.12.96, 3.2.97, 10.3.97, 3.4.97)

Sampling Site (no. of particles)	DFD ± S.D.	PFD ± S.D.	Equivalent Circle Diameter ± S.D. (nm)	Number Median Diameter (nm)
Roadside (199)	1.56 ± 0.09	1.13 ± 0.10	109 ± 189	69
Background (189)	1.57 ± 0.09	1.11 ± 0.08	122 ± 134	89
t-test pvalue	p = 0.68	p=0.03	p=0.43	

Table 4.3 The mean DFD, PFD and equivalent circle diameter from the normalised analysis of roadside and background aerosol (for the dates 3.4.97, 12.5.97, 2.6.97, 21.7.97)

The mean equivalent circle diameter of all particles measured during the sampling period (6.12.96 - 21.7.97) was fairly consistent at *ca.* 100-120nm, with a large standard deviation spanning ultra fine particles (< 100nm) to large particles (>500nm), and a number median diameter of 69-89nm (*cf.* Figure 4.25 and 4.26). The difference between roadside and background aerosol in both the fixed and normalised analyses were similar. Both data sets
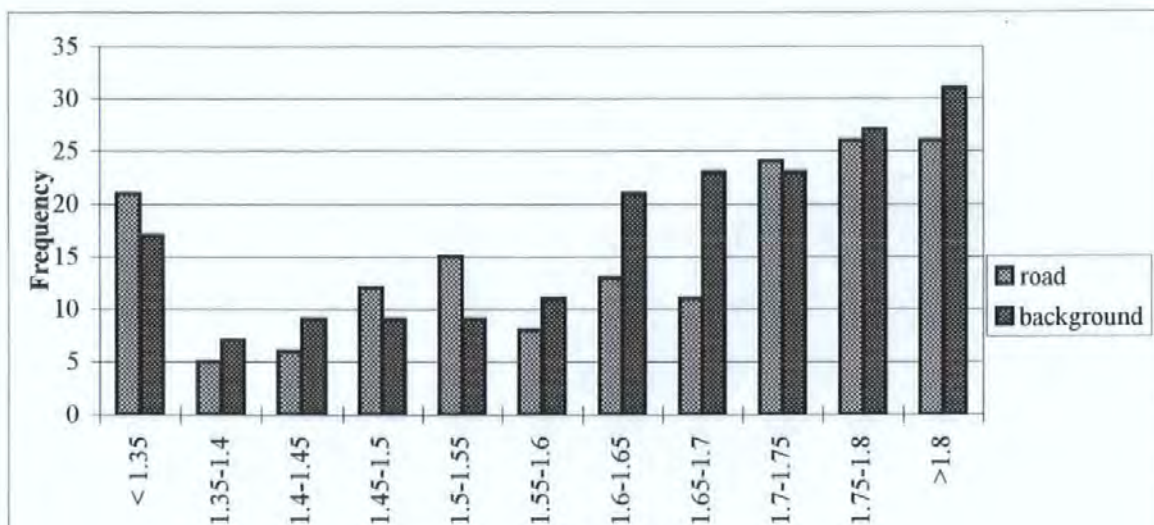
Density Fractal Dimension

Figure 4.23 Density Fractal Dimension distribution for all data at the Roadside and Background aerosol (Fixed analysis)
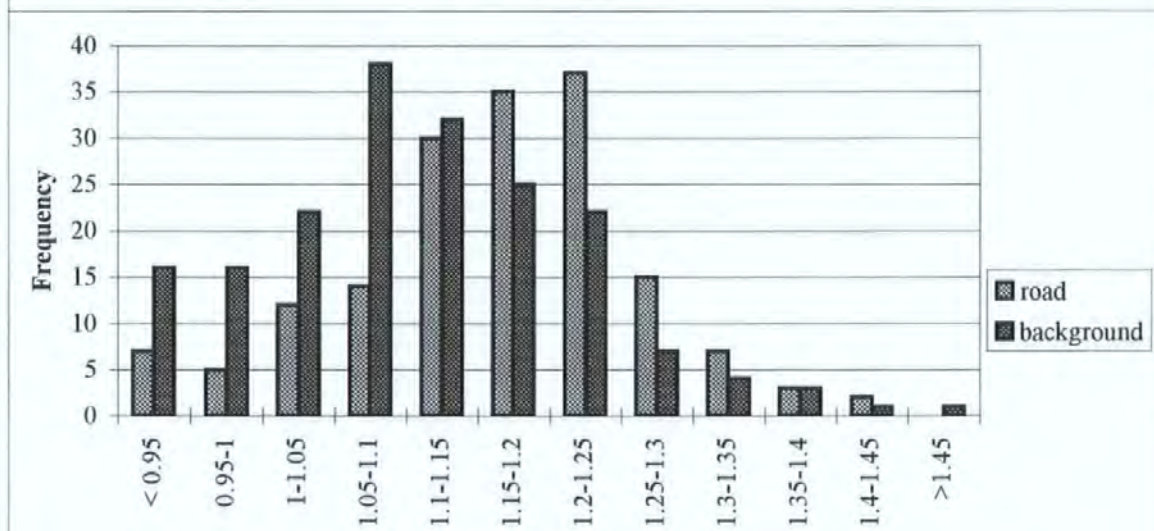
Perimeter Fractal Dimension

Figure 4.24 Perimeter Fractal Dimension distribution for all data at the Roadside and Background aerosol (Fixed analysis)
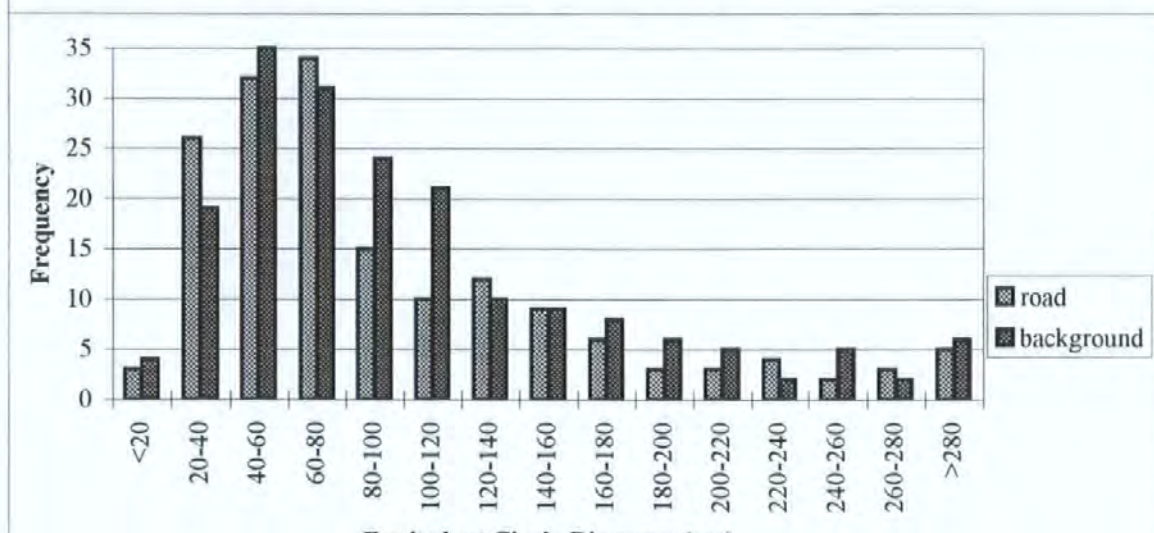
Equivalent Circle Diameter (nm)

Figure 4.25 Equivalent Circle Diameter distribution for all data at the Roadside and Background aerosol (Fixed analysis)
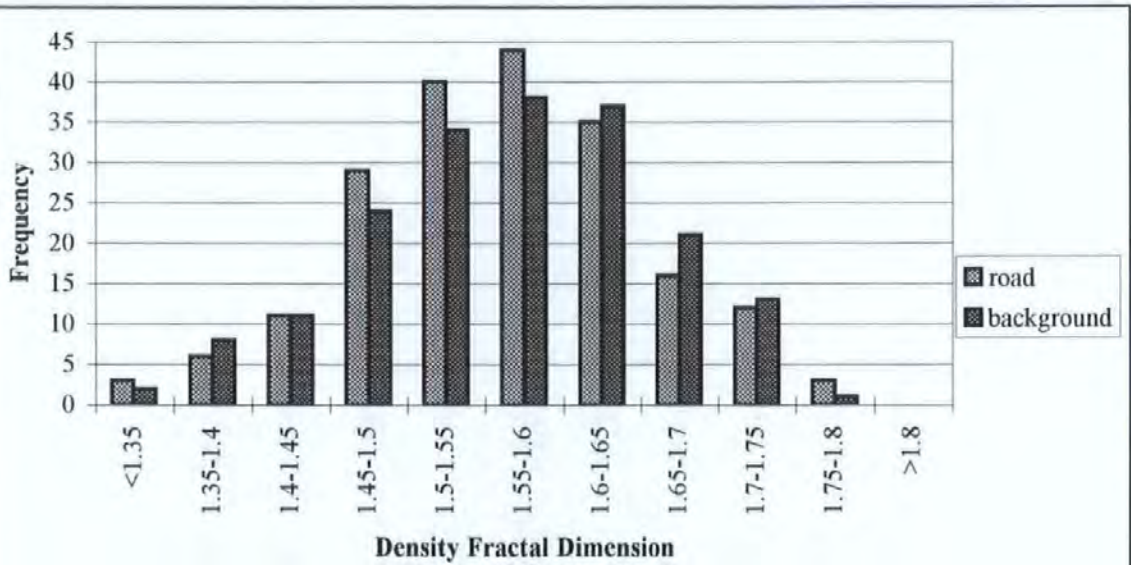
Figure 4.26 Density Fractal Dimension distribution for all data at the Roadside and Background aerosol (normalised analysis)
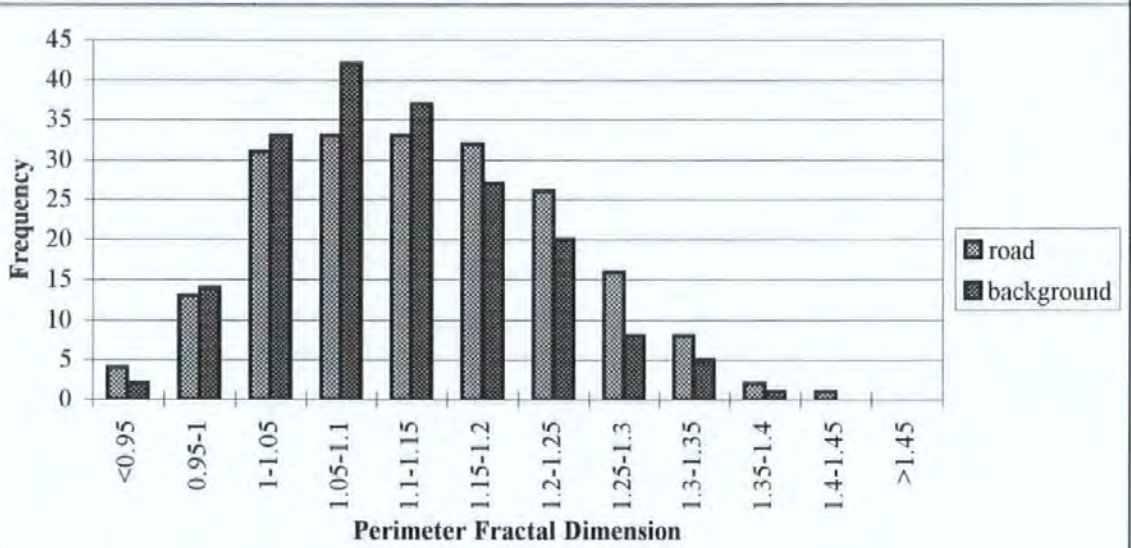
Figure 4.27 Perimeter Fractal Dimension distribution for all data at the Roadside and Background aerosol (normalised analysis)
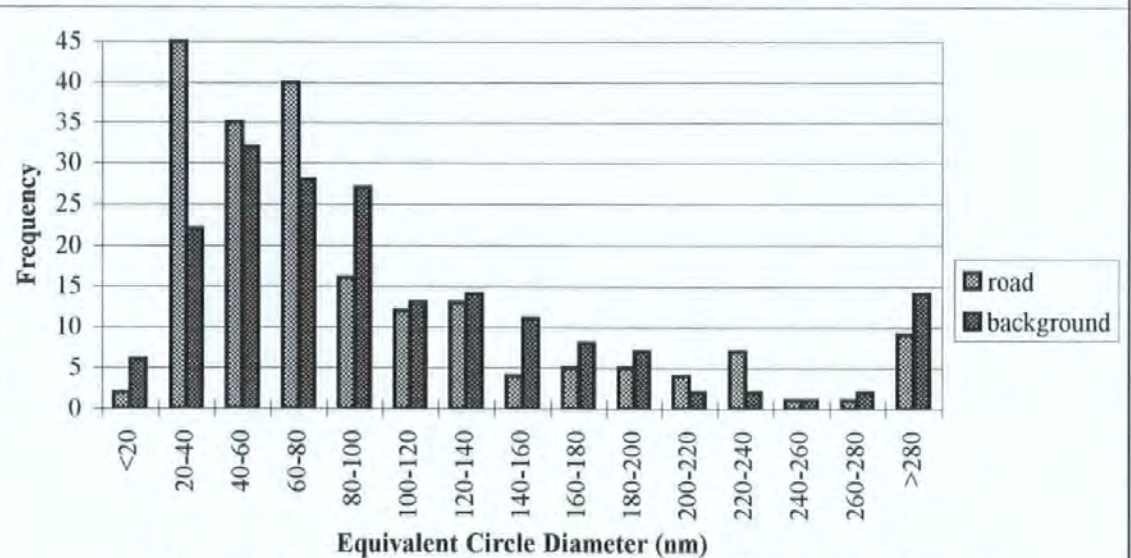
Figure 4.28 Size distribution for all data at the Roadside and Background aerosol (normalised analysis)

show that, on average, particles at the background site have a marginally higher DFD, lower PFD and larger diameter than particles at the roadside. Figure 4.22 indicates that a greater DFD is indicative of a more dense or space filling area while a lower PFD is indicative of a less rugged *i.e.* smoother, perimeter. On average background particles are smoother, more densely compacted and larger than roadside particles, owing to an ageing of aerosol. In the case of the PFD the difference between roadside and background aerosol is statistically significant at the 5% level (p=0.03).

The differences in average roadside and background aerosol morphology, as revealed by the fractal analysis calculated in this study, are the result of two processes, a mixing of sources and an ageing of agglomerated aerosol. At the background site the significantly lower PFD is caused by a mixing of agglomerate particles which are fractal in nature, *i.e.* the PFD is between one and two, with non agglomerate particles which are non-fractal, *i.e.* the PFD is less than one, or particles of low fractal dimension, thus acting to reduce the average fractal dimension (Kindrantenko *et al.*, 1994; Colbeck *et al.*, 1997). A source of aged agglomerates which have been smoothed and compacted through humidity changes, agglomeration and coating, will also reduce the average PFD (Katrinak *et al.*, 1992; Katrinak *et al.*, 1993; Huang *et al.*, 1994).

It seems that the PFD is most sensitive to differences between the roadside and background aerosol, and thus is useful for further analysis. The aerosol may be separated easily by PFD in to fractal (>1) and non fractal (≤1) particles to remove the influence of non fractal *i.e.* non agglomerate particles. This tentatively isolates the influence of ageing processes on the background aerosol as shown in Table 4.4 and 4.5.

	DFD ± S.D.		PFD ± S.D.		EC diameter (nm) ± S.D. (number median diameter)	
	Fractal	*Non fractal*	*Fractal*	*Non fractal*	*Fractal*	*Non fractal*
Road	1.64 ± 0.17	1.31 ± 0.29	1.18 ± 0.086	0.92 ± 0.067	101 ± 70 (74.5)	37 ± 28 (33)
Background	1.65 ± 0.17	1.54 ± 0.29	1.14 ± 0.091	0.91 ± 0.093	106 ± 66 (85)	92 ± 91 (59)
t-test pvalue	p=0.56	p = 0.02	p < 0.01	p=0.72	p=0.48	p=0.05

Table 4.4 Fixed road and background fractal and non fractal particle means (for the dates 6.12.96, 3.2.97, 10.3.97, 3.4.97), number median diameter in brackets.

	DFD ± S.D.		PFD ± S.D.		EC diameter (nm) ± S.D. (number median diameter)	
	Fractal	*Non fractal*	*Fractal*	*Non fractal*	*Fractal*	*Non fractal*
Road	1.56 ± 0.09	1.56 ± 0.09	1.15 ± 0.09	0.97 ± 0.01	111 ± 196 (69)	91 ± 91 (60.8)
Background	1.57 ± 0.09	1.56 ± 0.10	1.13 ± 0.08	0.97 ± 0.02	123 ± 134 (84)	122 ± 146 (77.2)
t-test pvalue	p=0.64	p=0.92	p=0.01	p=0.79	p=0.49	p=0.63

Table 4.5 Normalised road and background fractal and non fractal particle means (for the dates 3.4.97, 12.5.97, 2.6.97, 21.7.97), number median diameter in brackets

With the non-fractal particles removed the difference in PFD between roadside and background is increased in the case of normalised analysis as shown in Table 4.5, and decreased in the case of the fixed focus analysis as shown in Table 4.4. In both cases the differences in PFD between the roadside and the background particles is still significant at the 5% level. The trend is the same as was indicated previously *i.e.* that the average particle morphology at the background site is larger in diameter, but more dense (DFD) and significantly smoother (PFD) than roadside aerosol (*cf.* Table 4.4 and 4.5). This is good evidence for a structural difference between roadside and background agglomerate aerosol, caused by post emission processes. The differences may still be partly owing to non-

agglomerate sources at the background site but the effect of this proportion of aerosol in Tables 4.4 and 4.5 is much reduced. It is demonstrated that there is a clear difference in agglomerate aerosol between roadside and background detected by PFD.

The DFD differences for non fractal particles in the fixed analysis data (*cf.* Table 4.5), are due to a size related effect (*cf.* Section 3.6). Many of the particles which are non-fractal are very small and these may be typically identified as individual carbon ceno-spheres. In fact, the mean of 37nm for the roadside fixed analysis non fractal particles is within the quoted values for carbon ceno-spheres produced in diesel combustion, typically 30-70nm (Medalia and Rivin, 1982). Within this non fractal component there are also larger non-fractal particles which are not from hydrocarbon combustion sources (Colbeck *et al.*, 1997). This is especially the case at the background site, the effect of which increases the overall DFD. Separation of non-fractal particles by size distinguishes hydrocarbon sources of fine ceno-spheres from other non fractal particle sources (*cf.* Chapter 6).

The average fractal dimensions found in this work are comparable to other studies of urban aerosol which used different techniques and which are summarised in Table 4.6. Kindratenko *et al.* (1994) and Xie *et al.* (1994) measured PFD for various urban background aerosol (*cf.* Table 4.6). The PFD's found by both of these studies are within the standard deviations of the mean background aerosol PFD in this Plymouth research for both fixed and normalised analysis (*cf.* Tables 4.2 and 4.3). Katrinak *et al.*, (1993) measured the average DFD of urban aerosol in Phoenix, Arizona, USA (*cf.* Table 4.6). and the background aerosol is within the standard deviation of DFD results found herein (*cf.* Table 4.2 and 4.3).

Study (number of particles analysed in parenthesis)	DFD	PFD			Mean diameter (µm)
Kindratenko *et al.* (1994)[1]		*Textural*	*Structural*		> 1
Irregular fly ash (21)	------	1.09 ± 0.02	1.28 ± 0.02	------	
Soil dust (37)	------	1.04 ± 0.01	------	------	
Katrinak *et al.* (1993)[2]					> 0.2
All urban aerosol (38)	1.75 ± 0.2	------	------	-------	1.17 ± 0.7
Fractal particles from urban aerosol (23)	1.65 ± 0.15	------	------	-------	1.13 ± 0.68
Xie *et al.* (1994)[3]		*Textural*	*Structural*	*Overall*	> 1
Spherical particle	------	1.07 ± 0.99	1.03 ± 0.98	1.04 ± 0.94	
Bladelike particle	------	1.05 ± 0.99	1.22 ± 0.94	1.07 ± 0.93	
Fused particle	------	1.09 ± 0.92	1.39 ± 0.89	1.15 ± 0.90	

1 and 3. Kindratenko et al 1994 and Xie et al 1994, PFD measured using a 'stepping' or 'yardsitck' edge detection technique and using SEM.
2. Katrinak *et al.* 1993, DFD measured using nested squares technique and using TEM.
4. For Textural and Structural Fractal Dimensions refer to Section 3.6

Table 4.6 Summary of DFD and PFD for particles measured in other studies making

fractal measurements of airborne particles

In Katrinak *et al.* (1993) the average DFD for exclusively fractal particles was lower (1.65) than the average DFD for all urban particles (1.75) (*cf.* Table 4.6). This was explained by the removal of the more dense, *i.e.* higher DFD (>2), non agglomerate and aged particles. However in the current study, for the fixed analysis the average DFD for exclusively fractal particles was higher (1.64-1.65) than the average DFD for all the urban aerosol (1.62-1.63) (*cf.* Table 4.2 and 4.4), and there was no change in the DFD between all aerosol and exclusively fractal aerosol for the normalised analysis (*cf.* Table 4.3 and 4.5). The reduction in DFD does not occur in this research because the separation in to fractal and non-fractal components was made according to the PFD, not DFD as in Katrinak *et al.* (1993). Thus both fractal and non-fractal groups of particles contain a range of DFD dimensions. The particles in this study also have a smaller mean (*ca.* 100nm) than those studied by Katrinak *et al.* (1993) (*ca.* 1µm, *ie.* 1000 nm). These ultra fine (*ca.* 100nm) agglomerates which make up the greatest proportion of the aerosol have much less scope for variation in space

filling structure than large space filling structures (*cf.* Figure 4.29). In short, the PFD fractal and non-fractal components have similar DFD because the particles are so small.

In all of these previous studies, the material analysed was generally micron sized (*cf.* Table 4.6). Micron sized material is simple to resolve in SEM and TEM, providing clear particle morphologies which are easy to detect with image analysis (*cf.* Section 3.5). The urban aerosol is on the contrary a far more complex mix. In London the number median diameter of aerosol has been measured from between 90 and 130nm (COMEAP, 1995) and in Birmingham number median diameters have been measured in the order of 40-50nm (COMEAP, 1995). The greatest number of aerosol particles will then be below the detection limits of these previous studies, so a representative sample was not analysed. The strength of the work reported here rests upon the collection of a representative sample using the PCF method (Dye *et al.*, 1997; *cf.* Section 3.2). In Plymouth a mean equivalent circle diameter of particles has been found in the order of 100nm (*cf.* Tables 4.2 and 4.3) and the number median of particles between 80-90 nm at the background site for all particle types. This is comparable with particles from London and Birmingham (COMEAP, 1995). Although this ultra fine (< 100nm) aerosol presents problems in resolution and analysis (*cf.* Section 3.5), it is representative of the urban aerosol. This work thus describes the representative fractal nature of the urban aerosol, in both density and perimeter fractal dimensions and may be analysed further by day and specific size ranges.

4.4.2.2 Fractal Analysis : Individual sampling days

An Analysis of Variance (ANOVA) statistical test on the mean size, DFD and PFD (*cf.* Figures 4.30, 4.31 and 4.32) show that there is little aerosol homogeneity between different sampling occasions (*cf.* Tables 4.7 and 4.8). For the fixed analysis, DFD is size sensitive so significant differences in diameter cause the significant difference in DFD (*cf.* Table 4.7).
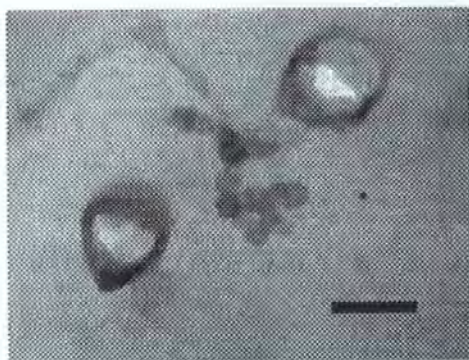
Scale bar = 100nm
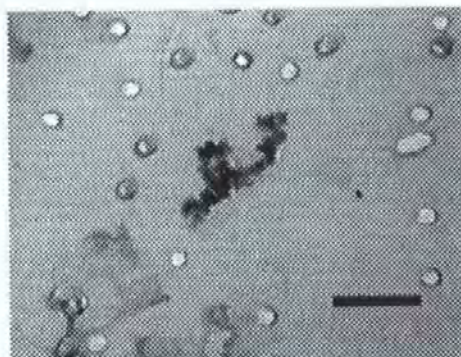
Scale bar = 500nm

11 cenospheres : not great scope for stuctural variation

42 cenospheres : large scope for stuctural variation

| 1.5804 | DFD | 1.4916 |
| 1.1841 | PFD | 1.1976 |

Estimated PFD & DFD
Compact structure

| 1.7 | DFD | 1.7 |
| 1.0 | PFD | 1.0 |

Possible Open structure

| 1.5 | DFD | 1.4 |
| 1.2 | PFD | 1.4 |

not a big diff in PFD and DFD

Big changes in DFD and PFD

Figure 4.29 The variation in agglomerate structure dependent upon the number of cenospheres.
DFD and PFD estimates from Figure 4.22
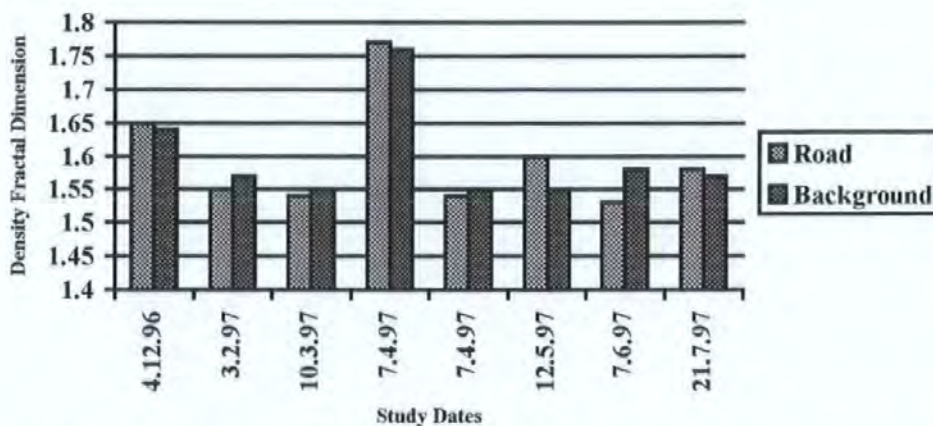
Figure 4.30 Average DFD for Fixed and Normalised Analysis Study days, at Roadside and Background Sites
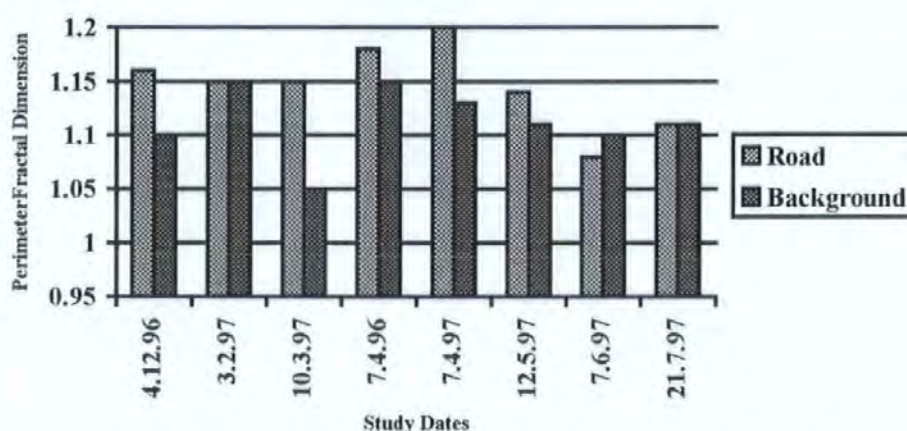
Figure 4.31 Average PFD for Fixed and Normalised Analysis Study Days, at the Roadside and Background sites
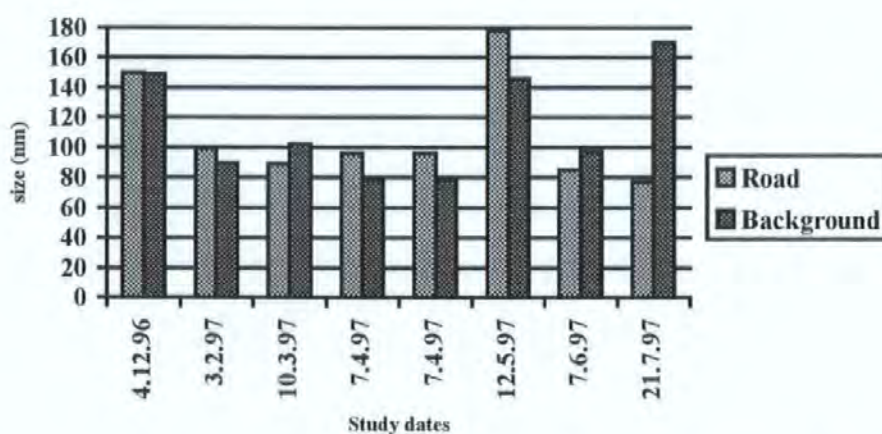
Figure 4.32 Mean Equivalent Circle Diameter (nm) for Fixed and Normalised Analysis Study Days at Roadside and Background Sites

The large variations in PFD, in the fixed analysis, also obscure any significant difference in the roadside sample. For the normalised analysis the background site looks a slightly more homogenous, in terms of DFD and PFD, than at the roadside. Again, for the normalised analysis (cf. Table 4.8), there is a significant variation in average equivalent circle diameters between the sampling days. The normalised data reveals that, while the mean aerosol size varies significantly at both the background and roadside sites, the background aerosol retains some homogeneity in compositional morphology. This suggests that the morphological composition of aerosol in the ambient air in Plymouth, UK, does not vary significantly over a period of months, whilst the mean diameter of aerosol may fluctuate.

Study Site	DFD (P values)	PFD (P values)	Diameter (P values)
Road	yes (<0.0001)	yes (0.043)	yes (0.0004)
Background	yes (<0.0001)	yes (0.0007)	yes (<0.0001)

Table 4.7 Date comparison, ANOVA test for any significant difference between any study days(fixed analysis data)

Study Site	DFD (P values)	PFD (P values)	Diameter (P values)
Road	yes (0.0021)	yes (0.00004)	yes (0.026)
Background	no (0.22)	no (0.29)	yes (0.0017)

Table 4.8 Date comparison test for any significant difference between study days (normalised data)

The variation between individual means at the road and background was also tested (cf. Table 4.9 and 4.10). Although there is at least one parameter which is significantly different between road and background on five of the seven study days, an overall trend is unclear (cf. Table 4.9). The mean DFD is different between roadside and background on two days but is larger at the roadside on the 12.5.97 and larger in background on the 7.6.97 (cf. Figure 4.30). Although the PFD is greater at the roadside than the background on most of the study days (cf. Figure 4.31), it is only significantly larger on three days (cf. Table 4.8).

The mean aerosol diameter is most consistent, only being significantly different on one day (21.7.97) (*cf.* Figure 4.32). The lack of significant difference may be owing to a number of factors. The samples taken for each day were small and therefore the variation in the sample will obscure any significant differences. Also the meteorological conditions are a major factor in the compositions of a complex multi-source aerosol (Twomey, 1977; QUARG, 1996), and so may affect any consistency in significant differences.

Date of Sample	DFD (p values)	PFD (p values)	Diameter (p values)
4.12.96	no (0.97)	no (0.12)	no (0.87)
3.2.97	no (0.51)	no (0.95)	no (0.69)
10.3.97	no (0.33)	yes (< 0.001)	no (0.88)
7.4.97	no (0.15)	yes (0.009)	no (0.59)

Table 4.9 Road vs Background comparison and significance of difference (Fixed Data)

Date of Sample	DFD (p values)	PFD (p values)	Diameter (p values)
7.4.97	no (0.72)	yes (0.0027)	no (0.15)
12.5.97	yes (0.04)	no (0.051)	no (0.59)
7.6.97	yes (0.00382)	no (0.29)	no (0.45)
21.7.97	no (0.68)	no (0.78)	yes (0.0011)

Table 4.10 Road vs Background comparison and significance of difference (Normalised Data)

A matched pair t-test using the mean roadside and background DFD for each day reveals there is no significant consistent DFD difference between the road and background samples over the study days. There is a mean significant difference of 0.3 ± 0.04 (p = 2.93, degrees of freedom = 7) between the roadside and the background average PFD, considering all of the study days. There is also a significant difference between the roadside and background aerosol diameter for the fixed and the normalised study days. Thus this shows the consistency of density of aerosol but the great variability in diameter and ruggedness of particles, occurring as a result of ageing and source additions at the background site. The

stability in density is due to the small size of particles studied as previously described in. Figure 4.29.

4.4.2.3 Size Grouped Fractal Analysis

The size of a particle can be a factor in the generation of fractal dimension of real particles (Kaye, 1993). The interpretation of PFD and DFD thus benefits from a breakdown of data into distinct particle size ranges. For this purpose size ranges 40nm wide in diameter were selected because this is the typical size of a single ceno-sphere of a diesel combustion agglomerate (Medalia and Rivin, 1982). The choice of the top size range of 120-220nm was designed to include enough particles for analysis. In addition fractal agglomerate measurement above 220nm is less useful because of the small sample population.

The mean values for DFD, PFD and diameter for the selected size ranges of aerosol for all fixed analysis sampling days are shown in Figures 4.33, 4.34 and 4.35. The means for the normalised sampling days are shown in all normalised study days, Figures 4.36, 4.37 and 4.38. Statistical analysis of fixed study data shows no significant differences between road and background mean diameter and DFD for any size range (*cf.* Figure 4.33). Analysis of the PFD reveals a significant difference between road and background at every size range and the lowest probability of similarity in the 120-220nm size range (*cf.* Appendix 2). At each size range the mean PFD of the roadside aerosol is larger than mean PFD of the background aerosol (*cf.* Figure 4.35). Analysis of the normalised study data shows the only significant difference between road and background samples for the PFD mean, in the 120-220nm size range (*cf.* Appendix 2; *cf.* Figure 4.37). Comparison of the means for the normalised roadside and background aerosol in Figure 4.37 shows that the roadside aerosol has a consistently larger PFD, which attains significance in the 120-220nm size range. The PFD has been shown in this analysis to be the most sensitive factor in distinguishing
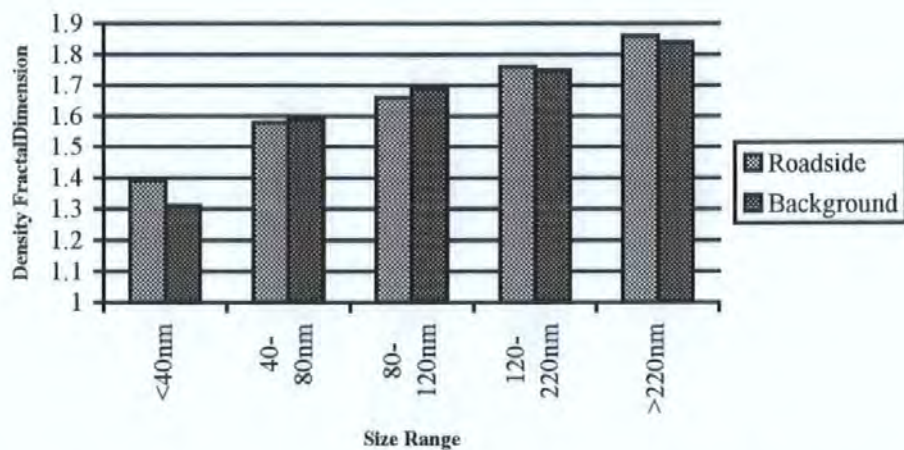
Figure 4.33 Average DFD according to size range for the fixed data
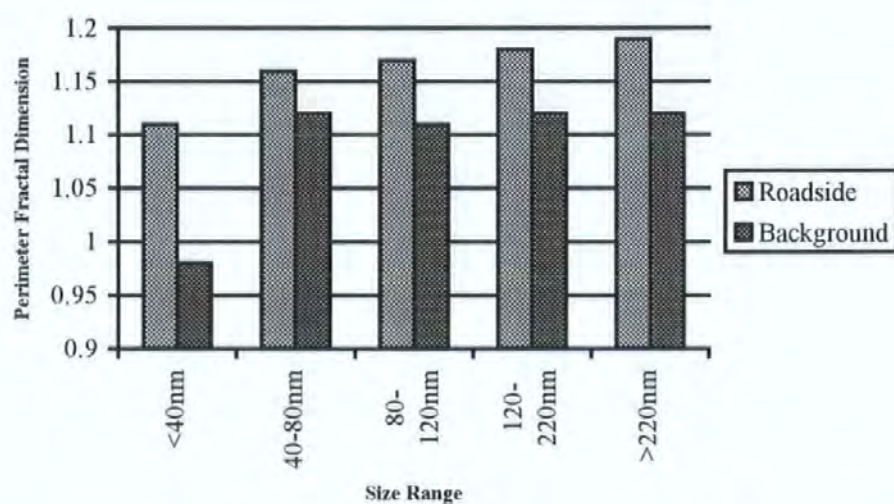
Figure 4.34 Average PFD according to size range for the fixed data
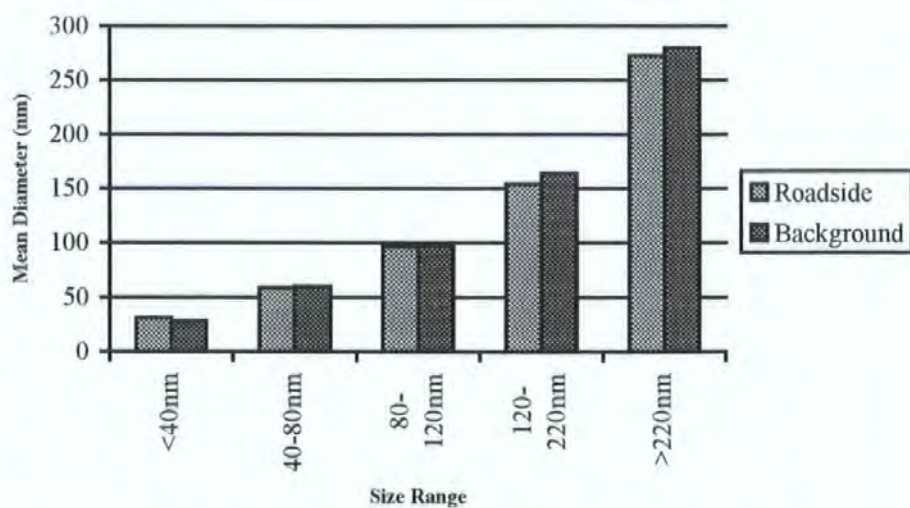
Fig 4.35 Mean Diameter according to size range for the fixed data
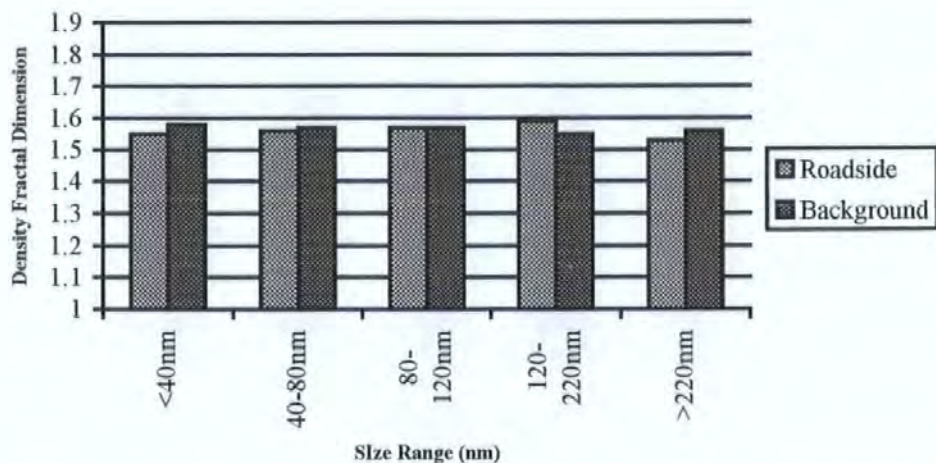
Figure 4.36 Average DFD according to size range for the normalised data
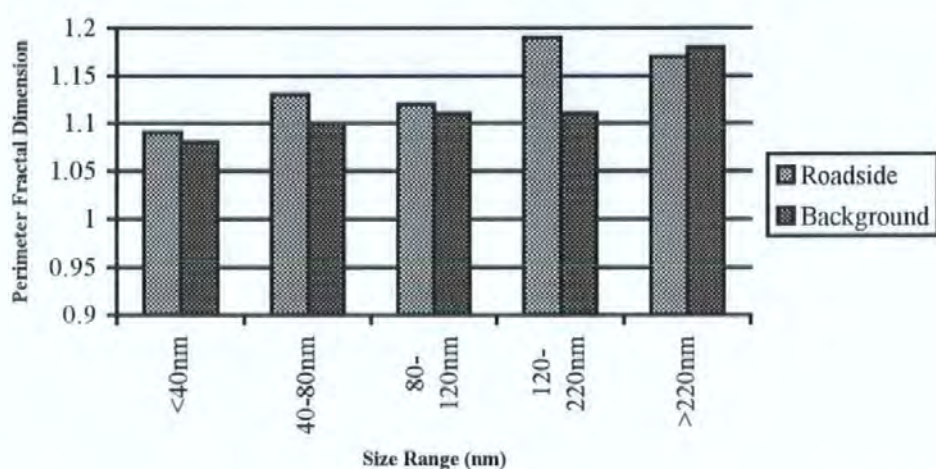
Figure 4.37 Average PFD according to the size range for the normalised data
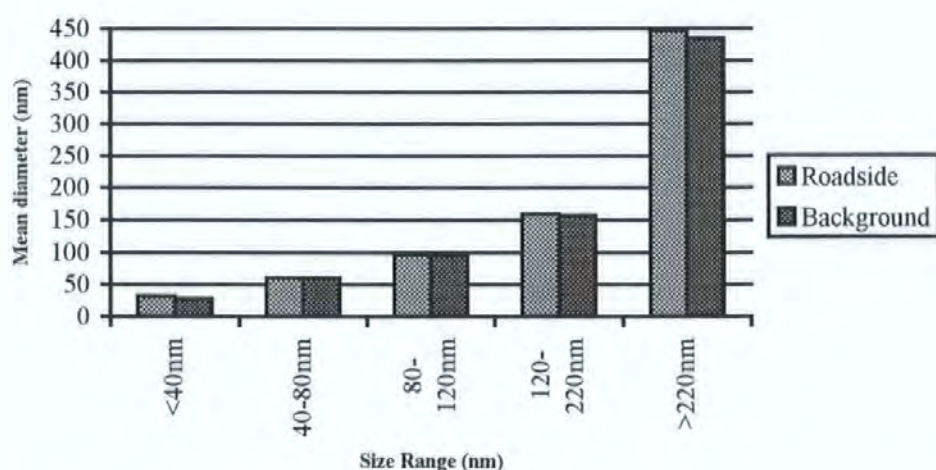
Figure 4.38 Average diameter according to the size range for the normalised data

morphological differences between the roadside and background. This is true on a daily basis and on an all data basis as shown previously.

In both the fixed and normalised analysis the >220nm size range should be considered with caution because of the open ended nature of this size range. In the fixed analysis the >220nm size range has an average size of 270nm for roadside and background aerosol, but for the normalised data the mean is 450nm therefore rendering doubtful any firm conclusions derived from this size range.

The difference between roadside and background aerosol are thus significantly owing to the 120-220nm size range, especially taking into account the size sensitive nature of the fixed study data (cf. Section 3.6). The significance in difference between background and roadside aerosol may also be owing to all aerosol above 120nm, but in general particles above 220nm account for a small proportion of the number of particles in the air (Seaton et al., 1995; QUARG, 1996; COMEAP, 1995). Therefore particles above 220nm have little effect on the number mean PFD of aerosol. In this work particles greater than 220nm only accounted for ca. 10% by number of all the particles, whereas the range 120-220nm accounted for ca. 20% of all the particles studied. So if all the aerosol above 120nm in diameter are considered it is the 120-220nm size range that is most influential in affecting the number mean PFD.

The largest PFD difference occurs in the 120-220nm size range rather than particles of <120nm, because of the increasing variety of source particles, and the larger size of agglomerates. At the 120-220nm size, sources which produce only particles greater that 120nm will be included. Such sources will include bacterial spores (QUARG, 1996), sea salts (Murphy, 1984), maybe some industrial dusts, and most nitrates (QUARG, 1996).

The decrease of PFD at the 120nm size range in background aerosol (Figure 4.34 and 4.37) is at least partly due to the introduction of particles having a smooth morphology. There may also be significant effect from the change in morphology of large agglomerates. Below the size 120nm, agglomerates consist of few individual carbon ceno-spheres. The possibility of structural change and collapse within these agglomerates is minimal. Above the size 120nm agglomerates consist of a greater number of individual carbon ceno-spheres (*cf.* Figure 4.29). These more complex structures have far more scope for the manifestation of processes leading to morphological change (*cf.* Figure 4.29). The change from filigree fresh roadside agglomerates to an aged, compacted, smoothed and coated background aerosol is therefore more important in the size range above 120nm. The critical nature of the 120-220nm size range is that it lies on the boundary of size and number, having a significant number to alter the overall aerosol character (Table 4.2, 4.3, 4.4, 4.5) and having significant size for structural changes to occur (*cf.* Figure 4.29).

The public health implications of particle collapse are two-fold. The roadside aerosol is fresh and open structure in general nature. This means that it has a large surface area and a small aerodynamic diameter, caused by the drag on the particle (Kaye, 1993; Huang *et al.*, 1994; cf. Figure 2.3, Page 49). Particles of the same actual size in the background ambient air have a lower PFD and higher DFD. In other words they have a smaller surface area and larger aerodynamic diameter caused by structural collapse. It is the aerodynamic diameter which governs respiratory penetration thus, on average, roadside particles will penetrate more deeply, with a larger active surface, than more aged aerosol particles of the same actual size more likely to be found in background sites.

4.4.2.4 Comparison of size grouped PFD distributions

The PFD is the most sensitive parameter in the comparison of roadside and background aerosols as shown in Section 4.4.2.1. For this reason it is useful to inspect the distributions of PFD for size range at the roadside and the background (*cf.* Figures 4.39, 4.40, 4.41 and 4.42). In this comparison it is important to note that while fixed and normalised data are both useful, only the normalised data has PFD's comparable between different size ranges.

The PFD mode or modes generally shifts towards larger values with increasing size, from *ca.* 0.95 to 1.3 for the fixed analysis PFD modes (*cf.* Figures 4.39 and 4.40) and from *ca.* 1 to 1.25 for the normalised analysis PFD modes (*cf.* Figures 4.41 and 4.42). The same increase in PFD with increasing size can be observed in the mean PFD within the size ranges (*cf.* Figures 4.34 and 4.37). This is indicative of a general increase in the ruggedness of particles with size, which is a reasonable effect of increasing particle size shown in Section 4.4.2.2.

Comparison of the histograms of roadside and background for the fixed data (Figures 4.39 and 4.40), shows there is a clear domination of the roadside aerosol with modes between 1.2 and 1.3, and one mode for <40nm at 0.95. For the background aerosol the modes are less clear. There is a mode at 0.95 for the <40nm aerosol, a wide mode between 1.05 and 1.2 for all of the aerosols and also modes at 1.25 for 120-220 and >220nm aerosols.

The 0.95 mode for roadside and background is caused predominantly by particles of small size because of size sensitivity of fixed magnification analysis in this size region (*cf.* Table 4.4). The single modes for aerosol at the roadside indicates the dominance of the aerosol by roadside generated aerosol all of similar fractal dimension. The wide mode and double
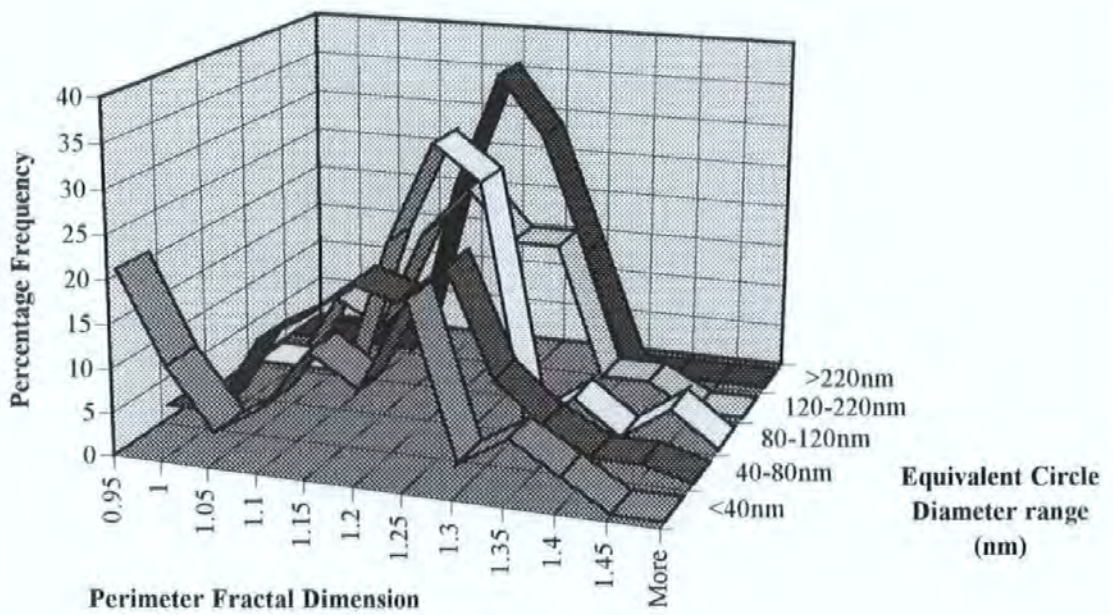
Figure 4.39 PFD distributions for roadside particles in size ranges (percentage histogram) fixed data
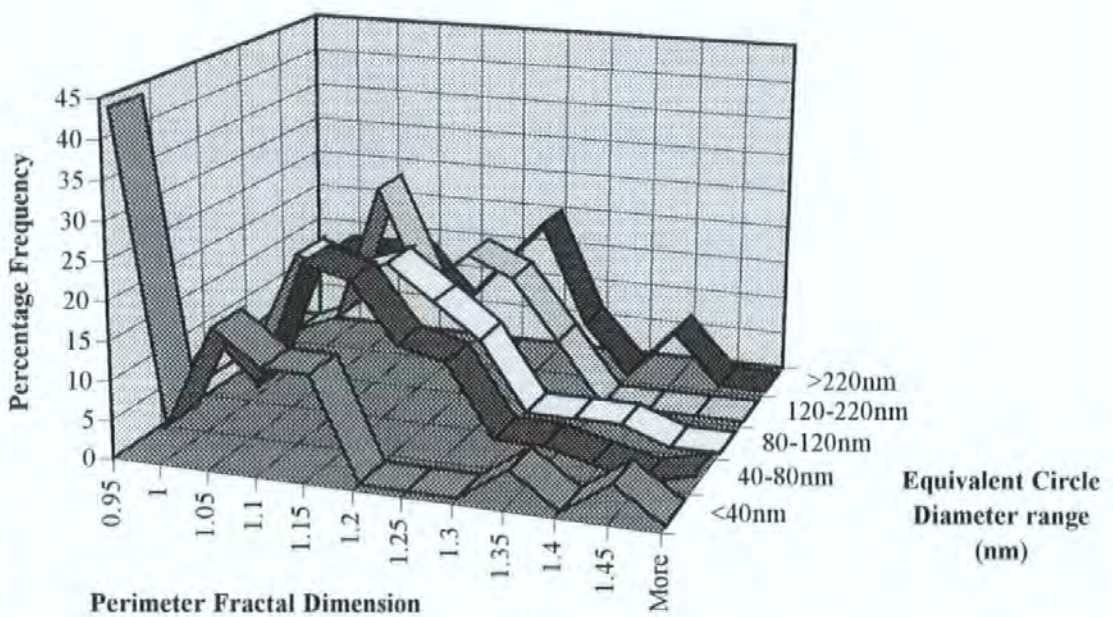
Figure 4.40 PFD distributions for background particles in size ranges (percentage histogram) fixed data
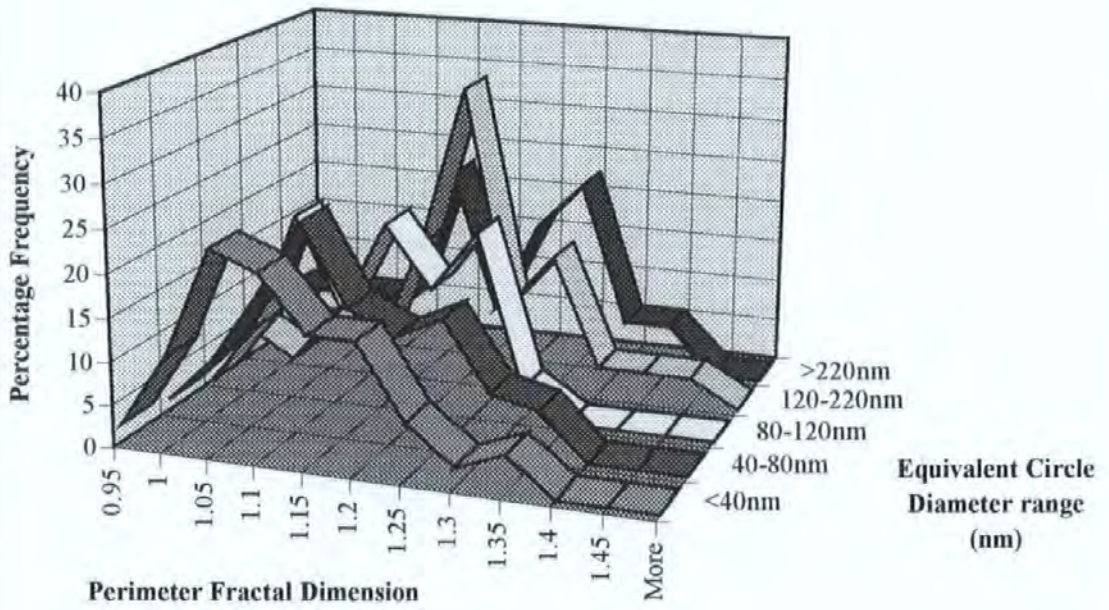
Figure 4.41 PFD distributions for roadside particles in size ranges (percentage histogram) normalised data
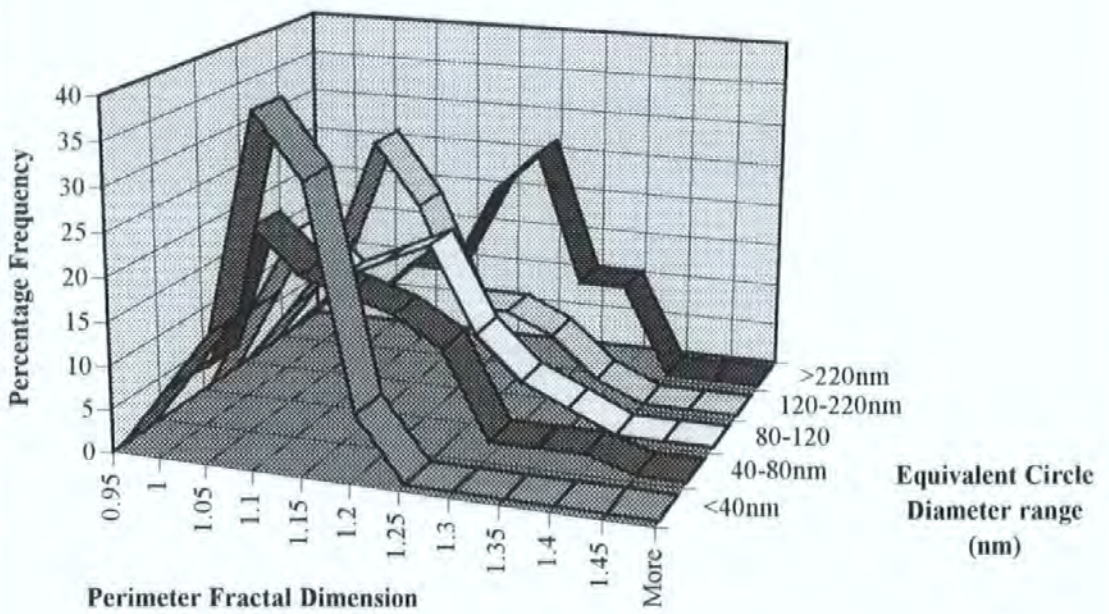
Figure 4.42 PFD distributions for background particles in size ranges (percentage histogram) normalised data

modes in the background fixed sample is evidence of a multi-source aerosol or changes in the original roadside aerosol by particle compaction or agglomeration.

The normalised data histograms also reveal the nature of the roadside and background aerosol (*cf.* Figure 4.41 and 4.42). Normalised analysis allows the comparison between size ranges but the resolution of some particles is greatly increased over others, and for these particles the fine textural data is measured. This effect broadens the modes for the PFD distribution of fine particles. Nevertheless there are some clear feature of the PFD histograms. The roadside data exhibits a bi-modal or extended modal nature in each size range (*cf.* Figure 4.41). In the < 40nm range the small second mode is not distinct and forms a broad mode with the lower mode. For size ranges <40nm, 40-80nm and 80-120nm, the lower mode is at 1.05-1.1, for size ranges 120-220nm and <220nm there are modes at 1.15 to 1.2. The second mode for <40nm is at 1.2 and at 1.25 for the rest of the size ranges. The background data (*cf.* Figure 4.42) does not exhibit this bi-modal nature. For <40nm there is one definite mode at 1.1. The size ranges 40-80, 80-120 and 120-220 have broad modes between 1 and 1.2 and >220nm shows a mode in 1.25.

The low PFD modes in both roadside and background particles below 80nm, is again due to the contribution of individual carbon ceno-spheres. The bi-modal nature of the roadside aerosol, suggests major contributions from two distinct sources, perhaps distinguishing fuel type, aged or fresh particles, or roadside and an artefact from carbon coating. The wide modes for background aerosol supports a multi source aged aerosol with wide ranging morphology. The mode for >220nm is disproportionally large because of the use of percentage histograms but is due to few particles and is not significant.

The breakdown of PFD and DFD for each size range and study date is shown in Figures 4.43 - 4.44. The roadside PFD is shown to be numerically greater for roadside than background aerosol in almost every case. A statistical difference in not found because of the small nature of the sample, however the consistency of differences supports the general rule that PFD at the roadside is greater than the background and this difference is greater above 120nm than below. The DFD is seen to be a very stable measure fluctuating by less than 10% between days, and shows no consistency of differences between roadside or background. Notably the DFD is significantly higher at the 5% level, at the background than the roadside on two occasions for < 40nm particles, (*cf.* Figure 4.44, 2.6.97, 21.7.97; cf. Appendix 2), signifying a greater particle density on these occasions at the background. When the data is separated by day and size the sample size is very small this means that size separated analysis combining the study days is probably the most useful (*cf.* Figures 4.39-4.42)

4.5   Summary of Urban Aerosol Analysis

• Representative samples of roadside and background aerosol were sampled and analysed by size and morphology, both as a whole and broken down into defined size ranges.

• The average perimeter fractal dimension (PFD) of aerosol was consistently and significantly greater at the roadside than the background, by a 0.02 increment of PFD. This is the case both with and without non PFD fractal particles. The reduction in PFD in the background aerosol was interpreted as indicative of an ageing and collapse of fractal aerosol.

• The removal of non PFD fractal dimensions decreases the significance of difference for fixed analysis particles and increases the significance of difference for normalised analysis particles.

Fractal Dimensions at Background and Roadside according to size range, 6.12.96 fixed

Fractal Dimensions at Background and Roadside according to size range, 3.2.97 fixed

Fractal Dimensions at Background and Roadside according to size range, 10.3.97 fixed

Fractal Dimensions at Background and Roadside according to size range, 3.4.97 fixed
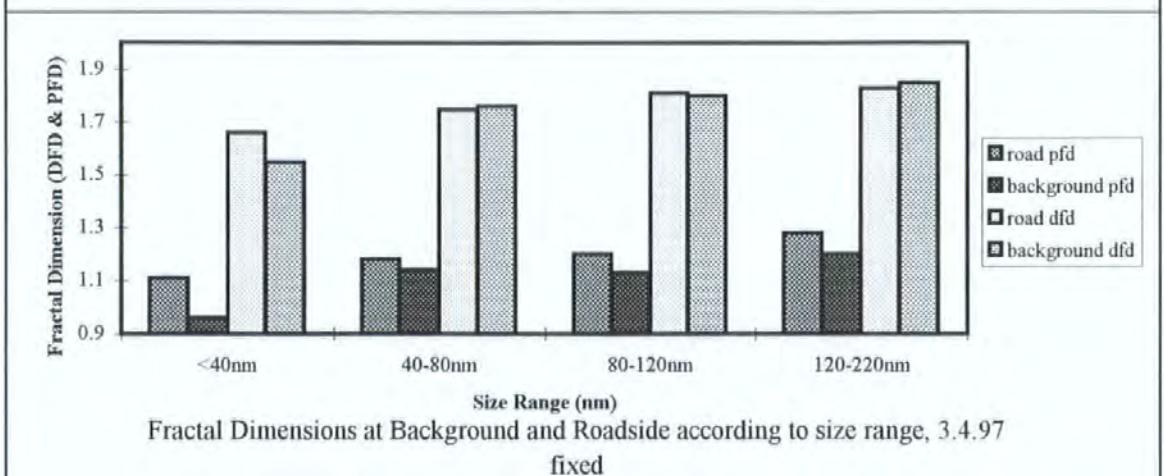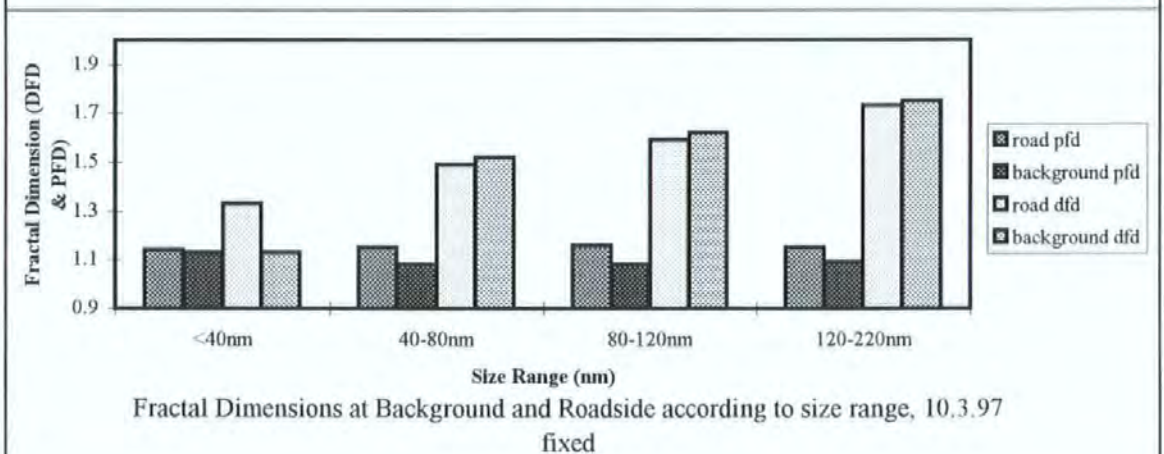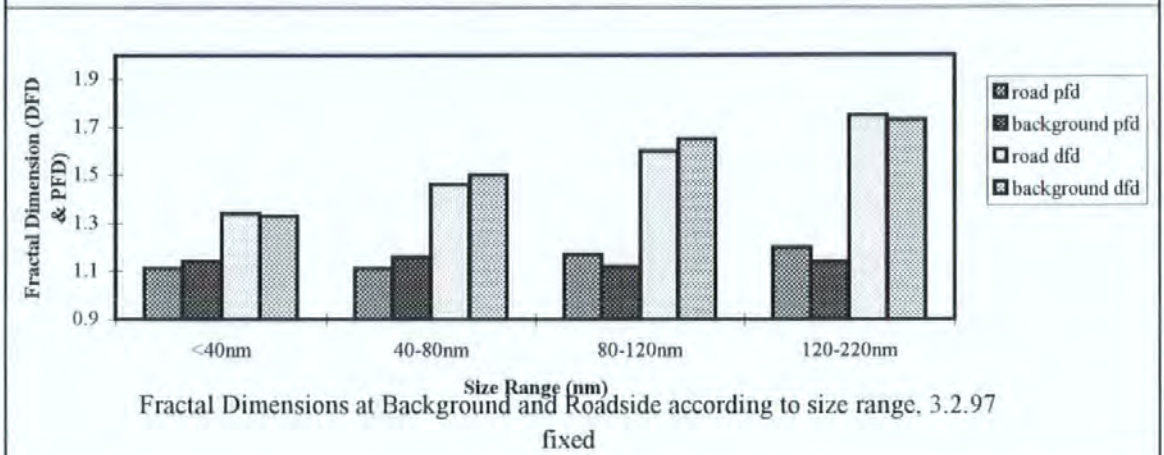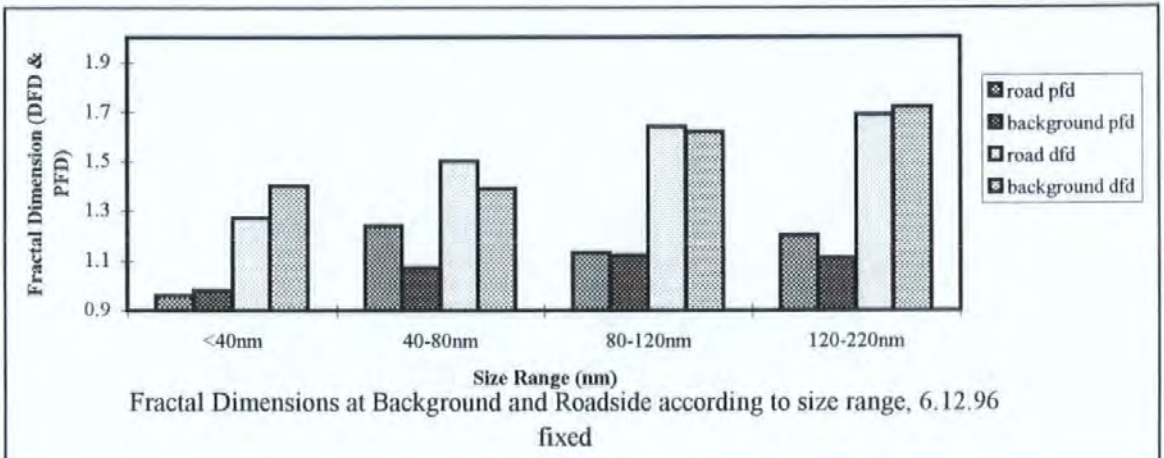
Figure 4.43 Average Daily Aerosol Morphology according to size range (Fixed Data)

Fractal Dimensions at Background and Roadside according to size range, 3.4.97, Nomalised

Fractal Dimensions at Background and Roadside according to size range, 12.5.97 Normalised

Fractal Dimensions at Background and Roadside according to size range, 2.6.97 Normalised

Fractal Dimensions at Background and Roadside according to size range, 21.7.97 Normalised
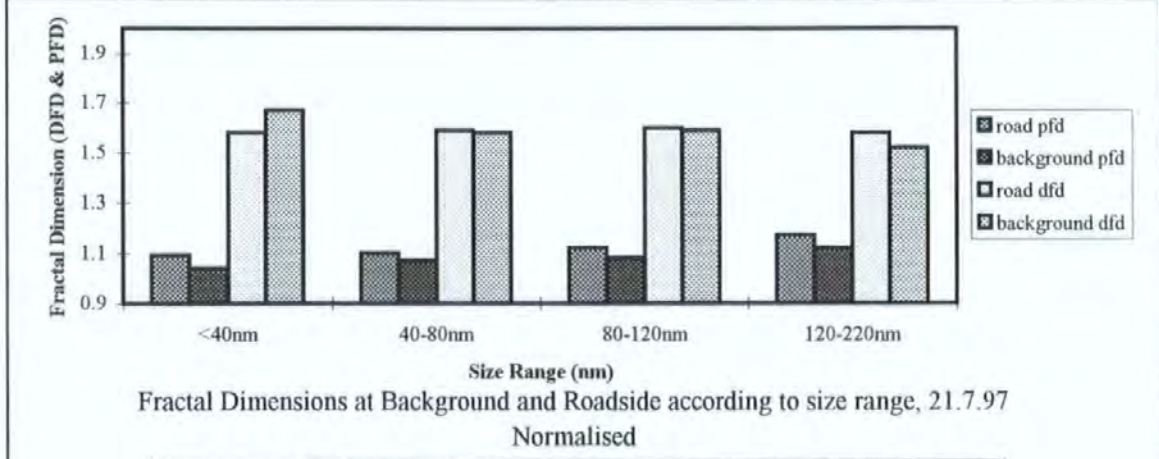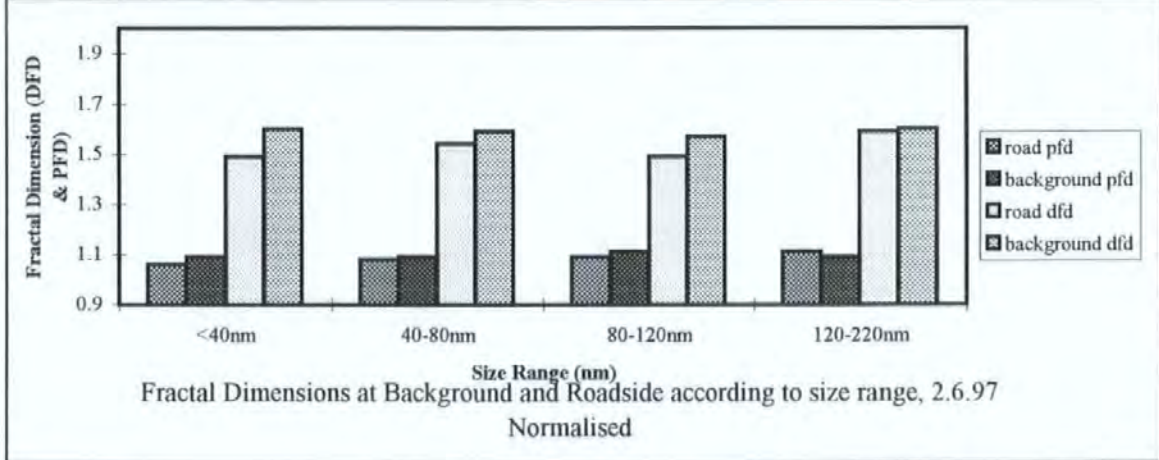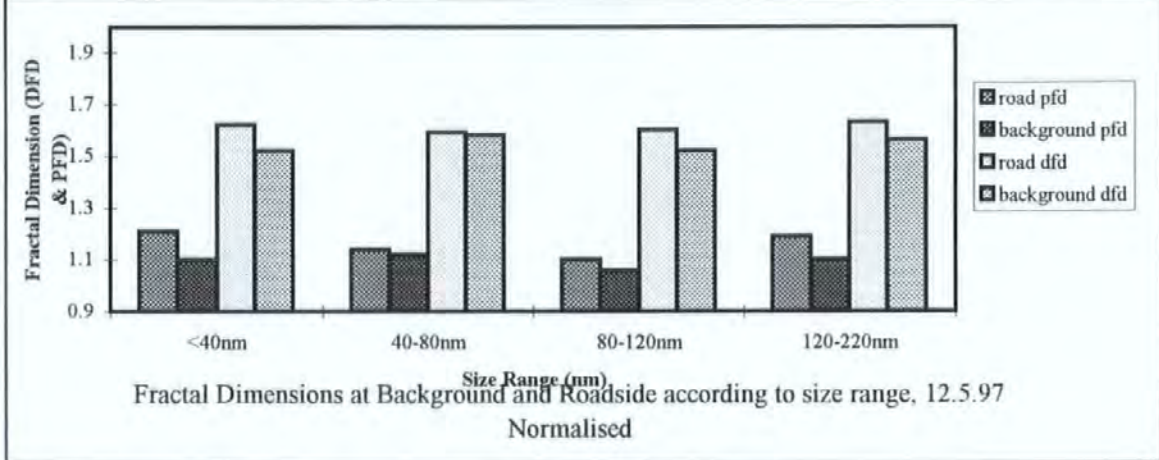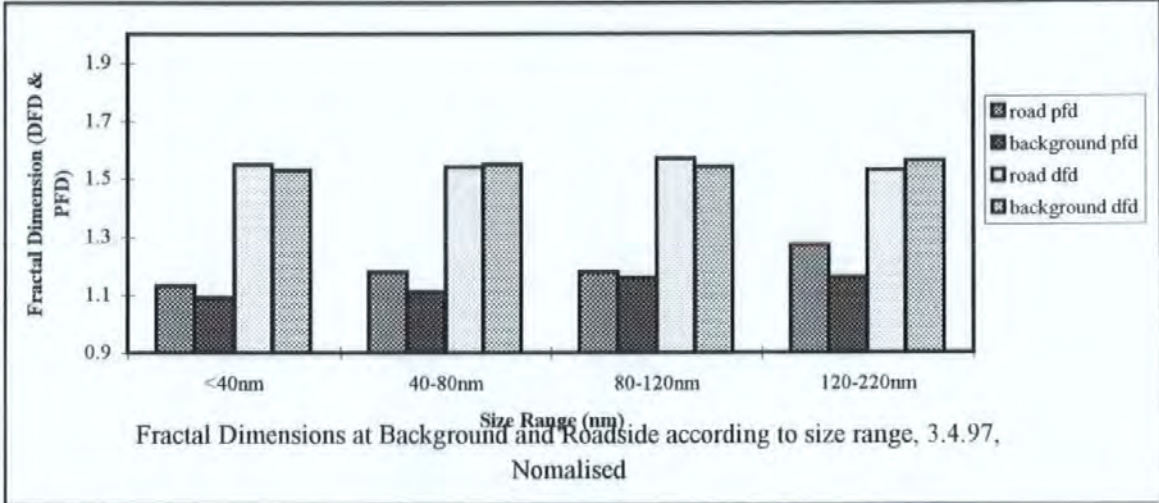
Figure 4.44 Average Daily Morphology according to size range (Normalised Data)

- Non-fractal particles have a smaller mean size at the roadside, because they are dominated by individual carbon ceno-spheres. The background aerosol contains non fractal particles of similar mean size to fractal particles, indicative of aged agglomerates and other aerosol sources.

- Size grouped analysis of the aerosol demonstrates no significant difference in DFD between roadside and background at any size range. However the PFD is significantly greater at the roadside than the background especially for the 120-220nm size range.

- It is suggested that the 120-220nm size range of particles is thus the most influential part of the urban aerosol in terms of morphological nature, being small, numerous and undergoing significant structural changes.

- The PFD distribution with size shows a very different pattern at roadside and background. The normalised data supports a one or two source input at the roadside and a mixed and aged aerosol input at the background. Fixed data shows the domination of size influence and is less useful for interpretation.

- The size separated histograms of PFD and DFD for roadside and background aerosol indicate distinct sources at the roadside, and an aged mix of particles in the background aerosol

- There is a low homogeneity of size, DFD or PFD between study days, this suggests the dominant effect of local meteorological conditions in governing overall atmospheric integrity.

CHAPTER FIVE
The Morphology of Aerosols
from Diesel and Spark Ignition Engines

5.1   Introduction

There have been a number of studies of the morphology of combustion aerosols using the concepts of fractal dimensions (*cf.* Section 1.5.2). In these studies, diesel engine particles (Huang *et al.*, 1994; Skillas *et al.*, 1998), have received greater attention than spark ignition (petrol) engine particles (Colbeck *et al.*, 1997), owing to the good fuming properties of diesel fuel (Kaye, 1993). The fractal measurements of combustion particles can be directly related to their physical properties (Nyeki and Colbeck, 1994), to the formation processes (Kaye and Clark, 1991), and ultimately to the sources of particles (Katrinak *et al.*, 1994). Source morphology measurements of particles are thus vital for the identification of urban sources of fine particles.

In this research aerosol source samples of diesel and spark ignition have been examined in the same way as urban aerosol (*cf.* Chapter 4). The novel sampling of aerosol developed in this research has allowed the analysis of a representative aerosol from a variety of sources (*cf.* Chapter 3). Measurement of the density fractal dimension, perimeter fractal dimension and size of aerosol has been made using computer aided image analysis. Source sample particles were examined with the aim of characterising their morphology and the identification of any source 'fingerprint'. Ultimately these engine samples have been used as an aid to the apportionment of sources to fine and ultra fine aerosol in the urban air (cf. Chapter 6).

5.2   Engine Review

5.2.1   Plymouth Test Engine

Raw diesel engine particles were collected from a diesel engine at the University of Plymouth. The engine used was a Perkins Prima 65 HSDI diesel engine fitted with a Bosch EPVE fuel injector pump and CAV multihole injector, detailed specifications are shown in

Table 5.1. The engine was mounted on a test bed with a Borgi and Saveri FA 1000 eddy current dynamometer controlled by a test automation series 2, 000 C-E compact controller. The Prima diesel engine was one of the earliest high speed DI engines to be fitted in passenger cars. It was used in Rover vans and Maestro and Montego cars in naturally aspirated and turbocharged forms (Pemberton, 1996).

Specifications	
Number of cylinders	4
Cylinder arrangement	In-line
Cycle	Four stroke
Induction system	Naturally aspirated
Fuel injection system	Bosch EPVE pump with CAV multihole injectors
Combustion system	Direct injection
Cubic capacity (cm^3)	1,994
Power 4500 rpm (bhp)	60
Torque at 2500 rpm (Nm)	119
Compression ratio	18.1:1
Bore (mm)	84.4
Stroke (mm)	88.9

Table 5.1 Perkins Prima Engine Specifications (Pemberton, 1996)

5.2.2   Other Engine Sources

A number of small comparative samples were taken at Ricardo Consulting Engineers (Bridgeworks, Shoreham, UK), using a dilution tunnel (*cf.* Figure 5.1), with exhaust from vehicles on a rolling road. A Fiat Tipo 2L spark ignition engine, Citroen 2L I.D.I. diesel and a test direct injection diesel engine were all sampled. The Tipo and Citroen were sampled under steady state conditions at 30kph with the Tipo also sampled at 70kph. The test direct injection diesel engine was sampled during an urban cycle test (Pemberton, 1996).
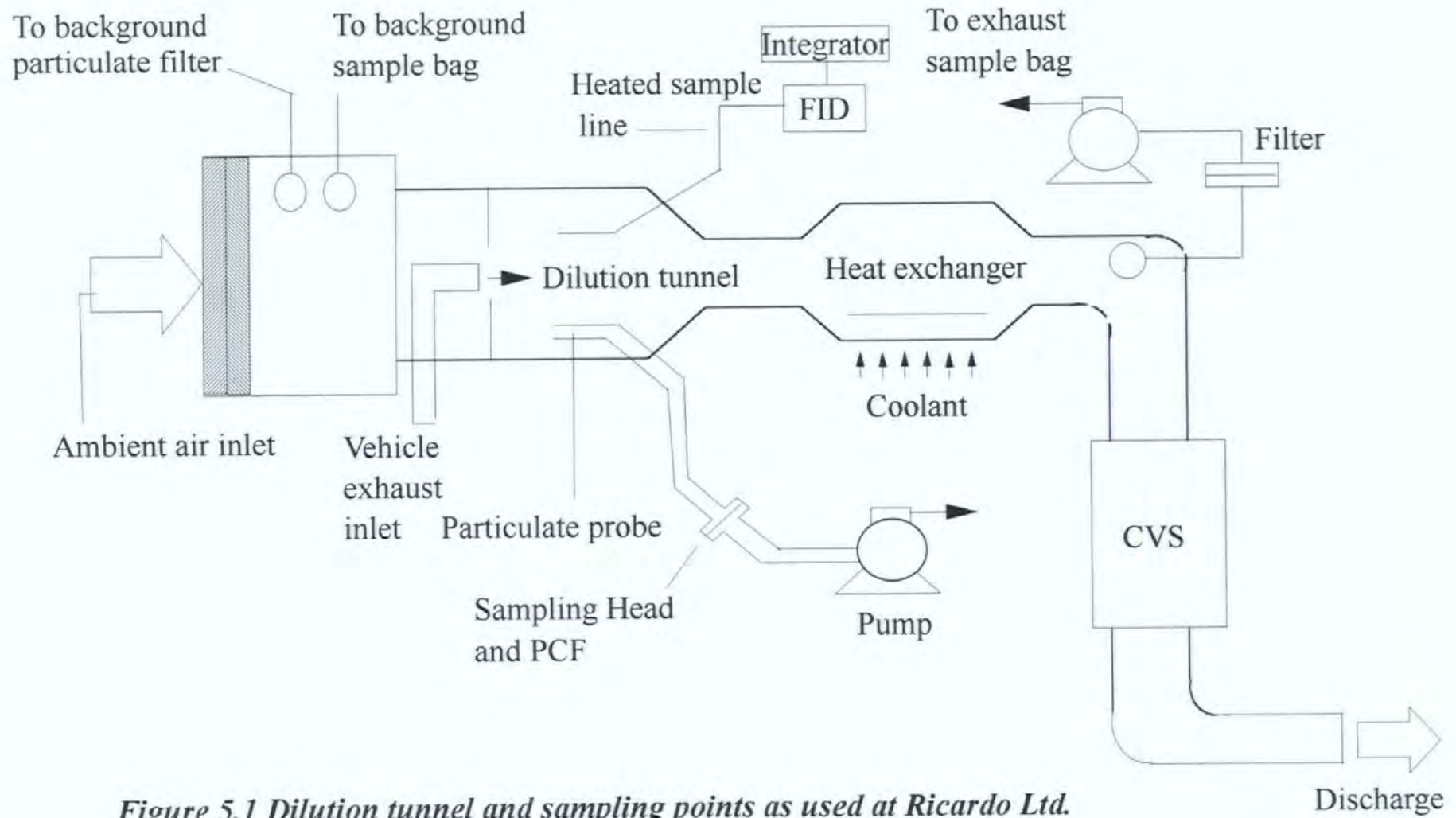
Figure 5.1 Dilution tunnel and sampling points as used at Ricardo Ltd.

5.3 Experimental

5.3.1 Sampling

Raw exhaust from the Perkins *Prima Engine* was extensively sampled at 5 speeds and loads. The porous carbon film (PCF) method as developed at the University of Plymouth, was used (Dye *et al.*, 1997; *cf.* Section 3.2.3.1). European cyclone sampling heads were used with pump sampling rates were set to 1.9 l min^{-1} (*cf.* Section 3.2.1). Sampling was made for periods of 1-10 minutes dependent on the speed and load on the engine. The sampling point was directly from the exhaust stream, with the cyclone sampling head.

Exhaust was also sampled from a series of vehicles on a rolling road and from a dilution tunnel. The direct sampling developed was used (*cf.* Section 3.2.3.1) and the cyclone sampling head was attached to the dilution tunnel *via* the sampling point used for aerosol number sampling (*cf.* Figure 5.1).

5.3.2 Analysis

Analysis of samples was made in a similar way to the aerosol sampling. For the Perkins Prima engine, six samples were made at each speed and load, and a t-test was used to test the repeatability of the experiment. The samples made at Ricardo Consulting Engineers (Bridgeworks, Shoreham, UK) were spot tests, *i.e.* consisting of only one or two samples, each of 50 particles.

5.4 Results and Discussion

5.4.1 Plymouth Test Engine

All of the diesel engine particulate (DEP) inspected was categorised as agglomerate or individual carbonaceous ceno-sphere. The average morphological characteristics for each

speed and load are shown in Table 5.2. Figures 5.2, 5.3 and 5.4 show the histograms of PFD, DFD and diameter, for each speed and load.

Speed and Load (RPM/NM)[1]	DFD ± S.D.	PFD ± S.D.	Equivalent Circle Diameter (nm) ± S.D.
1000/10 (95)	1.58 ± 0.08	1.13 ± 0.10	160 ± 123
1000/50 (99)	1.58 ± 0.08	1.15 ± 0.10	165 ± 174
2250/30 (120)	1.59 ± 0.09	1.12 ± 0.09	104 ± 94
3500/10 (120)	1.57 ± 0.08	1.12 ± 0.08	89 ± 61
3500/50 (119)	1.60 ± 0.07	1.12 ± 0.08	87 ± 48

1. Includes the number of particles analysed for each speed and load in parenthesis

Table 5.2 Mean DFD, PFD and Equivalent Circle Diameter at each speed and load for the Prima Engine

An ANOVA test showed that there were no significant differences between the diesel engine particles at different speeds and loads, apart from on a size basis. Two significantly different groups were found, the 1000 rpm groups and the >1000rpm groups. There was no significant difference between the two low speed groups (1000 rpm / 10 Nm and 1000 rpm / 50 Nm) and no significant difference between the > 1000 rpm groups (2250 rpm / 30 Nm, 3500 rpm / 10 Nm and 3500 rpm / 50 Nm). Table 5.3 shows the grouped data means, and Figures 5.2, 5.3 and 5.4 show the similarity of morphology distribution but the dissimilarity of size distribution.

Speed and Load (RPM/NM)[1]	DFD ± S.D.	PFD ± S.D.	Equivalent Circle Diameter (nm) ± S.D. (median)
All data (553)	1.58 ± 0.08	1.13 ± 0.09	117 ± 111 (90)
1000/10 and 1000/50 (194)	1.58 ± 0.08	1.14 ± 0.10	163 ± 151 (121)
2250/30, 3500/10 and 3500/50 (359)	1.59 ± 0.08	1.12 ± 0.08	93 ± 71 (76)

1. Includes the number of particles analysed for each group in parenthesis

Table 5.3 Grouped data mean DFD, PFD and Equivalent circle diameter
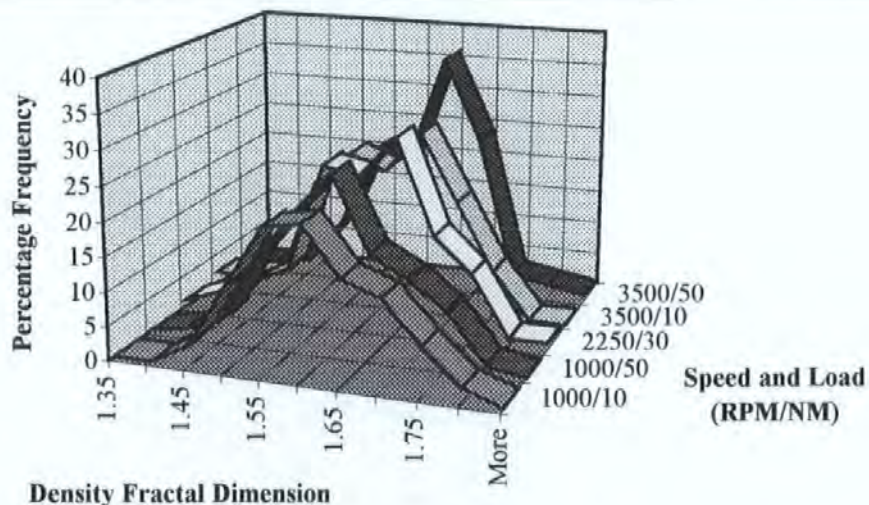
Figure 5.2 DFD distributions for Particles from a Perkins Prima D.I. 2L at different speeds and loads
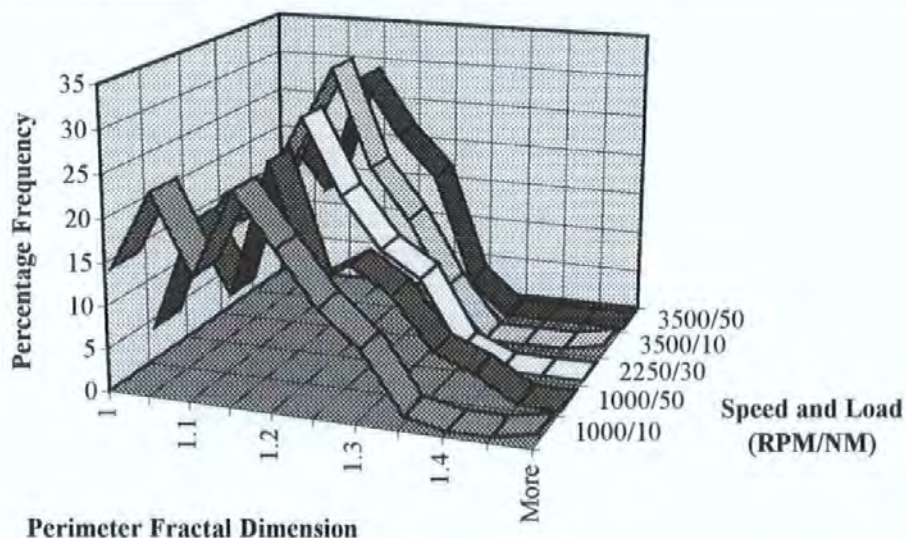
Figure 5.3 PFD distributions for Particles from a Perkins Prima D.I. 2L at different speeds and loads
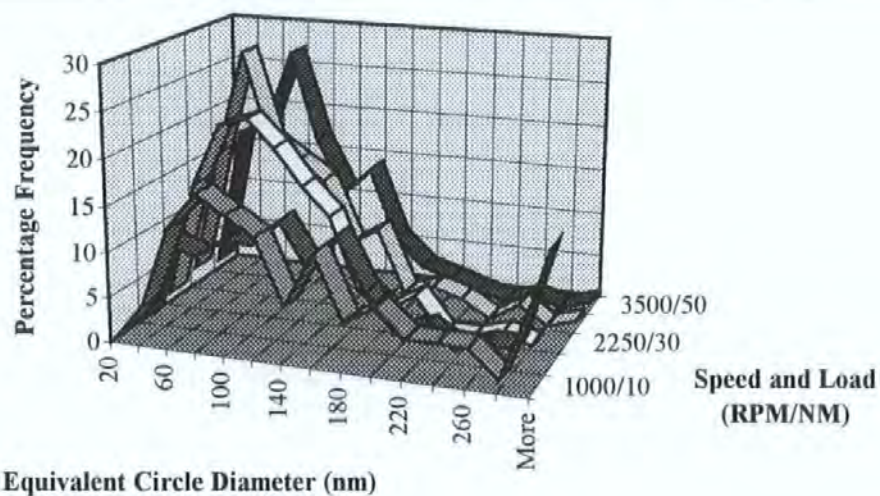
Figure 5.4 Equivalent Circle Diameter (nm) distributions for Particles from a Perkins Prima D.I. 2L at different speeds and loads

The grouped data means show that the low speed samples have a marginally lower mean DFD and greater mean equivalent circle diameter than the >1000rpm groups. This may be a real effect or due to a larger mean particle size at low speed. The mean particle size at low speed may be greater because of the lower rate of combustion of fuel. Fuel is combusted and exhausted from the engine more slowly therefore spending more time in this high concentration of particles (Skillas *et al.*, 1998). The particles therefore have more time to grow and agglomerate and so will grow larger.

Comparison of particle morphologies within set size ranges removes any size induced differences between mean fractal dimensions (*cf.* Section 4.4.2.3). Any significant difference between and speed and load was calculate using an ANOVA test as shown in Table 5.4.

Size range	DFD (p value)[1]	PFD (p value)[1]	Equivalent Circle Diameter (p value)[1]
< 40nm	no (0.46)	no (0.31)	no (0.73)
40-80nm	no (0.30)	yes (0.02) (1000/10)	no (0.43)
80-120nm	no (0.34)	no (0.054)	no (0.94)
120-220nm	yes (0.0002) (2250/30)	yes (0.002) (3000/50)	yes (0.022) (1000/10)
> 220nm	no (0.37)	no (0.14)	no (0.53)

1. The significantly different group within a size range is included in the second set of parenthesis

Table 5.4 Significant difference between any speed and load groups using ANOVA

Whilst there are some differences shown in Table 5.4, there is no evidence of any consistent significant difference between particles produced at different speeds and loads. At 40-80nm and 120-220nm some individual groups were found to be significantly different (*cf.* Table 5.4), but no pattern of group differences is apparent. The diesel engine may be therefore considered reasonably consistent in the size grouped morphology of particles which it produces. The histograms for different size ranges, show a consistency in shape and value

of the DFD mode generally between 1.6 and 1.7 (*cf.* Figure 5.6). The PFD distribution for
each size range exhibit a regular increase in the modal value (*cf.* Figure 5.7). This supports
the postulation of a predictable diesel engine source morphology useful for source
apportionment (Katrinak *et al.*, 1993). The grouped morphology characteristics are given
in Table 5.5.

Size Range (nm)		Equivalent Circle Diameter (nm)	Density Fractal Dimension	Perimeter Fractal Dimension
< 40	mean	31	1.62	1.05
	standard deviation	6	0.08	0.07
	median	33	1.63	1.04
40-80	mean	60	1.58	1.11
	standard deviation	10	0.08	0.08
	median	60	1.57	1.11
80-120	mean	98	1.58	1.13
	standard deviation	11	0.08	0.09
	median	97	1.58	1.13
120-220	mean	155	1.58	1.15
	standard deviation	26	0.08	0.09
	median	149	1.58	1.15
>220	mean	387	1.58	1.19
	standard deviation	202	0.10	0.09
	median	322	1.60	1.21

*Table 5.5 Grouped morphology characteristics for all speeds and loads of diesel engine
particles from the Perkins Prima*

The size grouped results for the prima engine (*cf.* Table 5.5) have a similar pattern to those
found in urban air (*cf.* Figures 4.36 - 4.38). In both cases the DFD is consistent with
increasing particle size, although the diesel engine particles have a slightly greater DFD
below 40nm of 1.62 as compared to less than 1.6 for both roadside and background air.
Also in both urban and the diesel engine samples the PFD increases with particle size (*cf.*
Table 5.5 and Figures 4.36 - 4.38). This may be indicative of similar particle types in both
urban and diesel engine samples.
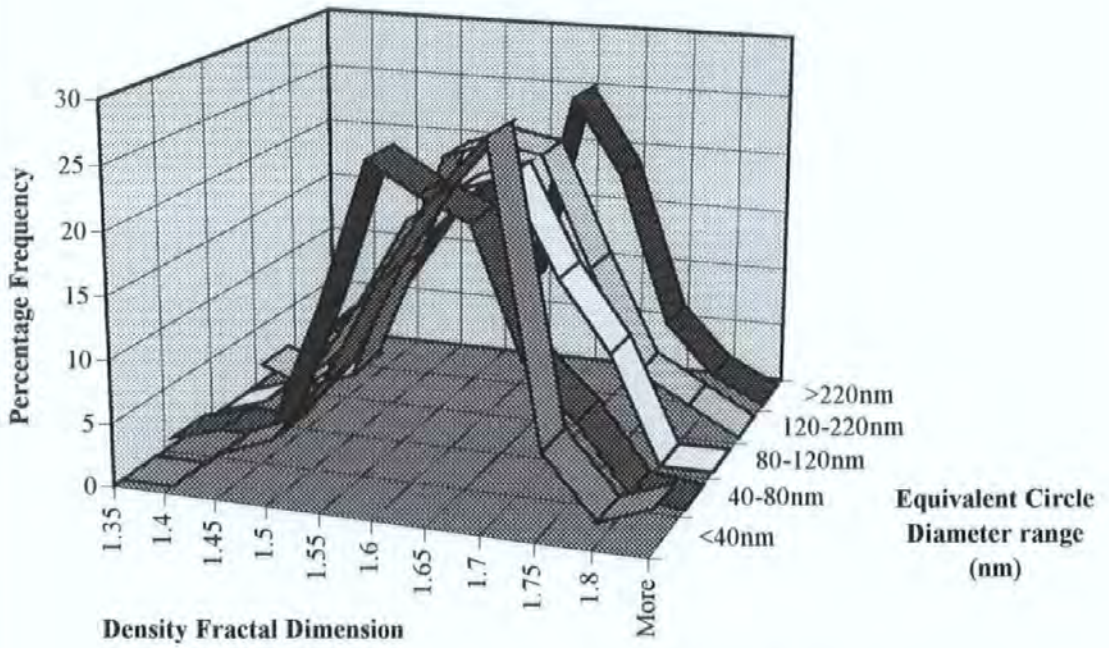
Figure 5.6 DFD distributions for All Prima Engine Particles in size ranges (percentage histogram)
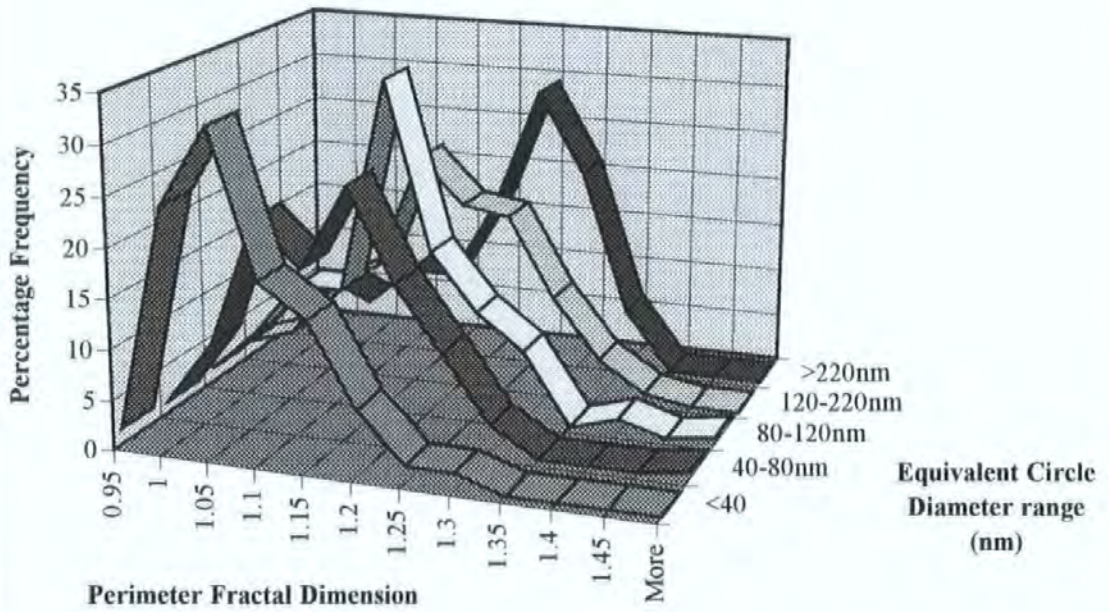
Figure 5.7 PFD distributions for All Prima Engine Particles in size ranges (percentage histogram)

The consistency of diesel engine combustion is shown in the comparison of measurements with other studies (*cf.* Table 5.6). The density fractal dimension of diesel engine particles (DEP) in this work using low sulphur fuel agrees closely with the work of Huang *et al.*, (1994) which examined fresh DEP from low sulphur fuel (*cf.* Table 5.6).

Study	DFD	PFD	Mean Diameter (μm)
Huang *et al.*, 1994[1]			
High Sulphur (0.84% wt) Diesel Particles	1.46 ± 0.3	----	0.55 ± 0.2
Collapsed High Sulphur Diesel Particles	1.46 ± 0.3	----	0.55 ± 0.2
Mid Sulphur (0.32% wt) Diesel Particles	1.40 ± 0.3	----	0.82 ± 0.2
Collapsed Mid Sulphur Diesel Particles	1.54 ± 0.3	----	0.81 ± 0.2
Low Sulphur (0.034% wt) Diesel Particles	1.56 ± 0.2	----	0.96 ± 0.2
Collapsed Low Sulphur Diesel Particle	1.76 ± 0.2	----	0.96 ± 0.2
Forrest and Witten, 1979[2]			
Iron, zinc, silicon dioxide aggregates	$1.7\text{-}1.9 \pm 0.02$	----	1-9
Samson *et al.*, 1987[3]			
Acetylene combustion	1.5-1.6	----	0.1-40
Colbeck et al., 1997[4]			
Petrol	----	1.27	> 0.4
Diesel	2.04 ± 0.2	1.25	> 0.4
Fuel oil	1.88 ± 0.2	1.15	> 0.4
Paraffin oil	----	1.19	> 0.4
Butane	1.97 ± 0.2	1.25	> 0.4
Wood	2.35 ± 0.2	1.12	> 0.4
Skillas *et al.*, 1997[5]			
Diesel			0.05-0.15
Load 0 kW	2.9	---	
Load 0.5 kW	2.9	---	
Load 1.0 kW	2.6	---	
Load 1.5 kW	2.4	---	
Load 2.0 kW	2.25	---	
Load 2.5 kW	2.4	---	

1. Two dimensional DFD calculated using nested circle method (Tence *et al.*, 1986)
2. Two dimensional DFD calculated using nested squares method (Mandelbrot, 1977)
3. Two dimensional DFD calculated using particle counting method (Meakin *et al.*, 1984) for <5µm particles, and using nested squares method for 5-40µm particles
4. Three dimensional DFD calculated using *in situ* method (Nyeki and Colbeck, 1994), PFD calculated using stepping method (Kaye, 1989), also called textural fractal dimension
5. 'Fractal like' Three dimensional DFD calculated from diameter and mass of particles.

Table 5.6 Fractal dimensions of sources from other studies

Both PFD and DFD in this study are similar to comparable values of diesel particles in other studies (*cf.* Table 5.6). Notably other hydrocarbon sources give similar PFD and DFD values (Samson *et al.*, 1987; Colbeck *et al.*, 1997) but non hydrocarbon sources are quite different (Forrest and Witten, 1979; Colbeck *et al.*, 1997). Skillas *et al.*, (1997), has shown some relationship between engine loading and particle DFD, that with increased load the particle DFD decreased (*cf.* Table 5.6). The result by Skillas *et al.*, (1997) was found by calculating the three dimensional fractal dimension of particles and thus is not directly comparable or able to be confirmed, using the two dimensional fractal dimensions in this work (Weber, 1992). For the Prima, Table 5.3 shows the exhaust was separated in to statistically different groups of low load, (DFD = 1.58) and high load (DFD = 1.59). However the significant difference between groups is more owing to the PFD than DFD. Thus the trend indicated by Skillas *et al.*, 1998, has been neither confirmed or contradicted in this research.

5.4.2 Ricardo sampled sources

The characteristics of the aerosol collected from the Ricardo test vehicles at different speeds and loads, are shown in Table 5.7. Although the integrity of these samples is not statistically supported, they are useful for the understanding of the variability of roadside generated aerosol. Figures 5.7, 5.8 and 5.9 show the histogram of Ricardo sources.

Source[1]	DFD ± S.D.	PFD ± S.D.	Equivalent Circle Diameter (nm) ± S.D. (median)
Tipo 30kph Petrol (48)	1.61 ± 0.09	1.09 ± 0.09	101 ± 109 (67)
Tipo 70kph Petrol (49)	1.56 ± 0.10	1.10 ± 0.08	160 ± 139 (115)
Citroen 30kph I.D.I. (51)	1.57 ± 0.09	1.10 ± 0.08	119 ± 70 (101)
Seria s4 D.I. (50)	1.56 ± 0.10	1.10 ± 0.08	120 ± 84 (80)
Seria s2 D.I. (50)	1.54 ± 0.11	1.12 ± 0.08	86 ± 43 (76)

1. The number of particles measured for each source in parenthesis

Table 5.7 Average Particle characteristics for Ricardo vehicle samples
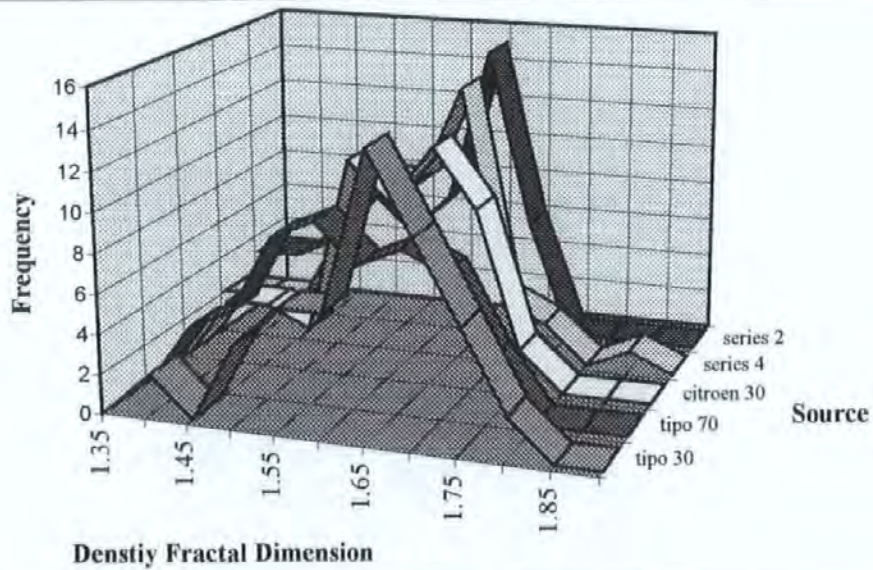
Figure 5.7 Histogram of DFD according to Ricardo Test Source
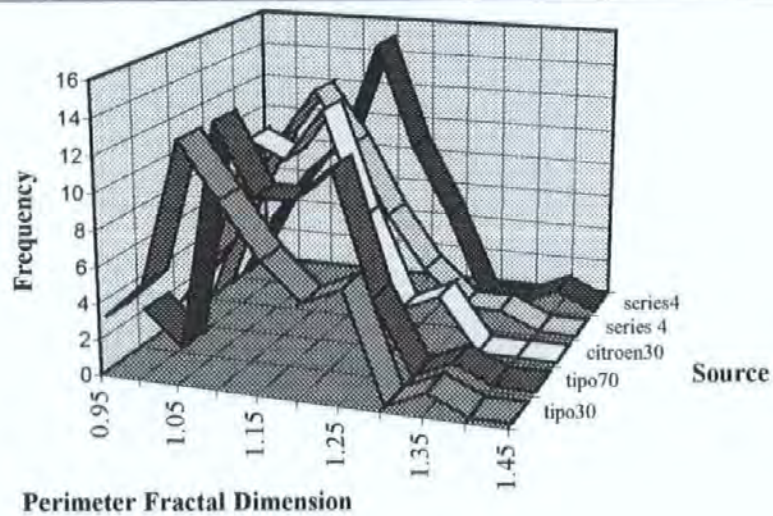
Figure 5.8 Histogram of PFD according to Ricardo Test Source
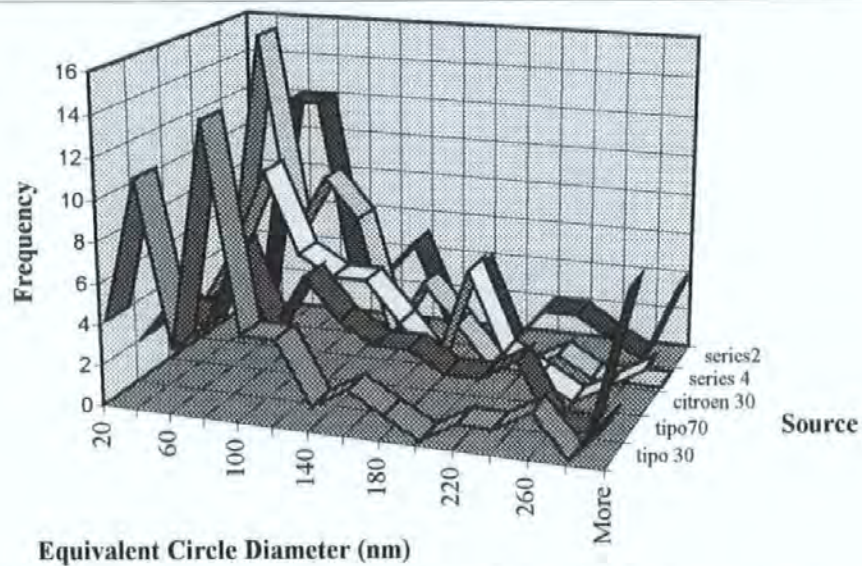
Figure 5.9 Histogram of particle size according to Ricardo Test Source

The DFD for each of these samples, except the Tipo 30 kph sample (*cf*. Table 5.7), were all less than the DFD found for the Prima engine (1.58). The PFD for all of the samples (*cf*. Table 5.7), was also less than that for the Prima engine (1.13). This effect of lowering density and yet smoothing of the particle is indicative of agglomeration in the dilution tunnel. The difference between the PFD and DFD for the Prima and the engines with the dilution tunnel is similar to that between the roadside and the background.

Because only single small samples were taken an ANOVA test between the means in table 5.7 is not very useful. As with the Prima engine data any size effects upon the means may be reduced by considering data within set size ranges. An ANOVA was used to determine any significant difference between any of the spot samples listed (*cf*. Table 5.7) within the size ranges, results are shown in Table 5.8.

Size range	DFD	PFD	Equivalent Circle Diameter (nm)
< 40nm	yes (0.026) (tipo70, citroen30)	no (0.64)	no (0.93)
40-80nm	no (0.50)	no (0.76)	no (0.20)
80-120nm	yes (0.0066) (sierra s2)	no (0.25)	no (0.90)
120-220nm	yes (0.0002) (sierra s2)	no (0.26)	no (0.94)
> 220nm	no (0.35)	no (0.98)	no (0.40)

P values are shown in the first parenthesis
The significantly different groups are shown in the second set of parenthesis

Table 5.8 Results of ANOVA indicating significance of difference between source samples within size ranges

As with the Prima engine there are significant differences between some groups. Notably the significant differences that do occur are only in terms of DFD. Although there is no one group or source which may be consistently separated as significantly different, the DFD exhibits that it could be sensitive parameter for the separation of different sources. This is

contrary to previous work where PFD was identified as the most useful parameter in aerosol morphology characterisation (*cf.* Section 4.4.2.1).

5.4.3 Comparison of Source Distributions

The morphology distribution has previously been used in an examination of the modal nature of the particle morphology distribution (*cf.* Figures 4.39 - 4.42; *cf.* Section 4.4.2.4). A similar analysis of the modal nature of the source distribution can be made. The percentage histograms of morphology are shown in Figures 5.10, 5.11. and 5.12. These figures compare PFD, DFD and equivalent circle diameter for all Prima engine DEP, all Ricardo diesel engine particles, and all Ricardo petrol engine particle sources.

The DFD distribution is very similar for each source group (*cf.* Figure 5.10). Each source exhibits a broad mode between 1.45 and 1.8, however both Ricardo petrol and diesel groupings show some tendency for a peak at 1.65. The second peak (1.65) for the Ricardo samples could be indicative of the similar sampling conditions, different from the Prima sampling conditions. This second peak is not shifted from the broad mode so there is no concrete argument for a difference. Figure 5.10 is supportive of the consistency of DFD across hydrocarbon combustion.

Figure 5.11 compares the PFD distribution for each source. All three source groups have a single mode between 0.95 and 1.35, but there are some notable features. Both Ricardo diesel source and Prima diesel source have a mode peak at 1.2 which is recognisably separate from the Ricardo Petrol mode peak at 1.05. The petrol histogram is distinct in that it has a peak at 1.05 but a large 'hump' between 1.1 and 1.3 which the diesel source histograms do no exhibit.
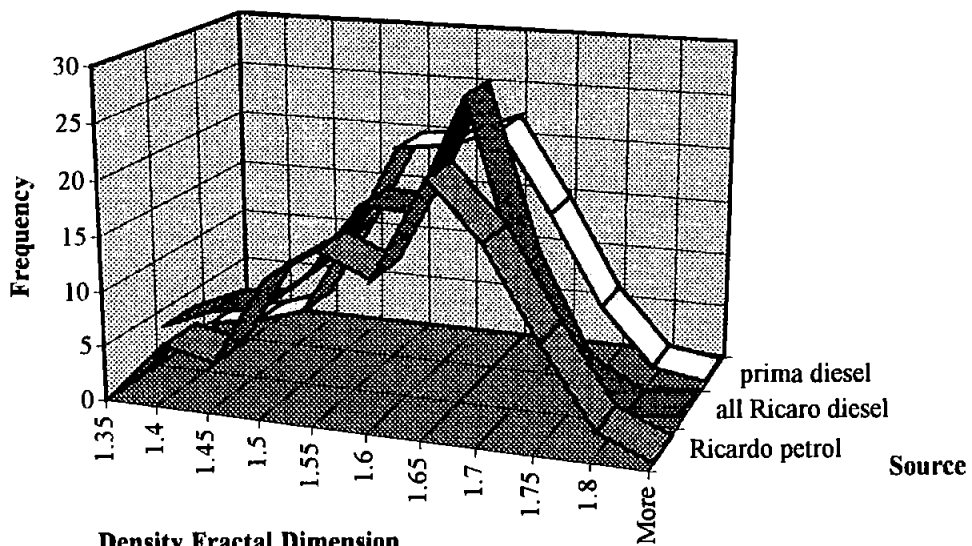
Figure 5.10 Histogram of DFD according to grouped Ricardo and Prima Sources
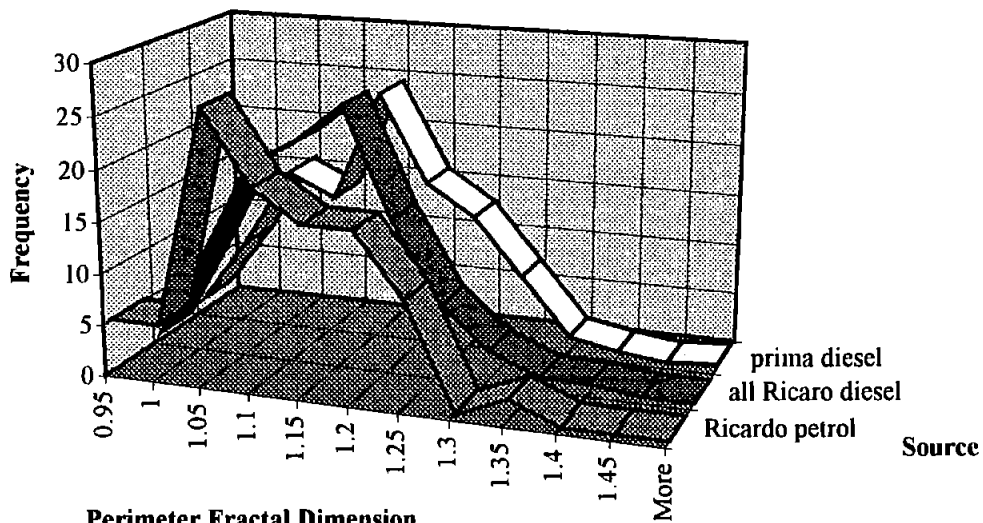
Figure 5.11 Histogram of PFD according to grouped Ricardo and Prima Sources
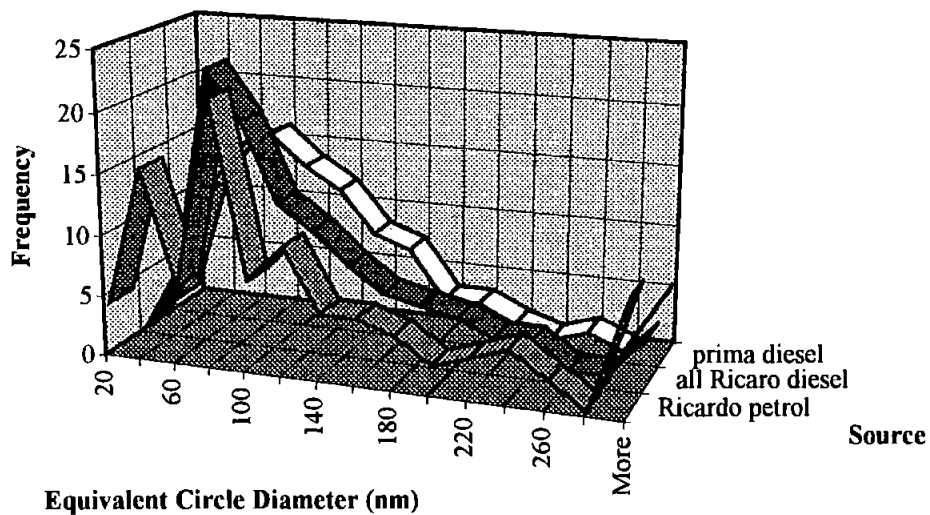
Figure 5.12 Histogram of size according to grouped Ricardo and Prima Sources

An ANOVA of all three reveals a significant difference between the groups ($p = 0.0003$), but the separation of the petrol peak is not statistically possible because of the skew of the histogram.

The equivalent circle diameter distribution is compared in Figure 5.12, and shows that there is no distinct differences the particle sizes measured. An ANOVA confirms the lack of significant difference ($p = 0.26$) and each source has a mean size between 110 and 130 nm.

Comparison of the sources within size ranges provides a more detailed picture of morphology. Figures 5.13-5.17 show the PFD distribution for each source according to size range. There is a large overlap between the sources in each group which makes separation difficult although some distinct features are discernable. In each chart the petrol histogram has a lower peak, between 1.05 and 1.15, and a broad 'hump' between 1.1 and 1.5. This broad hump is not shown in either diesel groups apart from in the <40nm grouping perhaps. The reason for this consistent shape of peak and hump is unknown but possibly exclusive to petrol combustion.

The consistency of the diesel combustion sources can again be identified. In the < 40nm, 40-80nm and 80-120nm histograms the mode for each diesel source occurs in the same place and in the 120-220nm is identifiably separate from the petrol source peak. In the 120-220nm size range both diesel engine sources have modes at a larger PFD than the petrol source.
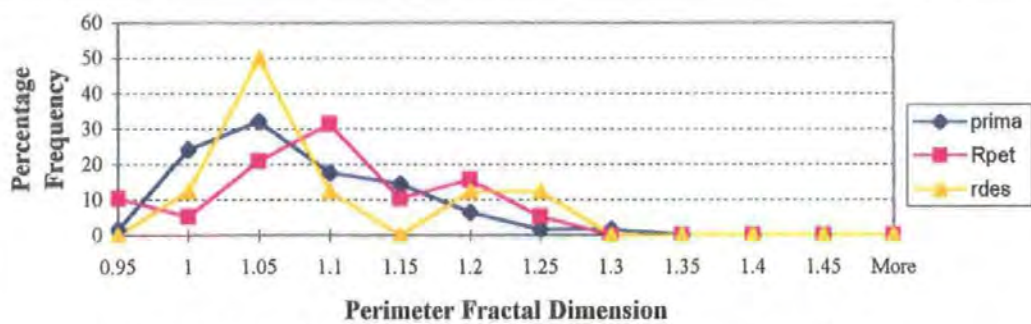
Figure 5.13 PFD distributions for grouped sources <40nm
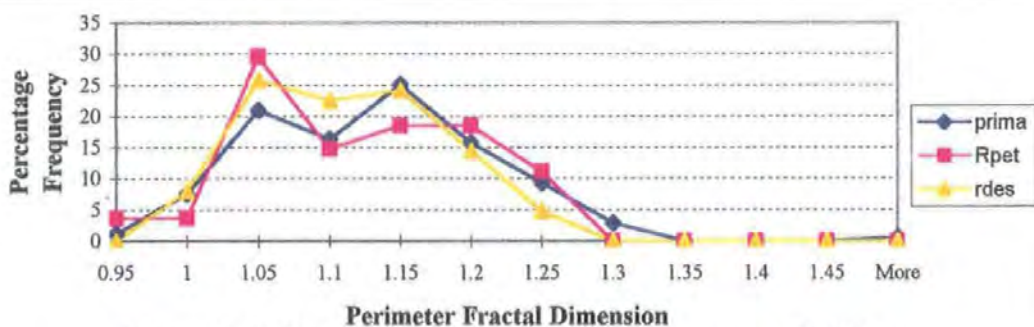
Figure 5.14 PFD distributions for grouped sources 40-80nm
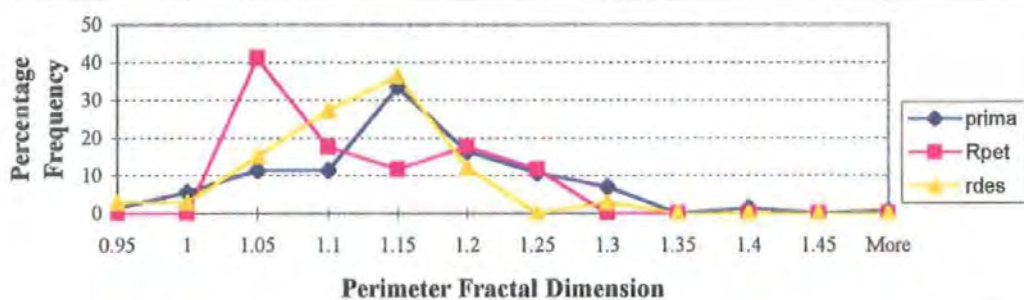
Figure 5.15 PFD distributions for grouped sources 80-120 nm
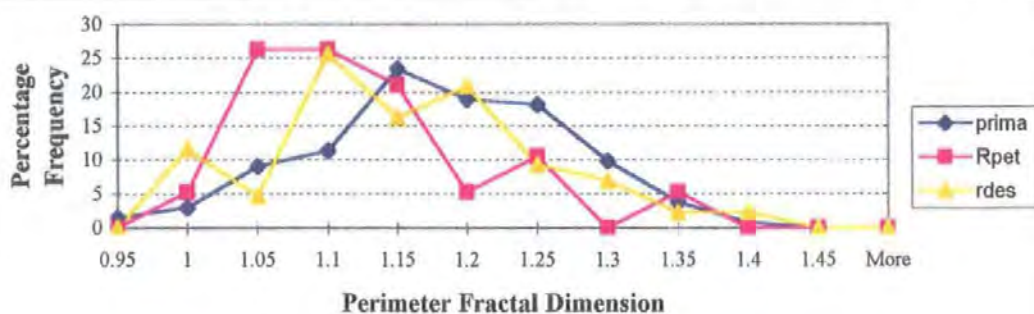
Figure 5.16 PFD distributions for grouped sources 120-220 nm
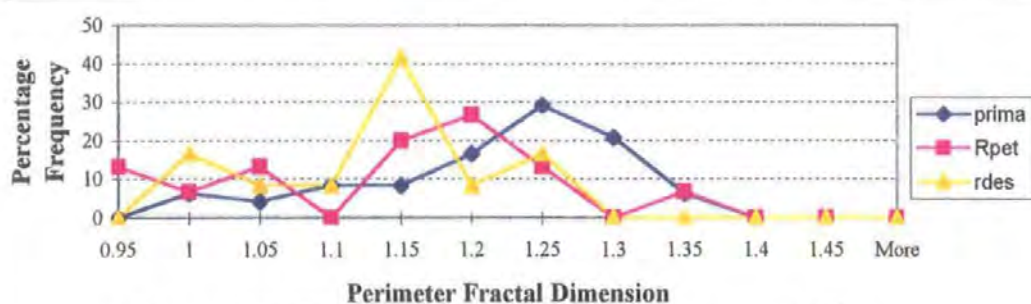
Figure 5.17 PFD distributions for grouped sources >220nm

Statistical analysis of the differences between size ranges shows no significant difference between groups apart from the 120-220nm size range (p=0.0007) where the petrol source may be separated as significantly different. Again the broad modes and petrol histogram skew prevent any statistical separation of the sources according to the means. However the identification of modes from the PFD histograms of urban aerosol sample could provide a tentative approach to source apportionment (*cf.* Chapter 6).

5.4.4 Size *vs.* Morphology of Source Particles

A study of acetylene soot by Samson *et al.* (1987) noted that the density fractal dimension could vary with the size of agglomerate. This size relationship is owing to soot being made up of carbon ceno-spheres of finite size and because of the different agglomeration regimes in which soot can form (Skillas *et al.*, 1998; *cf.* Section 1.5.2). However no work has found any conclusive trend relationship (Katrinak *et al.*, 1993), possibly for a number of reasons: sizing made by aerodynamic diameter is its self related to the morphology of particle and therefore morphology *vs.* physical agglomerate size relationship will be obscured; also the wide range of particle morphologies produced prevents the identification of any clear trends (Katrinak *et al.*, 1993).

The study of the relationship between size and fractal dimension is useful because of the direct relationship to ceno-sphere size and formation dynamics (Skillas *et al.*, 1998). The examination of source particle PFD at different sizes can thus give insights into the formation dynamics of the aerosol (Kaye and Clark, 1992). The PFD of sources is related to its formation conditions both in terms of variation within source (Huang *et al.*, 1994) and between different sources (Colbeck *et al.*, 1997). It may be surmised that a comparable size *vs.* PFD relationship relates to similar formation dynamics and a similar source of aerosol.

The combustion process produces a range of PFD values at any size, because of the varying agglomeration processes in the growth of engine particles (Katrinak *et al.*, 1993; Skillas *et al.*, 1998). As previously shown in this work there is an inherent difficulty in the separation of mean particle type at any particular engine condition *i.e.* the engine is consistent in production of a range of morphologies (*cf.* Section 5.4.1). For this reason comparison is made of PFD *vs.* the size range. The Figures 5.18 to 5.22 show the comparison of the PFD to the equivalent circle diameter for the Prima and Ricardo engine sources. Size ranges have been selected to give as many data points as possible, without losing the resolution of the charts (*cf.* Figures 5.18 to 5.22). The median PFD value of the size range is used so as to most accurately represent the sometimes skewed distribution of PFD and equivalent circle diameter. The error bars in Figures 5.18 to 5.22 show the interquartile range of the median value, always representing greater than ten particle PFD measures.

Figure 5.18 Shows the comparison of median particles PFD with median equivalent circle diameter for all Perkins Prima particles. The increase in median PFD follows a natural log relationship with respect to the median diameter. The regression value of 0.89 shows that this relationship is fairly strong. The trend line on the chart follows a natural log curve, which describes the overall relationship of diesel particle morphology and size. This relationship is governed by the agglomeration environments through which the particles are produced (*cf.* Section 1.5). Inspection of the first five data points (*cf.* Figure 5.19) suggests this tendency is towards one that is a highly rounded non-fractal particle. This is expected as below *ca.* 40nm the PFD will tend toward a median of one ,describing the spherical carbon ceno-spheres which make up the agglomerate. This breaks from the general trend line shown (*cf.* Figure 5.18) which is governed by the agglomeration characteristics of the particles.
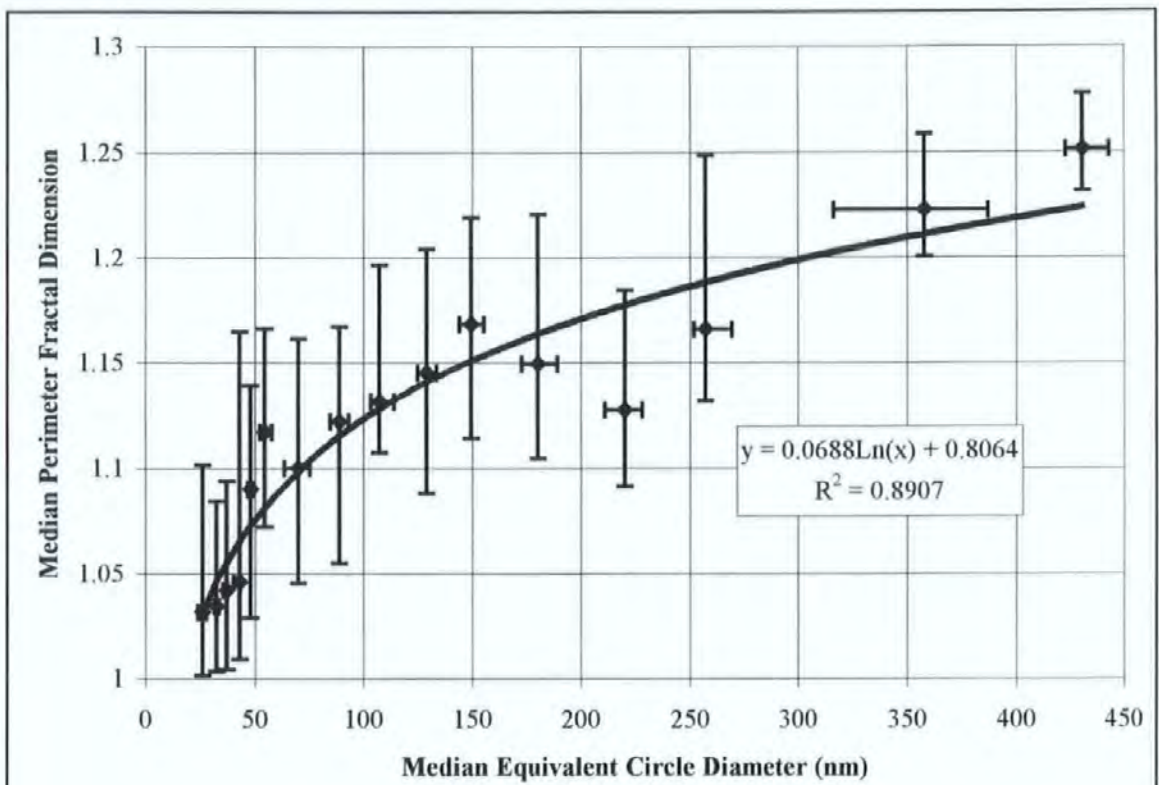
Figure 5.18 Comparison of size ranges and morphology using median values of PFD and Equivalent Circle Diameter (nm), for all particles from the Perkins Prima D.I. (error bars = interquartile range)
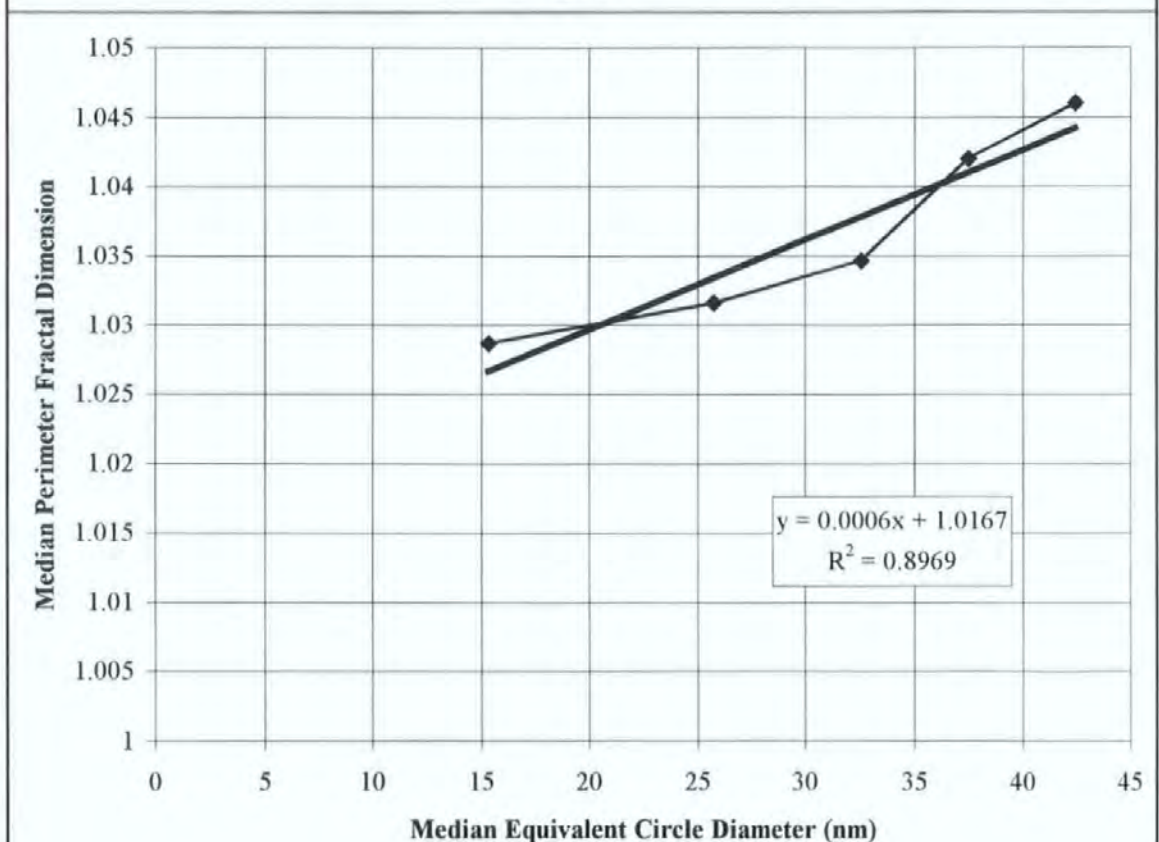
Figure 5.19 Comparison of size ranges and morphology using median values of PFD and Equivalent Circle Diameter (nm), for all particles from the Perkins Prima D.I. below 50nm
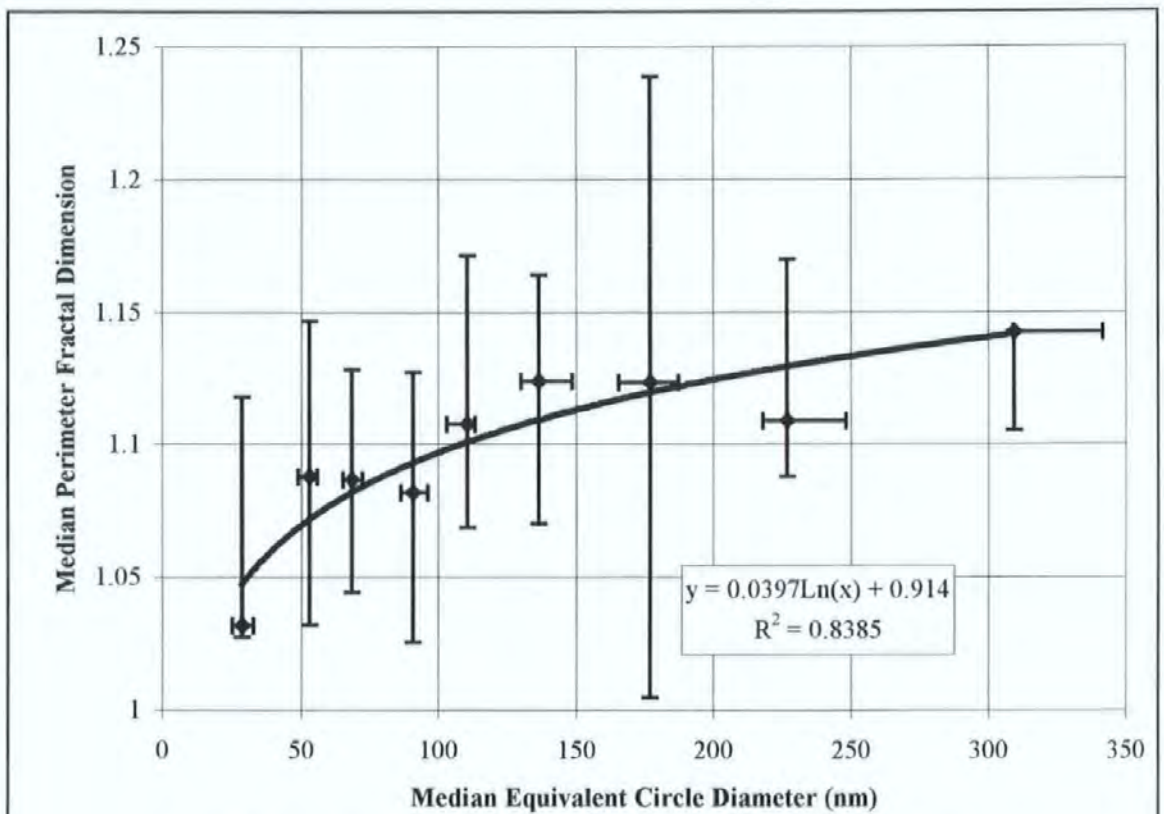
Figure 5.20 Comparison of size ranges and morphology using median values of PFD and Equivalent Circle Diameter (nm), for all particles from Ricardo Diesels, D.I and I.D.I. (Error bars show interquartile range)
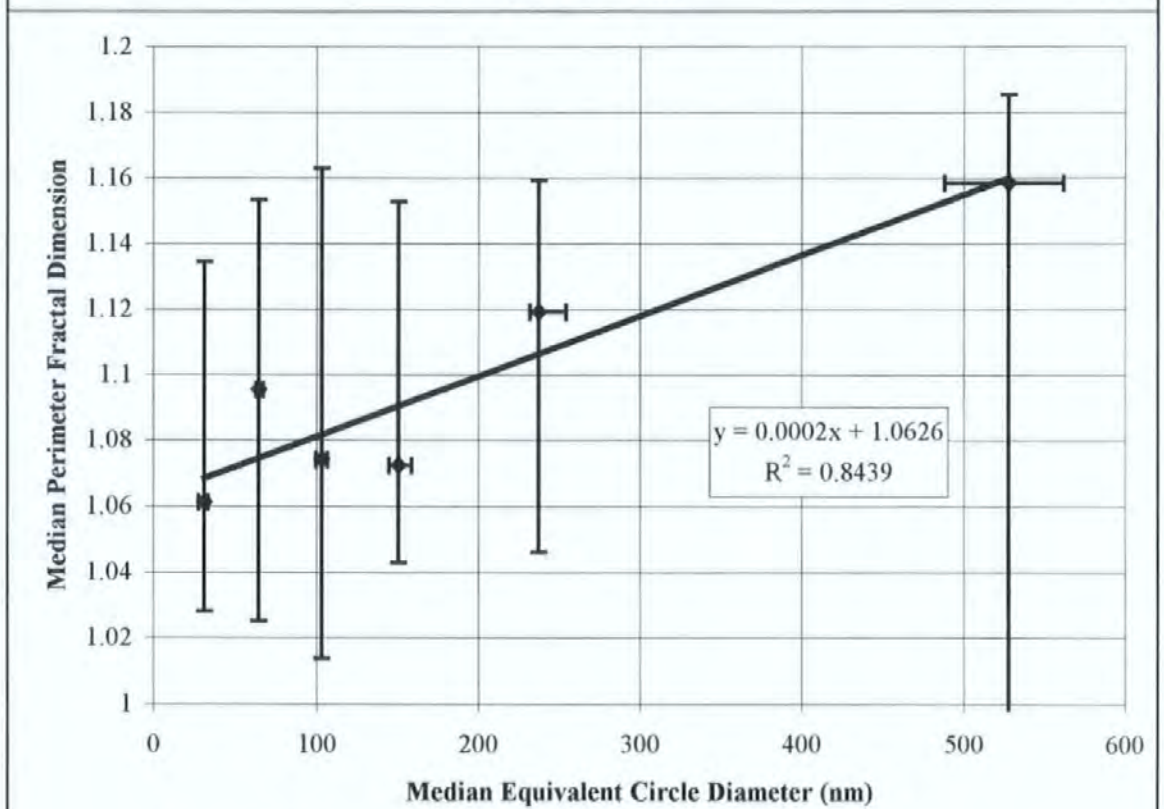
Figure 5.21 Comparison of size ranges and morphology using median values of PFD and Equivalent Circle Diameter (nm), for all particles from the ricardo petrol sources, (error bars show interquartile ranges)

Figure 5.20 shows the size morphology relationship between diesel particles collected from the Ricardo rolling road. This chart again follows a natural log relationship with a good fit ($r^2 = 0.83$), but the PFD tends toward smaller values. Samples of Prima engine were from raw exhaust whereas Ricardo samples were made from a dilution tunnel. Therefore particles from a dilution tunnel have time to undergo post emission structural changes, which can alter the morphology of the particles.

The petrol sources median diameter *vs.* median perimeter is shown in Figure 5.21. The data for this source follow a linear relationship with a fairly good fit to the trendline ($r^2=0.84$). However the error bars show the large variation of PFD within the size ranges especially at the largest size range, and there are only 6 points on the chart because of the relatively small amount of data (100 particles). For these reasons this relationship should be treated with caution. Comparison of petrol (Figure 5.21) and diesel engine charts (Figure 5.18 and 5.20) shows clear differences, both diesel groups closely follow the same natural log trend but the petrol chart follows a linear trend of median particle size and median PFD. The difference between trends may be directly attributable to different sources

The data from all diesel engine sources is combined in Figure 5.22. The fit of the trendline is slightly lower but still good ($r^2=0.80$). In fact Perkins Prima and Ricardo diesel plots follow similar patterns apart from the trendline, which reveal structural qualities of diesel engine particles. There seems to be a clear break in the data at a median diameter of 50nm, from below 1.05, which describes individual carbon spheres, to 1.08 at which simple compact agglomerates begin to be described.
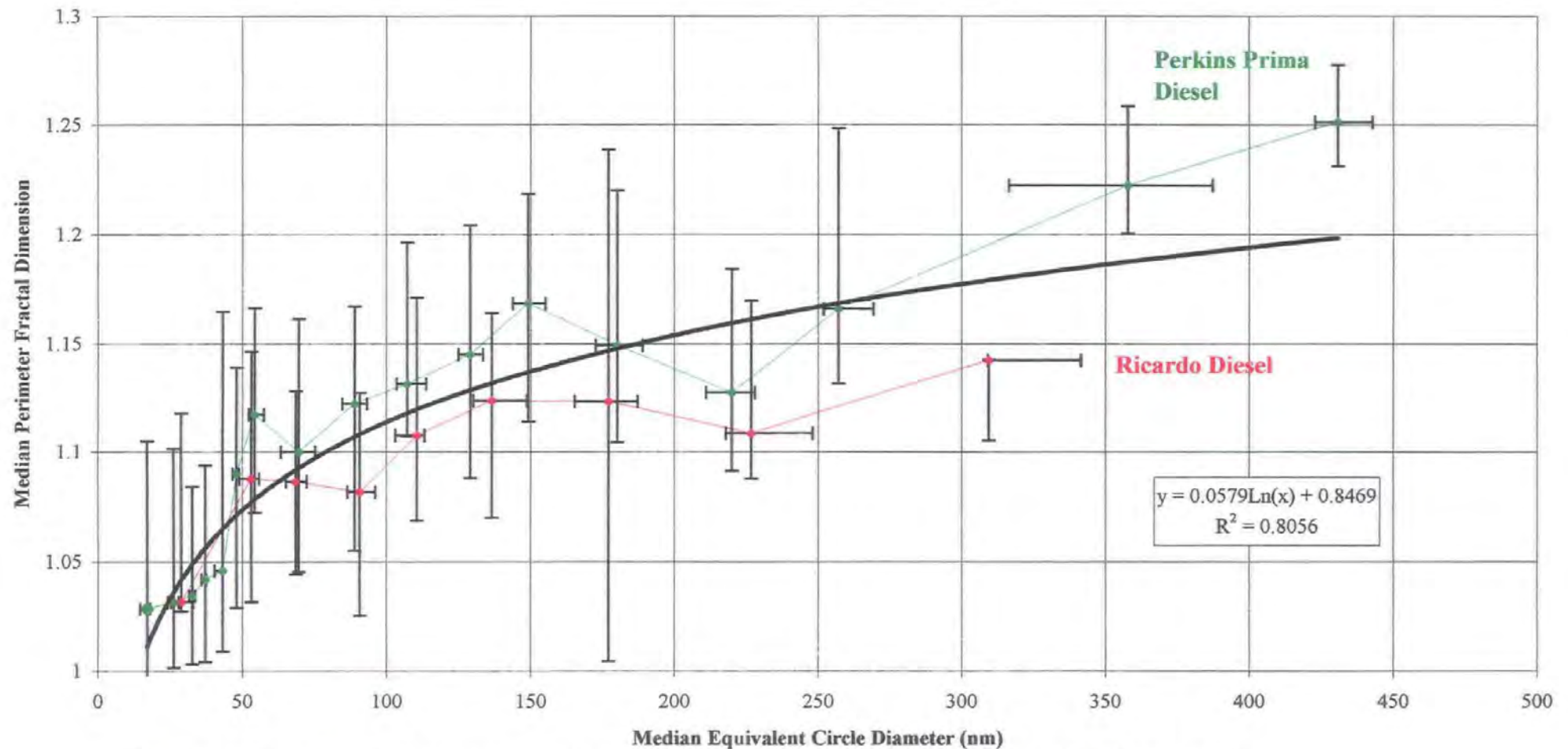
Figure 5.22 Comparison of size ranges and morphology using median values of PFD and Equivalent Circle Diameter (nm), for all particles from all the diesel engines(Error bars show the interquartile range)

Both trendlines in Figure 5.22 follow an increase in PFD but show a reduction in PFD between 150 and 250nm. It is likely that this dip shows the change from PFD measurement of fine textural qualities of small agglomerates to overall structural qualities of larger agglomerates. This effect is possibly as a result of the normalisation of agglomerates to the same image size.

The trendline in Figure 5.22, thus closely describes the bulk of particle morphologies from 3 different diesel engines, under a variety of speeds and loads. This supports the consistency of diesel engine combustion in production of average particle morphology and the size *vs.* PFD relationship may be tentatively considered as indicative of diesel combustion in general.

Comparison of the measured PFD for particles from other studies with the calculated value using the natural log trend in Figure 5.22, shows agreement for diesel generated particles within the error values (*cf.* Table 5.9)

Studies of source PFD	Diameter (estimated from study data)	PFD[1]	Calculated PFD median values from theory line ± Ave. Interquartile range[2]
Kaye, 1993 *Diesel*	~ 8-12 µm	1.43	1.36-1.38 ± 0.07
	~ 1.5-3.5 µm	1.21	1.27-1.31 ± 0.07
Colbeck *et al.*, **1997** *Diesel*	~ 0.5-2 µm	1.25	1.20-1.28 ± 0.07
Kaye, 1993 *Coal*	~ 0.75	1.05	1.23
Coal	~ 1.5	1.13	1.27
Thorium dioxide	~ 0.3	1.03	1.18
Thorium dioxide	~ 1	1.40	1.24

1. All the PFD's measured use methods from Kaye, (1993)
2. The calculated PFD values are from using the particle diameters from each study with the diesel engine trend line formula calculated in figure 5.22

Table 5.9 Comparison of measured PFD from other studies and the PFD calculated from the trend found in Figure 5.22

The agreement is good considering that the PFD values from other studies, are only for single particles, and the trend line describes the average particle type. This agreement supports the use of this trend as indicative of diesel source particles. The fact that the relationship calculated in Figure 5.22 poorly agrees with other particle sources such as coal fire particles (*cf.* Table 5.9) tends to indicate that the trend for diesel found here is specific to diesel combustion. This would agree with the source comparison made in Table 5.6, *i.e.* that different sources have distinct fractal producing properties.

5.5 Sources summary

- Diesel engine sources show great consistency of average particle morphology with varying speed and load, although there is a wide range of morphologies for particles of every size

- The morphology of diesel engine particles in this work was comparable to DFD and PFD values found in other studies of diesel combustion.

- A natural log relationship between the PFD morphology and the particle size has been found for the Perkins Prima diesel engine

- The natural log relationship was repeated in other diesel samples but not in petrol samples.

- The similarity of the PFD *vs.* size relationship between the diesel engines studied in this work, and also that other research fits the trend, demonstrates that diesel particle formation may be consistent across size ranges and between engines.

- This trend may be a tentative 'fingerprint' of diesel engine combustion.

CHAPTER SIX
Source Apportionment of Urban Aerosol

6.1 Introduction

There is a large body of work dealing with the apportionment of sources of PM_{10} by mass (Chow *et al.*, 1992 a, b; Kao and Friedlander, 1995; QUARG, 1996; Harrison *et al.*, 1997 a; b). Such work is dependent upon a chemical characterisation of sources and of the atmosphere. Fine particle sources of aerosol have been indicated as most important to public health (Seaton *et al.*, 1995; *cf.* Section 1.1.4), but such fine particles are poorly represented in mass apportioned studies (*cf.* Chapter 1.1.2). There have been some studies of the sources of PM_{10} by number using EDXS (Katrinak *et al.*, 1995), but for fine carbonaceous particles the elemental profile of particles is similar and so morphological identification of particles can be more useful (Kindrandenko *et al.*, 1994). Fractal measures have been used previously to apportion sources of micron sized atmospheric aerosol (Katrinak *et al.*, 1993; Xie *et al.*, 1994).

The work presented here involves the first known application of fractal geometry to the characterisation of a representative urban aerosol, of number median size of 100nm, from Plymouth, UK (*cf.* Chapter 5). Measurement of the morphology of sources from diesel and spark ignition combustion engines has been made using the same methods (*cf.* Chapter 6). In this chapter the identification of urban aerosol has been assisted using this source sample information.

6.2 Source Apportionment using the fractal and non-fractal PFD separation

In other work non-fractal particles and fractal particles have been separated. This separation is based on the fractal nature of fresh combustion particles (Katrinak *et al.*, 1993; Kaye, 1994; Colbeck *et al.*, 1997), as opposed to the non or very low fractal nature of other sources (Katrinak *et al.*, 1993; Colbeck *et al.*, 1997). A similar separation, by PFD, of the particles collected during the study, in Plymouth, is shown in Figures 6.1 and 6.2 for the

fixed analysis data (*cf.* Section 4.4) and in Figures 6.3 and 6.4 for the normalised analysis data (*cf.* Section 4.4).

In all samples the fractal proportion of particles far outweighs the non-fractal proportion (cf. Figure 6.1 to 6.4). Fractal aerosol can be apportioned to combustion generated aerosol, especially vehicle engine agglomerates (Medalia and Rivin 1983; Colbeck *et al.*, 1997; Katrinak *et al.*, 1993; Xie *et al.*, 1994). In the work of Katrinak *et al.*, (1993) non-fractal particles were identified as being from either: non-combustion sources, combustion sources with low fractal particles, or aged aerosols. Also the individual carbon ceno-spheres produced from diesel engine combustion, which are in the range of 30-70nm, have a low or non-fractal dimension (*cf.* Chapter 5). In the current research a large proportion of the particles analysed in the roadside and the background urban air are below 80nm in size (*cf.* Chapter 4). For this reason non-fractal particles below 80nm have been separated from other non-fractal particles (*cf.* Figures 6.1 to 6.4). This group may consist of a variety of sources but is dominated by individual carbon ceno-spheres from diesel combustion. Other sources of particles less than 80nm in diameter are : smelter fumes, of which there are very few sources in Plymouth, UK, and nitrate particles formed in the atmosphere. Nitrates can form coatings in the presence of carbon spheres (Katrinak *et al.*, 1993), therefore it is possible that the bulk of particles less than 80nm in diameter will be carbon ceno-spheres from combustion.

Above 80nm, non-fractal particles includes aged hydrocarbon combustion aerosols and non-hydrocarbon combustion aerosols. The greater proportion of non-fractal particles above 80nm, relative to <80nm, in background samples as opposed to roadside samples (*cf.* Figures 6.1 and 6.4), is evidence of contribution of non-hydrocarbon combustion sources to the ambient aerosol.

non-fractal non-fractal
<80nm >80nm
6% 1%
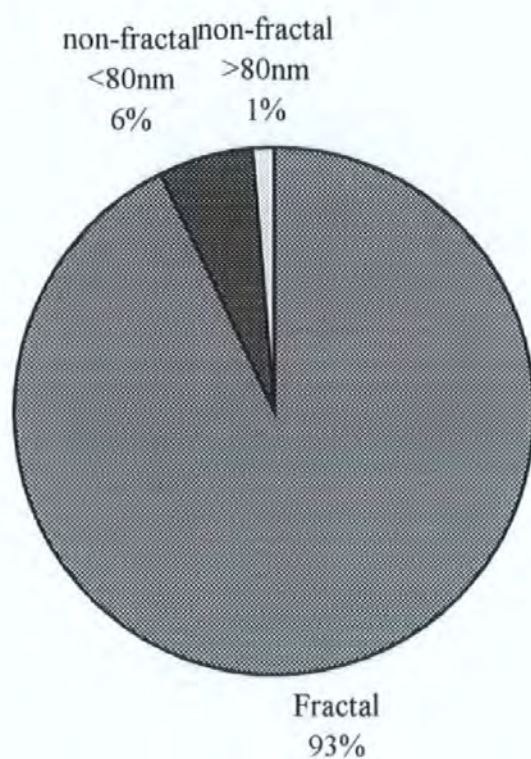
Fractal
93%

Figure 6.1 Proportions of fractal and non-fractal particles at the roadside (fixed analysis)

non-fractal
>80nm
6%

non-fractal
<80nm
11%
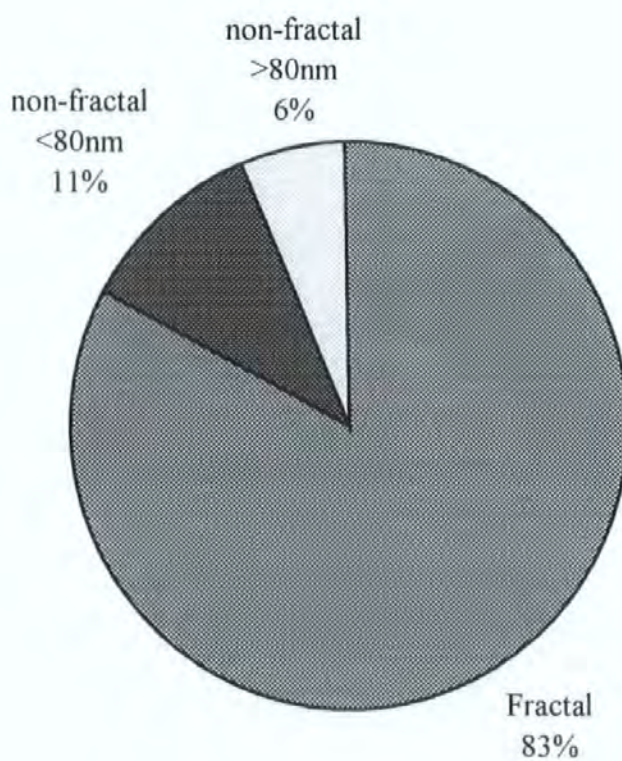
Fractal
83%

Figure 6.2 Proportions of the fractal and non-fractal particles at the background (Fixed analysis data)
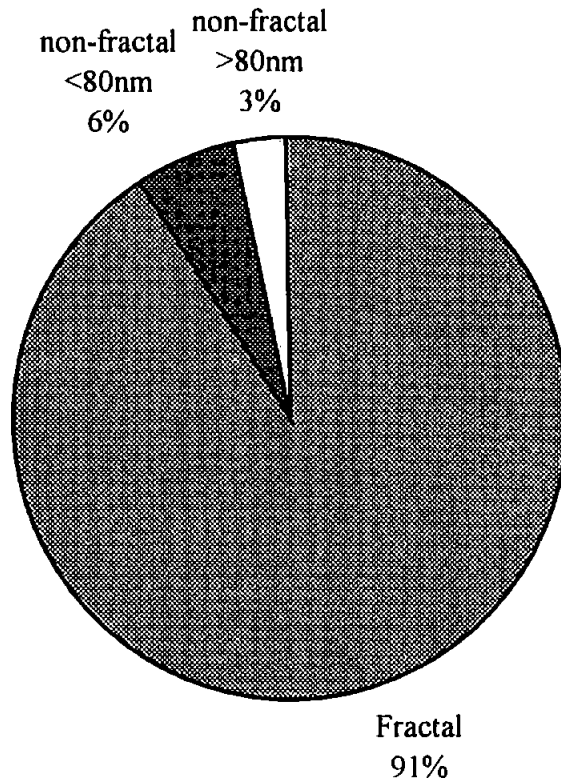
Figure 6.3 Proportions of fractal and non-fractal Particles at the roadside, (normalised analysis)
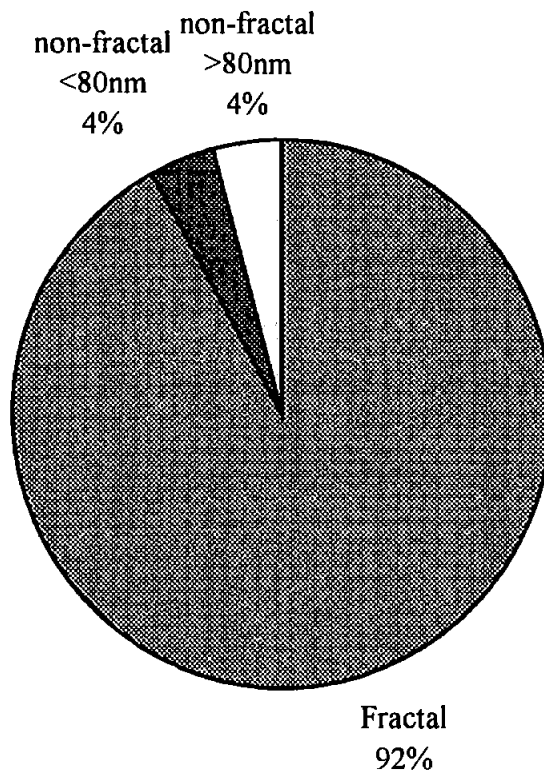
Figure 6.4 Proportion of fractal and non-fractal particles at the background (normalised analysis)

The proportions of particles separated into agglomerate and non-agglomerate by the qualitative means (*cf.* Chapter 4, Table 4.1) is within the standard deviation (± 10-15%) of particles separated by PFD (*cf.* Figures 6.1 to 6.4). This agreement suggests that contributions of vehicle generated aerosol, by number, of 90-99% at the roadside and 85-95% at the background, are not unreasonable (*cf.* Figures 6.1 to 6.4). The particle size, agglomerate classification (*cf.* Chapter 4, Table 4.1) and PFD can be combined for a more detailed classification of particles, which is shown in Table 6.1 with the inferred sources.

Class	Inferred Source
Fractal + agglomerates any size	Generally from hydrocarbon combustion
Fractal + non-agglomerates any size	Usually of low fractal dimension not from hydrocarbon combustion
Non-fractal + non-agglomerate + >80nm	Particles not from hydrocarbon combustion
Non-fractal + agglomerate + >80nm	Aged hydrocarbon combustion particles
Non-fractal + agglomerate + <80nm	1 or 2 ceno-spheres from hydrocarbon combustion
Non-fractal + non-agglomerate + <80nm	Ceno-spheres

Table 6.1 Particle size, fractal and agglomerate nature and the source which can be inferred from these qualities

The interpretation of groupings of fractal dimension, agglomerate nature and size, made in Table 6.1, is based upon the literature. Fractal particles are dominated by agglomerates formed in hydrocarbon combustion but may include some non-agglomerate particles at lower PFD's (Kindratenko *et al.*, 1994; Colbeck *et al.*, 1997). Thus a fractal/agglomerate group has an inferred hydrocarbon combustion source and a fractal/non-agglomerate group is inferred as from a non-combustion source (*cf.* Table 6.1). The non-fractal, non-agglomerate particles above 80nm are too large for ceno-spheres from hydrocarbon combustion (Carpenter and Johnson, 1979; Medalia and Rivin, 1983) and show no agglomerate structure, therefore they are considered to be from non-hydrocarbon combustion sources (*cf.* Table 6.1), but may include wood and coal combustion particles (BéruBé *et al.*, 1997; Colbeck *et al.*, 1997). Non-fractal, agglomerate particles above 80nm

will be exclusivly to aged agglomerates (*cf.* Table 6.1), compacted and coated through atmospheric processes (Katrinak *et al.*, 1993). Any non-fractal particle below 80nm in size is defined as a ceno-sphere (*cf.* Table 6.1), probably from hydrocarbon combustion which is the major source of particles of this size (Medalia and Rivin, 1983; QUARG, 1996; Seaton *et al.*, 1995).

6.2.1 Classification of normalised and fixed analysis particles

The apportioned sources and percentages for both normalised and fixed analysis data using the classification in Table 6.1, are shown in Table 6.2. For the normalised analysis 91% of particles at the roadside and 92% of particles in at the background were classed as fractal (*cf.* Figures 6.3 and 6.4). The vast majority of these particles at both the roadside (88.5%) and the background (86%) were agglomerates by inspection (*cf.* Chapter 4, Table 4.1). The non-agglomerate fractal particles accounted for *ca.* 3% of roadside and *ca.* 6% of background particles (*cf.* Table 6.2). Inclusive of both the roadside and backgrounds aerosol, 13 of the 33 non-agglomerates qualitatively identified (*cf.* Chapter 4, Table 4.1), were classified by PFD in to non-fractal groups. These non-fractal non-agglomerates were ceno-spheres less than 80nm (*ca.* 2% of roadside; 1% of background) and non-ceno-spheres greater than 80nm (*ca.* 1.5%, of roadside; 1.6% of background). Only 6 particles classified as non-agglomerate had a PFD above 1.05. In total 19 particles identified as agglomerates by visual classification (*cf.* Chapter 4, table 4.1), were non-fractal. Those non-fractal agglomerates below 80nm accounted for 4% of the roadside and *ca.* 3% of the background and those above 80nm accounted for 1% of the roadside and *ca.*2% of the background aerosol (*cf.* Table 6.2).

In the fixed analysis 93% of the roadside aerosol and 83% of the background aerosol was fractal (*cf.* Figure 6.1 and 6.2). The majority of these were agglomerate, accounting for

92% of the roadside and 77% of the background aerosol (*cf.* Table 6.2). Non-agglomerates accounted for a small proportion of fractal particles at both the roadside (1%) and the background (6%). 10 of the 29 non-agglomerates in the fixed magnification analysis were non-fractal and placed in to ceno-sphere (0% at roadside; 2.1% at background) and non ceno-sphere groups (0% at roadside; 3.2% of background). 34 particles identified as agglomerate were detected as non-fractal. Those above 80nm accounted for ca. 1% of roadside and ca. 3% of background aerosol and those below 80nm accounted for 6.4% of the roadside and 9% of the background aerosol (*cf.* Table 6.2).

Normalised Data Grouping (Inferred source)	Roadside (max.-min)	Background (max.-min))
Fractal agglomerates (from hydrocarbon combustion)	88.5% (92-75%)	86% (91-73%)
Fractal, non-agglomerates (not from hydrocarbon combustion)	3% (6-1%)	6% (8-2%)
Non-fractal non-agglomerate >80nm (non combustion particles)	1.5%(0-2.5%)	1.6% (0-3.7%)
Non-fractal agglomerates > 80nm (aged combustion particles)	1.0% (1-4.5%)	2.2% (0-8.8%)
Non-fractal agglomerates < 80nm (1 or 2 ceno-spheres)	4.0% (0-14%)	3.2% (0.5-9.4%)
Non-fractal non-agglomerates <80nm (ceno-spheres)	2.0% (1-3%)	1.0% (0.5-3.1)%

Fixed Data Grouping (Inferred source)	Roadside (max.-min)	Background (max.-min)
Fractal agglomerates (from hydrocarbon combustion)	92% (95-85%)	77% (92-70%)
Fractal, non-agglomerates (not from hydrocarbon combustion)	1% (1-1%)	6% (7-5%)
Non-fractal non-agglomerate >80nm (non combustion particles)	0% (0-0%)	3.2% (1-3.7%)
Non-fractal agglomerates > 80nm (aged combustion particles)	0.6% (0-3%)	2.7% (1.1-9.5%)
Non-fractal agglomerates < 80nm (1 or 2 ceno-spheres)	6.4% (4-11%)	9.0% (4.2-12.7%)
Non-fractal non-agglomerates <80nm (ceno-spheres)	0% (0-0%)	2.1% (2.1-2.6%)

1. The maximum. and minimum in brackets is calculated according to the ± 6% standard deviation in PFD calculation

Table 6.2 Sources apportioned using the agglomerate, size and PFD criteria[1]

About half of the particles found to be non-fractal in both normalised and fixed analysis, were visually classified as agglomerate in nature. Inspection of these particles shows that below 80nm these agglomerates consist of 1-3 individual ceno-spheres (*cf.* Chapter 4, Figure 4.7 and Figures 4.13-4.15). Above 80nm non-fractal agglomerates exhibit compacted agglomerate structures with a smoothed boundary (*cf.* Figure 6.5), such as those aged agglomerates found by Katrinak *et al.*, (1993). As expected the proportion of these smoothed non-fractal agglomerates greater than 80nm in diameter, increases at from 1% of all particles at the roadside to 2.2% at the background for normalised analysis. The proportion of non-fractal agglomerates increases from less than 1 % at the roadside to 2.7% at the background. This corresponds to the aged nature of the background aerosol.
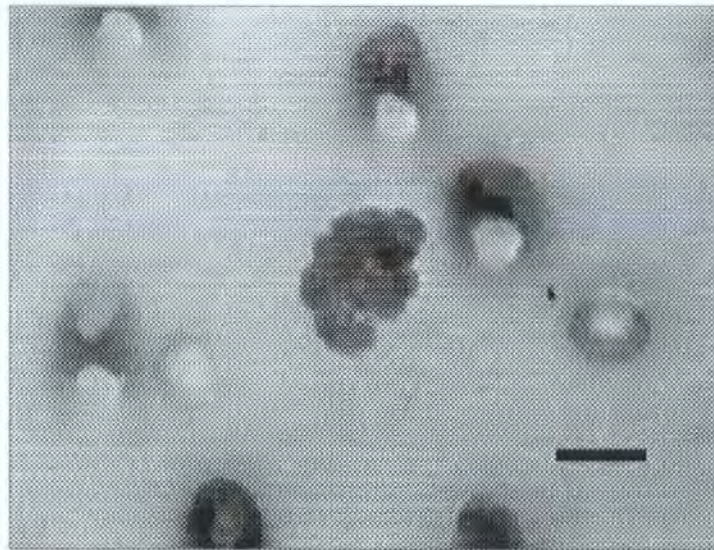
Figure 6.5 Compacted agglomerate greater than 80 nm in diameter (Scale bar = 100nm)

The best agreement of agglomerate/non-agglomerate classification (*cf.* Chapter 4, Table 4.1) with fractal/ non-fractal is made with the maximum standard deviation of 6% to include all particles below 1.05 PFD as non-agglomerates, and using the normalised analysis. The fixed analysis data is less effective for the classification of particle types because of the inherent size effects (*cf.* Section 3.4.3.1) and misplacement of particles is made. This agreement in results shows that PFD is a useful measure for the apportionment of sources

of aerosol. The underestimate from the true fractal dimension is not accounted for because it is not possible to quantify for each particle. The under estimate will be less for small particles than larger particles. In any case the under estimate would make less particles non-fractal and therefore increase the estimation of the source proportion from combustion sources.

6.2.2   Daily Contribution of Fractal and Non-fractal sources

The small daily samples of particles makes such a detailed source apportionment, as in Section 6.2.1, untenable.   The basic difference between roadside and background percentage contributions of fractal, non-fractal greater than 80nm and non-fractal particles less than 80nm are shown in Figures 6.6 and 6.7.   These charts show that the non-fractal component is greater in the background aerosol on three of the four fixed analysis dates and greater in the roadside aerosol on only one date.

The non-fractal component greater than 80nm in diameter accounts for a much greater proportion of the background aerosol than the roadside aerosol.   Figures 6.8 and 6.9 show that at the roadside non-fractal particles larger than 80nm vary between 20% to 50% of the non-fractal component of the aerosol on only four occasions.   At the background the non-fractal proportion larger than 80nm in diameter varies from 20%-50% on six of the dates and is greater than the roadside non-fractal contribution larger than 80nm on five of the seven study days.   There is then no clear consistency of difference in *non-fractal* contribution of the aerosol, but the background aerosol consistently exhibits a greater proportion of non-fractal particles larger than 80nm.   It is the non-fractal particles larger than 80nm in diameter which are indicative of both aged agglomerates and non combustion source particles, as previously discussed in Section 6.2.

176
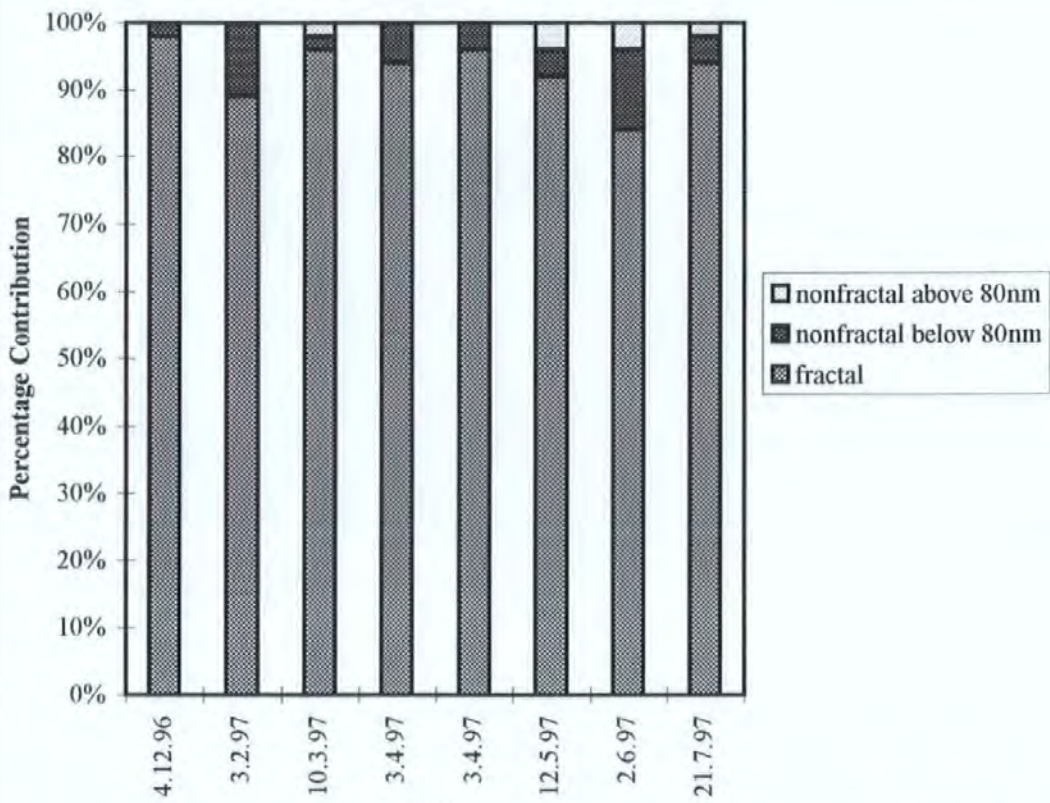
*Figure 6.6 Percentage contribution of fractal, <80 non-fractal >80
non-fractal particles at the roadside*
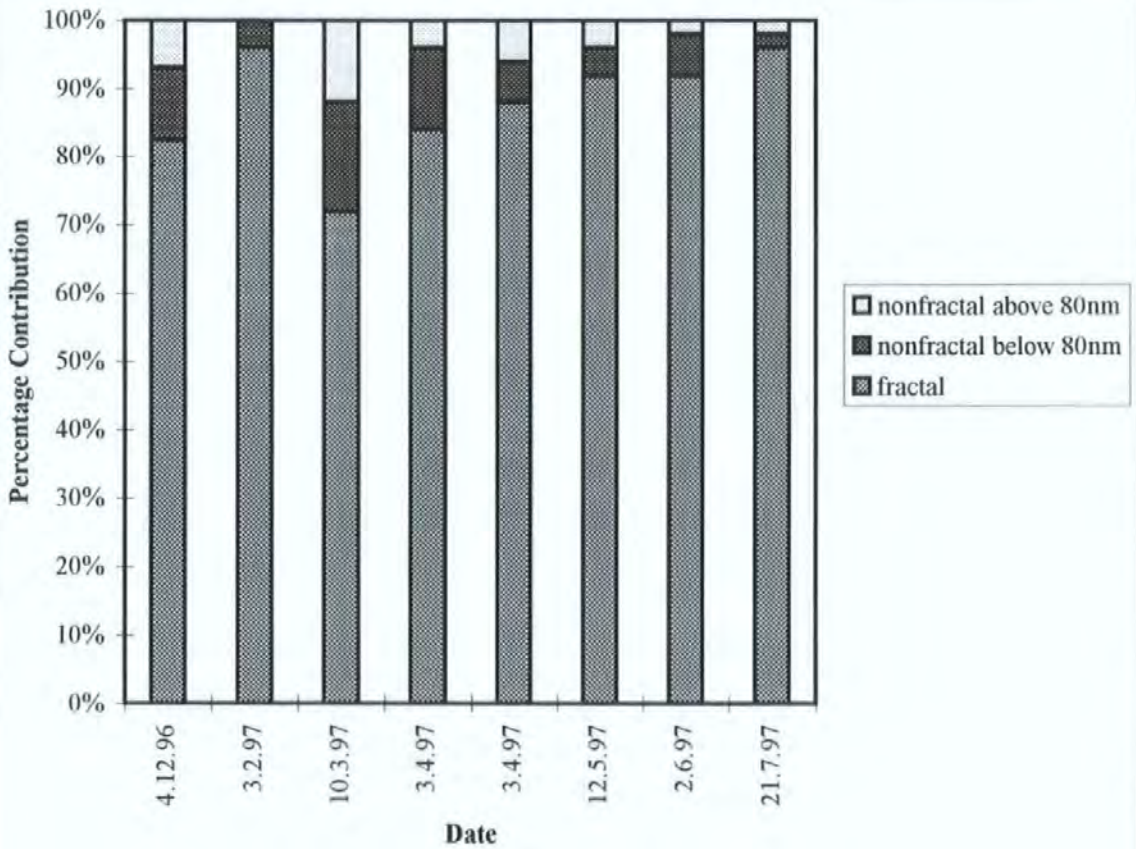
*Figure 6.7 Percentage contribution of fractal, <80nm non- fractal
and >80nm non-fractal particles at the background*
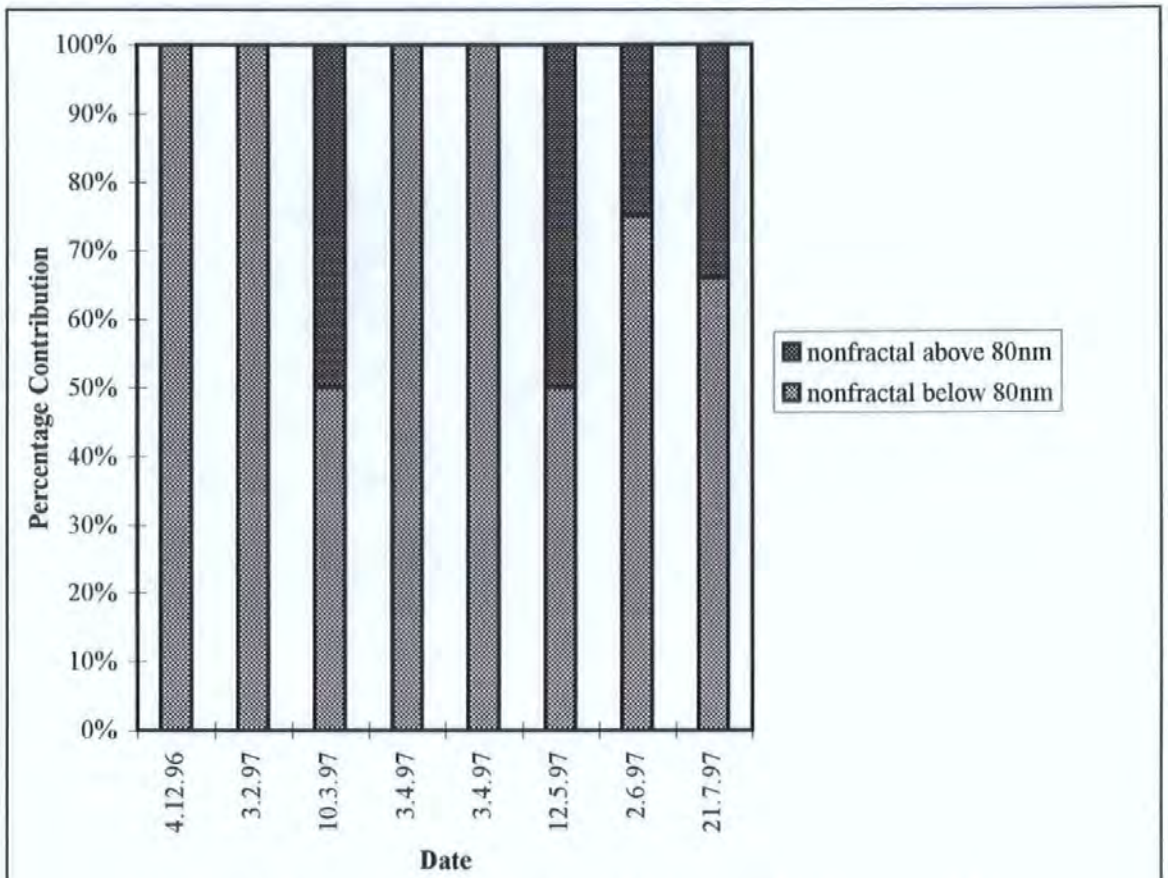
*Figure 6.8 Percentage contribution of <80nm and >80nm particles
to the non-fractal component of aerosol at the road side*
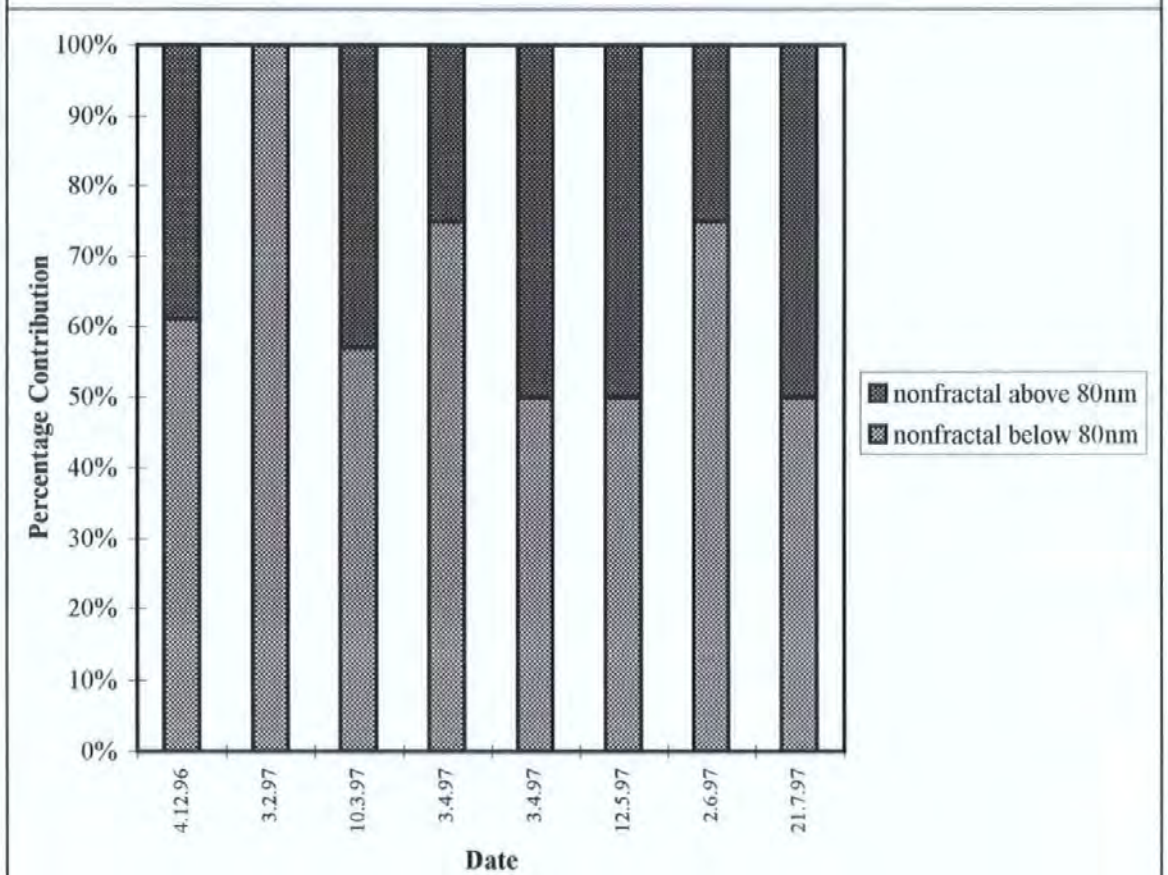
*Figure 6.9 Percentage contribution of <80nm and >80nm particles
to the non-fractal component of aerosol at the background*

6.3 Histogram mode comparison

As shown in Chapter 5, some separation of diesel and petrol engine sources may be attempted using a comparison of PFD histograms. Specifically a comparison of histograms showed some qualitative differences, whilst not being statistically different in a comparison of means (*cf.* Chapter 5, Figures 5.10, 5.11, 5.12). It is useful to compare the histograms of source samples with the normalised urban aerosol samples. In this way it may be possible to identify modes in the urban aerosol PFD histograms, and apportion an inferred source. This method is certainly not statistically rigorous but is useful in a qualitative sense of identification.

The comparison of all urban air samples with the source samples is shown in Figures 6.10-6.12. Here the similarity of the combustion engine source morphology with the urban aerosol samples is shown. The DFD morphology for all samples exhibit similar distributions. The DFD histogram (*cf.* Figure 6.10) shows that all samples have a broad mode between 1.35 and 1.8, with modes between 1.6 and 1.65. The similarity of histograms supports the evidence for the domination of fine urban aerosol by vehicle generated aerosol, discussed previously in Section 6.2.1 (*cf.* Table 6.2). As previously discussed (Section 5.4.3), the PFD histograms show some modal separation (*cf.* Figure 6.11). In the comparison with the sources, the roadside sample histogram exhibits a broad modal peak, between both a petrol mode (1.05) and a diesel mode (1.15), at a PFD of 1.10. This supports a tentative identification of the roadside mode as motor vehicle generated, but impossible to distinguish if petrol or diesel. The background sample shows a single mode, indicative perhaps of the homogenous morphological nature of the aged aerosol. The equivalent circle diameter histograms (Figure 6.12) demonstrate the generally similar distributions of particles examined.
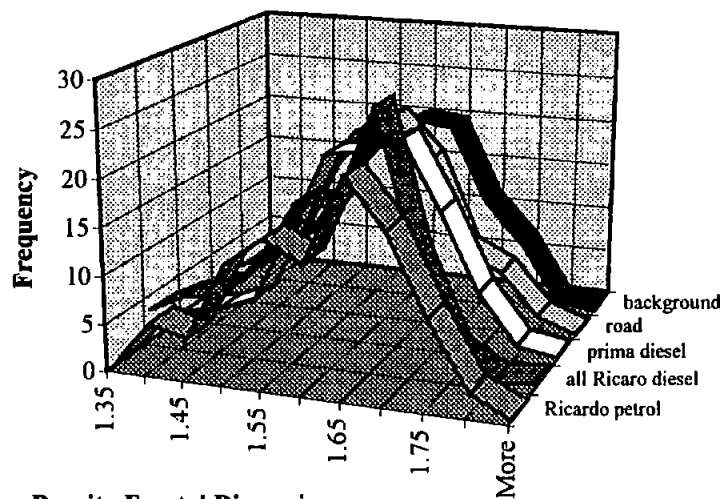
Density Fractal Dimension

Figure 6.10 Comparison of sources and urban air sample, DFD percentage histogram
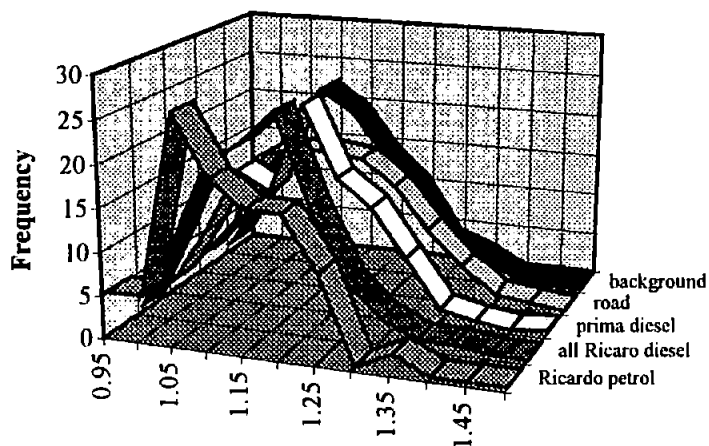
Perimeter Fractal Dimension

Figure 6.11 Comparison of sources and urban air samples, PFD percentage histogram
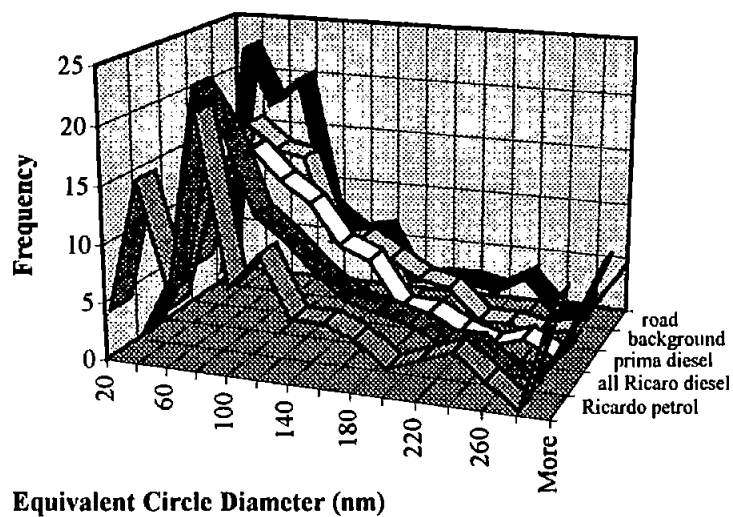
Equivalent Circle Diameter (nm)

Figure 6.12 Comparison of sources and urban air samples, Size percentage histogram

A further detailed comparison of air samples and source morphology, within size ranges, was made using the PFD. The Figures 6.13 - 6.17 compares PFD distributions for roadside, background, Prima engine, Ricardo petrol samples and Ricardo diesel samples, within the size ranges postulated in section 4.4.2.3.

For particles less than 40nm (*cf.* Figure 6.13) the roadside mode is broad but peaks at the same PFD as the diesel mode peak (1.05). The background mode peaks at the same value of PFD as the petrol engine peak (1.10). An ANOVA comparison of samples revealed no significant difference between any groups (p=0.077).

For particles between 40 and 80nm (*cf.* Figure 6.14) the roadside modes (PFD = 1.1 and 1.25), most closely follow the diesel mode peaks (1.15). The background mode is at the same PFD value as the petrol mode peak (1.05), and part of Ricardo peak. However an ANOVA comparison showed no significant difference between any of the groups (p=0.079).

For particles from 80-120nm (*cf.* Figure 6.15) there are three roadside modes, the lower peak (1.05) matches the petrol source peak, the middle matches the diesel source peaks (1.15), the upper mode (1.25) is not matched to any source. The background sample has a lower mode which matches the petrol mode (1.05) and an upper mode (1.20) just above the diesel engine modes (1.15). An ANOVA comparison revealed no significant differences between any groups (p=0.096).

Figure 6.13 PFD distributions for grouped sources and urban air samples <40nm

Figure 6.14 PFD distributions for grouped sources and urban air samples 40-80 nm

Figure 6.15 PFD distributions for grouped sources 80-120nm
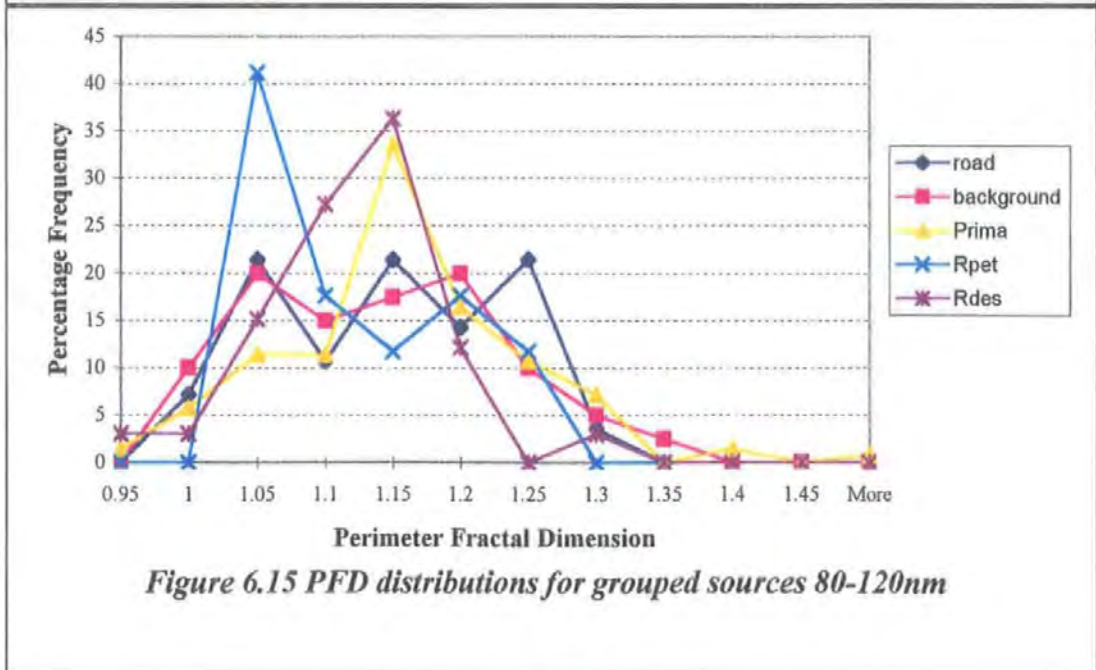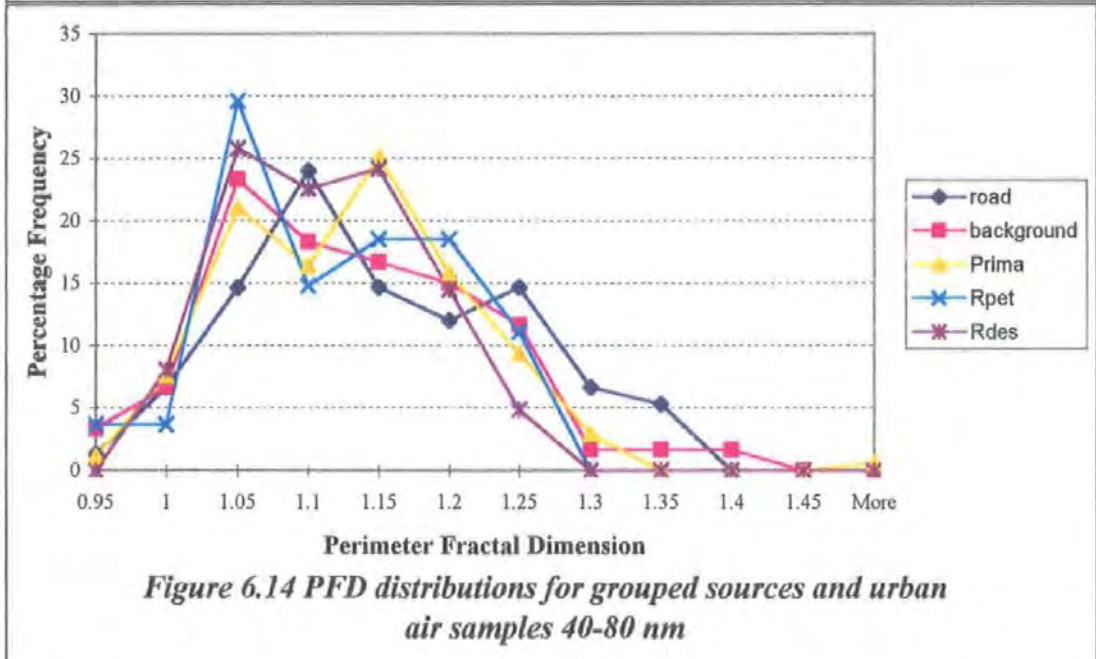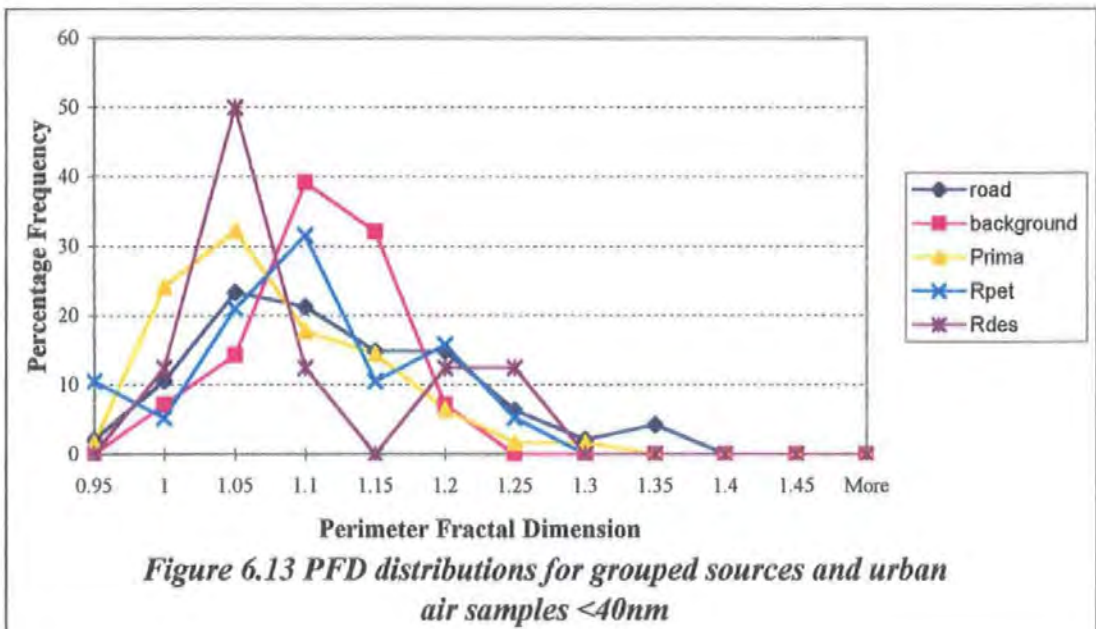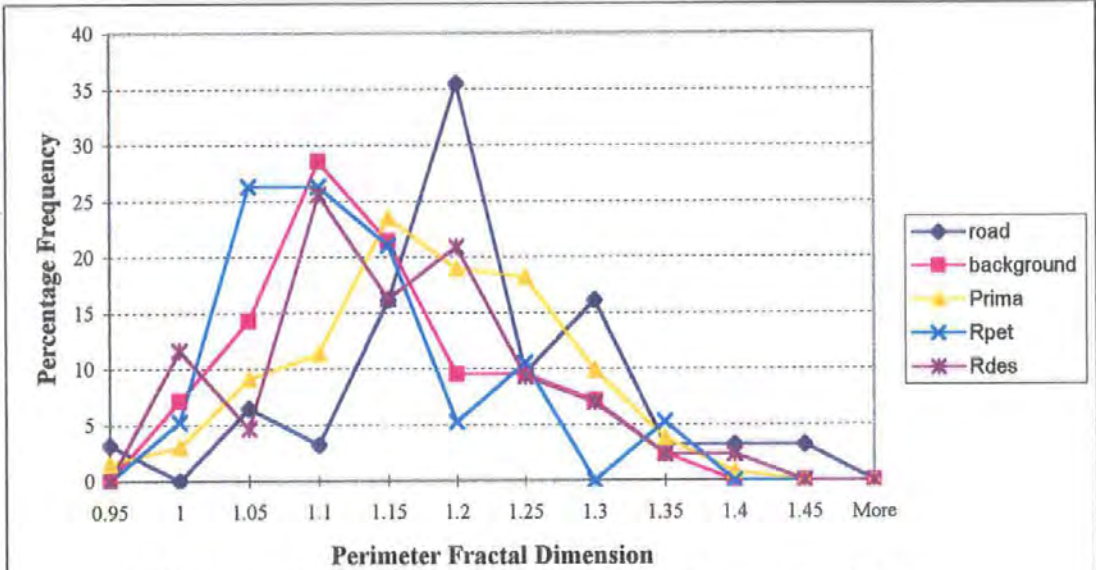
Figure 6.16 PFD distributions for grouped sources and urban air samples 120-220nm
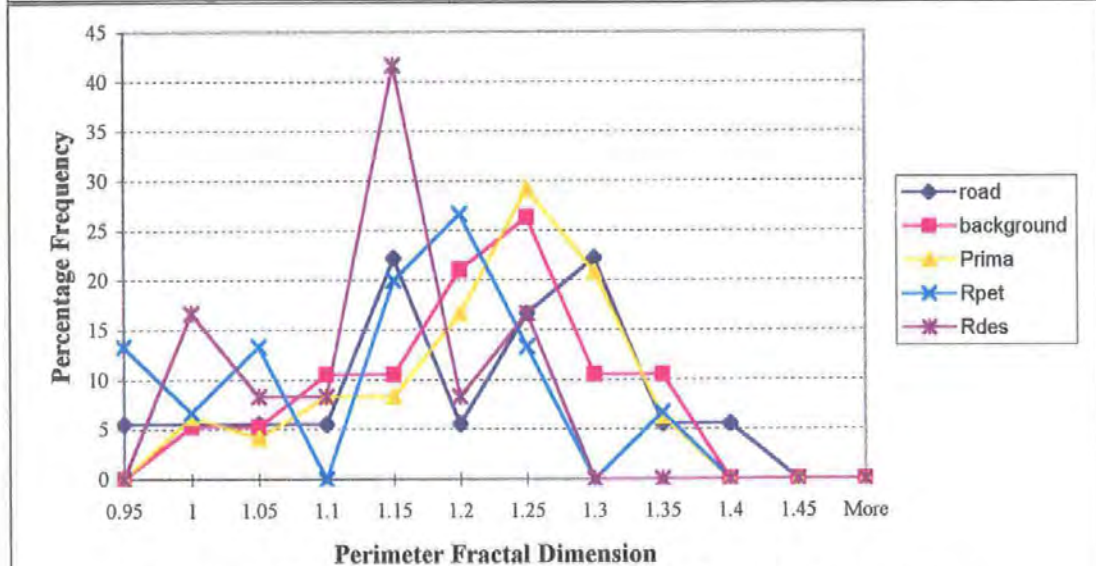
Figure 6.17 PFD distributions for grouped sources and urban air samples >220nm

The particles between 120 and 220nm have been previously indicated as most influential in average aerosol morphology (*cf.* Section 4.4.2.3). Comparison of the PFD distributions for 120-220nm is made in Figure 6.16. The roadside PFD mode matches that for the Prima diesel source (1.20), and part of the Ricardo diesel source. The background mode (1.10) matches that of the petrol source (1.05-1.10). An ANOVA revealed a significant difference between the groups (p=0.0008). A Fisher's least significant difference multiple comparison was used to separate the differences.

Sample	Ricardo petrol	Background	Ricardo diesel	Prima	Roadside
PFD mean	1.10	1.11	1.13	1.15	1.19
Groups	[--]				
		[------------------------------]			
			[------------------------------]		

At the 95% significance level any two means not underlined by the same segment are significantly different.

Figure 6.17 compares the fraction of particles larger than 220nm, for each sample. Roadside modes (1.15 and 1.30), partially match the Ricardo diesel mode (1.15) and the prima diesel mode (1.25) respectively. The background mode (1.25) matches that of the prima diesel mode. An ANOVA showed no significant difference between the means (p=0.055).

The ANOVA comparison of size grouped means thus shows that the only significant difference in the 120-220nm size range. In which the background aerosol was grouped with both Ricardo sources by a Fisher's least significant difference test. This is reasonable in that in the dilution tunnel (*cf.* Figure 5.1), the Ricardo source samples underwent ageing similar

to the background aerosol. The roadside sample was shown to be significantly different from Ricardo dilution tunnel sources and background sources, but similar to the raw prima diesel source by the same test. Also the two diesel sources were placed in the same group.

The comparison of means is useful, but ANOVA tests rely on an assumed normal population distribution. This is not reconcilable with the skew of the PFD histograms (cf. Figures 6.13 - 6.17), and in effect statistical differences between the bulk of the samples are obscured. Thus a comparison of modes has only been made qualitatively. A more rigorous comparison may be made when the PFD medians for selected size ranges of urban aerosol are plotted (cf. Figures 6.18 and 6.19) and compared with the charts for sources (cf. Chapter 5, Figures 5.18 - 5.22). The correlation of the median PFD from selected size ranges (cf. Section 4.4.2.3), for each source and environmental sample are compared in table 6.3.

Sources	Prima	Background	Roadside	Ricardo Petrol	Ricardo Diesel
Prima	1				
Background	0.849	1			
Roadside	0.931	0.664	1		
Ricardo Petrol	0.814	0.946	0.665	1	
Ricardo Diesel	0.963	0.683	0.938	0.650	1

1. size ranges used <40nm, 40-80nm, 80-120nm, 120-220nm, >220nm

Figure 6.3 Table of correlation coefficients of median PFD vs. size ranges, between sources and air samples[1]

The charts for roadside and background PFD median vs. size median, suggest different trends for roadside and background aerosol (cf. Figures 6.18 and 6.19). The roadside aerosol follows a log normal trend (cf. Figure 6.18), which the background aerosol (cf. Figure 6.19) does not follow. The log normal trend of the roadside aerosol is similar to that shown for the diesel engine sources (cf. Chapter 5, Figure 5.22).
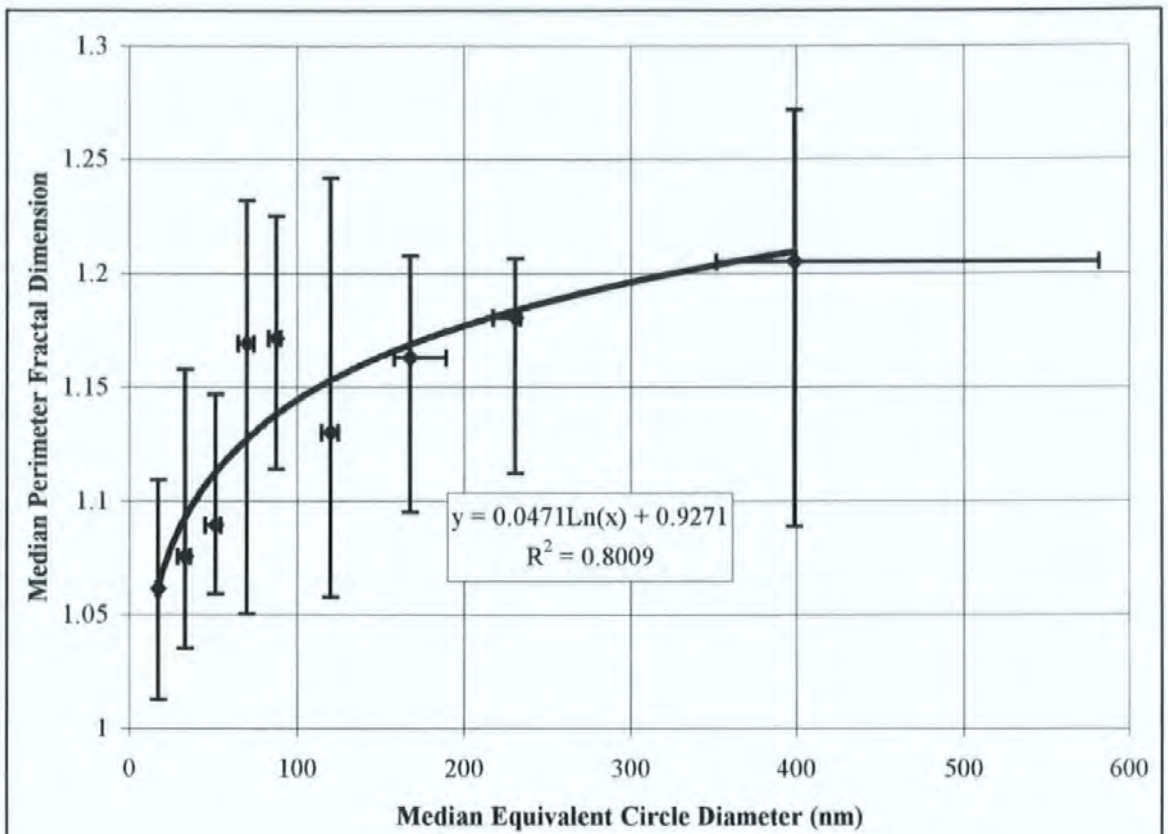
Figure 6.18 Comparison of size ranges and morphology using median values of PFD and Equivalent Circle Diameter (nm), for all particles from the Roadside from 3.4.97-21.7.97
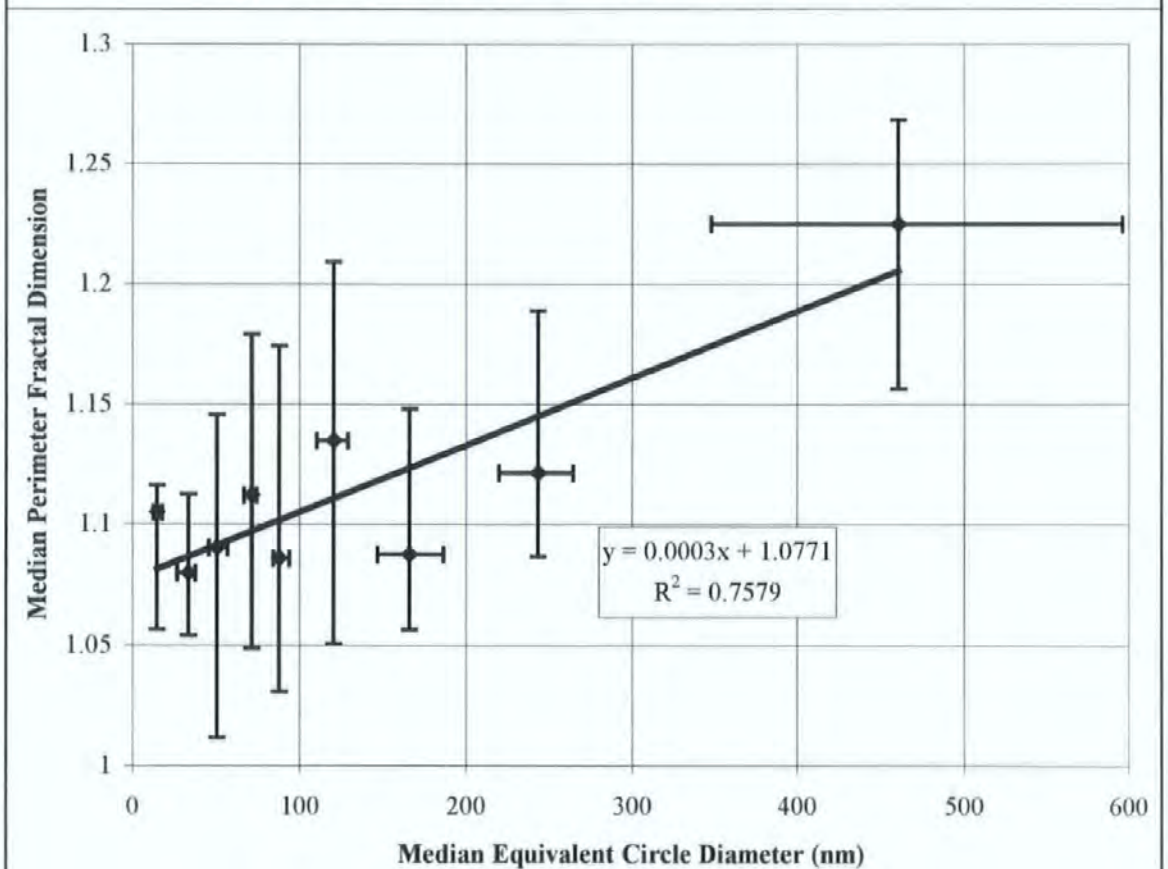
Figure 6.19 Comparison of size ranges and morphology using median values of PFD and Equivalent Circle Diameter (nm), for all particles from urban background samples.

The best correlation of source median PFD is shown for the roadside sample with the Prima diesel (0.931) and the Ricardo diesel (0.938) (*cf.* Table 6.3). The is also a high correlation of the Background aerosol to the Ricardo Petrol source (0.946) (*cf.* Table 6.3).

Thus it has been shown that the roadside aerosol is statistically and qualitatively similar in morphological character to different diesel sources. The roadside aerosol is also statistically significantly different to the petrol source in the 120-220nm size range and there is a low correlation between the petrol source and roadside median PFD's. This evidence tends to suggest that the roadside aerosol is dominated by diesel engine particles.

The background aerosol shows similarities to both diesel and petrol sources. The high correlation of petrol source to background aerosol is tentative because of the small petrol source sample. It is possible that the high correlation of petrol to background sources is due more to the dissimilarity with the diesel source rather than any true similarity. Neither the background PFD *vs.* size (Figure 6.19), or the petrol PFD *vs.* Size charts (*cf.* Chapter 5, Figures 5.21), follow the log normal trend. In the case of the petrol source this seems to be indicative of a different particle formation. In the case of the background aerosol this would seem to be indicative of the dilution of roadside aerosol by non combustion particles and the ageing of combustion aerosol.

6.4   Source analysis summary

It has been demonstrated in Sections 6.2 and 6.3 that hydrocarbon combustion may dominate as much as 90%-95% of roadside and background aerosols. With non-combustion sources contributing 4% to roadside aerosol increasing to 8% at the background, and an increased proportion of aged agglomerates in the background aerosol. These proportions of input to the urban aerosol support the argument that although non-

combustion sources may be significant by mass they are much less significant by number .

The number of particles is of most concern in terms of health since the distribution by number is dominated by ultra fine particles (< 100nm) (Seaton *et al.*, 1995; QUARG, 1996). It is these fine particles which contribute most to the deep alveolar penetration in the lungs, where the most damage and irritation can occur (COMEAP, 1995). It is further suggested, by this research, that the roadside aerosol is dominated specifically by diesel source particles, as identified from their morphological characteristics. The results of tentative source apportionment in this work are compared with other studies in Table 6.4. The major difference that can be highlighted between this and the other studies is that most have apportioned sources by mass contribution to the urban aerosol whereas in this work apportionment has been made by number. The mass apportionment of PM_{10} will be dominated by contributions from particles greater than $1\mu m$ (COMEAP, 1995). However the most important particles in terms of public health are smaller than $1\mu m$ (*cf.* Section 1.1), and therefore apportionment by number gives a better indication of the sources of most concern in terms of their respiratory penetration. The mode of vehicle engine particles is *ca.* 100nm (*cf.* Section 5.3), so is important in terms of its potential respiratory penetration

When apportioned by mass the vehicle contribution is between 11% and 33% by mass in the US (*cf.* Table 6.4; Chow *et al.*, 1992; Kao and Friedlander, 1995), where diesel vehicles are less common. In the UK a vehicle contribution of 24% of PM_{10} by mass has been apportioned (*cf.* Table 6.4), but when taking into account secondary sources estimates rise to 70-80% of PM_{10} (Harrison *et al.*, 1997 a, b).

Study	Vehicle source (%)	Non vehicle source (%)	Aged vehicle (%)	Combustion Ceno-spheres or chemically formed <80nm particles (%)
This research **Plymouth UK :** *number* Roadside Background (0.01-10μm)	88 - 92 77 - 86	1 - 4 8 - 9	*ca.* 1 2 - 3	*ca.* 6 4 - 11
Harrison *et al.,* **1997 a** **Birmingham, UK:** *mass* Background (*ca.* 0.4-2.1)μm	25 ± 8 (80[1])	11 ± 7 (Coal) 7 ± 2 (Incineration) 2 ± 2 (marine) 32 ± 5 (Road dust)[1]	---	23[1] (Secondary)
Harrison *et al.,* **1997 b** **Birmingham, UK:** *mass* Background PM[10]	32 (71[1])	29	---	39[1] (Secondary)
Katrinak *et al.,* **1995** **Phoenix, AZ, US :** *number* Background (0.1-2.5μm)	32	36 (Crustal) 12 (metal rich) 0.2 (Salt) 7.4 (Sulphur rich)	---	---
Kao and Friedlander, 1995 **California, US :** *mass* Background (PM[10])	12-33	35-52 (Crustal) 1-9 (Marine) 3.0 (Oil)	---	17-23 (NH_4NO_3) 6-11 ((NH_4)$_2SO_4$)
Chow *et al.,* **1992 a** **Rubidoux, CA, US:** *mass* Background (PM[10])	11	6 (Lime/Gypsum) 48 (Crustal) 2 (Marine)	---	23 (NH_4NO_3) 6 ((NH_4)$_2SO_4$)
QUARG, 1996 **UK :** *mass* (Total Suspended Particles): London, Bloomsbury Liverpool Bristol	79[2] 78[2] 76[2]	---	---	---

The particle size range of the study is shown in parenthesis

1. Harrison *et al.,* argue for 80% vehicle and secondaries contribution, considering that genuine road dusts will probably occur greatly only above 2.1μm.

2. Fraction of 'Traffic related' particles, including secondaries

Table 6.4 Sources apportionment studies of urban aerosol

The higher estimate of the total contribution of vehicle sources in Birmingham, London, Liverpool and Bristol (70%-80%), would seem to agree with the contribution of vehicle sources calculated in this work (*cf.* Table 6.4). This is even though these studies have used mass apportionment, not number apportionment of particles as in this work. The agreement occurs because the studies in Birmingham, London, Liverpool and Bristol are all in more vehicle polluted areas than Plymouth (NETCEN, 1998), and also all included the secondary sources in the vehicle apportioned fraction of PM_{10} (Harrison *et al.*, 1997 a, b; QUARG, 1996). In Plymouth secondary sources are accounted for quite differently. A grouping has been allowed for which may include chemically formed secondary particles (*cf.* Table 6.4), however without chemical characterisation it is impossible to make positive identification. There is some evidence to suggest that in the presence of carbon ceno-spheres that nitrates and sulphates will tend to form coatings (Katrinak *et al.*, 1992). The apportionment by number in Plymouth does not recognise the secondary mass contribution as coatings, unless the particle in question is significantly aged (*cf.* Table 6.4). The number apportionment performed in this research has attempted to fingerprint the source from the morphology of the particles, thus for mixed source particles, minor coatings can be overlooked. For mass apportionment of particles secondary sources show up whether from coatings or discrete particles. It follows that the mass apportionment, as performed in London, Liverpool, Birmingham and Bristol (*cf.* Table 6.4), highlights the secondary sources of particles and added to the mass of combustion engine particles account for the vast majority of the mass of aerosol in the air. The number apportionment, as performed in Plymouth, has tended to hide the secondary sources, but the majority of particles are from vehicle sources and so there is an agreement between the mass studies in the four UK cities and the number study in Plymouth (*cf.* Table 6.4).

The only other study of particle source by number is by Katrinak *et al.* (1995) in Phoenix, AZ, USA (*cf.* Table 6.4). In Phoenix the apportionment clearly highlighted the significance of motor vehicle sources of aerosol by number. It must be also considered that in the US, diesel vehicles are less common, so for a similar vehicle loading the particles generated in this way will be much less apparent than in the UK. The difference between Katrinak *et al.* (1995) and this research are various. The larger proportion of diesel vehicles in the UK is one reason. Phoenix is situated in the middle of Arizona, US, a much drier place than Plymouth UK and therefore the crustal contribution to aerosol is obviously much greater. The study in Phoenix employed a minimum particle size of $0.1\mu m$, below which the majority of motor vehicle generated and urban aerosol occur.

CHAPTER SEVEN
Conclusions and Future Work

7.1 Conclusions

The epidemiological evidence for a link between respiratory health and the mass of fine particulate matter below 10 μm (PM_{10}) in urban air is well documented. However, a small increase in PM_{10} mass concentration causes the same percentage increase in health effects whether at a high or low ambient PM_{10} level. Since a small change in PM_{10} mass may correspond to a large fluctuation in the number of nano-metre sized particles, current research suggests that the number, size and shape of particles may be of most concern. Also, in the urban atmosphere combustion sources of aerosol, especially diesel engine sources, have been singled out as the largest contributor of these numerous fine (< 1 μm) and ultra-fine (<0.1 μm) particles. Despite this, the number, size and shape of particles in urban air has not been reported to any great extent or detail, and the percentage contribution to the numbers of particles from different sources is largely unknown or ignored.

The ultimate objectives of this research were to characterise particles with respect to their physical parameters and thus to proceed to apportion the sources of particles by number. More specifically, the study has developed through a number of stages. Urban aerosol above 1 μm was initially examined with the aims of studying the fluctuations in PM_{10} number and retrospective analysis of periods of elevated PM_{10}, for source identification in Plymouth, UK. Building upon this work it was further aimed to; collect and analyse sub-micron aerosol both in urban air and in combustion engine exhausts, to identify the morphological variations in sub-micron aerosols, to relate urban aerosol morphological data to the aerosol sources and thus discuss the implications of these results for public health.

In the first stage of research a method was developed for the collection and analysis of aerosol above 1 μm in urban air for the study of the number distribution of particles (*cf.*

Chapter 2). The method was required to be automated in some way because of the large number of airborne particles and the need for a reproducible daily procedure. Collection of airborne particles was made using a Burkard spore trap, which has been widely used for pollen studies but has been little used in the analysis of non-biological aerosols (Battarbee *et al.*, 1997). The collection of a permanent continuous particle trace, in the form of slides, from the Burkard trap allows retrospective analysis of periods of interest. This is an advantage over other studies which have used particle number counters over a time period without keeping a permanent record for further analysis. The slides were optimised for examination using optical microscopy and image analysis. Optical analysis sets a lower operational limit on particle size of about 0.5 μm, but by using image analysis high quality data within this limited size was obtained. A macro programme was developed (Written by Paul Russell, University of Plymouth, UK) for the image analyser allowing user input into detection and thresholding of images collected from slides, but automating measurement procedures. In this way large numbers of particles were measured within reasonable time constraints. Thus repeatable uniform daily measurements of the number, size and shape of particles were made.

The method of collection and analysis of 1-10 μm aerosol was used during the period 16 March 1995 to 31 August 1996, at a background aerosol site in Plymouth, UK. The results show the interaction of a number of effects upon aerosol number and size distribution. Two periods, 19 January-4 February 1996 and 10-25 March 1996, identified as UK-wide PM_{10} episodes, were retrospectively studied and compared with PM_{10} mass measurements. Also a detailed 24 hour retrospective study of the fluctuation in particulate size distribution was made. The study results show:

- large periodical variations in number count following a similar pattern to the PM_{10} mass recorded by tapered element oscillation micro-balance (TEOM) on a monthly rolling

average. The mass of PM_{10} from a TEOM is therefore closely associated with 1-10 micron particles and much more so than fine sub-micron particles.

- Elevated average number concentrations of $13.5 \pm 7.6 \times 10^4$ particles m^{-3} for 19 Jan-4 Feb 1996, and $13.0 \pm 9.7 \times 10^4$ particles m^{-3} for 10-25 March 1996, were found.

- The correlation between PM_{10} mass (TEOM) and the number count was found to be non existent (-0.05) for 19 January-February 4, 1996and low (0.49) for 10-25 March 1996.

- During January and February 1996, outside of the peak period of PM_{10}, the correlation of fine particles (< 2.5 μm) to PM_{10} (TEOM) mass is good (0.79). However during the peak period fine particles are poorly correlated to PM_{10} (TEOM) mass (-0.07) but coarse particles (>2.5 μm) show a good correlation (>0.62)

- During March 1996 the correlation of < 5 μm particles to PM_{10} (TEOM) mass, stays fairly consistent during the whole period (0.45-0.47), but the correlation of > 5 μm particles increases from 0.26 outside the peak period of PM_{10} to 0.42 during the peak period.

- The results suggest a domination of the urban aerosol on a daily basis by the fine fraction of aerosol which generally makes up 30-50% of the number count, however elevated periods of PM_{10} cause an increase in particle numbers of all sizes examined, but are closely related to > 2.5 μm particles. This is highly suggestive of a different source of aerosol during these periods.

- These results correspond to the work by King and Dorling (1997) and Stedman (1997). They suggest that periods of elevated PM_{10} in the UK occur because of the introduction of a continental air mass. The research presented here is in agreement with their work, in that continental aged aerosol would be expected to have the related > 2.5 μm component, found herein, as a result of agglomeration and inorganic mineral sources.

- As with other research (Battarbee et al., 1997), local sources of fine aerosol, generally vehicle generated, contribute greatly to diurnal fluctuations.

- Periods of exceedence of the 50 μg m^{-3} PM$_{10}$ recommended level are traditionally considered to be the worst times for public health. However, the exceedence periods during 1996 have both been shown to be generated through continental inputs (King and Dorling 1997, Stedman 1997), which this research correlated to the > 2.5 μm aerosol. Since < 2.5 μm aerosol is considered worst for public health (Seaton *et al.*, 1995), it follows that the EPAQS recommendation and TEOM mass measure of PM$_{10}$ do not adequately address the potential health effects of an aerosol. This is especially the case during the periods of exceedence, when continental air masses dominate. In some cases, exceedances due to a high mass, large sized, aerosol, from continental sources, may be of far less health concern than the low mass, small size, high number vehicle generated aerosol consistently found in urban areas during non-exceedance periods.

- This research has demonstrated that current mass measurements of PM$_{10}$ are inadequate and the study of particle size distribution and morphology is needed for a better understanding of the possible toxicity of an aerosol.

Analysis of the 1-10 μm size fraction, demonstrated the importance of <2.5 μm particles in terms of their number, but little morphological analysis was possible with optical microscopy, so further techniques were developed for the collection and analysis of sub-micron particles. Other work has measured the number of particles in urban areas, however the morphological nature of the urban aerosol has largely been ignored. In this work the morphological nature of the aerosol was studied in detail, with the ultimate aim of identifying source identification of individual particles.

The technique developed for the collection of sub-micron aerosol had to provide a representative sample, be un-powered, except for filtration pump, for portability and allow transmission electron microscopy (TEM), for nano-meter scale analysis. Other studies have

collected samples for TEM but either fail to provide a representative sample in size distribution or morphology (Farrants *et al.*, 1988; Spurney, 1994), or require other power sources (Maynard *et al.*, 1995). A method was developed through a combination of techniques. Porous carbon films (PCF), transparent to the electron beam were made using carbon coated nuclepore filters (0.1 μm pore size) in a Jaffe washer (*cf.* Chapter 3). The PCF made were clean and porous. These films were then attached to nuclepore filters (NPF) for the direct sampling of urban aerosol. The efficiency of collection is low (*ca.* 5%) but the sample collected is representative in terms of size distribution and morphology of aerosol particles.

Measurement techniques using fractal analysis were developed on a Quantimet 540 image analyser (*cf.* Chapter 3). Previous to this work there have been few studies using fractal techniques to measure urban aerosol. Katrinak *et al.*, (1993) made a study of aerosol in Phoenix, Az. USA, using one density fractal dimension and a limited size range of micron sized material. In this work an analysis of a representative sub-micron aerosol has been sought, using both density and perimeter fractal dimensions for analysis. Thus the method developed has allowed a more representative and thorough analysis of urban aerosol morphology than previously completed.

The sampling technique developed was applied to the collection of urban aerosol from background and roadside sites in Plymouth, UK (*cf.* Chapter 4). Analysis of the urban aerosol was made using a TEM, with subsequent morphological analysis using the image analysis methods developed (*cf.* Chapter 3). From the analysis of urban aerosol the following conclusions were made:

- The average perimeter fractal dimension (PFD) of aerosol was consistently and significantly greater by a 0.02 increment at the roadside than the background, both with

and without non-PFD fractal particles. Thus roadside aerosol is more rugged than background aerosol. Without non-fractal particles the influence of non-fractal/non-agglomerate particles is removed, the remaining difference is thus indicative of an ageing of fractal aerosol at the background site.

- In the roadside samples the non-fractal group of particles is made up almost exclusively of individual carbon ceno-spheres (35-45 nm in size). In the background aerosol the PFD non-fractal group of particles consists of particles of similar mean size to fractal particles. This is indicative of large agglomerates which have become non-fractal through ageing as well as non-agglomerate particles from non-combustion sources.

- The variation of perimeter fractal dimension with aerosol size has a very different distribution at roadside as compared to the background. The evidence from normalised analysis supports a one or two source input at the roadside and a mixed and aged aerosol input at the background. Fixed data shows the dominance of size influences and is less useful for interpretation.

- An analysis of variance showed that there were few similarities in aerosol size and mean morphology between study days, thus showing the importance of local meteorological conditions which fluctuate daily.

- Histograms indicate distinct sources at the roadside, and an aged mix of particles in the background aerosol.

- The 120-220nm aerosol was argued to be important in contribution to the average morphology of the aerosol, being significant in number and large enough for structural re-arrangement.

The collection and analysis techniques were also applied to the detailed sampling of a Perkins Prima 2 litre D.I. diesel engine and the limited spot sampling of a number of other engines from a dilution tunnel for comparison. A similar data analysis, as for urban aerosol, was performed on the results (*cf.* Chapter 5).

These results show that:

- The Perkins Prima 2L D.I. diesel engine source showed great uniformity of particle morphology with varying speed and load and no consistently significant differences were found.

- The morphology results were comparable to other density fractal dimensions and perimeter fractal dimension values found in other studies for diesel particulates.

- A natural log relationship between the PFD morphology and the median particle size has been found for the Perkins Prima diesel engine

- The natural log relationship was repeated in other diesel samples but not in petrol samples.

- The evidence points to the fact that diesel particle formation is reasonably consistent in its pattern across size ranges and between engines and holds for other studies.

- It may be tentatively argued that the combination of mostly cluster-cluster aggregation, with a mixture of ballistic trajectories at high temperature and diffusion limited aggregation at low temperature gives unique but consistent formation process for diesels, as opposed to petrol engines where monomer-cluster aggregation and other processes, such as condensation, may dominate.

- The natural log trend may be a tentative 'fingerprint' of diesel engine combustion, but is indicative of the aggregates formed in combustion.

The sources and atmospheric samples from Plymouth, UK. were compared as an aid to source apportionment (*cf.* Chapter 6). Fractal analysis has been used previously to apportion sources of micron sized atmospheric aerosol (Katrinak *et al.*, 1993; Xie *et al.*, 1994). The work here involves the first known application of two fractal measures to the identification of the source of a representative urban aerosol, in Plymouth UK. The identification of particle sources has involved knowledge of aerosol size, morphology and qualitative user classification.

- Firstly the combination of particle size, measured PFD and user classification was used to identify six groups of particles, from which sources were inferred.

- Using this classification the vast majority of aerosol was identified as agglomerate particles formed in hydrocarbon combustion; 75-95% of the roadside and 70-92% of background aerosol. A significant component of carbon ceno-spheres were also identified ranging from 0-12% of the roadside and background aerosol. Non combustion particles increased from the roadside (1-8.5%) to the background (2-11.7%), as did the proportion of particles identified as aged combustion particles, 0-1% of aerosol at the roadside to 0-9.5% of the aerosol at the background.

- The background aerosol was found to consistently exhibit, on a day by day basis, a greater proportion of particles inferred as from aged combustion or non-combustion sources.

- Comparison of histograms of the distributions of DFD for the sources and urban aerosol samples also provides qualitative evidence of the similarity between motor vehicle sources and the urban aerosol. Comparison of PFD at different size ranges shows a close comparison between the histogram modes for diesel sources and the roadside aerosol. At the 120-220nm size range an ANOVA test showed that the background aerosol could be grouped with all of the sources, the diesel sources form a sub-group, and the roadside aerosol showed significant differences to all groups except the Prima diesel engine.

- A strong correlation for the median size *vs.* morphology curve between, the roadside and Prima diesel (0.93), and the roadside and Ricardo diesel (0.94) was found. Also a high correlation of the background and petrol sources was found (0.95).

- Thus the roadside aerosol is statistically and qualitatively similar in morphology to diesel engine sources of aerosol. The roadside aerosol is significantly different to the petrol source in the 120-220nm size range and there is a low correlation of the petrol source

and the roadside size *vs.* morphology curve. This evidence tends to suggest the domination of roadside aerosol by diesel engine particles.

- The background aerosol shows similarities to both diesel and petrol engine sources, especially those sources sampled from a dilution tunnel and this is indicative of a mix of sources and an aged combustion aerosol.

Other source apportionment studies have given a vehicle contribution of 11-33% by mass in the US (Chow *et al.*, 1992; Kao and Friedlander, 1995), and 25-32% in the UK (Harrison *et al.*, 1997 a; b), but when accounting for secondary sources, estimates rise to 70-80% of PM_{10} in the UK (QUARG, 1996; Harrison *et al.*, 1997 b). The higher estimates of vehicle contributions by mass from Birmingham and London, UK compare most closely to the results in this work. The percentage number contribution of vehicle sources would be expected to be much larger than these mass studies because one 1μm particle from a non combustion source may have the same mass as up to a thousand 0.1μm particles (COMEAPS, 1995).

Without chemical characterisation secondary particles have not been identified. There is some evidence to suggest that in the presence of carbon spheres nitrates and sulphates will tend to form coatings (Katrinak *et al.*, 1992). However there is probably a proportion of these particles that will either be counted as vehicle generated particles or lost during sample heating in the electron microscope.

The only other study of particle source by number is by Katrinak *et al.* (1995) in Phoenix, AZ., US (*cf.* Table 4.22). In Phoenix, the apportionment clearly highlighted the significance of motor vehicle sources of aerosol by number. It must be also considered that in the US, diesel vehicles are less common, so for a similar vehicle loading the particles generated in this way will be much less apparent than in the UK. The difference between Katrinak *et al.*,

(1995) and this research are various. The larger proportion of diesel vehicles in the UK is one reason. Phoenix is in the middle of Arizona, USA, a much drier place than Plymouth UK, therefore the crustal contribution to aerosol is greater. Also the study in Phoenix only particles to $0.1\mu m$ below which the majority of motor vehicle generated and urban aerosol occur.

In this work, roadside and background aerosol was dominated by vehicle generated aerosol (70-95%). The roadside aerosol closely correlates in morphology terms to diesel engine sources and it is suggested that the background aerosol exhibits a mix of aged aerosol sources. The most important particles in terms of public health are below $1\mu m$ (*cf.* Section 1.1), therefore apportionment by number gives a better indication of the sources of most concern in terms of their repiratory penetration. The mode of vehicle engine particles is less than 100nm (*cf.* Section 4.3), so it is important in terms of its potential respiratory penetration. Thus it is shown in this research that diesel engine sources of aerosol are of the greatest concern in relation to their potential health effect, especially at the roadside, both in terms of percentage number contribution and morphology.

7.2 Future work

Future developments of the research presented could be made in sampling and analysis of either the 1-10 μm aerosol monitoring using the Burkard spore trap or in the analysis of sub-micron material made using transmission electron microscopy.

Despite reservations, the analysis of PM_{10} on spore trap slides has a number of advantages and is a novel technique open to development. Burkard spore samplers are quite widespread and therefore it would be straightforward to extend PM_{10} measurements using this method to many other areas. The slides give a permanent record of the airborne

particulate matter hour by hour which can be stored or transported for image analysis in another area. In chapter 2 comparisons were made between the Burkard number count and the PM_{10} mass as measured in Bristol, UK. A better comparison in future work could be made between mass and number sampling in the same area, thus allowing comparison of local as well as regional or national periods of PM_{10} recommendation exceedences. Development of the shape analysis capabilities of image analysis could allow the automatic identification of pollens, spores and maybe even more irregular particle types. The Burkard trap may also be useful in the examination of pollens coated with diesel engine particles, which may work synergistically in causing hayfever and asthma.

Although a representative sub-micron sample was analysed in this work, further developments could be made. The sampling technique developed in this work in Chapter 3 could be improved in efficiency. By using a larger pore size for PCF construction, there should be an optimum size of pore for maximum efficiency without loosing the representative nature of the sampling. The fractal analysis of images could be extended to include a greater number of fractal dimension measurements, so giving a more specific fingerprint of particles and allowing a closer comparison of measured values to the agglomeration models developed in other studies (Jullien *et al.*, 1987; Skillas *et al.*, 1998).

In the research reported, some elemental analysis using energy dispersive x-ray spectroscopy (EDXS) was made initially (*cf.* Chapter 4), but not used as a matter of course in analysis. In future chemical analysis and morphological analysis at the same time, would aid the identification of coatings and secondary sources of aerosol on the electron microscope. It may be possible in this way to substantiate if nitrates predominate as discrete particles or if they are mostly found in the form of coatings, using carbonaceous particles as seeds for deposition.

The sampling of aerosol can be extended and improved. In the research presented here the sampling and analysis was made for a single day, each month, over a number of months. There is obvious scope for more samples on more days allowing work looking at the fluctuations in the sub-micron aerosol and its morphology relating to the meteorology and traffic flows. In future work source sampling could be made in a co-ordinated program looking at number, size, shape, mass and chemistry of combustion engine particles both immediately after the combustion chamber, at the exhaust outlet and after dilution. Both transmission electron microscopy and scanning electron microscopy can be used, as well as image analysis in this process to assist in the interpretation of morphology and the three dimensional nature of the aerosol. Thus a more detailed 'fingerprint' of particles could be made for use in individual particle identification and elucidation of formation mechanisms.

The number of particles measured in this work was small relative to studies using computer controlled scanning electron microscopy (CCSEM), but allowed the analysis of much smaller particles. If TEM image collection from the microscope was automated in a similar way to CCSEM then a far larger sample at high resolution could be measured within set time limits. Thus the quality of the analysis would be improved and the results more statistically significant.

At present epidemiological links have been made between the mass of particles and health effects (Dockery *et al.*, 1993; Pope *et al.*, 1995). Toxicological studies have also been made of the mass of particles and heath effects in rats (Warheit *et al.*, 1990; Ferin *et al.*, 1992; Nikula *et al.*, 1995; Heirich *et al.*, 1995; Driscoll *et al.*, 1996). In both fields it would be useful for further work to also measure the numbers and morphology of particles to assess the current concern about the numbers, size and shape of particles (Seaton *et al.*,

1995). The research reported here has shown the inadequate nature of mass measures of PM_{10} currently used and further work could be attempted to assess true exposures to particles numbers. The exposure to PM_{10} during a day may be more significant, in terms of number and morphology, from a short exposure whilst walking by a roadside than the exposure experienced away from the roadside for the rest of the day. Therefore, measurements of personal activity and the exposure to PM_{10} could be monitored, using the portable sub-micron aerosol collection developed in this work in conjunction with a portable particle counter. Thus the true PM_{10} exposure could be calculated, which would be useful for directing recommendations on areas of activity and standards of air quality.

REFERENCES

References

Abrahamson, J. (1977) Saturated platelets are new intermediates in hydrocarbon pyrolysis and carbon formation, **Nature**, *266*, 24 March, 323-327.

Anderberg, M.R.(1973) **Cluster Analysis for applications**, Academic Press, London, ISBN 0-12-057650-3.

Barnard, J.A. and Bradley, J.N. (1984) **Flame and Combustion**, 2nd Edition, Chapman and Hall, London, ISBN 0-412-23030-5.

Basu, S and Millette (eds.) (1986) **Electron Microscopy in Forensic, Occupational, and Environmental Sciences**, Plenum Press, ISBN 0-306-42466-5.

Battarbee, J.L., Rose, R.L. and Long, X. (1997) A continuous high resolution record of urban airborne particulates suitable for retrospective microscopical analysis, **Atmospheric Environment**, *31*, 2, 171-181.

Bayona, J.M., Casellas, M., Fernández, P., Solanas, A.M. and Albaigés, J. (1994) Sources and Seasonal Variability of Mutagenic agents in the Barcelona city aerosol, **Chemosphere**, *29*, 441-450.

Barnsley, M.F., Devaney, R.L., Mandelbrot, B.B., Peitgen, H.-O., Saupe, D. and Voss, R.F. (1988) **The Science of Fractal Images** : Ed. Peitgen, H.-O. and Saupe, D., Springer-Verlag, New York, ISBN 0 387 96608 0.

BéruBé, K.A., Jones, T.P. and Williamson, B.J. (1997) Electron Microscopy of Urban Airborne Particulate Matter, **Microscopy and Analysis**, Sept, 11-13.

Brown, W.(1994) Dying from too much dust, **New Scientist**, *141*, 1916, 12-13.

Burkard Manufacturing Co. Ltd., Woodcock Hill Industrial Estate, Rickmansworth, Hertfordshire, WD3 1PJ, 01923 773134.

Carpenter, K and Johnston, J.H. (1979) Analysis of the Physical Characteristics of Diesel Particulate Matter using Transmission Electron Microscope Techniques; in : **The Measurement and Control of Diesel Particulate Emissions Part 2**, Society of Automotive Engineers, Inc., Warrendale, USA, pp 95-101 Paper 790815.

Chan, Y.C., Simpson, R.W., McTainsh, G.H. Vowles, P.D., Cohen, D.D. and Bailey, G.M. (1997) Characterisation of chemical species in $PM_{2.5}$ and PM_{10} Aerosols in Brisbane, Australia, **Atmospheric Environment**, *31*, 22, 3773-3785.

Chow, J.C., Liu, C.S., Cassmassi, J., Watson, J.G., Lu, Z. and Pritchett, L.C. (1992 a) A neighborhood - scale study of PM_{10} source contributions in Rubidoux, California, **Atmospheric Environment**, *26A*, 4, 693-706.

Chow, J.C., Watson, J.G., Lowenthal, D.H., Solomon, P.A., Magliano, K.L., Ziman, S.D and Richards, L.W. (1992 b) PM10 source apportionment in California's San Joaquin valley, **Atmospheric Environment**, *26A*, 18, 3335 -3354.

Clover, C.(1995) £50 bn is true cost of traffic, The front page, **The Electronic Telegraph**, Monday 6 November, http://www.telegraph.co.uk.

Colbeck, I. And Wu, Z. (1994) Measurement of the fractal dimensions of smoke aggregates, **Journal of Physics. D: Applied Physics**, *27*, 670-675.

Colbeck, I., Appleby, L., Hardman, E.J. and Harrison, R.M. (1990) The optical properties and morphology of cloud-processed carbonaceous smoke, **Journal of Aerosol Science**, *21*, 4, 527-538.

Colbeck, I., Atkinson, B. and Johar, Y. (1997) The morphology an optical properties of soot produced by different fuels, **Journal of Aerosol Science**, *28*, 5, 715-723

Cole, S., (1996) Lung damage linked to combined fine-particle ozone exposure in a new toxicological study, **Environmental Science and Technology**, *30*, 9, 382A.

Committee on the Medical Effects of Air Pollutants (COMEAP) (1995) **Health Effects of Non-Biological Particles**, Department of Health, HMSO, London.

Cookson, W.O.C.M. and Moffatt, M.F. (1997) Asthma : An Epidemic in the Absence of Infection?, **Science**, *275*, 3 January, 41-42.

Department of the Environment (1996) **Minerals Planning Guidance : Provision of Silica Sand in England**, September 1996, HMSO Publications.

Department of the Environment, Transport and the Regions (DETR) (1997) **Recent Statistics**, Spring 1997, http://www.detr.gov.uk/transtat/spring97/spring97.html.

Destephen, J.A. and Choi, K.J.(1996) Modeling of filtration processes of fibrous filter media, **Separations Technology**, *6*, 1, 55-67.

Devon County Council (1996) **Personal Communication**, Traffic Survey Data, Environment Department, Devon County Council.

Dockery, D.W., Pope, C.A., Xu, X., Spengler, J.D., Ware, J.H., Fay, M.E., Ferris, B.G and Speizer, F.E. (1993) An Association between Air Pollution and Mortality in Six U.S. Cities, **The New England Journal of Medicine**, *329*, 24, 1753-1759.

Dockery, D.W. and Pope, C.A. (1994) Acute Respiratory Effects of Particulate Air Pollution, **Annual Review of Public Health,** *15*, 107-132.

Dowdy, S. and Wearden, S. (1991) **Statistics for Research**, John Wiley & Sons, Chichester, ISBN 0 471 85703 3.

Driscoll, K.E., Carter, J.M., Howard, B.W., Hassenbein, D.G., Pepelko, W., Baggs, R.B. and Oberdörster, G. (1996) Pulmonary Inflammatory, Chemokine, and Mutagenic Responses in Rats after Subchronic Inhalation of Carbon Black, **Toxicology and Applied Pharmacology**, *136*, 372-380.

Dye, A.L., Rhead, M.M. and Trier, C.J. (1997) A porous carbon film for the collection of atmospheric aerosol for transmission electron microscopy, **Journal of Microscopy**, *187*, 2, 134-138.

ECC International (1986) **China Clay Production**, ECC International Paper division.

Fahmy, T.(1996) **xlSTAT 2.0**, Microsoft Excel add-in, fahmy@engref.fr.

Farrants, G., Rieth, A., Schuler, B., Feren, K. (1988) A simple, direct method for the collection of particles from air for transmission electron microscopy and digital image analysis, **Journal of Microscopy,** *149*, 2, 159-164.

Ferin, J., Oberdörster, G. and Penney, D.P.(1992) Pulmonary retention of ultrafine and fine particles in rats, **American journal of respiratory cell molecular biology**, 6, 535 - 542.

Ferin, J., Oberdörster, G., Penney, D.P., Soderholm, S.C., Gelein, R. and Peper, H.C. (1990) Increased Pulmonary Toxicity of Ultrafine particles? I. Particle Clearance, Translocation, Morphology, **Journal of Aerosol Science**, *21*, 381-384.

Forrest, S.R. and Witten, T.A. Jr. (1979) Long-range correlations in smoke-particle aggregates, **Journal of Physics A.**, *12*, L109-L117.

Freeman, V. (1994) Fuel for long-term thought, **The Times**, Friday February 25, 37-38.

Frenklach, M. and Wang, H. (1990) Detailed Modelling of soot particle nucleation and growth, **In : Twenty Third Symposium (International) on Combustion,** The Combustion Institute, Pittsburgh, Pennsylvania, 1559-1566.

Frenklach, M. and Warnatz, J. (1987) Detailed modelling of PAH profiles in a sooting low-pressure Acetylene flame, **Combustion Science and Technology,** *51*, 265-283.

Fukami, K., Shizuma, K., Iwatana, K., and Hasai, H. (1992) Collection Efficiency of the Nuclepore Membrane Filter for Aerosol Sampling and its Application to ^{218}Po Measurement, **Japanese Journal of Applied Physics,** *31*, 3699-3700.

Gangopadhyay, S., Elminyawi, I. and Sorensen, C.M. (1991) Optical structure factor measurements of soot particles in a premixed flame, **Applied Optics,** *30*, 4859-4863.

Glikson, M., Rutherford, S., Simpson, R.W., Mitchell, C.A. and Yago, A. (1995) Microscopic and submicron components of atmospheric particulate matter during high asthma periods in Brisbane, Queensland, Australia, **Atmospheric Environment,** *29*, 4, 549-562.

Goodge, E.M. (1979) **Combustion Calculations,** Macmillan Press Ltd., ISBN 0-333-21801-9, 10-14.

Green, M. (1995) Air pollution and health, **British Medical Journal,** *311*, 401-402.

Haddad, S. and Watson, N. (1984) **Principles and Performance in Diesel Engineering,** John Wiley and Sons Ltd., ISBN 0-85312-732-8, 13-28.

Hamilton, R.S., Kershaw, P.R., Segarra, F., Spears, C.J. and Watt, J.M. (1994) Detection of airborne carbonaceous particulate matter by scanning electron microscopy, **The Science of the Total Environment,** *146/147,* 303-308.

Hannigan, M.P., Cass, G.R., Lafleur, A.L., Longwell, J.P. and Thilly, W.G. (1994) Bacterial Mutagenicity of Urban Organic Aerosol Sources in Comparison to Atmospheric Samples, **Environmental Science and Technology,** *28,* 2014-2024.

Harrison, R.M., Smith, D.J.T., Pio, C.A. and Castro, L.M. (1997 a) Comparative receptor modelling study of airborne particulate pollutants in Birmingham (United Kingdom), Coimbra (Portugal) and Lahore (Pakistan), **Atmospheric Environment,** *31,* 20, 3309-3324.

Harrison, R.M., Deacon, A.R. and Jones, M.R. (1997 b) Sources and Processes affecting concentrations of PM_{10} and $PM_{2.5}$ particulate matter in Birmingham (U.K.), **Atmospheric Environment,** *31,* 24, 4103-4117.

Health and Safety Executive (1998) **Health and Safety in the Workplace,** http : // www.open.gov.uk/hse/pubns/workplac.htm.

Hirst, J.M. (1952) An Automatic Volumetric Spore Trap, **Annals of Applied Biology,** *39,* 257-265.

Hopke, P.K. and Song, X.H. (1997) Classification of single particles by neural networks based on the computer controlled scanning electron microscopy data, **Analytica Chimica Acta**, *348*, 375-388.

Huang, P., Turpin, B.J., Pipho, M.J., Kittleson, D.B and McMurry, P.H. (1994) Effects of water condensation and evaporation on diesel chain-agglomerate morphology, **Journal of Aerosol Science**, *25*, 3, 447-459.

Jain, S. and Kodas, T.T. (1998) Asymptotic widths if size distributions resulting from collisional growth assuming Log-normally distributed fractal aggregates, **Journal of Aerosol Science**, *29*, 3, 259-261.

Jullien, R., Botet, R. and Mors, P.M. (1987) Computer simulations of cluster - cluster aggregation, **Faraday discussions of the chemical society**, *83*,125-137.

Kado, N.Y., Colome, S.D., Kleinman, M.T., Hsieh, D.P.H. and Jaques, P. (1994) Indoor-Outdoor Concentrations and Correlations of PM10-Associated Mutagenic Activity in Nonsmokers' and Asthmatics Homes, **Environmental Science and Technology**, *28*, 1073-1078.

Kao, A.S. and Friedlander, S.K. (1995) Frequency Distributions of PM_{10} Chemical Components and Their Sources, **Environmental Science and Technology**, *29*, 19-28.

Karlsen, J.T., Farrants, G., Torgrimsen, T. and Reith, A. (1992) Chemical Composition and Morphology of Welding Fume Particles and Grinding Dusts, **American Industrial Hygiene Association Journal**, *53*, (5), 290-297.

Katrinak, K.A., Anderson, J. R. and Buseck, P.R.(1995) Individual Particle Types in the Aerosol of Phoenix, Arizona, **Environmental Science and Technology**, *29*, 321-329.

Katrinak, K.A., Rez, P., Buseck, P.R. (1992) Structural Variations in Individual Carbonaceous Particles from an Urban Aerosol, **Environmental Science and Technology**, *26*, 1967 - 1976.

Katrinak, K.A., Rez, P., Perkes, P.R. and Buseck, P.R. (1993) Fractal Geometry of Carbonaceous Aggregates from an Urban Aerosol, **Environmental Science and Technology**, 27, 539-547.

Katsouyanni, K., Touloumi, G., Spix, C., Schwartz, J., Balducci, F., Medina, S., Rossi, G., Wojtyniak, B., Sunyer, J., Bacharova, L., Schouten, J.P., Ponka, A., Anderson, H.R. (1997) Short term effects of ambient sulphur dioxide and particulate matter on mortality in 12 European cities: results from time series data from the APHEA project, **British Medical Journal**, *314*, 1658 - 63.

Kaye, B.H. (1992) The impact of fractal geometry on fine particle characterisation, **RSC special publication**, *102*, 300-313.

Kaye, B.H.(1993) **Chaos & Complexity : discovering the surprising patterns of science and technology**. VCH, Weinheim, ISBN 3-527-29007-9.

Kaye, B.H. (1991) Characterising the Structure of Fumed Pigments using the Concepts of Fractal Geometry, **Particle and Particle System Characterisation**, *8*, 63 -71,

Kaye, B.H., Clark, G.G., Kydar, Y. (1994) Strategies for Evaluating Boundary Fractal Dimensions by Computer Aided Image Analysis, **Particle and Particle System Characterisation,** *11*, 411-417.

Kaye, B.H. and Clark, G.G. (1991) Formation Dynamics Information, **Proceedings of the American Chemical Society: Particle Size Distribution 2: Assessment and Characterisation 1991 Washington D.C.**, 472, Chapter 24, 372-385.

Kim, D.S., Hopke, P.K., Massart, D.L., Kaufman, L. and Casuccio, G.S. (1987) Multivariate Analysis of CCSEM Auto emission data, **The Science of the Total Environment**, *59*, 141 - 155.

Kim, D. and Hopke, P.K. (1988) Classification of Individual Particles Based on Computer - Controlled Scanning Electron Microscopy Data, **Aerosol Science and Technology**, *9*, 133 -151.

Kindratenko, V.V., Van Espen, Piet., J.M., Treiger, B.A., Van Grieken, R.E. (1994) Fractal Dimensional Classification of Aerosol Particles by Computer-Controlled Scanning Electron Microscopy, **Environmental Science and Technology**, *28*, 2197-2202.

King, A.M. and Dorling, S. (1997) PM$_{10}$ particulate matter - the significance of ambient levels, **Atmospheric Environment**, *31*, 15, 2379-2383.

Kleinman, M.T., Bhalla, D.K., Mautz, W.J. and Phalen, R.F. (1995) Cellular and Immunological injury with PM-10 inhalation, **Inhalation Toxicology**, *7*, 589 - 602.

Köylü, Ü.Ö., Xing, Y and Rosner, D.E. (1995) Fractal Morphology Analysis of Combustion-Generated Aggregates Using Angular Light Scattering and Electron Microscope Images, **Langmuir**, *11*, 4848-4854.

Kruis, F.E., van Denderen, J., Buurman, H., Scarlett, B.(1994) Characterisation of Agglomerated Aerosol Particles Using Image Analysis, **Particle and Particle System Characterisation,** *11*, 426 - 435.

Langley, P.(1996 a) Road rage is driving Britain to distraction, Home News, **Electronic Telegraph**, Wed 24 January, http://www.telegraph.co.uk.

Langley, J. (1996 b) How the dirty diesel is cleaning up its act, **The Daily Telegraph**, Saturday, February 3, 14-15.

Lawther, P.J., Ellison, J.McK., Waller, R.E. (1968) Some medical aspects of aerosol research, **Proceedings of the Royal Society A**, 307, 223-234.

Leake, J. and Macaskill, J. (1998) Diesel fumes proved to be cancer risk, **The Sunday Times**, Sunday, 10 May.

Mandelbrot, B.B. (1977) **Form, Change and Dimension**, W.H. Freeman, San Francisco, USA.

Maynard, A.D. (1995) The Development of a New Thermophoretic Precipitator for Scanning Transmission Electron Microscope Analysis of Ultrafine Aerosol Particles, **Aerosol Science and Technology**, *23*, 521-533.

Medalia, A.I. and Hornik, G.J. (1975) Pattern Recognition Problems in the Study of Carbonblack, **Pattern Recognition**, *4*, 155.

Medalia, A.I. and Rivin, D. (1982) Particulate carbon and other Components of Soot and Carbon Black, **Carbon**, *20*, 481-492.

Meteorological Data Archive at : http://hydrography.ims.plym.ac.uk/ims/default.htm.

Miller, J.C. and Miller, J.N. (1993) **Statistics for Analytical Chemistry**, 3rd Edition, Elis Horwood Ltd, Chichester, ISBN 0 13 030990 7.

Mountain, R.D., Mulholland, G.W. and Baum, H. (1986) Simulation of aerosol agglomeration in the free molecular and continuum flow regimes, **Journal of Colloid and interface Science**, *114*, 1, 67-81.

Murayama, T., Miyamoto, N., Chikahisa T. and Yamane K. (1986) Effects of combustion and injection systems on unburned hydrocarbon and particulate emissions from a DI diesel engine, **Society of Automotive Engineers**, Paper no. 932685, 1-17.

Murphy, C.H. (1984) **Handbook of Particle Sampling and Analysis Methods**, Verlag Chemie, International Inc., Weinheim, ISBN 0-89573-116-9.

NETCEN (1998) air quality home page of the National Environmental Technology Centre at :- **http://www.aeat.co.uk/netcen/airqual/welcome.html.**

Newbury, D.E., Joy, C.D., Echlin, P., Fiori, C.E., Goldstein, J.I. (1992) **Scanning Electron Microscopy and X-ray microanalysis**, 2nd Edition, Plenum Press, London.

Nikula, K.J., Snipes, M.B., Barr, E.B., Griffith, W.C., Henderson, R.F. and Mauderly, J.L. (1995) Comparative pulmonary toxicities and carcinogenities of chronically inhaled diesel exhaust and carbon-black in F344 rats, **Fundamental and Applied Toxicology**, *25*, 80-94.

Nyeki, S. and Colbeck, I.(1994) The measurement of the fractal dimension of individual in situ soot agglomerates using a modified Millikan cell technique, **Journal of Aerosol Science**, *25*, 75-90.

Oke, T. (1978) **Boundary Layer Climates**, Methuen & Co. Ltd., London, ISBN 0 416 70520 0.

O'Neill, P. (1985) **Environmental Chemistry**, George Allen and Unwin Ltd., London, ISBN 0 04 551086 5.

Pagano P., Zaiacomo T.D., Scarcella E., Bruni S. and Calamosca M. (1996): Mutagenic Activity of Total and Particle - Sized Fractions of Urban Particulate Matter. **Environmental Science & Technology**, *30*, 3512 -3516.

Peitgen, H-O., Jürgens, H., Saupe, D.(1992) **Chaos and Fractals : New frontiers of Science**, Springer-Verlag, Berlin, ISBN 3-540-97903-4.

Pemberton, R.D. (1996) **The Fate of Napthalene and n-Alkylnapthalenes during combustion and evaluation of the sources of these compounds in diesel exhaust emissions**, Ph. D. Thesis, University of Plymouth, pp197.

Peters, A., Doring, A., Wichmann, H., Koenig, W.(1997) Increased plasma viscosity during an air pollution episode: a link to mortality?, **The Lancet**, *349*, May 31, 1582 - 1587.

Pope, C.A., Dockery, D.W. and Schwartz, J. (1995 a) Review of Epidemiological evidence of Health Effects of Particulate Air Pollution, **Inhalation Technology**, *7*, 1, 1- 18.

Pope, C.A., Thun, M.J., Namboodiri, M.M., Dockery, D.W., Evans, J.S., Speizer, F.E. and Heath, C.W. (1995 b) Particulate air pollution as a predictor of mortality in a prospective study of U.S. adults, **American Journal of Respiratory Critical Care Medicine**, *151*, 3, 669-674.

Pope, C.A., Dockery, D.W., Spengler, J.D., and Raizenne, M.E. (1994) Respiratory Health and PM_{10} Pollution, **American Review of Respiratory Disease**, *144*, 3, 668-674.

Quality of Urban Air Review Group (QUARG) (1993) a, **Urban Air Quality in the United Kingdom,** HMSO.

Quality of Urban Air Review Group (QUARG) (1993) b, **Diesel Vehicle Emissions and Urban Air Quality,** HMSO.

Quality of Urban Air Review Group (QUARG) (1996) , **Airborne Particulate Matter in the United Kingdom: Third Report of the Quality of Urban Air Review Group,** HMSO.

Read, C. (1994) **How vehicle pollution affects our health**, Ashden Trust, London, EC4A 3EB.

Rao, K.K., Winterborne, D.E. and Clough, E. (1993) Influence of swirl on high pressure injection in hydra diesel engine, **Society of Automotive Engineers**, Paper no. 930978, 1-11.

Robards, A.W. and Wilson, A.J. eds. (1993) **Procedures in Electron Microscopy**, John Wiley & Sons, Chichester.

Rodgers, G.F.C. and Mayhew, Y. (1992) **Engineering Thermodynamics, Work and Heat Transfer**, Longman group Ltd., ISBN 0-582-04566-5, 395-415.

Samson, R.J., Mulholland, G.W. and Gentry, J.W. (1987) Structural Analysis of Soot Agglomerates, **Langmuir**, *3*, 272-281.

Satio, T., Gordon, A.S., Williams, F.A. and Stikle, W.F. (1991) A study of the early history of soot formation in various diffusion flames, **Combustion Science and Technology**, *80*, 103-119.

Saucy, D.A., Anderson, J.R. and Buseck, P.R. (1991) Aerosol Particle Characteristics by Combined Cluster and Principle Component Analysis, **Journal of Geophysical Research**, *96*, D4, 7407 -7414.

Scheepers, P.T.J. and Bos, R.P. (1992) Combustion of diesel fuel from a toxicological perspective, **International Archives of Occupational and Environmental Health**, *64*, 163-177.

Schenker, M. (1993) Air Pollution and Mortality, **The New England Journal of Medicine**, *329*, 24, 1807-1808.

Schlesinger, R.B. (1995) Interaction of gaseous and particulate pollutants in the respiratory tract: mechanisms and modulators, **Toxicology**, *105*, 315-325.

Schwartz, J. (1994) Air Pollution and Daily Mortality: A Review and Meta Analysis, **Environmental Research**, *64*, 36-52.

Schwartz, H and Exner, E. (1980) The Implementation of the Concept of Fractal Dimension on a Semi-Automatic Image Analyser, **Powder Technology**, *27*, 207 -213.

Seaton, A., Godden, D.J. and Brown, K. (1994) Increase in asthma: a more toxic environment or a more susceptible population, **British Medical Association**, *49*, 2, 171-174.

Seaton, A., MacNee, W., Donaldson, K. and Godden, D.(1995) Particulate Air Pollution and Acute Health Effects, **The Lancet**, *345*, 176-178.

Shirakawa, T., Enomoto, T., Shimazu, S. and Hopkin, J.M. (1997) The inverse association between Tuberculin Responses and Atopic Disorder, **Science**, *275*, 77-78.

Shrimsley, R. (1997) Government aims to put brakes on motorists, UK News, **Electronic Telegraph**, Thursday 21 August, *818*, http://www.telegraph.co.uk.

Siak, J., Chan, T.L., Gibson, T.L. and Wolff, G.T. (1985) Contribution to bacterial mutagenicity from Nitro-PAH compounds in ambient aerosols, **Atmospheric Environment**, *19*, 369-376.

Skillas, G., Künzel, S., Burtscher, H. (1997) On the morphology if internal combustion engine exhaust particles, **Journal of Aerosol Science**, *28*, S43-S44.

Skillas, G., Künzel, S., Burtscher, H., Baltensperger, U. and Siegmann, K. (1998) High fractal-like dimension of diesel soot agglomerates, **Journal of Aerosol Science**, *29*, 4, 411-419.

Sorensen, C.M., Cai, J. and Lu, N.(1992) Light-scattering measurements of monomer size, monomers per aggregate, and fractal dimension for soot aggregates in flames, **Applied Optics**, *31*, 6547-6557.

Spurny, K.R. (1994) Sampling, Analysis, Identification and Monitoring of Fibrous Dust and Aerosols, **Analyst**, *119*, 41-51.

Spurny, K. and Lodge, J.P. (1968) Analytical Methods for determination of aerosols by means of membrane ultrafilters, structural and filtration properties of nuclear pore filters, **Collection of Czechoslovakian Chemical Communications**, *33*, 3697 - 3693.

Stedman, J.R. (1997) A U.K. - wide episode of elevated particle (PM_{10}) concentration in March 1996, **Atmospheric Environment**, *31*, 15, 2379-2383.

Steiner, D., Burtscher, H. and Gross, H. (1992) Structure and Disposition of Particles from a Spark- Ignition Engine, **Atmospheric Environment**, *26A*, 6, 997-1003.

Tence, M., Chevalier, J.P. and Jullien, R. (1986) On the measurement of the fractal dimension of aggregated particles by electron-microscopy - experimental method, corrections and comparison with numerical - models, **Journal of Physics**, *47*, 11, 1989-1998.

Thurston, G.D., Ito, K., Hayes, C.G., Bates, D.V. & Lippmann, M. (1994) Respiratory Hospital Admissions and Summertime Haze Air Pollution in Toronto, Ontario: Consideration of the Role of Acid Aerosols, **Environmental Research**, *65*, 271-290.

Thurston, G.D. and Spengler, J.D. (1985) A Quantitative Assessment of Source Contributions to Inhalable Particulate Matter Pollution in Metropolitan Boston, **Atmospheric Environment**, *19*, 1, 9-25.

Twomey, S. (1977) **Atmospheric Aerosols**, Elsevier, Scientific Publishing Company, Amsterdam, ISBN 0 444 41527 0.

van Borm, W.A. and Adams, F.C.(1988) Cluster Analysis of Electron Microprobe Analysis Data of Individual Particles for Source Apportionment of Air Particulate Matter, **Atmospheric Environment,** *22*, 2297 -2307.

van Houdt, J.J. (1990) Mutagenic activity of airborne particulate matter in indoor and outdoor environments, **Atmospheric Environment**, *24B*, 207-220.

Vincent, J.H. (1989) **Aerosol Sampling : Science and Practice,** John Wiley & Sons, ISBN 0-471-92175-0.

Viras, L.G., Athanasiou, K. and Siskos, P.A. (1990) Determination of mutagenic activity of airborne particulates and of the Benzo[α]Pyrene concentrations in Athens Atmosphere, **Atmospheric Environment**, *24B*, 267-274.

von Mutius, E., Fritzsch, C., Weiland, S.K., Röll, G. and Magnussen, H. (1992) Prevalence of asthma and allergic disorders among children in united Germany: a descriptive comparison, **British Medical Journal**, *305*, 1395-1398.

von Mutius, E., Martinez, F.D., Fritzsch, C., Nicolai, T., Reitmeir, P. and Thiemann, H-H. (1994) Skin test reactivity and number of siblings, **British Medical Journal**, *308*, 692-695.

Waller R.E. (1967) Studies on the Nature of Air Pollution, London Conference on Museum Climatology, **International Institute for Renovation of Works of Art**, 65 - 69.

Warheit, D.B., Seidel, W.C., Carakostas, M.C. and Hartsky, M.A. (1990) Attenuation of Perfluoropolymer fume pulmonary toxicity - effect of filters, combustion method, and aerosol age, **Experimental and Molecular Pathology**, *52*, 309-329.

Weber, A.P. (1992) **Characterisation of the Geometrical Properties of Agglomerated Aerosol Particles**, Paul Scherrer Institut.

Wienke, D., Xie, Y., and Hopke, P.K.(1994) An adaptive resonance theory based artificial neural network (ART - 2a) for rapid identification of airborne particle shapes from their scanning electron microscopy images, **Chemometrics and Intelligent Laboratory Systems**, *25*, 367-387.

Wu, Z., Colbeck, I and Simons, S. (1994) Determination of the fractal dimension of aerosols from kinetic coagulation, **Journal of Physics. D: Applied Physics**, *27*, 2291-2296.

Wu, Z. and Colbeck, I. (1996) Studies of the dynamic shape factor of aerosol agglomerates, **Europhysics Letters**, *33*, 9, 719-724.

Xie, Y, Hopke, P.K., Casuccio, G., Henderson, B. (1994 a) Use of Multiple Fractal Dimensions to Quantify Airborne Particle Shape, **Aerosol Science and Technology**, *20*, 161 - 168.

Xie, Y., Hopke, P.K., and Wienke, D. (1994 b) Airborne Particle Classification with a Combination of Chemical Composition and Shape Index Utilizing an Adaptive Resonance Artificial Neural Network, **Environmental Science and Technology**, *28*, 11, 1921-1928.

APPENDIX ONE

A1 Quic BASIC macro progammes for Image Analysis using the QUANTIMET 540 (Cambridge Instruments Cambridge) written by Paul Russell, University of Plymouth, UK.

A1.1 Burkard Spore Trap Slide Image analysis macro programme (*cf.* Section 2.2.3)

Initial set up , microscope, camera, and magnification

```
10      rem x y w ht blue yellow double border
20      panel 0,0,80,79,1,14,3"WELCOME":coltext 44:coltext 33:coltext 1
30      posttext 12,14
40      print " Place 3.5 disc in bottom drive then press space bar"
50      g$=inkey$;if g$="" then 50
60      test g$=" " then 70 else 50
70      cls
80      panel 0,0,80,79,1,14,3"SET UP" :coltext 45:coltext 32:coltext 1
90      postext 12,15
100     rem WHAT MICROSCOPE, MAG AND ILLUMINATION????????
110     print "PLACE COL CAM ON ZEISS X16 OBJECTIVE AND 3.3 EYEPIECE"
120     postext 13,26
130     print "FOCUS AND POSITION OBJECT"
140     postext 14,26
150     print"                    "
160     postext 15,26:coltext 35
170     print "WHEN READY PRESS SPACE BAR"
180     r$=inkey$:if r$="" then 180
190     TEST r$=" " THEN 200 else 180
200     CLS
210     c=1
220     camera 4
230     scanner 20 14
240     setlamps 55 1
```

Set the background darkness at the beginning of each session.

```
250     pausetext 1"AT THE BEGINNING OF EVERY SESSION YOU NEED TO SET SHADING"
260     pausetext 2"MOVE TO A BLANK AREA AND THEN HIGHLIGHT SET WITH MIDDLE
TRAKERBALL KEY"
270     pausetext 3 "THEN PRESS MIDDLE KEY, THEN CONTINUE"
280     qmenu 'shading'
290     pausetext 1""
300     pausetext 2"CHECK MAG IS X20"
310     pausetext 3""
320     calibrate 3, 't'
330     qmenu 'calibrate'
340     riasettings 'cal_value' k
```

File set up

```
350     panel 0,0,80,79,1,14,3"FILE":coltext 44:coltext 33:coltext 1
360     postext 14,5
370     input "Please type the name of the file you wish to save this image under".N$
380     open#1 "b:"+n$+".prn"
390     c=1
400     postext 16,5
410     input 'HOW MANY FIELDS DO YOU WISH TO SAVE? ' F$
420     CLS
430     PAUSETEXT 1""
440     pausetext 2"FIND THE FIELD YOU WISH TO MEASURE"
450     pausetext 3""
```

Image Measurement

```
460     qmenu 'image_setup'
```

```
470    panel 0,0,80,79,1,14,3"WORK":coltext 44:coltext 33:coltext 1
480    postext 12,23
490    print "PLEASE WAIT I'M WORKING ON "N$ ", FIELD "C"!"
500    postext 13,28
510    print "I WILL BE ABOUT 10 SECS"
520    mframe 85 106 353 406              |set measurment frame particles that partially fall
                                          in this frame are measured|
530    iframe 0 0 512 512                 |set image frame to account for the particles that
                                          fall partly outside the measument area|
540    multiacquire 5 1 4                 [Picture aquired and saved]
550    delin 1 2 256 3                    |noise reduced|
560    greyfill 1 3 2 2                   |grey scale picture saved|
570    greydetect 1 192 231 4 1 0   [grey scale detected and saved in bin 1|
580    pausetext 2"DETECT THE ORIGINAL IMAGE LEAVING A FEW HOLES"
590    qmenu 'detect'
600    binmove 1 10                       [Picture in bin 1 moved to bin 10]
610    pausetext 2"DETECT THE TRANSFORMED IMAGE TO FILL IN THE HOLES"
620    greydetect 3 217 231 4 1 0         |grey picture detected|
630    qmenu 'detect'
640    binx 1 10 2 2 0 0                  [binary picture in bin 1 added to picture in 10|
650    binerode 2 3 0 1                   |removes noise and small objects|
660    build 2 3                          [rebuilds edges to original resolution|
670    setftrpar "1,3,2,15,34,31,39,13"   |Setting to measure parameters|
680    ftrgrey 3 : measfeat 3 1 1 300000 : clraccept
690    acceptxfer 3 4
700    pausetext 2 " ERE THEY BE!"
710    qmenu 'feature_results'
720    rem transform, detect, amend, measure, display
730    rfeatnum n(1)
740    for f=0 to n(1)-1
750    rfeatres f 1 a(1)                  |measure area of particle image|
760    rfeatres f 13 p(1)                 |measure perimeter of particle image|
770    rfeatres f 15 r(1)                 |measure roundness of particle image|
780    rfeatres f 31 g(1)                 |measure greyness of particle image|
790    rfeatres f34 ed(1)                 |measure equivalent circle diameter of image|
800    rfeatres f39 gv(1)                 [measure the variance in the greyness of the image|
810    print #1:c,n(1),k*k*a(1),K*P(1),R(1)/1000,g(1),K*ED(1),gv(1)   [Print data in microns]
820    next f
830    c=c+1
```

Programme end and repeat option
```
840    C$=STR$(C)
850    test f$<C$ then 860 else 460
860    panel 0,0,80,79,1,14,3,3"THE END":coltext 44:coltext 33:coltext 1
870    panel 20,5,40,12,4,14,2"COPYRIGHT":coltext 41:coltext 33:coltext 1
880    postext 8,33
890    print "PPPPP  RRRRR"
900    POSTEXT 9,33
910    PRINT"P  P R   R"
920    POSTEXT10,33
930    PRINT"PPPPP  RRRRR"
940    POSTEXT 11,33
950    PRINT"P        RR"
960    POSTEXT 12,33
970    PRINT"P        R R"
980    POSTEXT 13,33
990    PRINT"P         R   R"
1000   panel 20,18,40,6,5,4,2""
1010   postext 19,32
1020   coltext 1:coltext 32:coltext 45
1030   print"Wasn't that fun!"
1040   postext 20,32
```

```
1050  print "That is "n$" done"
1060  postext 21,22:COLTEXT 35
1070  print "Do you wish  to do another? y or n"
1080  a$=inkey$;if a$="" then 1080
1090  test a$ = 'y' then 370 else 1100
1100  coltext 0
1110  close#1
1120  cls
1130  end
```

A1.2 Determination of PM_{10} number per m^3

Six field are viewed across the slide

For each field the total number of particles between 1 and 10 microns is given

The PM1-10 number for each field is added together to give a total **P**

Each field has an area of 1.3×10^{-2} mm^2

P particles are counted in $6 \times 1.3 \times 10^{-2}$ $mm^2 = 7.8 \times 10^{-2}$ mm^2

The area of the slide = 48×14 mm = 672 mm^2

Total number of PM1-10 on the trace = **P** $\times 672/7.8 \times 10^{-2}$

14.4 m^3 of air was sampled

Assuming 100% efficiency of sampling between 1-10 microns the number of particles in 1 m^3 of air = **P** x

$672/(7.8 \times 10^{-2}$ $mm^2 \times 14.4) = \underline{\mathbf{P} \times 598}$

A1.3 Image analysis macro programme for the measurement of fractal dimension (*cf.* Section 3.5.1.1)

Image analysis from negatives (*cf.* Section 3.5.1.2)
FRACBOX
```
5 mframe 0 0 511 512
  6 iframe 0 0 481 481
  10 qmenu 'acquire'
  15 PAUSETEXT 2 'ACQUIRE INTO 0'
  20 greydetect 0 163 208 4 1 0
  30 qmenu 'detect'
  33 PAUSETEXT 2 'KEEP AREAS OF INTEREST INPUT 1 OUTPUT 1'
  35 qmenu 'bin_edit'
  40 binx 3 1 10 1 0 0
  50 build 3 10
  55 PAUSETEXT 2 'INPUT PLANE 10'
  60 qmenu 'measure_field'
  70 BINX 4 1 10 1 0 0
  80 BUILD 4 10
  90 QMENU 'MEASURE_FIELD'
  100 BINX 5 1 10 1 0 0
  110 BUILD 5 10
  120 QMENU 'MEASURE_FIELD'
  130 BINX 6 1 10 1 0 0
  140 BUILD 6 10
```

228

```
150 QMENU 'MEASURE_FIELD'
160 BINX 7 1 10 1 0 0
170 BUILD 7 10
180 QMENU 'MEASURE_FIELD'
190 END
```

FRACBOX2
```
10 mframe 0 0 511 512
20 iframe 0 0 481 481
25 qmenu 'image_setup'
30 qmenu 'acquire'
40 PAUSETEXT 2 'ACQUIRE INTO 0'
45 REM DETECT WHITE FOR NEG +70+80 TO CLEAN
50 greydetect 0 159 160 1 1 0
60 qmenu 'detect'
70 binopen 1 2 0 3
80 binmove 2 1
90 PAUSETEXT 2 'KEEP AREAS OF INTEREST INPUT 1 OUTPUT 1'
100 qmenu 'bin_edit'
110 binx 3 1 10 1 0 0
120 build 3 10
130 PAUSETEXT 2 'INPUT PLANE 10'
140 qmenu 'measure_field'
150 BINX 4 1 10 1 0 0
160 BUILD 4 10
170 QMENU 'MEASURE_FIELD'
180 BINX 5 1 10 1 0 0
190 BUILD 5 10
200 QMENU 'MEASURE_FIELD'
210 BINX 6 1 10 1 0 0
220 BUILD 6 10
230 QMENU 'MEASURE_FIELD'
240 BINX 7 1 10 1 0 0
250 BUILD 7 10
260 QMENU 'MEASURE_FIELD'
270 END
```

FRACBOX3
```
10 mframe 0 0 511 512
20 iframe 0 0 481 481
25 qmenu 'image_setup'
30 qmenu 'acquire'
40 PAUSETEXT 2 'ACQUIRE INTO 0'
45 REM DETECT WHITE FOR NEG +70+80 TO CLEAN
50 greydetect 0 159 160 1 1 0
55 greyfill 0 1 2 1
60 qmenu 'detect'
70 binopen 1 2 0 3
80 binmove 2 1
90 PAUSETEXT 2 'KEEP AREAS OF INTEREST INPUT 1 OUTPUT 1'
100 qmenu 'bin_edit'
110 binx 3 1 10 1 0 0
120 build 3 10
130 PAUSETEXT 2 'INPUT PLANE 10'
140 qmenu 'measure_field'
150 BINX 4 1 10 1 0 0
160 BUILD 4 10
170 QMENU 'MEASURE_FIELD'
180 BINX 5 1 10 1 0 0
190 BUILD 5 10
```

```
200 QMENU 'MEASURE_FIELD'
210 BINX 6 1 10 1 0 0
220 BUILD 6 10
230 QMENU 'MEASURE_FIELD'
240 BINX 7 1 10 1 0 0
250 BUILD 7 10
260 QMENU 'MEASURE_FIELD'
270 END
```

FRACBOX4
```
10 mframe 0 0 511 512
 20 iframe 0 0 481 481
 30 qmenu 'image_setup'
 40 multiacquire 5 0 4
 50 PAUSETEXT 2 'ACQUIRE INTO 0'
 60 REM DETECT WHITE FOR NEG +70+80 TO CLEAN
 70 greydetect 0 159 160 1 1 0
 80 qmenu 'detect'
 90 binopen 1 2 0 3
100 binmove 2 1
110 PAUSETEXT 2 'KEEP AREAS OF INTEREST INPUT 1 OUTPUT 1'
120 qmenu 'bin_edit'
130 OUTLINE 1 9
140 binx 3 1 10 1 0 0
145 BINX 3 9 11 1 0 0
150 build 3 10
160 build 3 11
170 PAUSETEXT 2 'INPUT PLANE 10 MEASURE THEN DO 11'
180 qmenu 'measure_field'
190 BINX 4 1 10 1 0 0
195 BINX 4 9 11 1 0 0
200 BUILD 4 10
210 build 4 11
220 QMENU 'MEASURE_FIELD'
230 BINX 5 1 10 1 0 0
235 BINX 5 9 11 1 0 0
240 BUILD 5 10
250 build 5 11
260 QMENU 'MEASURE_FIELD'
270 BINX 6 1 10 1 0 0
275 BINX 6 9 11 1 0 0
280 BUILD 6 10
290 build 6 11
300 QMENU 'MEASURE_FIELD'
310 BINX 7 1 10 1 0 0
315 BINX 7 9 11 1 0 0
320 BUILD 7 10
330 build 7 11
340 QMENU 'MEASURE_FIELD'
350 END
```

FRACBOX5
```
10 dim a(100)
 20 input 'filename? ' n$
 30 open#1 'b:' +n$+'.prn'
 40 c=1
 50 riasettings 'cal_value' k
 60 mframe 0 0 511 512
 70 iframe 0 0 481 481
 80 qmenu 'image_setup'
 90 multiacquire 5 0 4
```

```
100 PAUSETEXT 2 'ACQUIRE INTO 0'
110 REM DETECT WHITE FOR NEG +70+80 TO CLEAN
120 greydetect 0 159 160 1 1 0
130 qmenu 'detect'
140 binopen 1 2 0 3
150 binmove 2 1
160 PAUSETEXT 2 'KEEP AREAS OF INTEREST INPUT 1 OUTPUT 1'
170 qmenu 'bin_edit'
180 OUTLINE 1 9
190 binx 3 1 10 1 0 0
200 BINX 3 9 11 1 0 0
210 build 3 10
220 build 3 11
230 PAUSETEXT 2 'INPUT PLANE 10 MEASURE THEN DO 11'
240 measfield 10
250 rfieldres a(1)
260 print#1: a(1)*k,a(5)
270 measfield 11
280 rfieldres a(1)
290 print#1: a(1)*k,a(5)
300 c=c+1
310 if c=6 goto 560
320 if c=5 goto 510
330 if c=4 goto 460
340 if c=3 goto 410
350 if c=2 goto 360
360 BINX 4 1 10 1 0 0
370 BINX 4 9 11 1 0 0
380 BUILD 4 10
390 build 4 11
400 goto 240
410 BINX 5 1 10 1 0 0
420 BINX 5 9 11 1 0 0
430 BUILD 5 10
440 build 5 11
450 goto 240
460 BINX 6 1 10 1 0 0
470 BINX 6 9 11 1 0 0
480 BUILD 6 10
490 build 6 11
500 goto 240
510 BINX 7 1 10 1 0 0
520 BINX 7 9 11 1 0 0
530 BUILD 7 10
540 build 7 11
550 goto 240
560 close#1
570 END
```

Image analysis with TIFF images (*cf.* Section 3.5.1.3)
FRACTIF5

```
10 PAUSETEXT 2 'PLACE TIFF IMAGE INTO GREY 1'
20 qmenu 'acquire'
30 PAUSETEXT 2 "
40 greyinvert 1 0
50 PAUSETEXT 2 'ACQUIRE INTO 0'
60 REM DETECT WHITE FOR NEG +70+80 TO CLEAN
70 greydetect 0 159 160 1 1 0
80 qmenu 'detect'
90 binopen 1 2 0 3
100 binmove 2 1
```

```
110 PAUSETEXT 2 'KEEP AREAS OF INTEREST INPUT 1 OUTPUT 1'
120 qmenu 'bin_edit'
130 OUTLINE 1 9
140 binx 3 1 10 1 0 0
150 BINX 3 9 11 1 0 0
160 build 3 10
170 build 3 11
180 PAUSETEXT 2 'INPUT PLANE 10 MEASURE THEN DO 11'
190 qmenu 'measure_field'
200 BINX 4 1 10 1 0 0
210 BINX 4 9 11 1 0 0
220 BUILD 4 10
230 build 4 11
240 QMENU 'MEASURE_FIELD'
250 BINX 5 1 10 1 0 0
260 BINX 5 9 11 1 0 0
270 BUILD 5 10
280 build 5 11
290 QMENU 'MEASURE_FIELD'
300 BINX 6 1 10 1 0 0
310 BINX 6 9 11 1 0 0
320 BUILD 6 10
330 build 6 11
340 QMENU 'MEASURE_FIELD'
350 BINX 7 1 10 1 0 0
360 BINX 7 9 11 1 0 0
370 BUILD 7 10
380 build 7 11
390 QMENU 'MEASURE_FIELD'
400 END


FRACTIF6
10 dim a(100)
 20 input 'filename? ' n$
 30 open#1 'b:' +n$+'.prn'
 40 c=1
 50 riasettings 'cal_value' k
 80 mframe 0 0 482 401
 81 iframe 0 0 481 401
 85 PAUSETEXT 2 'ACQUIRE INTO 0'
 90 loadimage 0 "D:"+n$+".TIG"
110 REM DETECT WHITE FOR NEG +70+80 TO CLEAN
120 greydetect 0 159 160 1 1 0
130 qmenu 'detect'
140 binopen 1 2 0 3
150 binmove 2 1
160 PAUSETEXT 2 'KEEP AREAS OF INTEREST INPUT 1 OUTPUT 1'
170 qmenu 'bin_edit'
180 OUTLINE 1 9
190 binx 3 1 10 1 0 0
200 BINX 3 9 11 1 0 0
210 build 3 10
220 build 3 11
230 PAUSETEXT 2 'INPUT PLANE 10 MEASURE THEN DO 11'
240 measfield 10
250 rfieldres a(1)
260 print#1: a(1)*k,a(5)
270 measfield 11
280 rfieldres a(1)
290 print#1: a(1)*k,a(5)
300 c=c+1
```

232

```
310 if c=6 goto 560
320 if c=5 goto 510
330 if c=4 goto 460
340 if c=3 goto 410
350 if c=2 goto 360
360 BINX 4 1 10 1 0 0
370 BINX 4 9 11 1 0 0
380 BUILD 4 10
390 build 4 11
400 goto 240
410 BINX 5 1 10 1 0 0
420 BINX 5 9 11 1 0 0
430 BUILD 5 10
440 build 5 11
450 goto 240
460 BINX 6 1 10 1 0 0
470 BINX 6 9 11 1 0 0
480 BUILD 6 10
490 build 6 11
500 goto 240
510 BINX 7 1 10 1 0 0
520 BINX 7 9 11 1 0 0
530 BUILD 7 10
540 build 7 11
550 goto 240
560 close#1
570 END
```

FRACTIF7
```
10 dim a(100)
 20 input 'filename? ' n$
 30 open#1 'b:' +n$+'.prn'
 40 c=1
 50 riasettings 'cal_value' k
 60 mframe 0 0 482 401
 70 iframe 0 0 481 401
 80 PAUSETEXT 2 'ACQUIRE INTO 0'
 90 loadimage 0 "D:"+n$+".TIG"
100 REM DETECT WHITE FOR NEG +70+80 TO CLEAN
110 greydetect 0 206 209 4 1 0
120 qmenu 'detect'
130 binopen 1 2 0 3
140 binmove 2 1
150 PAUSETEXT 2 'KEEP AREAS OF INTEREST INPUT 1 OUTPUT 1'
160 qmenu 'bin_edit'
170 OUTLINE 1 9
180 binx 3 1 10 1 0 0
190 BINX 3 9 11 1 0 0
200 build 3 10
210 build 3 11
220 PAUSETEXT 2 'INPUT PLANE 10 MEASURE THEN DO 11'
230 measfield 10
240 rfieldres a(1)
250 print#1: a(1)*k,a(5)
260 measfield 11
270 rfieldres a(1)
280 print#1: a(1)*k,a(5)
290 c=c+1
300 if c=6 goto 550
310 if c=5 goto 500
320 if c=4 goto 450
```

```
330 if c=3 goto 400
340 if c=2 goto 350
350 BINX 4 1 10 1 0 0
360 BINX 4 9 11 1 0 0
370 BUILD 4 10
380 build 4 11
390 goto 230
400 BINX 5 1 10 1 0 0
410 BINX 5 9 11 1 0 0
420 BUILD 5 10
430 build 5 11
440 goto 230
450 BINX 6 1 10 1 0 0
460 BINX 6 9 11 1 0 0
470 BUILD 6 10
480 build 6 11
490 goto 230
500 BINX 7 1 10 1 0 0
510 BINX 7 9 11 1 0 0
520 BUILD 7 10
530 build 7 11
540 goto 230
550 close#1
560 END


FRACTIF8
10 dim a(100)
 20 input 'filename?  ' n$
 30 open#1 'b:' +n$+'.prn'
 40 c=1
 50 riasettings 'cal_value' k
 60 mframe 0 0 482 401
 70 iframe 0 0 481 401
 80 PAUSETEXT 2 'ACQUIRE INTO 0'
 90 loadimage 0 "C:\andy\"+n$+".tig"
100 REM DETECT WHITE FOR NEG +70+80 TO CLEAN
110 greydetect 0 206 209 4 1 0
120 qmenu 'detect'
130 binopen 1 2 0 3
140 binmove 2 1
150 PAUSETEXT 2 'KEEP AREAS OF INTEREST INPUT 1 OUTPUT 1'
160 qmenu 'bin_edit'
170 OUTLINE 1 9
180 binx 3 1 10 1 0 0
190 BINX 3 9 11 1 0 0
200 build 3 10
210 build 3 11
220 PAUSETEXT 2 'INPUT PLANE 10 MEASURE THEN DO 11'
230 measfield 10
240 rfieldres a(1)
250 print#1: a(1)*k,a(5)
260 measfield 11
270 rfieldres a(1)
280 print#1: a(1)*k,a(5)
290 c=c+1
300 if c=6 goto 550
310 if c=5 goto 500
320 if c=4 goto 450
330 if c=3 goto 400
340 if c=2 goto 350
350 BINX 4 1 10 1 0 0
```

```
360 BINX 4 9 11 1 0 0
370 BUILD 4 10
380 build 4 11
390 goto 230
400 BINX 5 1 10 1 0 0
410 BINX 5 9 11 1 0 0
420 BUILD 5 10
430 build 5 11
440 goto 230
450 BINX 6 1 10 1 0 0
460 BINX 6 9 11 1 0 0
470 BUILD 6 10
480 build 6 11
490 goto 230
500 BINX 7 1 10 1 0 0
510 BINX 7 9 11 1 0 0
520 BUILD 7 10
530 build 7 11
540 goto 230
550 close#1
560 END
```

APPENDIX TWO

A2   Data Tables

A2.1   Data for Average Aerosol Morphology for each study day (cf. Section 4.4.2.2, Figures 4.30, 4.31 and 4.32)

All data	DFD	DFD S.D.	PFD	PFD S.D.	EC Diameter (nm)	EC Diameter S.D.
4.12.96	1.65	0.22	1.16	0.10	149.7	93.2
3.2.97	1.55	0.24	1.15	0.13	99.1	79.3
10.3.97	1.54	0.16	1.15	0.09	89.2	53.2
7.4.97	1.77	0.07	1.18	0.10	95.9	78.2

Table A2.1 Average Daily Morphology of Roadside Aerosol (fixed data)

All data	DFD	DFD S.D.	PFD	PFD S.D.	EC Diameter (nm)	EC Diameter S.D.
4.12.96	1.64	0.18	1.10	0.13	149.0	84.0
3.2.97	1.57	0.16	1.15	0.12	89.5	60.2
10.3.97	1.55	0.24	1.05	0.12	102.0	77.1
7.4.97	1.76	0.09	1.12	0.12	78.4	34.8

Table A2.2 Average Daily Morphology of Background Aerosol (fixed data)

All data	DFD	DFD S.D.	PFD	PFD S.D.	EC Diameter	EC Diameter S.D.
7.4.97	1.54	0.09	1.20	0.10	95.90	78.20
12.5.97	1.60	0.09	1.14	0.10	178.13	346.93
7.6.97	1.53	0.10	1.08	0.09	85.08	80.7
21.7.97	1.58	0.10	1.11	0.08	77.08	71.13

Table A2.3 Average Daily Morphology of Roadside Aerosol (normalised data)

All data	DFD	DFD S.D.	PFD	PFD S.D.	EC Diameter	EC Diameter S.D.
7.4.97	1.55	0.08	1.13	0.10	78.40	34.80
12.5.97	1.55	0.09	1.11	0.08	146.46	163.87
7.6.97	1.58	0.09	1.10	0.08	97.33	89.38
21.7.97	1.57	0.10	1.11	0.09	170.93	184.38

Table A2.4 Average Daily Morphology of Background Aerosol (normalised data)

A2.2 Data for Size grouped DFD, PFD and Equivalent Circle Diameter and the statistical significance of difference between the roadside and background. (cf. Section 4.4.2.3 and figure 4.33 to 4.38)

	All Fixed	Road ± S.D	Background ± S.D	Sig diff
< 40nm	DFD	1.39 ± 0.23	1.31 ± 0.23	no (0.24)
	PFD	1.11 ± 0.16	0.98 ± 0.19	yes (0.013)
	Diameter	30.8 ± 7.8	27.6 ± 7.16	no (0.315)
40 - 80 nm	DFD	1.58 ± 0.15	1.59 ± 0.16	no (0.73)
	PFD	1.16 ± 0.10	1.12 ± 0.11	yes (0.035)
	Diameter	58.6 ± 11.5	59.6 ± 11.1	no (0.60)
80-120nm	DFD	1.66 ± 0.12	1.69 ± 0.09	no (0.26)
	PFD	1.17 ± 0.09	1.11 ± 0.10	yes (0.017)
	Diameter	96.7 ± 12.4	98.3 ± 11.9	no (0.60)
120 - 220nm	DFD	1.76 ± 0.07	1.75 ± 0.08	no (0.87)
	PFD	1.18 ± 0.09	1.12 ± 0.09	yes (0.0023)
	Diameter	154.0 ± 26.1	163.8 ± 29.0	no (0.14)
>220nm	DFD	1.86 ± 0.07	1.84 ± 0.07	no (0.45)
	PFD	1.19 ± 0.05	1.12 ± 0.13	yes (0.046)
	Diameter	272.5 ± 45.7	280.1 ± 44.4	no (0.65)

t-test p values in parenthesis

Table A2.5 All Fixed data size grouped morphology and the statistical significance of difference between the roadside and background

	All Normalised	Road	Roof	Sig diff
< 40nm	DFD	1.55 ± 0.10	1.58 ± 0.09	no (0.141)
	PFD	1.09 ± 0.09	1.08 ± 0.05	no (0.502)
	Diameter	31.9 ± 6.0	28.6 ± 9.0	no (0.065)
40 - 80 nm	DFD	1.56 ± 0.10	1.57 ± 0.09	no (0.440)
	PFD	1.13 ± 0.09	1.10 ± 0.09	no (0.126)
	Diameter	60.3 ± 11.2	60.0 ± 11.5	no (0.871)
80-120nm	DFD	1.57 ± 0.09	1.57 ± 0.10	no (0.489)
	PFD	1.12 ± 0.09	1.11 ± 0.09	no (0.655)
	Diameter	97.8 ± 13.1	96.0 ± 10.9	no (0.546)
120 - 220nm	DFD	1.59 ± 0.09	1.55 ± 0.10	no (0.099)
	PFD	1.19 ± 0.10	1.11 ± 0.09	yes (0.0009)
	Diameter	158.7 ± 31.5	157.1 ± 27.2	no (0.815)
>220nm	DFD	1.53 ± 0.07	1.56 ± 0.11	no (0.304)
	PFD	1.17 ± 0.12	1.18 ± 0.10	no (0.696)
	Diameter	446.6 ± 511.6	434.6 ± 232.0	no (0.927)

t-test p values in parenthesis

Table A2.6 All Normalised data size grouped morphology and the statistical significance of difference between the roadside and background

A2.3 The Daily Data for Size grouped DFD, PFD and Equivalent Circle Diameter and the statistical significance of difference between the roadside and background. (cf. Section 4.4.2.4 and figure 4.43 to 4.44)

	6.12.96	Road	Roof	Sig diff
< 40nm	DFD	1.27 ± 0.005	1.40 ± 0.15	no (0.32)
	PFD	0.96	0.98 ± 0.07	no (0.96)
	Diameter	28.3 ± 11.4	29.5 ± 4.5	no (0.85)
40 - 80 nm	DFD	1.50 ± 0.11	1.39 ± 0.10	no (0.051)
	PFD	1.24 ± 0.07	1.07 ± 0.16	no (0.13)
	Diameter	56.6 ± 9.8	53.9 ± 12.8	no (0.62)
80-120nm	DFD	1.64 ± 0.07	1.62 ± 0.07	no (0.52)
	PFD	1.13 ± 0.08	1.12 ± 0.07	no (0.85)
	Diameter	96.4 ± 11.9	104.8 ± 12.7	no (0.20)
120 - 220nm	DFD	1.69 ± 0.26	1.72 ± 0.06	no (0.59)
	PFD	1.20 ± 0.08	1.11 ± 0.09	no (0.07)
	Diameter	170.2 ± 32.4	172.8 ± 29.5	no (0.81)

t-test p values in parenthesis

Table A2.7 Size grouped morphology means for 6.12.96 (fixed analysis)

	3.2.97	Road	Roof	Sig diff
< 40nm	DFD	1.34 ± 0.24	1.33 ± 0.19	no (0.92)
	PFD	1.11 ± 0.18	1.14 ± 0.21	no (0.21)
	Diameter	28.6 ± 7.8	27.4 ± 5.9	no (0.75)
40 - 80 nm	DFD	1.46 ± 0.10	1.50 ± 0.09	no (0.34)
	PFD	1.11 ± 0.13	1.16 ± 0.11	no (0.31)
	Diameter	54.7 ± 11.5	59.7 ± 8.2	no (0.18)
80-120nm	DFD	1.60 ± 0.11	1.65 ± 0.038	no (0.18)
	PFD	1.17 ± 0.08	1.12 ± 0.09	no (0.26)
	Diameter	98.1 ± 9.9	93.8 ± 7.8	no (0.32)
120 - 220nm	DFD	1.75 ± 0.05	1.73 ± 0.05	no (0.48)
	PFD	1.20 ± 0.09	1.14 ± 0.07	no (0.18)
	Diameter	153.3 ± 23.4	157.8 ± 18.0	no (0.71)

t-test p values in parenthesis

Table A2.8 Size grouped morphology means for 3.2.97 (fixed analysis)

	10.3.97	Road	Roof	Sig diff
< 40nm	DFD	1.33 ± 0.18	1.13 ± 0.19	no (0.07)
	PFD	1.14 ± 0.10	0.91 ± 0.13	yes (0.003)
	Diameter	33.7 ± 9.6	27.7 ± 8.9	no (0.23)
40 - 80 nm	DFD	1.49 ± 0.09	1.52 ± 0.12	no (0.30)
	PFD	1.15 ± 0.09	1.08 ± 0.09	yes (0.011)
	Diameter	61.4 ± 12.5	59.5 ± 13.6	no (0.64)
80-120nm	DFD	1.59 ± 0.07	1.62 ± 0.05	no (0.31)
	PFD	1.16 ± 0.08	1.08 ± 0.08	no (0.051)
	Diameter	102.8 ± 12.7	102.2 ± 13.0	no (0.91)
120 - 220nm	DFD	1.73 ± 0.06	1.75 ± 0.07	no (0.60)
	PFD	1.15 ± 0.09	1.09 ± 0.10	no (0.24)
	Diameter	156.4 ± 28.6	168.8 ± 29.4	no (0.35)

t-test p values in parenthesis

Table A2.9 Size grouped morphology means for 10.3.97 (fixed analysis)

	3.4.97	Road	Roof	Sig diff
< 40nm	DFD	1.66 ± 0.06	1.55 ± 0.13	no (0.12)
	PFD	1.11 ± 0.16	0.96 ± 0.17	no (0.20)
	Diameter	33.6 ± 4.2	26.2 ± 8.2	no (0.11)
40 - 80 nm	DFD	1.75 ± 0.04	1.76 ± 0.03	no (0.22)
	PFD	1.18 ± 0.09	1.14 ± 0.10	no (0.13)
	Diameter	58.2 ± 10.7	61.3 ± 10.2	no (0.31)
80-120nm	DFD	1.81 ± 0.04	1.80 ± 0.03	no (0.74)
	PFD	1.20 ± 0.11	1.13 ± 0.12	no (0.21)
	Diameter	89.7 ± 13.1	95.6 ± 12.0	no (0.32)
120 - 220nm	DFD	1.83 ± 0.03	1.85 ± 0.03	no (0.14)
	PFD	1.28 ± 0.30	1.20 ± 0.08	no (0.48)
	Diameter	147.7 ± 31.1	140.7 ± 23.7	no (0.61)

t-test p values in parenthesis

Table A2.10 Size grouped morphology means for 3.4.97 (fixed analysis)

	3.4.97	Road	Roof	Sig diff
< 40nm	DFD	1.55 ± 0.05	1.53 ± 0.03	no (0.51)
	PFD	1.13 ± 0.09	1.09 ± 0.07	no (0.45)
	Diameter	33.6 ± 4.2	26.2 ± 8.2	no (0.11)
40 - 80 nm	DFD	1.54 ± 0.10	1.55 ± 0.08	no (0.53)
	PFD	1.18 ± 0.09	1.11 ± 0.10	yes (0.03)
	Diameter	58.2 ± 10.7	61.3 ± 10.2	no (0.30)
80-120nm	DFD	1.57 ± 0.08	1.54 ± 0.10	no (0.69)
	PFD	1.18 ± 0.09	1.16 ± 0.11	no (0.71)
	Diameter	89.7 ± 13.1	95.6 ± 12.0	no (0.32)
120 - 220nm	DFD	1.53 ± 0.08	1.56 ± 0.06	no (0.50)
	PFD	1.27 ± 0.07	1.16 ± 0.11	yes (0.04)
	Diameter	147.7 ± 31.1	140.3 ± 23.7	no (0.61)

t-test p values in parenthesis

Table A2.11 Size grouped morphology means for 3.4.97 (normalised analysis)

	12.5.97	Road	Roof	Sig diff
< 40nm	DFD	1.62 ± 0.10	1.52 ± 0.09	no (0.08)
	PFD	1.21 ± 0.13	1.10 ± 0.07	no (0.13)
	Diameter	33.4 ± 7.0	24.5 ± 12.5	no (0.18)
40 - 80 nm	DFD	1.59 ± 0.07	1.58 ± 0.08	no (0.81)
	PFD	1.14 ± 0.10	1.12 ± 0.06	no (0.72)
	Diameter	63.9 ± 10.2	61.6 ± 14.3	no (0.64)
80-120nm	DFD	1.60 ± 0.06	1.52 ± 0.10	no (0.051)
	PFD	1.10 ± 0.08	1.06 ± 0.07	no (0.35)
	Diameter	98.4 ± 12.9	95.8 ± 8.2	no (0.63)
120 - 220nm	DFD	1.63 ± 0.10	1.56 ± 0.10	no (0.10)
	PFD	1.19 ± 0.84	1.10 ± 0.06	yes (0.006)
	Diameter	172.3 ± 31.4	159.8 ± 32.5	no (0.36)

t-test p values in parenthesis

Table A2.12 Size grouped morphology means for 12.5.97 (normalised analysis)

	2.6.97	Road	Roof	Sig diff
	DFD	1.49 ± 0.09	1.60 ± 0.08	yes (0.002)
< 40nm	PFD	1.06 ± 0.07	1.09 ± 0.03	no (0.19)
	Diameter	31.7 ± 7.6	30.2 ± 9.1	no (0.63)
	DFD	1.54 ± 0.12	1.59 ± 0.10	no (0.21)
40 - 80 nm	PFD	1.08 ± 0.09	1.09 ± 0.10	no (0.70)
	Diameter	57.9 ± 11.5	59.9 ± 12.3	no (0.62)
	DFD	1.49 ± 0.08	1.57 ± 0.08	no (0.11)
80-120nm	PFD	1.09 ± 0.09	1.11 ± 0.07	no (0.64)
	Diameter	103.3 ± 14.3	95.3 ± 12.4	no (0.31)
	DFD	1.59 ± 0.07	1.60 ± 0.07	no (0.78)
120 - 220nm	PFD	1.11 ± 0.09	1.09 ± 0.07	no (0.55)
	Diameter	149.7 ± 29.0	166.1 ± 28.4	no (0.26)

t-test p values in parenthesis

Table A2.13 Size grouped morphology means for 2.6.97 (normalised analysis)

	21.7.97	Road	Roof	Sig diff
	DFD	1.58 ± 0.08	1.67 ± 0.05	yes (0.04)
< 40nm	PFD	1.09 ± 0.08	1.04 ± 0.02	no (0.17)
	Diameter	31.2 ± 4.7	32.2 ± 2.3	no (0.63)
	DFD	1.59 ± 0.08	1.58 ± 0.10	no (0.94)
40 - 80 nm	PFD	1.10 ± 0.71	1.07 ± 0.09	no (0.38)
	Diameter	62.3 ± 12.0	54.6 ± 10.4	no (0.12)
	DFD	1.60 ± 0.10	1.59 ± 0.09	no (0.89)
80-120nm	PFD	1.12 ± 0.09	1.08 ± 0.07	no (0.33)
	Diameter	101.7 ± 10.8	97.5 ± 11.6	no (0.49)
	DFD	1.58 ± 0.08	1.52 ± 0.11	no (0.40)
120 - 220nm	PFD	1.17 ± 0.02	1.12 ± 0.09	no (0.40)
	Diameter	157.7 ± 34.9	157.6 ± 22.5	no (0.99)

t-test p values in parenthesis

Table A2.14 Size grouped morphology means for 21.7.97 (normalised analysis)

A2.4 Tables of the percentages of non-fractal particles (cf. Chapter 6)

fractal vs. non fractal	7.4.97	12.5.97	2.6.97	21.7.97
non-fractal road	4% (0 - 8 %)	8% (2 - 24%)	16% (9 - 36%)	6% (0 - 28%)
above 80nm	0% (0-2%)	4% (2-14%)	4% (2-10%)	2% (0-0)
non-fractal roof	12% (0 - 22%)	8% (0 - 26%)	8% (2 - 22%)	4% (4-- 32%)
above 80nm	6% (6-6%)	4% (0-15%)	2% (0-8%)	2% (0-14%)

figures in parethesis account for the ±6% error on PFD from 0.95-1.05
figures given are percentages relative to the total particle number

Table A2.15 The proportion of non-fractal particles at the roadside and the background and the proportion above 80nm in size for the normalised study days (cf. Section 6.2.2, figures 6.6 and 6.7)

fractal vs. non fractal	4.12.96	3.2.97	10.3.97	7.4.97
non-fractal road	2% (2-2%)	11% (11-21%)	4% (0-14%)	6%(2-8%)
above 80nm	0%(0%)	0% (0-2%)	2%(0-6%)	0%(0-2%)
non-fractal roof	16% (4 - 26%)	4%(2-11%)	28% (6-44%)	16%(4-24%)
above 80nm	7% (2-11%)	0%(0-5%)	12% (2-22%)	4%(0-12%)

figures in parethesis account for the ±6% error on PFD from 0.95-1.05
figures given are percentages relative to the total particle number

Table A2.16 The proportion of non-fractal particles at the roadside and the background and the proportion above 80nm in size for the fixed study days (cf. Section 6.2.2, figures 6.6 and 6.7)

	7.4.97	12.5.97	2.6.97	21.6.97	All
< 40nm	20%	0 - 20%	18 - 41%	10 - 40%	13 - 26% (47)
40-80nm	4%	12.5 - 25 %	18 - 35%	0 - 30%	8 - 20% (74)
80-120nm	0 - 14%	10 - 40%	0 - 40%	17%	7 - 26% (27)
120 - 220nm	0 %	0 - 8%	12.5 - 25%	0	3 - 13% (31)

figures given as a range where applicable to account for the ±6% error on PFD from 0.95-1.05
figures given are the percentages relative to the number of particles in that size range

Table A2.17 The proportion of non-fractal particles at the roadside within each size range for the normalised study days (cf. Section 6.2.2, figures 6.6 and 6.7)

	7.4.97	12.5.97	2.6.97	21.6.97	All
< 40nm	20%	17%	0 ± 8%	0 - 60%	7- 11%
40-80nm	8 - 29%	0 - 20%	18 - 41%	11 - 44%	10 - 32%
80-120nm	14%	25 - 50% (8)	0 - 12.5%	0 - 50%	10 - 25%
120 - 220nm	14%	0 - 27%	11 - 22%	7 - 20 %	7 -16%

figures given as a range where applicable to account for the ±6% error on PFD from 0.95-1.05
figures given are the percentages relative to the number of particles in that size range

Table A2.18 The proportion of non-fractal particles at the background within each size range for the normalised study days (cf. Section 6.2.2, figures 6.6 and 6.7)

	Fixed		Nomalised	
	Road	Roof	Road	Roof
All	7 % (4-14%)	17% (1-25%)	8.5% (1.5-24%)	8% (1-25%)
Above 80nm	<1% (0-2%)	6 (2-14%)	2.5% (1-7%)	4% (0-13)

Table A2.19 The Percentage of non fractal particles for the normalised and fixed analysis data at roadside and background sites and the proportion above 80nm in size (cf. Section 6.2, Figures 6.1 to 6.4)